Homologous antimicrobial proteins in plants and fungi: conserved mechanisms shaping the plant microbiota

Doctoral thesis

for

the award of the doctoral degree

of the Faculty of Mathematics and Natural Sciences

of the University of Cologne

submitted by

Gabriella Cosmo Petti

accepted in the year 2026

Table of content

Abstract

Plants form close association with a diverse and dynamic community of microorganisms, including bacteria, fungi, protists, nematodes, and viruses, collectively referred to as their microbiota. These microorganisms form complex associations with their hosts and play critical roles in plant health. It has therefore been proposed that plants and their microbiota function together as a single ecological unit, the holobiont. The plant microbiota plays an important role in plant defence, influencing the outcome of plant-pathogen interactions. Microbiota members can suppress pathogens directly through competition, antibiosis, and nutrient sequestration, or indirectly by priming host immune responses, thereby enhancing disease resistance. Together, these mechanisms expand the plant capacity to withstand invading pathogens. To establish themselves within the host, plant pathogens secrete effector proteins. Initially defined as modulators of host immunity, effectors are now known to serve broader roles in microbial self-protection as well as in the manipulation of host physiology. Increasing evidence indicates that some pathogens deploy effectors with antibacterial activity to inhibit microbial competitors and reshape host-associated communities, thereby promoting pathogen establishment and persistence within their niche. The studies presented in this thesis aim to deepen our understanding of antimicrobial effector proteins by elucidating the mechanisms of action and ecological functions of selected effectors in fungal pathogens and their homologs in other organisms.

In this PhD thesis, I describe the first *Verticillium dahliae* effector protein identified with antifungal activity, VdAMP3. This effector belongs to the cysteine-stabilized αβ defensin family, an ancient antimicrobial protein family. *V. dahliae* secretes VdAMP3 during the formation of resting structures in senescing plant tissues, where it modulates the host mycobiota by suppressing fungal competitors and safeguarding the development of its resting structures.

V. dahliae also secretes the bactericidal effector VdAve1 to promote niche colonization by inhibiting bacterial antagonists. In this thesis, I present the structural and functional characterization of VdAve1. I demonstrate that VdAve1 binds lipoteichoic acid, a key component of Gram-positive bacterial cell walls, and disrupts microbial membranes in a charge-dependent manner. Moreover, its antimicrobial activity extends beyond bacteria, as VdAve1 also inhibits eukaryotic microbes.

Finally, I show that plant homologs of VdAve1, known as plant natriuretic peptides (PNPs), from diverse plant species as well as the the plant-derived PNP horizontally acquired by the whitefly *Bemisia tabaci,* exhibit both antibacterial and antifungal activities. Loss of PNP genes in *Arabidopsis thaliana* alters bacterial, but not fungal, phyllosphere communities, suggesting that PNPs are involved in microbiota manipulation.

Zusammenfassung

Pflanzen bilden eine enge Verbindung mit einer vielfältigen und dynamischen Gemeinschaft von Mikroorganismen, darunter Bakterien, Pilze, Protisten, Nematoden und Viren, die zusammen als ihre Mikrobiota bezeichnet werden. Diese Mikroorganismen gehen komplexe Verbindungen mit ihren Wirten ein und spielen eine entscheidende Rolle für die Pflanzengesundheit. Daher wurde vorgeschlagen, dass Pflanzen und ihre Mikrobiota zusammen als eine einzige ökologische Einheit, das Holobiont, funktionieren. Die Pflanzenmikrobiota spielt eine wichtige Rolle bei der Abwehr von Pflanzen und beeinflusst den Ausgang von Wechselwirkungen zwischen Pflanzen und Krankheitserregern. Mitglieder der Mikrobiota können Krankheitserreger direkt durch Konkurrenz, Antibiosis und Nährstoffbindung oder indirekt durch die Aktivierung der Immunantwort des Wirts unterdrücken und so die Krankheitsresistenz verbessern. Zusammen erweitern diese Mechanismen die Fähigkeit der Pflanzen, eindringenden Krankheitserregern zu widerstehen. Um sich im Wirt festzusetzen, scheiden Pflanzenpathogene Effektorproteine aus. Ursprünglich als Modulatoren der Wirtsimmunität definiert, spielen Effektoren heute bekanntermaßen eine umfassendere Rolle beim Selbstschutz von Mikroorganismen sowie bei der Manipulation der Wirtsphysiologie. Immer mehr Hinweise deuten darauf hin, dass einige Pathogene Effektorproteine mit antibakterieller Wirkung einsetzen, um mikrobielle Konkurrenten zu hemmen und die mit dem Wirt assoziierten Gemeinschaften umzugestalten, wodurch sie ihre Etablierung und Persistenz in ihrer Nische fördern. Die in dieser Arbeit vorgestellten Studien zielen darauf ab, unser Verständnis von antimikrobiellen Effektorproteinen zu vertiefen, indem sie die Wirkmechanismen und ökologischen Funktionen ausgewählter Effektorproteine in pilzlichen Pathogenen und ihren Homologen in anderen Organismen aufklären.

In dieser Doktorarbeit beschreibe ich das erste Effektorprotein von Verticillium dahliae, das mit antimykotischer Aktivität identifiziert wurde: VdAMP3. Dieser Effektor gehört zur Familie der cystein-stabilisierten αβ-Defensine, einer alten Familie antimikrobieller Proteine. V. dahliae sezerniert VdAMP3 während der Bildung von Ruhezuständen in alternden Pflanzengeweben, wo es die Mykobiota des Wirts moduliert, indem es konkurrierende Pilze unterdrückt und die Entwicklung seiner Ruhezustände schützt.

V. dahliae sezerniert auch den bakteriziden Effektor VdAve1, um die Besiedlung der Nische durch Hemmung bakterieller Antagonisten zu fördern. In dieser Arbeit stelle ich die

strukturelle und funktionelle Charakterisierung von VdAve1 vor. Ich zeige, dass VdAve1 an Lipoteichonsäure, einen wichtigen Bestandteil der Zellwände grampositiver Bakterien, bindet und mikrobielle Membranen auf ladungsabhängige Weise zerstört. Darüber hinaus erstreckt sich seine antimikrobielle Aktivität über Bakterien hinaus, da VdAve1 auch eukaryotische Mikroben hemmt.

Schließlich zeige ich, dass pflanzliche Homologe von VdAve1, bekannt als pflanzliche natriuretische Peptide (PNPs), aus verschiedenen Pflanzenarten sowie das pflanzliche PNP, das horizontal von der Weißen Fliege Bemisia tabaci erworben wurde, sowohl antibakterielle als auch antimykotische Aktivitäten aufweisen. Der Verlust von PNP-Genen in Arabidopsis thaliana verändert die bakterielle, aber nicht die pilzliche Phyllosphären-Gemeinschaft, was darauf hindeutet, dass PNPs an der Manipulation der Mikrobiota beteiligt sind.

Chapter 1: General introduction

The plant microbiota

Plants live in close association with a diverse and dynamic community of microorganisms collectively known as their microbiota. This community includes bacteria, fungi, oomycetes, archaea, and protists (Trivedi et al. 2020). Microbial colonization can occur in different plant habitats: belowground in the rhizosphere, aboveground in the phyllosphere, or within internal tissues, known as the endosphere (Bulgarelli et al. 2013).

Microbial acquisition occurs both vertically, via seed transmission, and horizontally, from sources such as bulk soil, air, insects, pollen and rain (Abdelfattah et al. 2023). Among these sources, soil serves as a major microbial reservoir, characterized by a high microbial diversity. This diversity generally declines along a gradient from bulk soil to the rhizosphere and further into the endosphere, reflecting increasing levels of selectivity and microbial filtering by the plant (Edwards et al. 2015). Plants influence their microbial community assembly through the release of root exudates, which contain sugars, amino acids, secondary metabolites, and signalling molecules that can attract or repel specific microbes (Sasse et al. 2018).

The composition and structure of these microbial communities are shaped by a multitude of biotic and abiotic factors, including plant genotype and compartment, developmental stage, soil physicochemical properties, climatic conditions, and complex microbial interactions (Trivedi et al. 2020). Despite this complexity, the plant microbiota is not a random assemblage of microorganisms, as across diverse environmental conditions, plant species consistently associate with a specific set of microbes known as the core microbiota (Yeoh et al. 2017; Durán 2024). Members of this core group can promote plant health by increasing mineral bioavailability and facilitating uptake, confer tolerance to abiotic stressors, suppress pathogen proliferation (Cheng et al. 2024; Lemanceau et al. 2017).

Given the functional interdependence between plants and their microbiota, they are increasingly viewed as a single ecological entity; the holobiont (Vandenkoornhuyse et al. 2015).

The plant immune system

Plant microbiota members comprise microbes with beneficial, mutualistic, or pathogenic potential. To defend against microbial invasion, plants have evolved both intracellular and extracellular immune receptors capable of detecting microbial presence and initiating immune responses. The most widely accepted framework for describing plant immunity is the zigzag model (Jones and Dangl 2006). According to this model, plants utilize cell surface-localized receptors called pattern-recognition receptors (PRRs) to recognize either conserved microbial molecules, known as microbe-associated molecular patterns (MAMPs), or endogenous molecules and damaged self-molecules called damage-associated molecular patterns (DAMPs) in the extracellular space (Boutrot and Zipfel 2017). MAMP/DAMP recognition by PRRs activates an immune response known as MAMP-triggered immunity (MTI). MTI constitutes a basal immune barrier and it is typically sufficient to make plants immune against invading microbes. However, successful pathogens have evolved virulence-promoting proteins, referred to as effector proteins, that aid the pathogen to evade or suppress MTI and consequently to cause disease, leading to effector-triggered susceptibility (ETS). Plants in turn have evolved resistance proteins, mainly intracellular receptors, which recognize microbial effectors either directly or indirectly, activating effector-triggered immunity (ETI). Pathogens can overcome ETI by modifying or losing recognized effector proteins to evade recognition, or evolving novel effectors to suppress ETI. These processes are shaped by continuous co-evolution between pathogens and their host plants, altering the outcome of the plant-pathogen interaction.

The zigzag model was originally proposed with the assumption that MTI and ETI represent two distinct branches of the plant immune system. However, this dichotomy has proven overly simplistic, as the boundaries between MTI and ETI have become increasingly blurred (Thomma et al. 2011; Pritchard and Birch 2014). To address these limitations, the Invasion Model was proposed (Cook et al. 2015). In this model, plants utilize invasion pattern receptors (IPRs) to detect invasion patterns (IPs), molecules of any kind and origin that signal microbial invasion, to initiate appropriate immune responses (Cook et al. 2015). Today, MTI and ETI are understood as part of a continuum of plant immune responses (Ngou et al. 2021; Yuan et al. 2021; Pruitt et al. 2021), making the Invasion Model a more accurate and integrative framework.

Detection of IPs by IPRs activates a cascade of immune responses, including the production of reactive oxygen species, callose deposition and the induction of defence-related genes (Tsuda & Katagiri, 2010). Among the defence components that are induced are antimicrobial proteins, which act through diverse mechanisms to inhibit microbial growth (van Loon et al. 2006). Some of the best-characterized antimicrobial proteins in plants are the pathogenesis-related (PR) proteins, which are typically upregulated in response to infection. PR proteins encompass several distinct families, many of which directly target microbial cell walls or membranes. These include glucanases, chitinases, thionins, and defensins (van Loon et al. 2006; Sels et al. 2008). PR proteins contribute to both local and systemic immune responses, and numerous studies have shown that their overexpression can enhance plant resistance to a range of pathogens (Terras et al. 1995; Epple et al. 1997; Gao et al. 2000). Beyond defence against pathogens, antimicrobial proteins also play roles in regulating symbiotic interactions. For instance, legume plants produce specific antimicrobial peptides that modulate the differentiation of nitrogen-fixing symbionts within root nodules (van de Velde et al. 2010).

Upon perception of microbes, the plant can enter an elevated defensive state known as induced resistance (IR) (Mauch-Mani et al. 2017). This state can be triggered by both pathogenic and beneficial microbes and leads to a stronger and/or faster defence response against future microbial challenges, which is often effective against a broad spectrum of pathogens (Kesel et al. 2021). Two major forms of IR have been described: systemic acquired resistance (SAR) and induced systemic resistance (ISR). SAR is typically triggered by pathogen infections, depends on salicylic acid (SA) signalling, and is associated with accumulation of PR proteins (Durrant and Dong 2004). In contrast, ISR is typically elicited by beneficial root-associated microbes such as rhizobacteria and mycorrhizal fungi. It relies on jasmonic acid (JA) and ethylene (ET) signalling pathways and functions independently of SA and PR protein accumulation (Pieterse et al. 2014).

The plant microbiota as an additional layer of the plant immune system

The plant microbiota plays a key role in plant defence. These microbial communities influence the outcome of plant–pathogen interactions, acting both directly and indirectly to suppress disease (Vannier et al. 2019). A well-known example of microbiota-mediated protection is found in plant-driven assembly of disease-suppressive soil microbiota. Following an initial

disease outbreak, plants can alter their root exudates to recruit beneficial microbes, a strategy referred to as a “cry for help”, resulting in the assembly of a disease-suppressive microbial community (Spooren et al. 2024). Subsequent plants grown in these soils benefit from this legacy, as disease severity and incidence are reduced. This phenomenon is attributed to the activity of specific microbial taxa within the soil community that inhibit pathogen proliferation (Mendes et al. 2011; Kwak and Weller 2013; Carrión et al. 2018). One famous example is the suppression of the wheat root disease take-all, caused by *Gaeumannomyces graminis*, which has been linked to the enrichment of fluorescent *Pseudomonas* spp. that produce the antibiotic 2,4-diacetylphloroglucinol (2,4-DAPG) in the rhizosphere (Weller et al. 2002; Kwak and Weller 2013). Beyond antibiosis, microbiota members can inhibit pathogens by limiting access to key nutrients. Iron sequestration through siderophore production, for example, has been implicated in restricting pathogen growth in both rhizosphere and phyllosphere communities (Gu et al. 2020; Shalev et al. 2022).

Plant-associated microbes can contribute to disease resistance by modulating plant immune responses. Plants grown under axenic (microbe-free) conditions exhibit increased susceptibility to pathogens and display defects in MTI, underscoring the microbiota’s essential role in immunocompetence (Paasch et al. 2023). Beneficial microbes are able to stimulate the host immune system, increasing the capacity to withstand pathogen attack (Pieterse et al. 2014). For instance, rhizosphere-associated *Pseudomonas* spp. have been extensively characterized for their ability to trigger ISR, resulting in the suppression of both root and foliar pathogens (Bakker et al. 2007; van de Mortel et al. 2012).

Together, these direct and indirect mechanisms of pathogen suppression by the plant microbiota expand the plant’s capacity to withstand invading pathogens, making plant-associated microbial communities an additional barrier for invading pathogens (Hacquard et al. 2017).

Effectors as tools for holobiont-level manipulation

Plant pathogens secrete effector proteins to facilitate host colonization (Lo Presti et al. 2015). Initially, effector proteins were regarded as small, secreted proteins that modulate host immune responses by targeting signalling pathways, suppressing immune responses, or

reprogramming metabolic networks. However, this definition has since expanded to include roles in microbial self-protection and the manipulation of host physiology to extract nutrients and create a more favourable niche (Cox et al. 2017; de Jonge et al. 2010; Hu et al. 2022). Recent studies have shown that plant pathogens also deploy effectors with antibacterial activity, aimed at suppressing microbial competitors in the host microbiota (Kettles et al. 2018; Snelders et al. 2020; Chang et al. 2021; Gómez-Pérez et al. 2023; Ökmen et al. 2023; Snelders et al. 2023; Chavarro-Carrero et al. 2024; Kraege et al. 2025; Mesny et al. 2024). These antibacterial effectors help to shape the plant-associated microbiota, thereby aiding pathogen niche colonization.

These findings prompted a paradigm shift in our understanding of effector biology. Rather than being exclusively host-directed, effectors are increasingly viewed as tools that aid niche colonization, by manipulating both plant and its associated microbial communities, but also microbial communities encountered by the pathogen during life stages outside the host (Kettles et al. 2018; Snelders et al. 2020; Chang et al. 2021; Gómez-Pérez et al. 2023; Ökmen et al. 2023; Snelders et al. 2023; Chavarro-Carrero et al. 2024; Kraege et al. 2025; Mesny et al. 2024).

Microbiota manipulation by the soil-borne plant pathogen *Verticillium dahliae*

Verticillium dahliae is a soil-borne fungal plant pathogen, and the most notorious pathogenic species within the *Verticillium* genus since it causes vascular wilt in a broad spectrum of plant hosts (Fradin and Thomma 2006). *V. dahliae* survives in the soil as persistent, melanized resting structures called microsclerotia that offer protection against (a)biotic stresses (Klosterman et al. 2011). Following microsclerotia germination, fungal hyphae grow saprophytically through the soil and rhizosphere towards the roots of its host. The fungus then colonizes the root cortex before invading the xylem vessels. Inside the xylem, *V. dahliae* forms conidiospores, which are transported with the sap stream to distal parts of the plant. Once conidiospores get trapped, they germinate and the hyphae colonize new xylem vessels, leading to systemic colonization and consequently wilting and necrosis (Klosterman et al., 2009). At the onset of host senescence, *V. dahliae* emerges from the xylem vessels and colonize decaying tissues, a phase accompanied by the formation of new microsclerotia. Upon host tissue decomposition,

microsclerotia are released in the soil where they can survive for years in the absence of a host (Fradin and Thomma 2006).

To facilitate colonization of its niche, *V. dahliae* secretes a diverse array of antibacterial effector proteins that suppress microbial antagonists in a stage-specific manner. The effector VdAve1 modulates the composition of the host rhizosphere microbiota, causing shifts in multiple bacterial orders, including a depletion of Sphingomonadales, an order comprising bacteria antagonistic to *V. dahliae* (Snelders et al. 2020). VdAve1 shares sequence similarity with VdAve1L2, which also displays antibacterial activity and modulates the host rhizosphere microbiota. In particular, Actinobacteria were depleted in the presence of VdAve1L2, which also have antagonistic potential towards V. dahliae (Snelders et al. 2023). It was recently shown that *V. dahliae* utilizes the effector Av2 to suppress the growth of beneficial *Pseudomonas spp.* which are recruited by the host plant as a result of the 'cry for help' (Kraege et al. 2025). Several *Pseudomonas spp.* were shown to be antagonistic to *V. dahliae*, suggesting that *V. dahliae* secretes Av2 to suppress the recruitment of antagonistic *Pseudomonas* into the rhizosphere. Effector-mediated microbiome manipulation also occurs during *V. dahliae* saprophytic stages to facilitate soil colonization. The VdAve1 effector is expressed in soil and contributes to *V. dahliae* colonization of this niche. Additionally, the effector VdAMP2 exhibits antibacterial activity, though with a distinct activity spectrum compared to VdAve1, enhancing fungal competitiveness within the microbe-rich soil (Snelders et al. 2020).

These findings collectively demonstrate that *V. dahliae* employs a suite of antibacterial effectors with distinct activities to modulate microbial communities across multiple ecological niches.

VdAve1 and its homologs

The effector protein VdAve1 was initially identified as the IP recognized by the tomato immune receptor Ve1, activating Ve1-mediated resistance (de Jonge et al. 2012). Functional analysis revealed that in the absence of the Ve1 receptor, VdAve1 acts as a virulence factor by manipulating the host microbiota and suppressing the growth of microbial antagonists (de Jonge et al. 2012; Snelders et al. 2020). Sequence similarity searches uncovered homologs of VdAve1 in plants. Interestingly, analysis of the phylogenetic distribution of *VdAve1* and its

homologs appeared to be inconsistent with species phylogeny, supporting the hypothesis that *VdAve1* was horizontally acquired by *V. dahliae* from plants (de Jonge et al. 2012).

VdAve1 plant homologs belong to a widely conserved class of plant signalling peptides known as plant natriuretic peptides (PNPs) (de Jonge et al. 2012). PNPs regulate water and ion homeostasis in plants, influencing various physiological processes including stomatal aperture, photosynthesis, and stress responses (Wang et al. 2011). In *Arabidopsis thaliana*, the PNP AtPNP-A has been linked to plant defence, as its expression increases upon *Pseudomonas syringae* infection and contributes to resistance by limiting disease symptoms and bacterial growth. Conversely, plants lacking AtPNP-A exhibit heightened susceptibility, underscoring its role in immunity (Meier et al. 2008; Ficarra et al. 2018). Notably, *AtPNP-A* has been reported to inhibit the growth of *Bacillus subtilis*, suggesting that VdAve1 plant homologs also exhibit antimicrobial activity and that the antimicrobial activity of *VdAve1* was not a result of neofunctionalization following horizontal gene transfer (HGT) (Snelders et al. 2020).

Besides plants, *VdAve1* homologs have also been identified in a range of plant-associated organisms, including fungal plant pathogens such as *Colletotrichum higginsianum*, *Cercospora beticola*, and *Fusarium oxysporum* (de Jonge et al. 2012). Additionally, the bacterial plant pathogen *Xanthomonas citri* harbours a *VdAve1*-like gene, known as *XacPNP*, which appears to have been acquired via HGT from plants (Gottig et al. 2008). Functional studies revealed that *XacPNP* contributes to virulence by promoting host colonization: its deletion leads to increased necrotic lesion formation, earlier bacterial death, reduced photosynthetic efficiency, and impaired water flux in infected leaves (Gottig et al. 2008). Based on these findings, it was suggested that *XacPNP* facilitates infection by maintaining host water balance and limiting tissue damage (Gottig et al. 2008).

Thesis outline

With this doctoral thesis, I aim to deepen our understanding of antimicrobial (effector) proteins by dissecting their mechanisms of action and ecological roles in both fungal pathogens and plants.

Chapter 2 (Figure 1a):

In this chapter, titled **"An ancient antimicrobial protein co-opted by a fungal plant pathogen for in planta mycobiome manipulation"**, we identify and characterize the antifungal effector VdAMP3 from *V. dahliae*. We show that VdAMP3 evolved from an ancient antimicrobial protein and has been co-opted by *V. dahliae* for mycobiota manipulation. We show that VdAMP3 is expressed during the formation of resting structures in senescing plant tissues to fend off fungal niche competitors. These findings illustrate that fungal plant pathogens can co-opt ancient antimicrobial proteins for plant-microbiota manipulation and that antimicrobial effector can be exploited for microbiota-manipulating effectors in a life-stage specific manner.

Chapter 3 (Figure 1b):

In this chapter, titled **"Structural and functional characterization of a host microbiota-targeting antimicrobial protein from the plant pathogen *Verticillium dahliae*"**, we deepen our understating of the mode of action of the *V. dahliae* antimicrobial effector protein VdAve1 by structurally and functionally characterizing it. NMR-based structural analysis revealed a β-barrel-like fold, and functional assays demonstrated that VdAve1 exhibits broad-spectrum antimicrobial activity against bacteria, fungi, and amoebae. The protein disrupts microbial plasma membranes in a charge-dependent manner, with positively charged regions being key to its activity. In Gram-positive bacteria such as *Bacillus subtilis*, VdAve1 binds lipoteichoic acid (LTA), a major component of the bacterial cell wall, thereby targeting the plasma membrane and ultimately causing cell death. These findings provide a mechanistic understanding of how VdAve1 mediates microbial antagonism during *Verticillium* niche colonization.

Chapter 4 (Figure 1c):

In this chapter, titled **"Antimicrobial activity of plant natriuretic peptides and their potential role in microbiota interactions"**, we investigate the antimicrobial activity of the VdAve1 homologs, the PNPs. To explore the potential antimicrobial activity of these proteins, we produced PNPs from diverse plant species, including *Arabidopsis thaliana*, *Solanum lycopersicum*, and *Physcomitrium patens*, as well the plant-derived PNP horizontally acquired by *Bemisia tabaci*, and assessed their activity *in vitro*. PNPs exhibited antibacterial and antifungal activity if the protein had a positive net charge, suggesting a charge-dependent mechanism of action. In *A. thaliana*, deletion of PNP-encoding genes altered phyllosphere

bacterial community composition, while fungal communities remained largely unaffected. These findings suggest that plant PNPs function as endogenous antimicrobial proteins involved in microbiota modulation, extending their role beyond water regulation to direct microbial shaping.

Chapter 5:

In this chapter, I discuss the implications of the key findings of my PhD research within a broader scientific context.

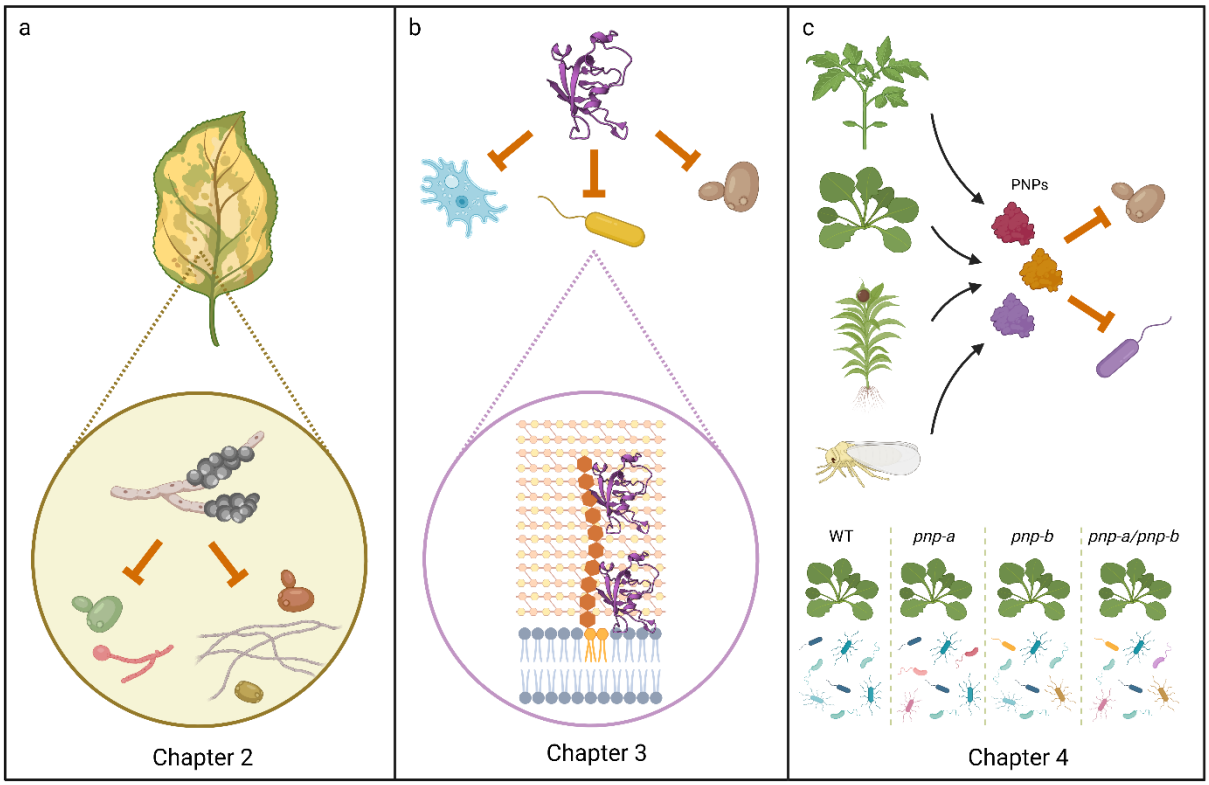

Figure 1. Graphical representation of the studies included in this thesis. a. Chapter 2 describes the identification and characterization of the antifungal effector VdAMP3 from *V. dahliae*, showing it evolved from an ancient antimicrobial protein and is expressed during resting structure formation in senescing plant tissues to inhibit fungal competitors. These findings illustrate that fungal plant pathogens can co-opt ancient antimicrobial proteins for life-stage-specific manipulation of the plant mycobiota. **b.** Chapter 3 details the structural and functional characterization of the *V. dahliae* effector VdAve1, revealing a β-barrel-like fold and broad-spectrum antimicrobial activity. The antibacterial activity is mediated by charge-dependent membrane disruption and, in Gram-positive bacteria, LTA binding. **c.** Chapter 4 explores the antimicrobial potential of PNPs, showing that positively charged PNPs from various plant species, and a PNP acquired by *Bemisia tabaci*, exert antibacterial and antifungal effects. Deletion of Arabidopsis PNPs result in the alteration of phyllosphere bacterial communities.

Chapter 2

An ancient antimicrobial protein co-opted by a fungal plant pathogen for in planta mycobiome manipulation

Nick C. Snelders[a,b,c] , Gabriella C. Petti[a] , Grardy C. M. van den Berg[c] , Michael F. Seidl[b] , and Bart P. H. J. Thomma[a,c]

[a] Cluster of Excellence on Plant Sciences, Institute for Plant Sciences, University of Cologne, Cologne D-50674, Germany;

[b] Theoretical Biology & BioinformaticsGroup, Department of Biology, Utrecht University, Utrecht 3584CH, The Netherlands;

[c] Laboratory of Phytopathology, Wageningen University & Research, Wageningen 6708PB, The Netherlands

DOI: 10.1073/pnas.2110968118

Author contributions:

N.C.S., G.C.P., and B.P.H.J.T. designed research; N.C.S., G.C.P., and G.C.M.v.d.B. performed research; N.C.S., G.C.P., M.F.S., and B.P.H.J.T. analyzed data; and N.C.S. and B.P.H.J.T. wrote the paper.

An ancient antimicrobial protein co-opted by a fungal plant pathogen for in planta mycobiome manipulation

Nick C. Snelders[a,b,c], Gabriella C. Petti[a], Grardy C. M. van den Berg[c], Michael F. Seidl[b], and Bart P. H. J. Thomma[a,c,1]

[a]Cluster of Excellence on Plant Sciences, Institute for Plant Sciences, University of Cologne, Cologne D-50674, Germany; [b]Theoretical Biology & Bioinformatics Group, Department of Biology, Utrecht University, Utrecht 3584CH, The Netherlands; and [c]Laboratory of Phytopathology, Wageningen University & Research, Wageningen 6708PB, The Netherlands

Edited by Steven E. Lindow, University of California, Berkeley, CA, and approved October 29, 2021 (received for review June 14, 2021)

Microbes typically secrete a plethora of molecules to promote niche colonization. Soil-dwelling microbes are well-known producers of antimicrobials that are exploited to outcompete microbial coinhabitants. Also, plant pathogenic microbes secrete a diversity of molecules into their environment for niche establishment. Upon plant colonization, microbial pathogens secrete so-called effector proteins that promote disease development. While such effectors are typically considered to exclusively act through direct host manipulation, we recently reported that the soil-borne, fungal, xylem-colonizing vascular wilt pathogen Verticillium dahliae exploits effector proteins with antibacterial properties to promote host colonization through the manipulation of beneficial host microbiota. Since fungal evolution preceded land plant evolution, we now speculate that a subset of the pathogen effectors involved in host microbiota manipulation evolved from ancient antimicrobial proteins of terrestrial fungal ancestors that served in microbial competition prior to the evolution of plant pathogenicity. Here, we show that V. dahliae has co-opted an ancient antimicrobial protein as effector, named VdAMP3, for mycobiome manipulation in planta. We show that VdAMP3 is specifically expressed to ward off fungal niche competitors during resting structure formation in senescing mesophyll tissues. Our findings indicate that effector-mediated microbiome manipulation by plant pathogenic microbes extends beyond bacteria and also concerns eukaryotic members of the plant microbiome. Finally, we demonstrate that fungal pathogens can exploit plant microbiome-manipulating effectors in a life stage–specific manner and that a subset of these effectors has evolved from ancient antimicrobial proteins of fungal ancestors that likely originally functioned in manipulation of terrestrial biota.

plant pathogenic fungus j microbiome j effector j antimicrobial j mycobiome

Microbes are found in a wide diversity of niches on our planet. To facilitate establishment within microbial communities, microbes secrete a multitude of molecules to manipulate each other. Many of these molecules exert antimicrobial activities and are exploited to directly suppress microbial coinhabitants in order to outcompete them for the limitedly available nutrients and space of a niche. Microbially secreted antimicrobials encompass diverse molecules including peptides and lytic enzymes but also nonproteinaceous molecules such as secondary metabolites. Soils are among the most biologically diverse and microbially competitive environments on earth. Microbial proliferation in the soil environment is generally limited by the availability of organic carbon (1), for which soil microbes continuously compete. Consequently, numerous saprophytic soil-dwelling microbes secrete potent antimicrobials that promote niche protection or colonization. Notably, these microbes are the primary source of our clinically used antibiotics (2, 3).

Like free-living microbes, microbial plant pathogens also secrete a multitude of molecules into their environment to mediate niche colonization (4, 5). The study of molecules secreted by microbial plant pathogens has been largely confined to the context of binary interactions between pathogens and hosts. To establish disease, plant pathogenic microbes secrete a plethora of so-called effectors, molecules of various kinds that promote host colonization and that are typically thought to mainly deregulate host immune responses (4, 6, 7). Upon host colonization, plant pathogens encounter a plethora of plant-associated microbes that collectively form the plant microbiota, which represent a key factor for plant health. Beneficial plant-associated microbes are found in and on all organs of the plant and help to mitigate (a)biotic stresses (8–13). Plants shape their microbiota and specifically attract beneficial microbes to suppress pathogens (14–16). Hence, the plant microbiome can be considered an inherent, exogenous layer that complements the plant's endogenous innate immune system. We previously hypothesized that plant pathogens not only utilize effectors to target components of host immunity as well as other aspects of host physiology to support host colonization but also to target the host microbiota in order to establish niche colonization (4, 5). We recently provided experimental evidence for this

Significance

Microbes secrete a diversity of molecules into their environment to mediate niche colonization. During host ingress, plant pathogenic microbes secrete effector proteins that facilitate disease development, many of which deregulate host immune responses. We recently demonstrated that plant pathogens additionally exploit effectors with antibacterial activities to manipulate beneficial plant microbiota to promote host colonization. Here, we show that the fungal pathogen Verticillium dahliae has co-opted an ancient antimicrobial protein, which likely served in microbial competition in terrestrial environments before land plants existed, as effector for the manipulation of fungal competitors during host colonization. Thus, we demonstrate that pathogen effector repertoires comprise antifungal proteins and speculate that such effectors could be exploited for the development of antimycotics.

Author contributions: N.C.S., G.C.P., and B.P.H.J.T. designed research; N.C.S., G.C.P., and G.C.M.v.d.B. performed research; N.C.S., G.C.P., M.F.S., and B.P.H.J.T. analyzed data; and N.C.S. and B.P.H.J.T. wrote the paper.

The authors declare no competing interest.

This article is a PNASDirect Submission.

[1]To whom correspondence may be addressed. Email: bthomma@uni-koeln.de.

This article contains supporting information online at http://www.pnas.org/lookup/suppl/doi:10.1073/pnas.2110968118/-/DCSupplemental.

Published December 1, 2021.

hypothesis by showing that the ubiquitously expressed effector VdAve1 that is secreted by the soil-borne fungal plant pathogen Verticillium dahliae acts as a bactericidal protein that promotes host colonization through the selective manipulation of host microbiomes by suppressing microbial antagonists (17, 18). Additionally, we demonstrated that VdAve1 and a further antibacterial effector named VdAMP2 are exploited by V. dahliae for microbial competition in soil and promote virulence of V. dahliae in an indirect manner (18). Collectively, these observations demonstrate that V. dahliae dedicates part of its effector catalog toward microbiota manipulation. Likely, the V. dahliae genome encodesfurther effectors that act in microbiome manipulation.

Evidently, bacterial and fungal evolution on land preceded land plant evolution. As a consequence,fungal pathogen effectors involved in the manipulation of (host-associated)microbial communities may have evolved from ancestors that served in microbial competition in terrestrial niches hundreds of millions of years ago prior to land plant evolution. However, evidence for this hypothesis is presently lacking.

V. dahliae is an asexual xylem-dwelling fungus that causesvascular wilt diseaseon hundreds of plant species(19). The fungus survivesin the soil in the form of multicellular melanized resting structures, called microsclerotia, that offer protection against (a)biotic stressesand can persist in the soil for many years (20). Microsclerotia represent the major inoculum source of V. dahliae in nature, and their germination is triggered by carbon- and nitrogen-rich exudates from plant roots (21). Following microsclerotia germination, fungal hyphae grow through the soil and rhizosphere toward the roots of host plants. Next, V. dahliae colonizes the root cortex and crossesthe endodermis, from which it invades xylem vessels. Once the fungus enters those vessels, it forms conidiospores that are transported with the water flow until they get trapped, for instance, by vesselend walls. This triggers germination of the conidiospores followed by penetration of cell walls, hyphal growth, and renewed sporulation, leading to systematic colonization of the plant (22). Once tissue necrosis commences and plant senescence occurs, host immune responses fade and V. dahliae enters a saprophytic phase in which it emerges from the xylem vesselsto invade adjacent host tissues, which is accompanied by the production of microsclerotia. Upon littering and decomposition of plant tissues, these microsclerotia are releasedinto the soil (23).

Results

To identify effectors potentially acting in microbiome manipulation, we recently queried the V. dahliae secretome for structural homologs of known antimicrobial proteins (AMPs), which led to the identification of 10 candidatesincluding the functionally characterized VdAMP2 (18). Among the remaining nine candidates, we now identified a small cysteine-rich protein of ~4.9 kDa, which we name VdAMP3 (Ensembl: VDAG_JR2_Chr3g05620a). As a first step in the characterization of VdAMP3, we assesseditspredicted structure. Interestingly, VdAMP3 is predicted to adopt a cysteine-stabilizedαβ(CSαβ)fold that isalso foundindefensin-likeproteins (Fig. 1A) (24–26).CSαβdefensins represent a widespread and well-characterized family of antimicrobial proteins that are presumed to share a single ancient origin in the last common ancestor of animals, plants, and fungi that produce these proteins today (24–27). It is important to note, however, that many typical small cysteine-rich pathogen effectors adopt AMP-like confirmations and that tertiary structures of several AMP families strongly resemble each other (27, 28). Hence, structure prediction can easily lead to false-positive classifications as AMP or allocation to the wrong AMP family.

CSαβdefensins, or so-called cis-defensins, owe their structure to highly conserved cis-orientated disulfide bonds that establish an interaction between a double- or triple-stranded antiparallel β-sheetwith an α-helix (25, 27). To validate the prediction of VdAMP3 as a member of this ancient antimicrobial protein family, we aligned its amino acid sequence with the antibacterial CSαβdefensins plectasin and eurocin, from the saprophytic Ascomycete species Pseudoplectania nigrella and Eurotium amstelodami (formerly Aspergillus amstelodami), respectively (29–31). Although the biological relevance of these defensins for the respective fungi remains unclear, their antibacterial activity and protein structure have been well characterized, which led to their recognition as genuine CSαβdefensins (29–31). Although the overall identity between the three proteins was rather low (25 to 40%), protein sequence alignment revealed that VdAMP3 contains the six highly conserved cysteine residues that are considered crucial for the structure of CSαβdefensins (Fig. 1B) (27). To further substantiate the emerging picture that VdAMP3 belongs to this particular protein family and that the detected similarities with plectasin and eurocin are not the result of convergent protein evolution, we

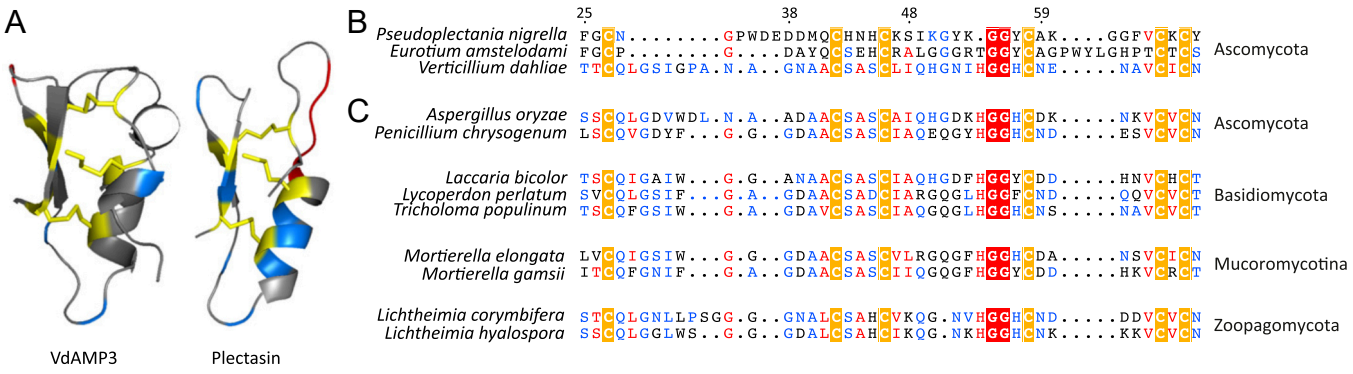

Fig. 1. The V. dahliae effector VdAMP3 evolved from an ancient fungal protein. (A) VdAMP3 (Left) is predicted to adopt a CSαβdefensin-like fold. The structure of the CSαβdefensin plectasin (Right) of the fungus P. nigrella is included as reference. The disulfide bonds stabilizing the antiparallel β-sheets and the α-helix are highlighted in yellow. Positively and negatively charged amino acid residuesare highlighted in blue and red, respectively. (B) Protein sequence alignment with CSαβdefensinsplectasin and eurocin (E. amstelodami) supports the structure prediction of VdAMP3. (C) VdAMP3 homologs are widespread in the fungal kingdom. Protein sequencealignment of VdAMP3 with a subset of its homologs identified in higher (Ascomycotaand Basidiomycota) and lower fungi (Mucoromycotina and Zoopagomycota). The alignment as shown in B and C displays the most conserved region of the CSαβ defensin protein family and was performed using HMMER and visualized with Espript3. The highly conserved cysteine and glycine residues that contribute to the CSαβdefensinstructure are highlighted by yellow and red backgrounds, respectively. The numbers on top of the alignment indicate the corresponding residue numbers of VdAMP3. The homologs displayed in C were identified using blastP in the predicted proteomes of the respective fungi included in the JGI1000 Fungal Genomes Project (32).

queried the predicted proteomes of the fungi from the Joint Genome Institute (JGI) 1000 Fungal Genomes Project (32) for homologs of VdAMP3 with higher sequence identity and included a subset of those in the protein alignment (Fig. 1C). Interestingly, besides homologs in Ascomycota and Basidiomycota, our sequence similarity search also revealed homologs in early-diverging fungi from the subphyla Mucoromycotina and Zoopagomycota [both formerly classified as Zygomycota (33)] (Fig. 1C). Importantly, this divergence is estimated to have taken place ~900 million years ago (34), indicating it preceded the evolution of the first land plants ~450 million years later (34–37). Consequently, this analysis indicates that VdAMP3 evolved from an ancestral fungal gene hundreds of millions of years ago before land plants existed.

As a first step to determine a potential role of VdAMP3 in V. dahliae infection biology, we assessedwhether we could find evidence for VdAMP3 expression during host colonization. Analysis of previously generated transcriptome datasets of diverse V. dahliae strains during colonization of a diversity of hosts did not reveal in planta expression of VdAMP3 (17, 38–40). However, strong induction of this effector gene was reported during microsclerotia formation in a transcriptome analysis of V. dahliae strain XS11 grown in vitro (24). To validate this finding, we analyzed in vitro expression of VdAMP3 in V. dahliae strain JR2. To this end, V. dahliae conidiospores were spread on nitrocellulose membranes placed on top of solid minimal medium and fungal material was harvested prior to microsclerotia formation after 48 h of incubation and after the onset of microsclerotia formation after 96 h of incubation. Expression of VdAMP3 was determined at both time points with real-time PCR alongside expression of the Chr6g02430 gene that encodes a putative cytochrome P450 enzyme that acts as a marker for microsclerotia formation (24, 41). Consistent with the observations for V. dahliae strain XS11 (24), no VdAMP3 expression was detected at 48 h, when Chr6g02430 was also not expressed and no visual microsclerotia formation could be observed on the growth medium (Fig. 2A). However, induction of VdAMP3, as well as Chr6g02430, was observed after 96 h of incubation, at which time point the formation of microsclerotia on the growth medium also became apparent (Fig. 2A). Collectively, these data demonstrate that expression of VdAMP3 coincides with microsclerotia formation in vitro also for V. dahliae strain JR2.

Although previous transcriptome analysesfailed to detect in planta expression of VdAMP3, we realized that these analyses were predominantly performed for infection stages when the fungus was still confined to the xylem vesselsand microsclerotia formation had not yet been initiated. Accordingly, in planta expression of VdAMP3 may have been missed. Thus, we inoculated Nicotiana benthamiana with V. dahliae and determined expression of VdAMP3 in leaves and petioles sampled at different time points and displaying different disease phenotypes, ranging from asymptomatic at 7 d postinoculation (dpi) to complete necrosis at 22 dpi. As expected, a strong induction of the previously characterized VdAve1 effector gene was detected at 7 and 14 dpi (Fig. 2B) (17, 18). In contrast, however, no expression of VdAMP3 was recorded, even at the latest time point, when the leaf tissue had become completely necrotic (Fig. 2B). Importantly, no Chr6g02430 expression was detected at any of these time points either (Fig. 2B), suggesting that microsclerotia formation had not yet started in these tissues. Indeed, visual inspection of the necrotic plant tissue collected at 22 dpi did not reveal microsclerotia presence. To induce microsclerotia formation, V. dahliae–inoculated N. benthamiana plants harvested at 22 dpi were sealed in plastic bags and incubated in the dark to increase the relative humidity and mimic conditions that occur during tissue decomposition in the soil. Interestingly, after 8 d of incubation, the first microsclerotia could be observed and induction of VdAMP3, as well as Chr6g02430, was detected (Fig. 2C). Notably, the induction of both genes in planta is markedly weaker when compared with their expression in vitro (Fig. 2A). However, this is likely explained by a much smaller proportion of the total population of V. dahliae cells undergoing synchronized development into microsclerotia, also because the time window from conidial germination through hyphal growth to microsclerotia formation is much smaller in vitro than in planta. Collectively, our findings suggest that in planta expression of VdAMP3 coincides with microsclerotia formation, similar to our observations in vitro. Moreover, our data suggestthat VdAMP3 expression primarily depends on a developmental stage of V. dahliae rather than on host factors such as tissue necrosis.

To determine more precisely where VdAMP3 is expressed and to improve our understanding of how V. dahliae may benefit from effector expressionduring microsclerotia formation, we generated a V. dahliae reporter strain expressing eGFP under control of the VdAMP3 promoter. Intriguingly, microscopic analysis of the reporter strain during microsclerotia formation stages in vitro (Fig. 2D) revealed that VdAMP3 is expressed by swollen hyphal cells that act as primordia that subsequently develop into microsclerotia but not by the adjacent hyphal cells or recently developed microsclerotia cells (Fig. 2 E–G). This highly specific expression of VdAMP3 suggeststhat the effector protein may facilitate the formation of microsclerotia in decaying host tissue. Given its presumed antimicrobial activity, VdAMP3 may be involved in antagonistic activity against opportunistic decay organisms in this microbially competitive niche.

To determine if VdAMP3 indeed exerts antimicrobial activity, we tried to produce VdAMP3 heterologously in the yeast Pichia pastoris and in the bacterium Escherichia coli, but these attempts failed, indicative of potential antimicrobial activity of the effector protein. Therefore, chemical synthesisof VdAMP3 was pursued. Next, we incubated a randomly selected panel of bacterial isolates with the effector protein and monitored their growth in vitro. VdAMP3 concentrations as high as 20 μM resulted in no or only marginal bacterial growth inhibition (SI Appendix, Fig. 1). A similar assay with fungal isolates showed that incubation with 5 μM VdAMP3 already markedly affected growth of the filamentous fungi Alternaria brassicicola and Cladosporium cucumerinum and the yeasts P. pastoris and Saccharomycescerevisiae(Fig. 3 A and B). This finding suggests that VdAMP3 displays more potent activity against fungi than against bacteria. Importantly, a thorough heat treatment involving boiling of VdAMP3 abolished its antifungal activity (SI Appendix, Fig. 2), indicating that the specificity of this activity depends on its correct three-dimensional confirmation.

Considering its antifungal activity, but also the highly controlled timely and topical expression of VdAMP3, we tested if exogenous VdAMP3 application negatively impacts hyphal growth of V. dahliae. Interestingly, incubation of V. dahliae with 5 μM VdAMP3 markedly affected its growth (SI Appendix, Fig. 3 A and B). However, it needs to be realized that this effector protein is produced by the time when most hyphae of the fungus have lost their function, as the host tissue has become senescent and will soon decompose, and the fungus produces microsclerotia for long-term survival. Next, to verify if growth or development of V. dahliae is affected by VdAMP3, we generated a VdAMP3 deletion mutant (SI Appendix, Fig. 4), which we cultivated in vitro alongside wild-type (WT) V. dahliae. As anticipated, deletion of VdAMP3 did not accelerate growth of the fungus (SI Appendix, Fig. 3C), confirming that the effector gene does not compromise the development of the fungus during the life stagesprior to microsclerotia formation. Moreover, deletion of VdAMP3 also did not impair the ability of V. dahliae to form resting structures, nor their ability to infect new plants and cause disease (SI Appendix, Fig. 3 C–E). Next, we aimed to

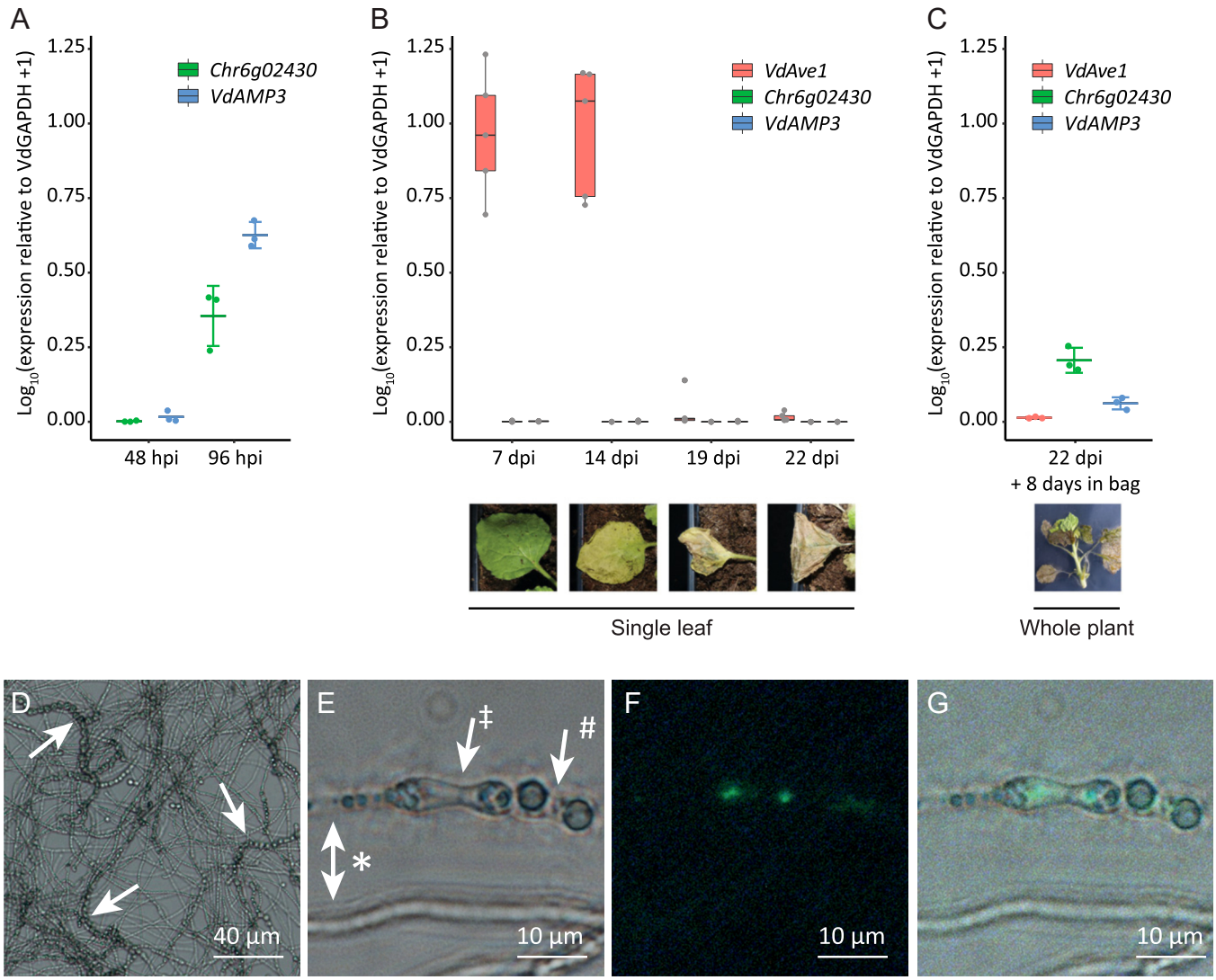

Fig. 2. VdAMP3 is specifically expressed in hyphal cells that develop into microsclerotia. (A) Expression of VdAMP3 and the marker gene for microsclerotia development Chr6g02430, relative to the household gene VdGAPDH at 48 and 96 h of in vitro cultivation (n = 3). (B) Expression of VdAve1, VdAMP3, and Chr6g02430 in N. benthamiana leaves from 7 to 22 dpi (n = 5). (C) Expression of VdAve1, VdAMP3, and Chr6g02430 in tissue of N. benthamiana plants harvested at 22 dpi after 8 d of incubation in sealed plastic bags (n = 3). (D) Microsclerotia formation of a pVdAMP3::eGFP reporter mutant as detected after 7 d of cultivation in Czapek Dox medium. Typical chains of microsclerotia (42, 43) are indicated by arrows. (E) Bright-field image of various V. dahliae cell types after 7 d of cultivation in Czapek Dox, including hyphae (*), swollen hyphal cells developing into microsclerotia (‡), and mature microsclerotia cells (#). (F) GFP signal for the image as shown in E, indicative for activity of the VdAMP3 promoter, is exclusively detected in the swollen hyphal cells developing into microsclerotia. (G) Overlay of E and F.

determine if the antifungal activity of VdAMP3 contributes to Verticillium wilt disease development. To this end, N. benthamiana plants were inoculated with V. dahliae WT as well as with VdAMP3 complementation and deletion mutants (SI Appendix, Fig. 4). In line with our inability to detect expression during early infection stages, disease phenotypes and V. dahliae biomass quantification using real-time PCR did not reveal a contribution of VdAMP3 to host colonization up to 2 wk after inoculation (Fig. 3 C and D). Considering the cell type–specific expression of VdAMP3 in developing microsclerotia, we speculated that the effector protein contributes to V. dahliae niche establishment during host plant senescence when the fungus has emerged from the xylem and has colonized the mesophyll. To test this hypothesis, we performed additional disease assays using V. dahliae WT and the VdAMP3 deletion mutant and sealed the N. benthamiana plants in plastic bags after harvesting to stimulate the onset of tissue decomposition and microsclerotia formation. Intriguingly, when we visually inspected the plants after 4 wk of incubation, we detected dispersed patches of dark mycelium, typical for V. dahliae microsclerotia, on the surface of plants colonized by V. dahliae WT (SI Appendix, Fig. 5). Strikingly, we did not identify such patches on plants colonized by the VdAMP3 deletion mutant, suggesting that V. dahliae depends on the antifungal activity of VdAMP3 to form microsclerotia in decaying host phyllospheres. It needs to be noted that an experimental setup that depends on a largely unpredictable occurrence of visibly detectable patches of microsclerotia on the surface of decaying plant parts that are colonized by diverse assemblages of opportunistic microbes that seize their opportunity to prosper while plant defenses fade is hardly feasible for standardized, robust quantification of microsclerotia formation. Also, this setup does not permit assessment of microsclerotia formation deeper in the decaying tissues. Instead, we quantified V. dahliae biomass using real-time PCR. As anticipated, we detected a

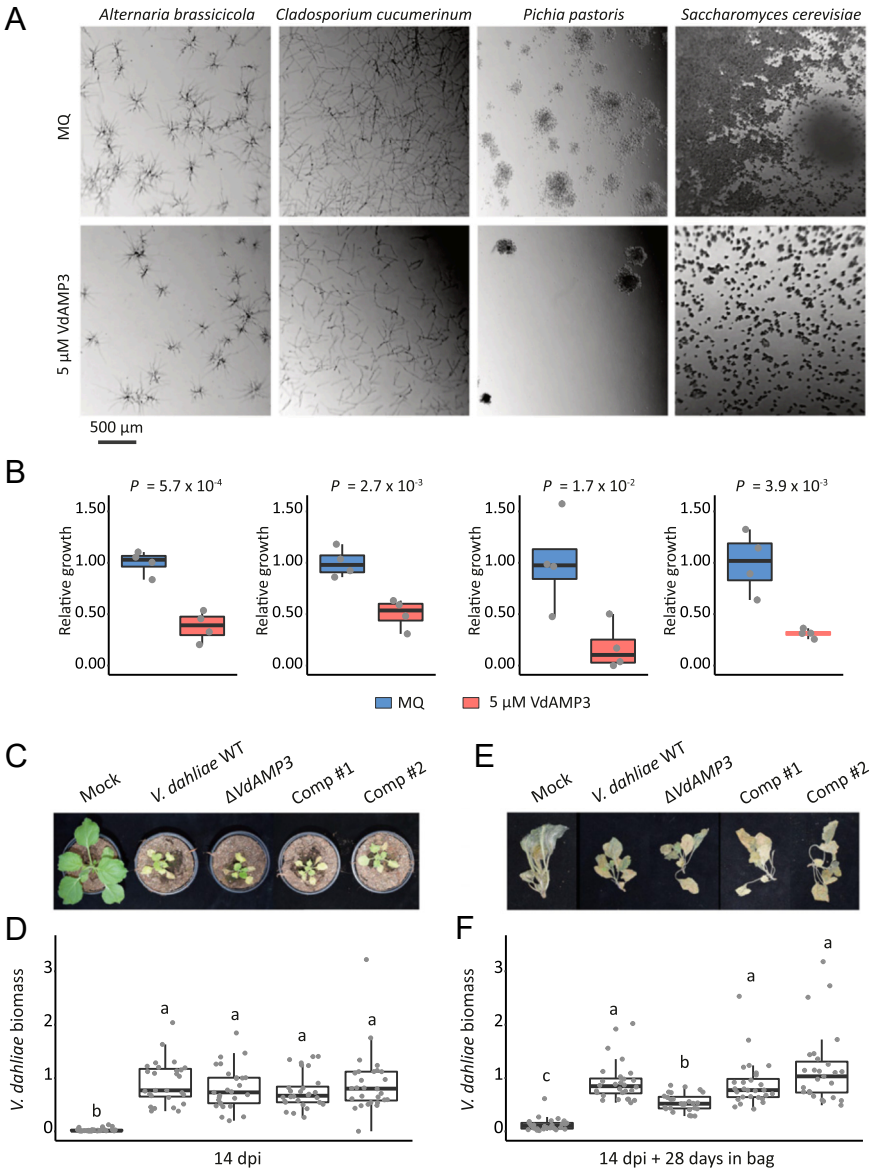

Fig. 3. VdAMP3 is an antifungal protein that contributes to V. dahliae biomass accumulation in the decaying host phyllosphere. (A) Microscopic pictures of fungal isolates grown in 5% PDB supplemented with 5 µM VdAMP3 or ultrapure water (Milli-Q). VdAMP3 impairs growth of A. brassicicola, C. cucumerinum, P. pastoris, and S. cerevisiae. Pictures were taken after 24 (A. brassicicola, C. cucumerinum, and S. cerevisiae) or 64 (P. pastoris) h of incubation. (B) Fungal growth as displayed in A was quantified using ImageJ (unpaired two-sided Student's t test; n = 4). (C) VdAMP3 does not contribute to establishment of Verticillium wilt disease in N. benthamiana. Photos display representative phenotypes of N. benthamiana plants infected by wild-type V. dahliae (WT), the VdAMP3 deletion (ΔVdAMP3), and two complementation (Comp) mutants 14 dpi. (D) Relative V. dahliae biomass in aboveground N. benthamiana tissues determined with real-time PCR. Different letter labels represent significant differences (one-way ANOVA and Tukey's post hoc test; $P < 0.05$; n ≥27). (E) Representative phenotypes of N. benthamiana plants as shown in C after 28 d of incubation in plastic bags. (F) Relative V. dahliae biomass in N. benthamiana tissues as displayed in E. Letters represent significant differences (one-way ANOVA and Tukey's post hoc test; $P < 0.05$; n ≥27).

significant reduction in biomass of the VdAMP3 deletion mutant when compared with V. dahliae WT and the complementation mutants (Fig. 3 E and F), confirming that VdAMP3 indeed is essential during microsclerotia formation in planta presumably by acting in self-protection against other microbes.

To investigate if the effects of VdAMP3 are limited to N. benthamiana or whether those also extend to other hosts, we inoculated Arabidopsis thaliana plants with V. dahliae WT and the VdAMP3 deletion mutant. Consistent with our observations for N. benthamiana, deletion of VdAMP3 did not affect establishment of Verticillium wilt in A. thaliana (SI Appendix, Fig. 6 A and B). However, V. dahliae biomass quantification in aboveground A. thaliana tissues at 3 wk postinoculation revealed reduced accumulation of V. dahliae in the absence of VdAMP3 (SI Appendix, Fig. 6C). Thus, the effects of VdAMP3 are not restricted to a single host.

As in vitro antimicrobial activity assays pointed toward fungi as the primary targets of VdAMP3, we speculated that V. dahliae exploits VdAMP3 to suppress fungal competitors in decomposing host tissues to safeguard the formation of its resisting structures. To characterize the microbiota associated with N. benthamiana decomposition and to determine the impact of VdAMP3 on these microbial communities, we characterized the phyllosphere microbiota of fresh mock-inoculated N. benthamiana plants, and decaying plants diseased by V. dahliae WT or the VdAMP3 deletion mutant incubated in plastic

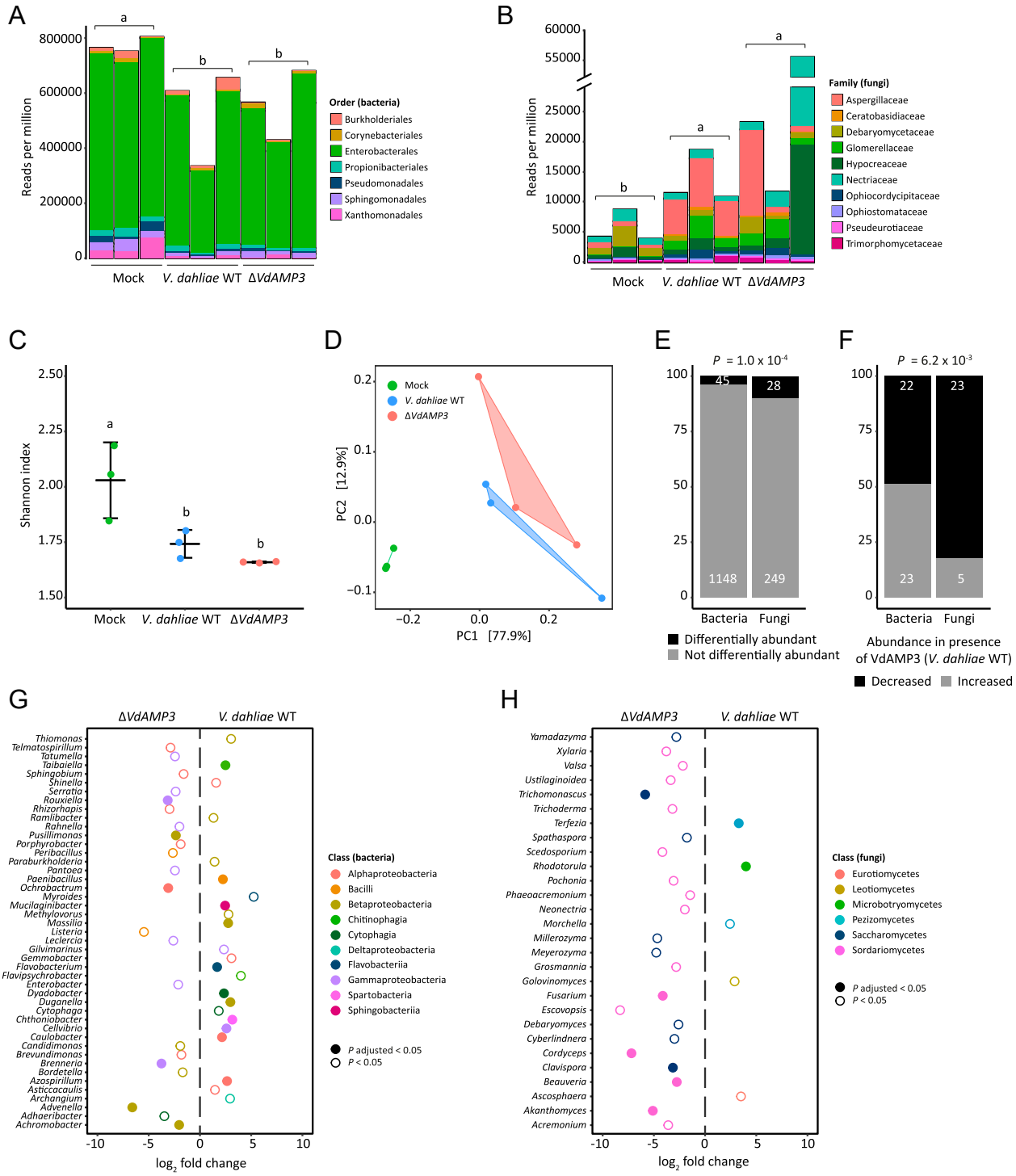

Fig. 4. VdAMP3 manipulates the mycobiome of the decaying N. benthamiana phyllosphere. (A and B) V. dahliae–induced decay of the N. benthamiana phyllosphere is associated with a decreased bacterial and increased fungal abundance. Relative abundance of bacteria (A) and fungi (B), excluding V. dahliae, in the phyllosphere of decaying N. benthamiana plants colonized by WT V. dahliae (WT) or the VdAMP3 deletion mutant (14 dpi and after 28 d of incubation in plastic bags) and in the phyllosphere of fresh N. benthamiana plants (mock). Letters represent significant differences in total bacterial/fungal abundance between the three treatments (one-way ANOVA and Tukey's post hoc test; $P < 0.05$; $n = 3$). (C) V. dahliae–induced decay of N. benthamiana plants impacts alpha diversity of the phyllosphere. The plot displays the average Shannon index ± SD; letters represent significant differences (one-way ANOVA and Tukey's post hoc test; $P < 0.05$; $n = 3$). (D) PCoA based on Bray–Curtis dissimilarities (beta diversity) reveals separation of the microbiomes based on the three different treatments. (E) Differential abundance analysis of microbial genera between the microbiomes colonized by V. dahliae WT and the VdAMP3 deletion mutant indicates that secretion of VdAMP3 significantly impacts a larger proportion of the fungi than of the bacteria (two-tailed Fisher's exact test). (F) Of the differentially abundant microbial genera, significantly more fungi display a decreased abundance in the presence of VdAMP3 when compared with the bacteria (two-tailed Fisher's exact test). (G and H) Overview of the differentially abundant bacterial (G) and fungal (H) genera. The plots display increased (positive $\log_2$ fold change) or decreased (negative $\log_2$ fold change) abundance in the presence of V. dahliae WT when compared with the VdAMP3 deletion mutant (Wald test, P adjusted < 0.05 and $P < 0.05$, $n = 3$). Differentially abundant fungal genera from the Saccharomycetes or Sordariomycetes are consistently suppressed in the presence of VdAMP3 (i.e., by V. dahliae WT).

bags, through shotgun metagenomic sequencing. Consistent with a primary role for fungi in the decomposition of dead plant material (44–48), we detected a significant increase of fungi and decrease of bacteria in the phyllosphere of the N. benthamiana plants diseased by the V. dahliae strains when compared with healthy mock-treated plants (Fig. 4 A and B). These changesare accompanied by a reduced alpha diversity in the decaying phyllospheres (Fig. 4C). Additionally, principal coordinate analysis (PCoA) based on Bray–Curtis dissimilarities (beta diversity) uncovered clear separation of the microbiota of the healthy plants from those in decay (Fig. 4D). The PCoA also revealed a weaker, yet potentially relevant, separation of the microbiota colonized by V. dahliae WT and the VdAMP3 deletion mutant, which suggests that secretion of VdAMP3 manipulates microbiome compositions (Fig. 4D). Intriguingly, when we compared the abundances of the identified microbial genera between the microbiomes colonized by V. dahliae WT and the VdAMP3 deletion mutant, we detected significantly more differentially abundant fungi (10.1%) than bacteria (3.8%) (Fig. 4E)(SI Appendix, Tables 1 and 2). Interestingly, whereas the number of bacterial genera that display an increased or a decreased abundance in the presence of VdAMP3 is more or less equal, the vast majority of the differentially abundant fungal genera (82.1%) are repressed in the presence of VdAMP3 (Fig. 4F). Moreover, while no consistent suppression of bacterial genera from the same class could be detected, we exclusively identified suppression of the differentially abundant fungal genera from the Saccharomycetesor Sordariomycetes in the presence of VdAMP3 (Fig. 4 G and H). Thus, these observations indicate that V. dahliae VdAMP3 mainly acts as an antifungal effector protein that displays selective activity that predominantly impacts the mycobiome in the decaying host phyllosphere.

To further substantiate that the suppression of the Saccharomycetes and Sordariomycetes is a direct consequence of the VdAMP3 activity, we incubated fungal speciesbelonging to the suppressedgenera with the effector to determine their sensitivity. In line with the previously observed sensitivity of the Saccharomycetes P. pastoris and S. cerevisiae, the Saccharomycete species Cyberlindnera jadinii, Debaryomycesvanrijiae, Rhodotorula bogoriensis, and Meyerozyma amylolytica also displayed markedly reduced growth in the presence of VdAMP3 (Fig. 5 A and B). Similarly, growth of the Sordariomycetes Cordyceps militaris and Trichoderma viride was inhibited by the effector (Fig. 5 A and B). Hence, these findings support the observed suppression of the Saccharomycetes and Sordariomycetes in the N. benthamiana phyllosphere mycobiome as a direct consequence of VdAMP3 activity.

The cell type–specific expression of VdAMP3, combined with its role in mycobiome manipulation, strongly suggeststhat VdAMP3 is exploited to ward off fungal niche competitors in planta to safeguard the formation of V. dahliae microsclerotia. To test if VdAMP3 indeed is essential for V. dahliae microsclerotia formation in the presence of other fungi, we cocultivated V. dahliae WT and the VdAMP3 deletion and complementation mutants with D. vanrijiae and M. amylolytica. Once microsclerotia formation by V. dahliae WT became apparent (Fig. 6A), we quantified the number of resting structures that were formed by the different V. dahliae genotypes. As anticipated, we detected a significant reduction of microsclerotia formed by the VdAMP3 deletion mutant when compared with V. dahliae WT and the complementation mutants in the presence of both fungal species, confirming that V. dahliae relies on the antifungal activity of VdAMP3 to form microsclerotia in the presence of particular fungal niche competitors (Fig. 6 B and C). Additionally, to confirm that this activity is not only relevant in the presence of a single microbial interactor but also facilitates microsclerotia formation in the presence of fungal communities,

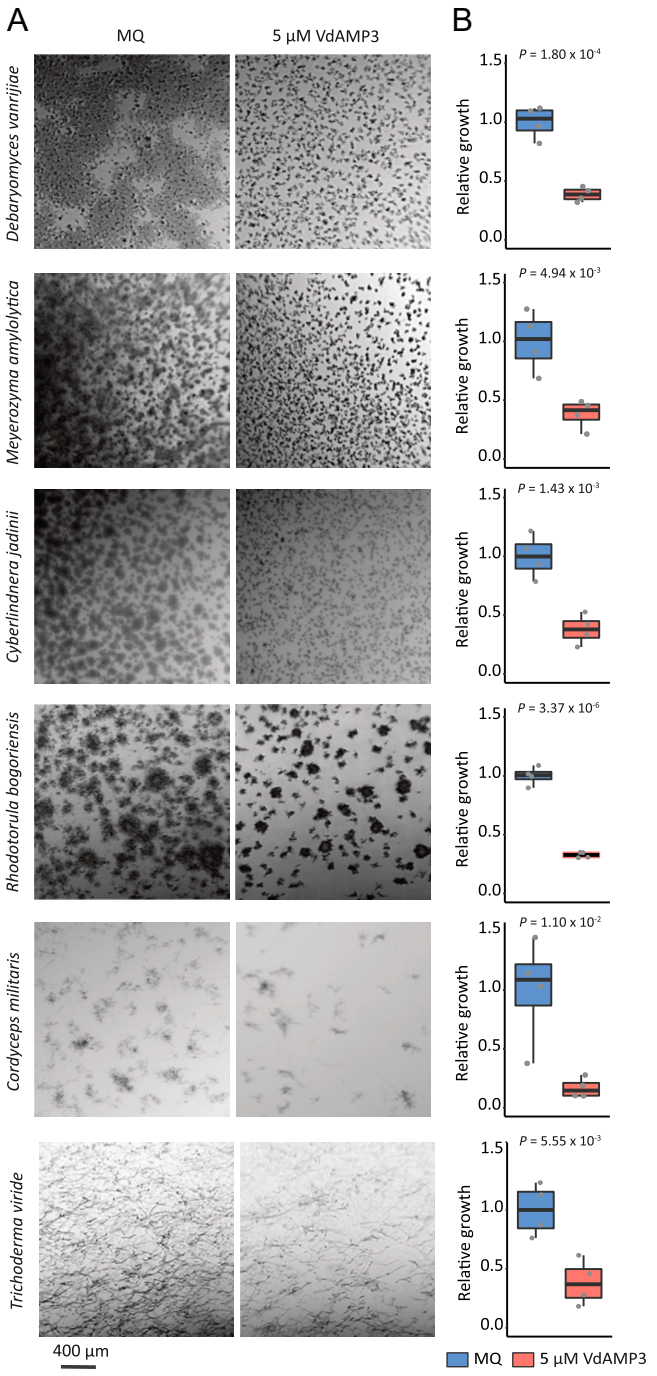

Fig. 5. VdAMP3 negatively affects Saccharomycetesand Sordariomycetes. (A) Microscopic pictures of fungal isolates grown in 5% PDBsupplemented with 5 µM VdAMP3 or ultrapure water (Milli-Q). VdAMP3 impairs growth of D. vanrijae, M. amylolytica, C. jadinii, R. bogoriensis, C. militaris, and T. viride. Pictures were taken after 10 (D. vanrijae and C. jadinii), 24 (M. amylolytica and R. bogoriensis), or 30 (C. militaris and T. viride)hof cultivation. (B) Fungal growth as displayed in A was quantified using ImageJ (unpaired two-sided Student's t test; n = 4).

we performed similar experiments using two synthetic communities that, besides D. vanrijiae and M. amylolytica, also comprised the filamentous fungus C. militaris or the yeastC. jadinii plus the filamentous mycoparasite T. viride. Also in these experiments, we detected a significant reduction of microsclerotia formed by the VdAMP3 deletion mutant when compared with V. dahliae WT and the complementation mutants (Fig. 6 B and C). Collectively,

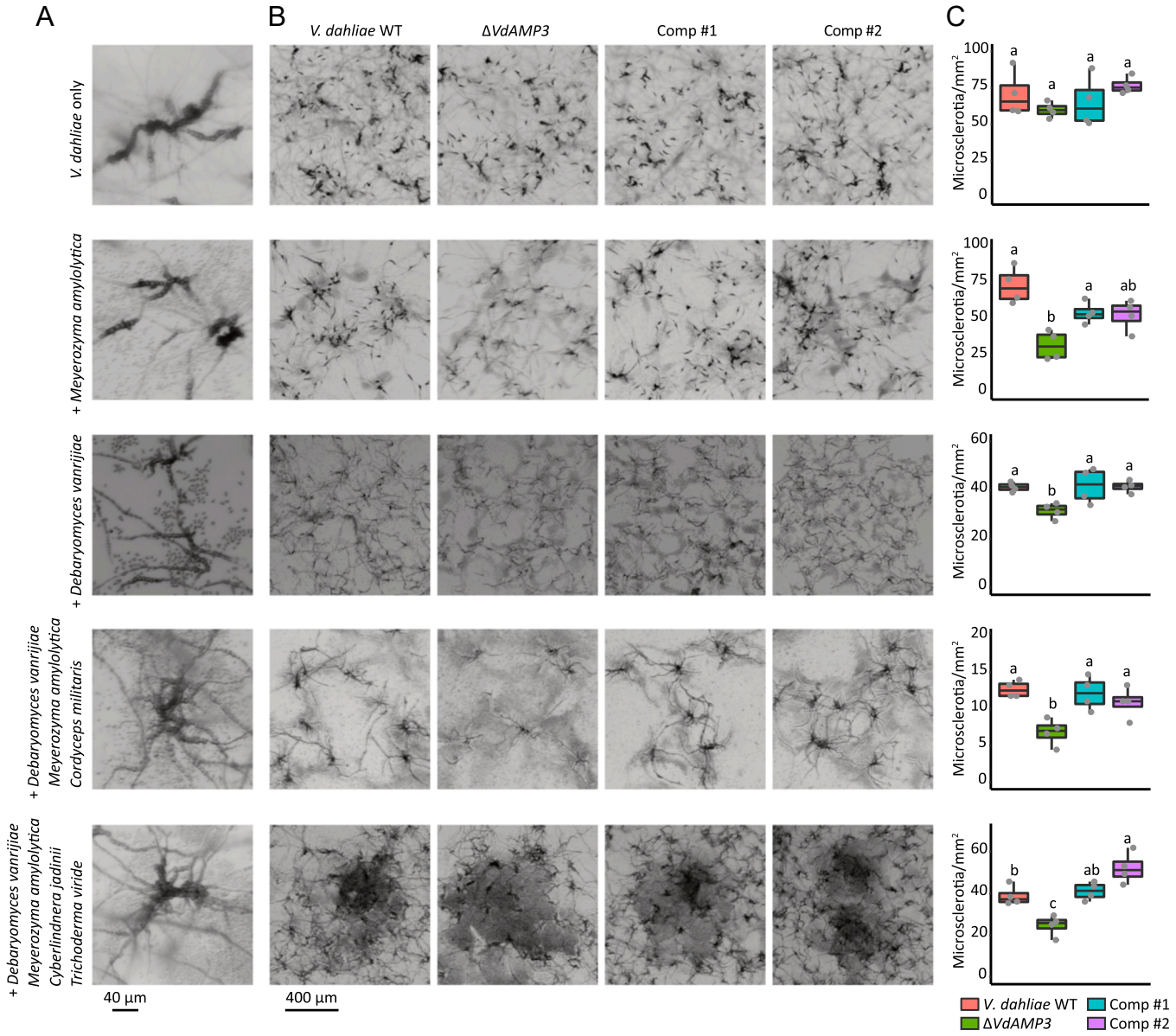

Fig. 6. VdAMP3 contributes to V. dahliae microsclerotia formation in the presence of fungal niche competitors. (A) Close-up of V. dahliae microsclerotia formed during cultivation in the presence of D. vanrijae (6 dpi), M. amylolytica (6 dpi), a syncom comprising D. vanrijae, M. amylolytica, and C. militaris (6 dpi), or a syncom comprising D. vanrijae, M. amylolytica, C. jadinii, and T. viride (9 dpi). (B) VdAMP3 contributes to V. dahliae microsclerotia formation in the presence of other fungal species. Representative microscopic pictures displaying V. dahliae WT, the VdAMP3 deletion mutant (ΔVdAMP3), and two complementation mutants (Comp) cultivated in the presence of the fungal species/communities as detailed in A. (C) Number of microsclerotia formed by V. dahliae in the presence of the fungal species or communities (one-way ANOVA and Tukey's post hoc test; $P < 0.05$; $n = 4$).

these findings underpin the idea that V. dahliae exploits the antifungal activity of VdAMP3 to safeguard the formation of its resting structures by warding off fungal niche competitors in senescing host mesophyll tissues.

Discussion

Microbes secrete a plethora of molecules to promote niche colonization (4). Free-living microbes are well-known producers of antimicrobials that are secreted to outcompete microbial coinhabitants to establish themselves in a microbial community. Microbial plant pathogens secrete a diversity of so-called effector molecules during host ingress, many of which are small cysteine-rich proteins that deregulate host immune responses to promote colonization (4, 6, 7). While investigating the vascular wilt fungus V. dahliae, we recently demonstrated that plant pathogens not only exploit effector proteins to promote disease establishment through direct host manipulation but also through the manipulation of plant microbiota by means of antibacterial activities (18). Considering that the advent of fungi on earth preceded land plant evolution, we speculated that a subset of the pathogen effectors involved in host microbiota manipulation may have evolved from antimicrobial proteins that originally functioned in microbial competition in terrestrial niches before the first land plants appeared and plant pathogenicity evolved. Here, we demonstrated that the soilborne fungal plant pathogen V. dahliae has co-opted an ancient antimicrobial protein as effector for mycobiome manipulation in planta to safeguard the formation of its resting structures. Thus, our findings indicate that plant pathogenicity in fungi is

not exclusively associated with the evolution of novel effectors that manipulate plants or their associated microbial communities but also with the co-option of previously evolved secreted proteins that initially served alternative lifestyles, such as saprotrophism, as effectors to promote host colonization. Moreover, our findings indicate that effector-mediated manipulation of plant microbiota by microbial plant pathogens is not confined to bacterial targets but extends to eukaryotic microbes.

Functional characterization of VdAMP3 unveiled that the effector evolved to play a life stage–specific role in microbiome manipulation during microsclerotia formation by V. dahliae. Recently, we described the characterization of the first microbiome-manipulating effectors secreted by V. dahliae, VdAve1 and VdAMP2 (18). VdAve1 is a ubiquitously expressed bactericidal effector that promotes V. dahliae host colonization through the selective manipulation of host microbiota in the roots as well as in the xylem by suppressing microbial antagonists. Moreover, VdAve1 is also expressed in the soil biome, where it similarly contributes to niche colonization. Intriguingly, VdAMP2 is exclusively expressed in soil and, like VdAve1, exerts antibacterial activity that contributes to niche establishment. Interestingly, VdAMP2 and VdAve1 display divergent activity spectra and, therefore, likely complement each other for optimal soil colonization. In decaying host tissue, neither VdAve1 nor VdAMP2 are expressed, yet VdAMP3 expression occurs. Collectively, our findings for VdAve1, VdAMP2, and VdAMP3 demonstrate that V. dahliae dedicates a substantial part of its catalog of effector proteins toward microbiome manipulation and that each of these effectors act in a life stage–specific manner.

The life stage–specific exploitation of the in planta secreted antimicrobial effectors VdAve1 and VdAMP3 is well reflected by their antimicrobial activities and by the microbiota of the niches in which they act. Contrary to previous V. dahliae transcriptome analyses that repeatedly identified VdAve1 as one of the most highly expressed effector genes in planta (17, 38–40), we detected a repression of the effector gene in decomposing N. benthamiana tissues (Fig. 1 B and C). Characterization of the antimicrobial activity exerted by VdAve1 previously uncovered that the protein exclusively affects bacteria and does not impact fungi (18). Thanks to their ability to produce a wide diversity of hydrolytic enzymes, fungi are the primary decomposers of plant debris on earth (44). The phyllosphere of plants comprises a diversity of fungi (49–51). Importantly, upon plant senescence, these fungi are provided the first access to decaying material on which they can act opportunistically once host immune responses have faded. Accordingly, we detected an increased abundance of fungi in the phyllosphere of the decomposing N. benthamiana plants diseased by V. dahliae when compared with healthy plants (Fig. 4B). The observed repression of VdAve1 and the subsequent induction of VdAMP3 in a niche in which V. dahliae encounters more fungal competition underscores the notion that V. dahliae tailors the expression of its microbiome-manipulating effectors according to the various microbiota that it encounters during the different life stages. Along these lines, it is tempting to speculate that during saprotrophism in soil, V. dahliae exploits antimicrobial effector proteins to ward off other eukaryotic competitors including soil-dwelling parasites such as fungivorous nematodes or protists. However, evidence for this hypothesis is presently lacking.

Antimicrobial resistance in bacteria and fungi is posing an increasing threat to human health. Possibly, microbiome-manipulating effectors represent a valuable source for the identification and development of novel antimicrobials that can be deployed to treat microbial infections. Arguably, our findings that microbiome-manipulating effectors secreted by plant pathogens also comprise antifungal proteins open up opportunities for the identification and development of antimycotics. Most fungal pathogens of mammals are saprophytes that generally thrive in soil or decaying organic matter but can opportunistically cause disease in immunocompromised patients (52–54). Azoles are an important class of antifungal agents that are used to treat fungal infections in humans. Unfortunately, agricultural practices involving massive spraying of azoles to control fungal plant pathogens, but also the extensive use of azoles in personal care products, ultraviolet stabilizers, and anticorrosives in aircrafts, for instance, gives rise to an enhanced evolution of azole resistance in opportunistic pathogens of mammals in the environment (52, 55). For instance, azole resistant Aspergillus fumigatus strains are ubiquitous in agricultural soils and in decomposing crop waste material, where they thrive as saprophytes (56, 57). Thus, fungal pathogens of mammals, like A. fumigatus, comprise niche competitors of fungal plant pathogens. Hence, we speculate that, like V. dahliae, other plant pathogenic fungi may also carry potent antifungal proteins in their effector catalogs that aid in niche competition with these fungi. Possibly, the identification of such effectors could contribute to the development of novel antimycotics.

Materials and Methods

Gene Expression Analyses. In vitro cultivation of V. dahliae strain JR2 for analysis of VdAMP3 and Chr6g02430 expression was performed as described previously (24). Additionally, for in planta expression analyses, total RNA was isolated from individual leaves or complete N. benthamiana plants harvested at different time points after V. dahliae root dip inoculation. To induce microsclerotia formation, N. benthamiana plants were harvested at 22 dpi and incubated in sealed plastic bags (volume = 500 mL) for 8 d prior to RNA isolation. RNA isolations were performed using the the Maxwell 16 LEV Plant RNA Kit (Promega). Real-time PCR was performed as described previously using the primers listed in SI Appendix, Table 3 (17).

Generation of *V. dahliae* Mutants. The VdAMP3 deletion and complementation mutants, as well as the eGFP expression mutant, were generated as described previously using the primers listed in SI Appendix, Table 3 (18). To generate the VdAMP3 complementation construct, the VdAMP3 coding sequence was amplified with flanking sequences (~0.9 kb upstream and ~0.8 kb downstream) and cloned into pCG (58). Finally, the construct was used for Agrobacterium tumefaciens–mediated transformation of V. dahliae as described previously (59). In vitro growth and microsclerotia production of the VdAMP3 deletion mutant were tested and quantified as described previously (18).

In Vitro Microbial Growth Assays. Bacterial isolates were grown on lysogeny broth agar at 28°C. Single colonies were selected and grown overnight in low-salt lysogeny broth (LB) (10 g/L tryptone, 5 g/L yeast extract, and 0.5 g/L sodium chloride) at 28°C while shaking at 200 rpm. Overnight cultures were resuspended to optical density $(OD)_{600}$ = 0.025 in fresh low-salt LB supplemented with 20 μM VdAMP3 or ultrapure water (Milli-Q). In vitro growth was quantified using a CLARIOstar plate reader (BMG Labtech) as described previously (18).

Fungal isolates were grown on potato dextrose agar (PDA) at 22°C. For yeasts, single colonies were selected and grown overnight in 0.05× potato dextrose broth (PDB) at 28°C while shaking at 200 rpm. Overnight cultures were resuspended to OD_{600} = 0.01 in fresh 5% PDB supplemented with ultrapure water (Milli-Q), 5 μM VdAMP3, or 5 μM VdAMP3 that was incubated in a PCR thermocycler at 95°C for 16 h. Alternatively, for filamentous fungi, spores were harvested from PDA and suspended in 5% PDB supplemented with 5 μM VdAMP3 or ultrapure water (Milli-Q) to a final concentration of 10^4 spores/mL. Next, 200 μL of the fungal suspensions was aliquoted in clear 96-well flat-bottom polystyrene tissue-culture plates. Plates were incubated at 28 °C, and fungal growth was imaged using an SZX10 stereo microscope (Olympus) with EP50 camera (Olympus).

Microbiome Analysis. Inoculation and incubation of N. benthamiana plants were performed as described above. Subsequent genomic DNA isolation and V. dahliae biomass quantification were performed as previously described using the primers listed in SI Appendix, Table 3 (60). After 4 wk of incubation in plastic bags at room temperature in the dark, the decaying N. benthamiana phyllosphere samples colonized by V. dahliae WT and the VdAMP3 deletion mutant were collected. The phyllospheres of fresh 3-wk-old N. benthamiana plants were included as controls. All samples were flash-frozen in liquid nitrogen and ground using mortar and pestle, and genomic DNA was isolated

using the DNeasyPowerSoil Kit (Qiagen). Sequencing libraries were prepared using the TruSeq DNA Nano kit (Illumina), and paired-end 150-bp sequencing was performed on the Illumina NextSeq500 platform at the Utrecht Sequencing Facility.

The sequencing data were processed as follows. Quality control of the reads, adapter trimming, and removal of N. benthamiana reads were performed with the ATLAS metagenomic workflow using the default parameters of the configuration file (61). Reads of the different samples were combined and assembled using metaSPAdes (used k-mer sizes: 21, 33, and 55) to obtain a single metagenome cross-assembly (62). Subsequently, the cross-assembled contigs were taxonomically classified using Contig Annotation Tool and binned per genus (63). The reads of the individual samples were mapped to the binned contigs using Burrows-Wheeler Aligner Maximal Exact Match (64). Next, the mapping files were converted to bam format using SAMtools (65) version 1.10, and the number of reads mapped to the contigs of a single genus were converted to "reads per million" for the individual samples. The generated taxonomy table and abundance table were subsequently transformed into a phyloseq (66) object (version 1.30.0) in R (version 3.6.1) to facilitate analysis of the microbiomes. The alpha diversity (Shannon index) and beta diversity (Bray–Curtis dissimilarity) were determined as described previously (66, 67). The DESeq2 extension of phyloseq was used to identify differentially abundant microbial genera (68). To this end, a parametric model was applied to the data and a negative binomial Wald test was used to test for significant differential abundance.

Fungal Cocultivation Assays. Fungal isolates were grown on PDA at room temperature. For D. vanrijiae, M. amylolytica, and C. jadinii, single colonies were selected and grown overnight in 5% PDB at 28°C while shaking at 200 rpm. The overnight cultures of D. vanrijiae and M. amylolytica were resuspended to OD_{600} = 0.0001 in fresh 5% PDB. For the synthetic communities, D. vanrijiae, M. amylolytica, and C. jadinii were resuspended to OD_{600} = 0.001 and spores of C. militaris and T. viride were harvested from PDA and resuspended to 10^4 spores/mL. Next, equal volumes of the various fungal suspensions were mixed to obtain two syncoms: (A) D. vanrijae, M. amylolytica, and C. militarisand (B) D. vanrijae, M. amylolytica, C. jadinii, and T. viride, which were stored at 20°C in 5% PDB supplemented with 10% glycerol (wt/vol). Upon use, the syncoms were thawed at room temperature and diluted 10× (A) or 25× (B) in fresh 5% PDB, after which they were mixed with V. dahliae. To this end, conidiospores of V. dahliae strain JR2 and the VdAMP3 deletion and complementation mutants were harvested from PDA plates and diluted in ultrapure water (Milli-Q) to a final concentration of 10^4 or 10^5 conidiospores/mL. Next, 150 µL of the fungal suspensions was mixed with 150 µL of the V. dahliae conidiospore suspensions (10^4 conidiospores/mL for cultivation with syncom A or M. amylolytica and 10^5 conidiospores/mL for cultivation syncom B or D. vanrijae) in clear 24-well flat-bottom polystyrene tissue-culture plates. Finally, after six to nine d of incubation at 22°C, fungal growth was imaged using an SZX10 stereo microscope (Olympus) with EP50 camera (Olympus). The number of microsclerotia formed by the different V. dahliae strains was quantified through counting.

Data Availability. The metagenomics data have been deposited in the National Center for Biotechnology Information GenBank database under BioProject accession no. PRJNA728211 (69) (https://www.ncbi.nlm.nih.gov/bioproject/?term=PRJNA728211).

ACKNOWLEDGMENTS. B.P.H.J.T. is supported by the Research Council Earth and Life Sciences of the Netherlands Organization of Scientific Research (NWO). B.P.H.J.T. acknowledges funding by the Alexander von Humboldt Foundation in the framework of an Alexander von Humboldt Professorship endowed by the German Federal Ministry of Education, and research is furthermore supported by the Deutsche Forschungsgemeinschaft (German Research Foundation) under Germany's Excellence Strategy—EXC 2048/1—Project identification: 390686111. We thank the Utrecht Sequencing Facility, subsidized by the University Medical Center Utrecht, Hubrecht Institute, Utrecht University, and The Netherlands X-omics Initiative (NWO Project 184.034.019) for providing sequencing service.

1. F. Demoling, D. Figueroa, E. Bååth, Comparison of factors limiting bacterial growth in different soils. Soil Biol. Biochem. 39, 2485–2495 (2007).
2. L. Katz, R. H. Baltz, Natural product discovery: Past, present, and future. J. Ind. Microbiol. Biotechnol. 43, 155–176 (2016).
3. A. van der Meij, S. F. Worsley, M. I. Hutchings, G. P. van Wezel, Chemical ecology of antibiotic production by actinomycetes. FEMS Microbiol. Rev. 41, 392–416 (2017).
4. H. Rovenich, J. C. Boshoven, B. P. H. J. Thomma, Filamentous pathogen effector functions: Of pathogens, hosts and microbiomes. Curr. Opin. Plant Biol. 20, 96–103 (2014).
5. N. C. Snelders, G. J. Kettles, J. J. Rudd, B. P. H. J. Thomma, Plant pathogen effector proteins as manipulators of host microbiomes? Mol. Plant Pathol. 19, 257–259 (2018).
6. M. C. Giraldo, B. Valent, Filamentous plant pathogen effectors in action. Nat. Rev. Microbiol. 11, 800–814 (2013).
7. L. Lo Presti et al., Fungal effectors and plant susceptibility. Annu. Rev. Plant Biol. 66, 513–545 (2015).
8. R. L. Berendsen, C. M. J. Pieterse, P. A. H. M. Bakker, The rhizosphere microbiome and plant health. Trends Plant Sci. 17, 478–486 (2012).
9. C. Dimkpa, T. Weinand, F. Asch, Plant-rhizobacteria interactions alleviate abiotic stress conditions. Plant Cell Environ. 32, 1682–1694 (2009).
10. G. Castrillo et al., Root microbiota drive direct integration of phosphate stress and immunity. Nature 543, 513–518 (2017).
11. C. R. Fitzpatrick et al., Assembly and ecological function of the root microbiome across angiosperm plant species. Proc. Natl. Acad. Sci. U.S.A. 115, E1157–E1165 (2018).
12. Y. Bai et al., Functional overlap of the Arabidopsis leaf and root microbiota. Nature 528, 364–369 (2015).
13. P. Durán et al., Microbial interkingdom interactions in roots promote Arabidopsis survival. Cell 175, 973–983.e14 (2018).
14. N. Lombardi et al., Root exudates of stressed plants stimulate and attract Trichoderma soil fungi. Mol. Plant Microbe Interact. 31, 982–994 (2018).
15. R. L. Berendsen et al., Disease-induced assemblage of a plant-beneficial bacterial consortium. ISMEJ. 12, 1496–1507 (2018).
16. V. J. Carrión et al., Pathogen-induced activation of disease-suppressive functions in the endophytic root microbiome. Science 366, 606–612 (2019).
17. R. de Jonge et al., Tomato immune receptor Ve1 recognizes effector of multiple fungal pathogens uncovered by genome and RNA sequencing. Proc. Natl. Acad. Sci. U.S.A. 109, 5110–5115 (2012).
18. N. C. Snelders et al., Microbiome manipulation by a soil-borne fungal plant pathogen using effector proteins. Nat. Plants 6, 1365–1374 (2020).
19. P. Inderbitzin et al., Phylogenetics and taxonomy of the fungal vascular wilt pathogen Verticillium, with the descriptions of five new species. PLoS One 6, e28341 (2011).
20. S. J. Klosterman et al., Comparative genomics yields insights into niche adaptation of plant vascular wilt pathogens. PLoS Pathog. 7, e1002137 (2011).
21. L. Mol, H. W. Van Riessen, Effect of plant roots on the germination of microsclerotia of Verticillum dahliae. Eur. J. Plant Pathol. 101, 673–678 (1995).
22. S. J. Klosterman, Z. K. Atallah, G. E. Vallad, K. V. Subbarao, Diversity, pathogenicity, and management of verticillium species. Annu. Rev. Phytopathol. 47, 39–62 (2009).
23. W. C. Schnathorst, "Life cycle and epidemiology of Verticillium" in Fungal Wilt Diseases of Food Crops, M. E. Mace, A. A. Bell, C. H. Beckman, Eds. (Elsevier, 1981), vol. 82.
24. D. Xiong et al., Deep mRNA sequencing reveals stage-specific transcriptome alterations during microsclerotia development in the smoke tree vascular wilt pathogen, Verticillium dahliae. BMC Genomics 15, 324 (2014).
25. Rde. O. Dias, O. L. Franco, Cysteine-stabilized αβ defensins: From a common fold to antibacterial activity. Peptides 72, 64–72 (2015).
26. L. A. Kelley, S. Mezulis, C. M. Yates, M. N. Wass, M. J. E. Sternberg, The Phyre2 web portal for protein modeling, prediction and analysis. Nat. Protoc. 10, 845–858 (2015).
27. T. M. A. Shafee, F. T. Lay, M. D. Hulett, M. A. Anderson, The defensins consist of two independent, convergent protein superfamilies. Mol. Biol. Evol. 33, 2345–2356 (2016).
28. M. Dal Peraro, F. G. van der Goot, Pore-forming toxins: Ancient, but never really out of fashion. Nat. Rev. Microbiol. 14, 77–92 (2016).
29. P. H. Mygind et al., Plectasin is a peptide antibiotic with therapeutic potential from a saprophytic fungus. Nature 437, 975–980 (2005).
30. T. Schneider et al., Plectasin, a fungal defensin, targets the bacterial cell wall precursor Lipid II. Science 328, 1168–1172 (2010).
31. J. S. Oeemig et al., Eurocin, a new fungal defensin: Structure, lipid binding, and its mode of action. J. Biol. Chem. 287, 42361–42372 (2012).
32. I. V. Grigoriev et al., MycoCosm portal: Gearing up for 1000 fungal genomes. Nucleic Acids Res. 42, D699–D704 (2014).
33. J. W. Spatafora et al., A phylum-level phylogenetic classification of zygomycete fungi based on genome-scale data. Mycologia 108, 1028–1046 (2016).
34. S. Kumar, G. Stecher, M. Suleski, S. B. Hedges, TimeTree: A resource for timelines, timetrees, and divergence times. Mol. Biol. Evol. 34, 1812–1819 (2017).
35. D. S. Heckman et al., Molecular evidence for the early colonization of land by fungi and plants. Science 293, 1129–1133 (2001).
36. M. L. Berbee, J. W. Taylor, "Fungal molecular evolution: Gene trees and geologic time" in Systematics and Evolution, D. J. McLaughlin, E. G. McLaughlin, P. A. Lemke, Eds. (Springer, 2001), pp. 229–245.
37. J. L. Morris et al., The timescale of early land plant evolution. Proc. Natl. Acad. Sci. U.S.A. 115, E2274–E2283 (2018).
38. L. Faino, R. de Jonge, B. P. H. J. Thomma, The transcriptome of Verticillium dahliae-infected Nicotiana benthamiana determined by deep RNA sequencing. Plant Signal. Behav. 7, 1065–1069 (2012).
39. J. Depotter et al., The interspecific fungal hybrid Verticillium longisporum displays subgenome-specific gene expression. mBio 12: e01496-01421 (2021).

40. H. Gibriel, J. Li, L. Zhu, M. F. Seidl, B. P. H. J. Thomma, Verticillium dahliae strains that infect the same host plant display highly divergent effector catalogs. bioRxiv [Preprint] (2019). https://www.biorxiv.org/content/10.1101/528729v1. Accessed 10 June 2021.
41. D. Duressa et al., RNA-seq analyses of gene expression in the microsclerotia of Verticillium dahliae. BMC Genomics 14, 607 (2013).
42. A. Klimes, K. F. Dobinson, A hydrophobin gene, VDH1, is involved in microsclerotial development and spore viability in the plant pathogen Verticillium dahliae. Fungal Genet. Biol. 43, 283–294 (2006).
43. H. C. Smith, The morphology of Verticillium albo-atrum, V. dahliae, and V. tricorpus. N. Z. J. Agric. Res. 8, 450–478 (1965).
44. M. R. Mäkelä, N. Donofrio, R. P. de Vries, Plant biomass degradation by fungi. Fungal Genet. Biol. 72, 2–9 (2014).
45. J. Voříšková, P. Baldrian, Fungal community on decomposing leaf litter undergoes rapid successional changes. ISME J. 7, 477–486 (2013).
46. T. Korkama-Rajala, M. M. Müller, T. Pennanen, Decomposition and fungi of needle litter from slow- and fast-growing Norway spruce (Picea abies) clones. Microb. Ecol. 56, 76–89 (2008).
47. T. Osono, Role of phyllosphere fungi of forest trees in the development of decomposer fungal communities and decomposition processes of leaf litter. Can. J. Microbiol. 52, 701–716 (2006).
48. T. Osono, Phyllosphere fungi on leaf litter of Fagus crenata: Occurrence, colonization, and succession. Can. J. Bot. 80, 460–469 (2002).
49. R. Sapkota, K. Knorr, L. N. Jørgensen, K. A. O'Hanlon, M. Nicolaisen, Host genotype is an important determinant of the cereal phyllosphere mycobiome. New Phytol. 207, 1134–1144 (2015).
50. T. Gomes, J. A. Pereira, J. Benhadi, T. Lino-Neto, P. Baptista, Endophytic and epiphytic phyllosphere fungal communities are shaped by different environmental factors in a Mediterranean ecosystem. Microb. Ecol. 76, 668–679 (2018).
51. A. E. Arnold, Understanding the diversity of foliar endophytic fungi: Progress, challenges, and frontiers. Fungal Biol. Rev. 21, 51–66 (2007).
52. P. E. Verweij, E. Snelders, G. H. J. Kema, E. Mellado, W. J. G. Melchers, Azole resistance in Aspergillus fumigatus: A side-effect of environmental fungicide use? Lancet Infect. Dis. 9, 789–795 (2009).
53. R. C. May, N. R. H. Stone, D. L. Wiesner, T. Bicanic, K. Nielsen, Cryptococcus: From environmental saprophyte to global pathogen. Nat. Rev. Microbiol. 14, 106–117 (2016).
54. E. Klein, M. Ofek, J. Katan, D. Minz, A. Gamliel, Soil suppressiveness to fusarium disease: Shifts in root microbiome associated with reduction of pathogen root colonization. Phytopathology 103, 23–33 (2013).
55. J. B. Buil et al., The fading boundaries between patient and environmental routes of triazole resistance selection in Aspergillus fumigatus. PLoS Pathog. 15, e1007858 (2019).
56. J. Zhang et al., Dynamics of Aspergillus fumigatus in azole fungicide-containing plant waste in the Netherlands (2016–2017). Appl. Environ. Microbiol. 87, e02295-20 (2021).
57. S. E. Schoustra et al., Environmental hotspots for azole resistance selection of Aspergillus fumigatus, the Netherlands. Emerg. Infect. Dis. 25, 1347–1353 (2019).
58. L. Zhou, J. Zhao, W. Guo, T. Zhang, Functional analysis of autophagy genes via Agrobacterium-mediated transformation in the vascular Wilt fungus Verticillium dahliae. J. Genet. Genomics 40, 421–431 (2013).
59. P. Santhanam, "Random insertional mutagenesis in fungal genomes to identify virulence factors" in Plant Fungal Pathogens, B. P. H. J. Thomma, M. D. Bolton, Eds. (Springer, 2012), pp. 509–517.
60. Y. Song et al., Transfer of tomato immune receptor Ve1 confers Ave1-dependent Verticillium resistance in tobacco and cotton. Plant Biotechnol. J. 16, 638–648 (2018).
61. S. Kieser, J. Brown, E. M. Zdobnov, M. Trajkovski, L. A. McCue, ATLAS: A Snakemake workflow for assembly, annotation, and genomic binning of metagenome sequence data. BMC Bioinformatics 21, 257 (2020).
62. S. Nurk, D. Meleshko, A. Korobeynikov, P. A. Pevzner, metaSPAdes: A new versatile metagenomic assembler. Genome Res. 27, 824–834 (2017).
63. F. A. B. von Meijenfeldt, K. Arkhipova, D. D. Cambuy, F. H. Coutinho, B. E. Dutilh, Robust taxonomic classification of uncharted microbial sequences and bins with CAT and BAT. Genome Biol. 20, 217 (2019).
64. H. Li, Aligning sequence reads, clone sequences and assembly contigs with BWA-MEM. arXiv [Preprint] (2013). https://arxiv.org/abs/1303.3997. Accessed 10 June 2021.
65. H. Li et al., 1000 Genome Project Data Processing Subgroup, The sequence alignment/map format and SAMtools. Bioinformatics 25, 2078–2079 (2009).
66. P. J. McMurdie, S. Holmes, phyloseq: An R package for reproducible interactive analysis and graphics of microbiome census data. PLoS One 8, e61217 (2013).
67. B. J. Callahan, K. Sankaran, J. A. Fukuyama, P. J. McMurdie, S. P. Holmes, Bioconductor Workflow for Microbiome Data Analysis: From raw reads to community analyses. F1000 Res. 5, 1492 (2016).
68. M. I. Love, W. Huber, S. Anders, Moderated estimation of fold change and dispersion for RNA-seq data with DESeq2. Genome Biol. 15, 550 (2014).
69. N. C. Snelders et al., Phyllosphere microbiome of Nicotiana benthamiana plants infected by Verticillium dahliae. National Center for Biotechnology Information GenBank database. https://www.ncbi.nlm.nih.gov/bioproject/?term=PRJNA728211. Deposited 8 May 2021.

EXTENDED MATERIALS AND METHODS

Chemical synthesis of VdAMP3

VdAMP3 was chemically synthesized and purified (≥ 95% purity) by GenScript (Piscataway, NJ, USA) using the PepPower™ platform. Lyophilized VdAMP3 was solubilized in ultrapure water (MQ) and stored at -20°C until use.

Microbial isolates

Bacterial strains *B. subtilis* AC95, *S. xylosus* M3, *P. corrugata* C26, *Streptomyces* sp. NE-P-8 and *Ralstonia* sp. M21 were obtained from our in-house endophyte culture collection. Bacterial strains *Novosphingobium* sp. (NCCB 100261) and *Sphingobacterium canadese* (NCCB100125) were obtained from the Westerdijk Fungal Biodiversity Institute (Utrecht, the Netherlands). Fungal strains *Saccharomyces cerevisiae* H15 and *Trichoderma viride* were obtained from our in-house culture collection. Fungal strains *Cyberlindnera jadinii* (DSM 70167), *Cordyceps militaris* (DSM 1153), *Debaryomyces vanrijiae* (DSM 70252), *Meyerozyma amylolytica* (DSM 27310) and *Rhodotorula bogoriensis* (DSM 70872) were obtained from the Leibniz Institute DSMZ.

Inoculation assays

Three-week-old *N. benthamiana* seedlings grown in the greenhouse at 21°C/19°C during 16h/8h day/night periods, respectively, with 70% relative humidity, were inoculated with *V. dahliae* through root-dip inoculation as described previously (60). After 14 days, above-ground parts of the *N. benthamiana* plants were harvested and stored at -20°C. Alternatively, above-ground parts were collected and transferred to plastic bags (volume = 500 mL) and incubated for four weeks at room temperature. Next, all *N. benthamiana* samples were ground using mortar and pestle. Subsequent genomic DNA isolation and *V. dahliae* biomass quantification was performed using the primers listed in Supplementary Table 3. Alternatively, to validate the integrity and activity of the microsclerotia formed by *V. dahliae* WT and the *VdAMP3* deletion mutant, we mixed the ground material of four

plants with 200 mL of potting soil and planted two-week-old *N. benthamiana* seedlings on this mixture. The phenotypes of the diseased *N. benthamiana* plants were imaged five weeks later.

Fluorescence microscopy

Conidiospores of the *pVdAMP3::eGFP* reporter strain were harvested from a PDA plate and diluted to a final concentration of 10^5 conidiospores/mL in 0.1x Czapek Dox medium. The suspension was incubated for one week at room temperature to allow hyphae to grow and microsclerotia to form. Finally, eGFP accumulating in the fungal cells was detected using a Nikon ECLIPSE 90i microscope.

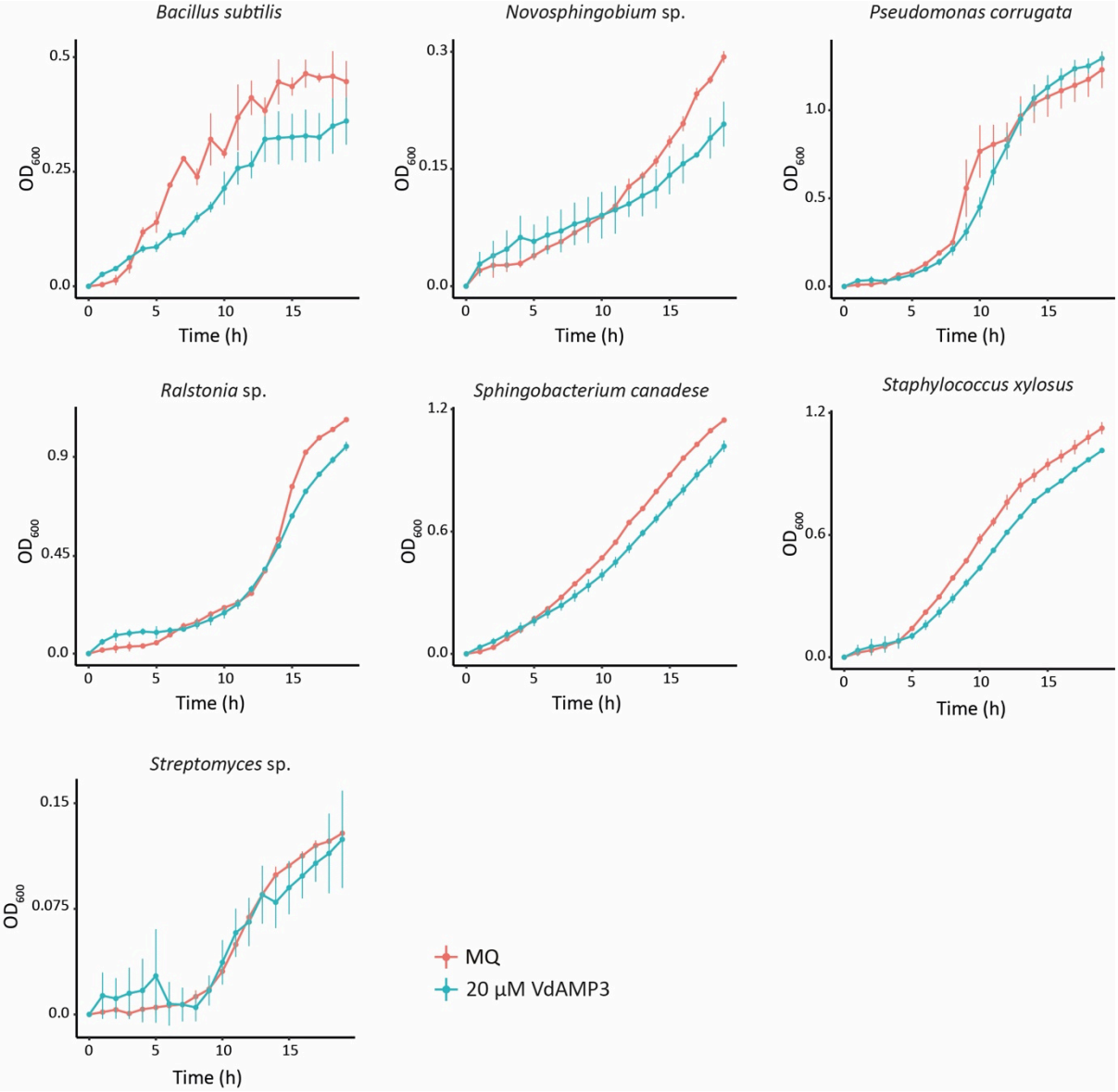

Supplementary Figure 1. VdAMP3 does not markedly impact bacterial growth. *In vitro* growth of plant-associated bacterial isolates in low salt LB is not, or only marginally, affected in the presence of 20 µM VdAMP3.

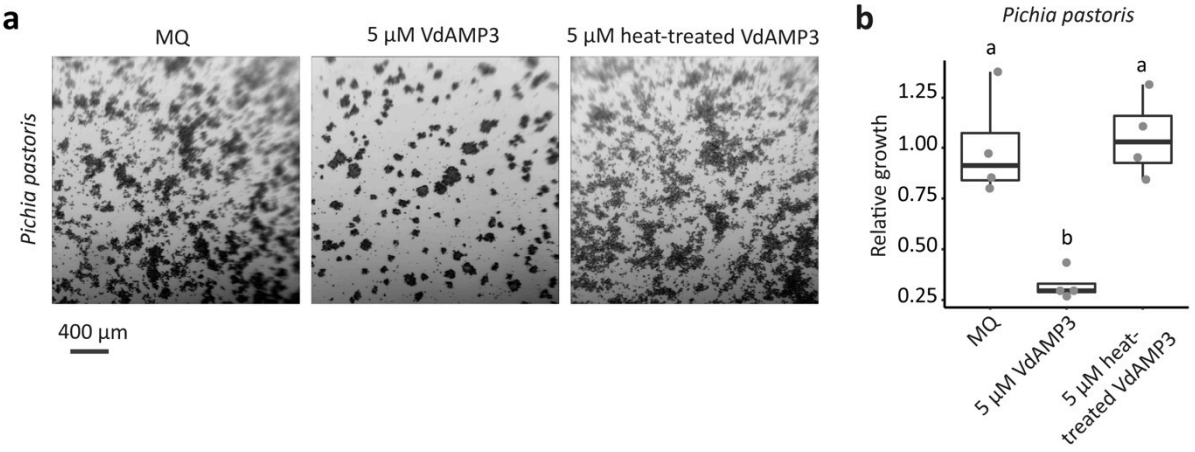

Supplementary Figure 2. Heat treatment abolishes antifungal activity of VdAMP3. Microscopic pictures of *Pichia pastoris* grown in 5% potato dextrose broth supplemented with ultrapure water (MQ), 5 µM VdAMP3 or 5 µM heat-treated VdAMP3. Pictures were taken after 48 hours of incubation. **(b)** Fungal growth as displayed in (**a**) was quantified using ImageJ (one-way ANOVA and Tukey's post-hoc test; $p<0.01$; N=4).

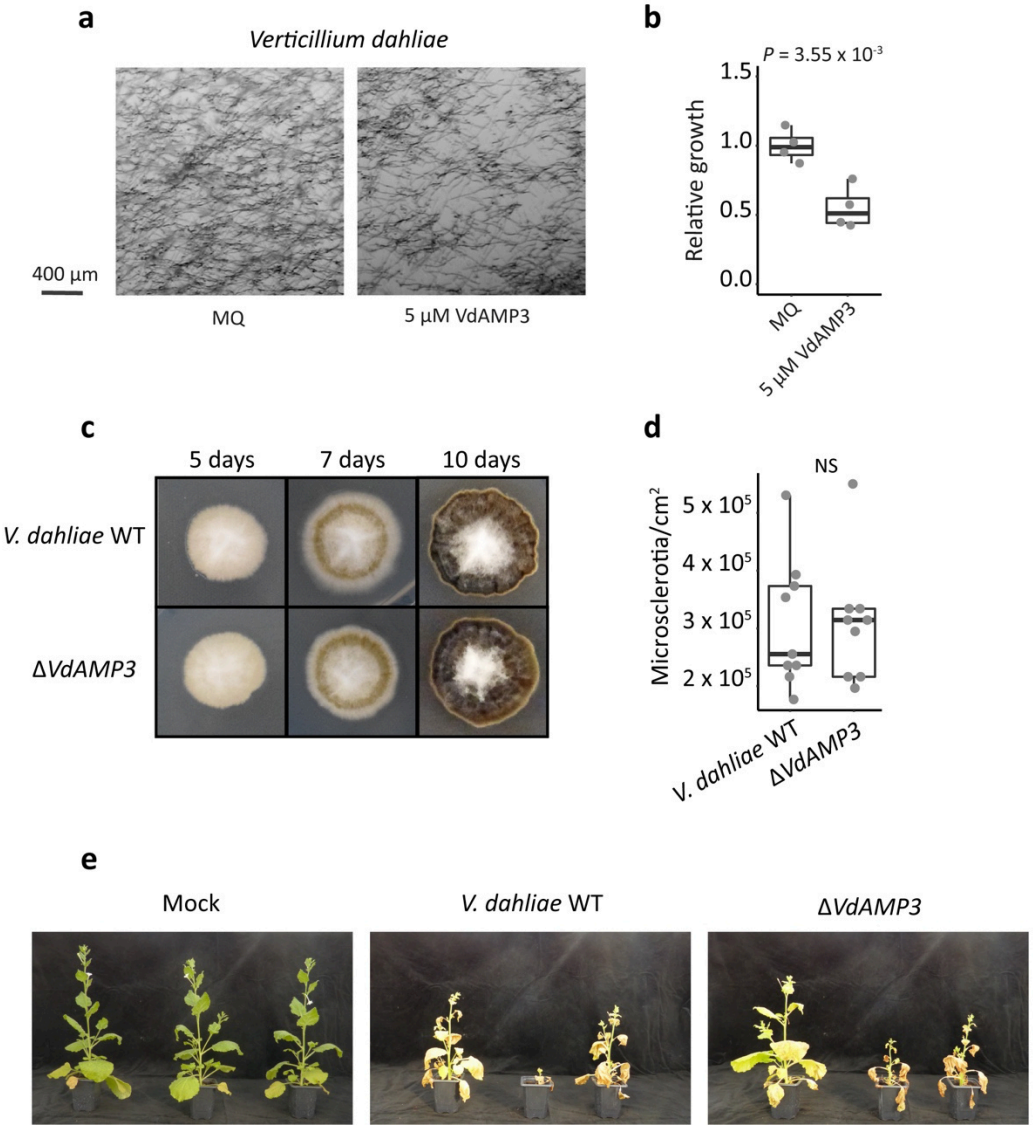

Supplementary Figure 3. *VdAMP3* does not impact *V. dahliae* growth and development. (a) Exogenously applied VdAMP3 impairs hyphal growth of *V. dahliae*. Microscopic pictures of *V. dahliae* grown in 5% potato dextrose broth supplemented with 5 µM VdAMP3 or ultrapure water (MQ), pictures were taken after 24 hours of incubation. **(b)** Growth as displayed in (**a**) was quantified using ImageJ (unpaired two-sided student's t-test; N=4). **(c-d)** Deletion of *VdAMP3* does not impact *V. dahliae* growth or microsclerotia formation *in vitro*. **(c)** Morphology of wild-type *V. dahliae* and the *VdAMP3* deletion mutant following five, seven and ten days of *in vitro* growth on PDA. **(d)** Deletion of *VdAMP3* does not impair microsclerotia formation. After ten days, the colonies as shown in **(c)** were processed and the number of microsclerotia per cm^2 was determined using a haemocytometer. No significant difference in microsclerotia formation was observed (unpaired student t-test N=9). **(e)** Deletion of *VdAMP3* does not impact the ability of microsclerotia to cause disease. Phenotypes of seven-week-old *N. benthamiana* plants grown on mock-treated potting soil or potting soil supplemented with microsclerotia of *V. dahliae* WT or the *VdAMP3* deletion mutant.

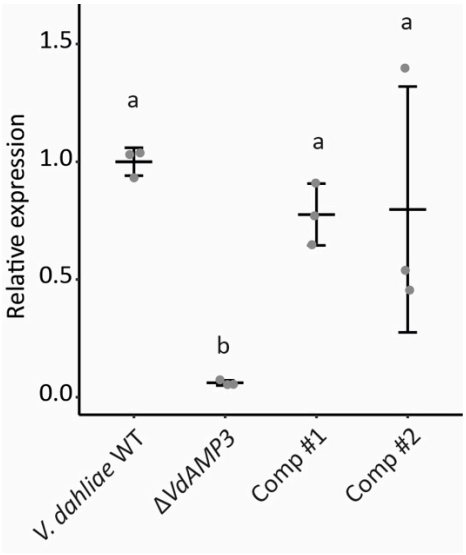

Supplementary Figure 4. Expression of *VdAMP3* in *V. dahliae* mutants. Expression of *VdAMP3* relative to *VdGAPDH* during microsclerotia formation by *V. dahliae* WT and the *VdAMP3* deletion and complementation mutants after seven days of cultivation in Czapek Dox medium. Letters represent statistically significant differences (one-way ANOVA and Tukey's post-hoc test; $p<0.05$; N=3).

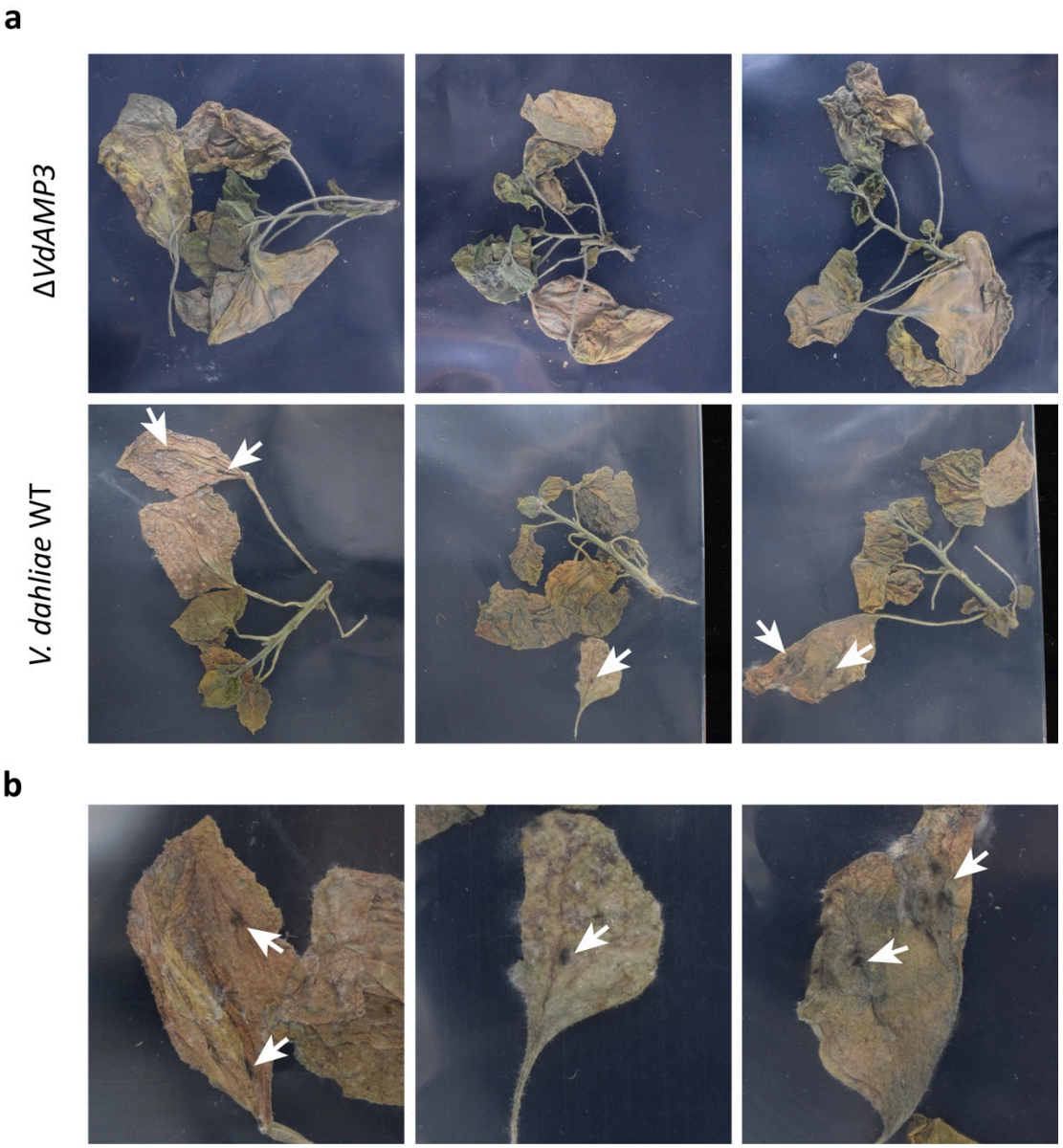

Supplementary Figure 5. *VdAMP3* contributes to *V. dahliae* microsclerotia formation in decaying *N. benthamiana* phyllosphere. (a) Phenotypes of *N. benthamiana* plants colonized by *V. dahliae* WT or the *VdAMP3* deletion mutant that were harvested at 14 days post inoculation and subsequently incubated in plastic bags for 28 days. The white arrows indicate dark patches of mycelium with *V. dahliae* microsclerotia found on plants colonized by *V. dahliae* WT, but not by the *VdAMP3* deletion mutant. **(b)** Close-up of the *N. benthamiana* tissues harboring the patches with microsclerotia.

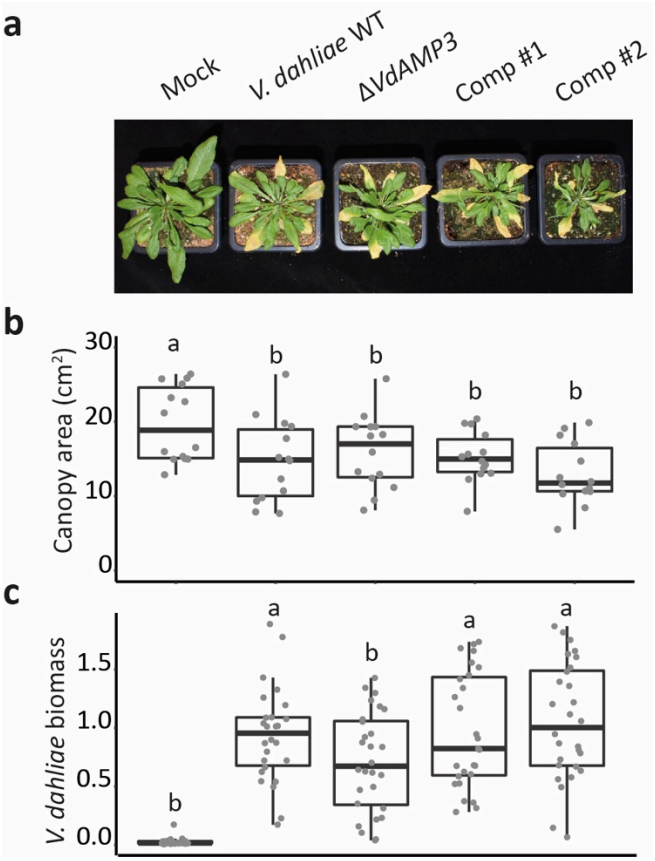

Supplementary Figure 6. VdAMP3 contributes to *V. dahliae* biomass accumulation in *Arabidopsis thaliana* but does not influence development of disease symptoms. (a) Deletion of *VdAMP3* does not affect establishment of Verticillium wilt disease in *A. thaliana*. Photos display representative phenotypes of *A. thaliana* plants 21 days post inoculation with *V. dahliae* WT and *VdAMP3* deletion and complementation mutants. **(b)** Canopy area of *A. thaliana* plants inoculated by the different *V. dahliae* genotypes. Different letter labels represent statistically significant differences when compared with *V. dahliae* WT (unpaired student's t-test; N=14). **(c)** Relative *V. dahliae* biomass in above-ground *A. thaliana* tissues determined with real-time PCR. Different letter labels represent statistically significant differences when compared with *V. dahliae* WT (unpaired student's t-test; N≥26).

Supplementary Table 1: DESeq2 output for the differentially abundant bacterial genera in the decaying phyllosphere of *N. benthamiana* plants colonized by *V. dahliae* wild type compared to the *VdAMP3* deletion mutant

Base mean	log2FC	lfcSE	stat	p value	p adjusted	Genus
6.57E+03	-6.60E+00	1.13E+00	-5.82E+00	5.88E-09	2.26E-06	*Advenella*
1.43E+01	-2.17E+01	3.91E+00	-5.54E+00	2.99E-08	5.76E-06	*Absicoccus*
8.83E+01	2.65E+00	6.25E-01	4.23E+00	2.31E-05	2.97E-03	*Azospirillum*
3.87E+01	2.97E+00	7.72E-01	3.85E+00	1.18E-04	6.00E-03	*Duganella*
8.74E+01	3.16E+00	8.36E-01	3.78E+00	1.56E-04	6.00E-03	*Chthoniobacter*
9.34E+03	2.76E+00	7.30E-01	3.78E+00	1.59E-04	6.00E-03	*Massilia*
3.16E+02	-3.09E+00	8.23E-01	-3.76E+00	1.71E-04	6.00E-03	*Ochrobactrum*
5.66E+01	-3.76E+00	1.08E+00	-3.47E+00	5.13E-04	1.52E-02	*Brenneria*
2.74E+01	2.24E+00	6.71E-01	3.34E+00	8.37E-04	2.12E-02	*Paenibacillus*
5.08E+01	-3.14E+00	9.45E-01	-3.33E+00	8.82E-04	2.12E-02	*Rouxiella*
1.32E+03	2.15E+00	6.62E-01	3.25E+00	1.15E-03	2.61E-02	*Caulobacter*
5.62E+02	2.59E+00	8.32E-01	3.11E+00	1.87E-03	3.99E-02	*Cellvibrio*
9.76E+02	2.46E+00	7.94E-01	3.09E+00	1.97E-03	3.99E-02	*Mucilaginibacter*
1.85E+01	-3.47E+00	1.13E+00	-3.08E+00	2.10E-03	4.04E-02	*Adhaeribacter*
7.36E+02	1.68E+00	5.55E-01	3.02E+00	2.50E-03	4.58E-02	*Flavobacterium*
6.39E+01	2.49E+00	8.28E-01	3.01E+00	2.63E-03	4.59E-02	*Taibaiella*
2.72E+03	2.34E+00	7.89E-01	2.97E+00	2.98E-03	4.59E-02	*Dyadobacter*
5.20E+01	-2.35E+00	7.98E-01	-2.94E+00	3.27E-03	4.84E-02	*Pusillimonas*
2.76E+03	1.43E+00	5.02E-01	2.84E+00	4.46E-03	6.13E-02	*Paraburkholderia*
1.21E+01	-2.97E+00	1.06E+00	-2.79E+00	5.25E-03	6.60E-02	*Rhizorhapis*
2.26E+01	-2.87E+00	1.08E+00	-2.65E+00	7.97E-03	8.98E-02	*Telmatospirillum*
4.21E+00	5.25E+00	1.98E+00	2.65E+00	8.03E-03	NA	*Myroides*
5.77E+03	-2.03E+00	7.67E-01	-2.65E+00	8.15E-03	8.98E-02	*Achromobacter*
1.02E+04	-1.59E+00	6.01E-01	-2.65E+00	8.16E-03	8.98E-02	*Sphingobium*
6.05E+00	4.00E+00	1.53E+00	2.61E+00	9.18E-03	9.80E-02	*Flavipsychrobacter*
7.67E+01	2.94E+00	1.13E+00	2.60E+00	9.42E-03	9.80E-02	*Archangium*
1.19E+04	-2.12E+00	8.21E-01	-2.58E+00	9.82E-03	9.89E-02	*Enterobacter*
1.29E+01	-2.64E+00	1.03E+00	-2.58E+00	1.00E-02	9.89E-02	*Peribacillus*
5.32E+01	2.79E+00	1.10E+00	2.53E+00	1.15E-02	1.08E-01	*Methylovorus*
2.90E+01	-1.92E+00	7.80E-01	-2.46E+00	1.40E-02	1.22E-01	*Candidimonas*
9.40E+01	-2.37E+00	1.01E+00	-2.35E+00	1.89E-02	1.58E-01	*Serratia*
1.54E+01	-2.60E+00	1.12E+00	-2.32E+00	2.04E-02	1.64E-01	*Leclercia*
7.76E+01	-2.00E+00	8.63E-01	-2.32E+00	2.04E-02	1.64E-01	*Rahnella*
8.42E+00	3.08E+00	1.37E+00	2.25E+00	2.46E-02	1.83E-01	*Gemmobacter*
4.26E+04	-2.44E+00	1.09E+00	-2.25E+00	2.48E-02	1.83E-01	*Pantoea*
7.68E+02	-1.68E+00	7.58E-01	-2.22E+00	2.63E-02	1.89E-01	*Bordetella*
2.47E+01	-2.43E+00	1.10E+00	-2.22E+00	2.65E-02	1.89E-01	*Tatumella*

5.52E+00	3.04E+00	1.39E+00	2.19E+00	2.87E-02	1.93E-01	*Thiomonas*
1.05E+01	2.34E+00	1.07E+00	2.19E+00	2.87E-02	1.93E-01	*Gilvimarinus*
3.93E+02	1.33E+00	6.08E-01	2.18E+00	2.91E-02	1.93E-01	*Ramlibacter*
3.53E+00	-5.46E+00	2.56E+00	-2.13E+00	3.31E-02	NA	*Listeria*
1.20E+02	-1.81E+00	8.69E-01	-2.08E+00	3.77E-02	2.34E-01	*Brevundimonas*
3.76E+02	1.47E+00	7.38E-01	1.99E+00	4.69E-02	2.77E-01	*Asticcacaulis*
7.80E+02	1.58E+00	7.95E-01	1.99E+00	4.71E-02	2.77E-01	*Shinella*
2.22E+01	1.84E+00	9.27E-01	1.98E+00	4.76E-02	2.77E-01	*Cytophaga*
9.32E+00	-1.88E+00	9.51E-01	-1.98E+00	4.83E-02	2.77E-01	*Porphyrobacter*

Supplementary Table 2: DESeq2 output for the differentially abundant fungal genera in the decaying phyllosphere of *N. benthamiana* plants colonized by *V. dahliae* wild type compared to the *VdAMP3* deletion mutant

Base mean	log2FC	lfcSE	stat	pvalue	padj	Genus
7.20E+01	-3.14E+00	7.70E-01	-4.08E+00	4.50E-05	3.87E-03	*Clavispora*
2.26E+01	-7.19E+00	1.77E+00	-4.05E+00	5.03E-05	3.87E-03	*Cordyceps*
1.55E+01	-5.85E+00	1.51E+00	-3.86E+00	1.11E-04	6.00E-03	*Trichomonascus*
2.64E+01	-5.10E+00	1.34E+00	-3.80E+00	1.43E-04	6.00E-03	*Akanthomyces*
9.44E+03	-4.13E+00	1.15E+00	-3.60E+00	3.19E-04	1.02E-02	*Fusarium*
7.01E+01	3.29E+00	9.81E-01	3.36E+00	7.91E-04	2.12E-02	*Terfezia*
2.22E+01	3.99E+00	1.34E+00	2.98E+00	2.84E-03	4.59E-02	*Rhodotorula*
1.82E+01	-2.76E+00	9.28E-01	-2.98E+00	2.92E-03	4.59E-02	*Beauveria*
4.87E+01	-8.30E+00	2.86E+00	-2.90E+00	3.71E-03	5.29E-02	*Escovopsis*
1.44E+02	-2.81E+00	9.97E-01	-2.81E+00	4.91E-03	6.51E-02	*Yamadazyma*
1.21E+01	3.51E+00	1.26E+00	2.79E+00	5.31E-03	6.60E-02	*Ascosphaera*
5.54E+03	-3.18E+00	1.19E+00	-2.68E+00	7.45E-03	8.96E-02	*Trichoderma*
6.49E+00	-3.79E+00	1.50E+00	-2.53E+00	1.14E-02	1.08E-01	*Xylaria*
5.53E+01	2.89E+00	1.16E+00	2.48E+00	1.32E-02	1.21E-01	*Golovinomyces*
1.88E+01	-2.17E+00	8.79E-01	-2.47E+00	1.36E-02	1.21E-01	*Valsa*
5.03E+00	-3.60E+00	1.48E+00	-2.44E+00	1.49E-02	1.27E-01	*Acremonium*
2.18E+00	-4.77E+00	2.04E+00	-2.34E+00	1.94E-02	NA	*Meyerozyma*
2.92E+00	-4.17E+00	1.79E+00	-2.33E+00	2.00E-02	NA	*Scedosporium*
4.94E+00	-3.36E+00	1.46E+00	-2.30E+00	2.14E-02	1.68E-01	*Ustilaginoidea*
2.98E+01	-2.60E+00	1.15E+00	-2.26E+00	2.35E-02	1.81E-01	*Debaryomyces*
6.66E+01	-1.45E+00	6.64E-01	-2.19E+00	2.86E-02	1.93E-01	*Phaeoacremonium*
1.58E+01	2.43E+00	1.15E+00	2.11E+00	3.46E-02	2.26E-01	*Morchella*
2.10E+01	-1.97E+00	9.38E-01	-2.11E+00	3.52E-02	2.26E-01	*Neonectria*
1.09E+01	-1.77E+00	8.45E-01	-2.10E+00	3.59E-02	2.26E-01	*Spathaspora*
5.98E+00	-3.07E+00	1.51E+00	-2.04E+00	4.12E-02	2.52E-01	*Pochonia*
2.02E+00	-4.67E+00	2.30E+00	-2.02E+00	4.29E-02	NA	*Millerozyma*
3.54E+00	-2.82E+00	1.41E+00	-2.00E+00	4.52E-02	NA	*Grosmannia*
3.47E+00	-2.99E+00	1.50E+00	-1.99E+00	4.68E-02	NA	*Cyberlindnera*

Supplementary Table 3: Primers used in this study

Name	Sequence (5' --> 3')	Application
VdAve1_qPCR_Fw	TGTTACCAAAGCAGCACACAAGG	Real-time PCR
VdAve1_qPCR_Rv	CCTTATGCCTCGTTCCCTTCCAC	Real-time PCR
VdGAPDH_Fw	CGAGTCCACTGGTGTCTTCA	Real-time PCR
VdGAPDH_Rv	CCCTCAACGATGGTGAACTT	Real-time PCR
VdAMP3_qPCR_Fw	ATGAAGCTCATTTCTGC	Real-time PCR
VdAMP3_qPCR_Rv	CTAGTTGCAAATGCACAC	Real-time PCR
Chr6g02430_qPCR_Fw	CAGAGCACCACTCACCACAT	Real-time PCR
Chr6g02430_qPCR_Rv	ATCAGGAGTGGCGTGAAGTC	Real-time PCR
ITS1-Fw	AAAGTTTTAATGGTTCGCTAAGA	Real-time PCR
St-Ve1-Rv	CTTGGTCATTTAGAGGAAGTAA	Real-time PCR
NbRUB_Fw	TCCGGGTATTAGCAAAAGCGT	Real-time PCR
NbRUB_Rv	CCCAAGATCTCGGTCAGAGC	Real-time PCR
AtRUB_Fw	GCAAGTGTTGGGTTCAAAGCTGGTG	Real-time PCR
AtRUB_Rv	CCAGGTTGAGGAGTTACTCGGAATGCTG	Real-time PCR
JR2_VdAMP3_LB_Fw	GGTCTTAAUTTTGAGGGGTTCAGCCGATG	To generate VdAMP3 deletion mutant
JR2_VdAMP3_LB_Rv	GGCATTAAUGACGATATGAGTGCTTGCGG	To generate VdAMP3 deletion mutant
JR2_VdAMP3_RB_Fw	GGACTTAAUAATGCTTGAGATGACGACGC	To generate VdAMP3 deletion mutant
JR2_VdAMP3_RB_Rv	GGGTTTAAUCTGCTCACCAAGCCTCCTTC	To generate VdAMP3 deletion mutant
VdAMP3_Comp_Fw	GGGGACAGCTTTCTTGTACAAAGTGGTTTGAGGGGTTCAGCCGATG	To generate VdAMP3 complementation mutant
VdAMP3_Comp_Rv	GGGGACAACTTTGTATAATAAAGTTGCTGCTCACCAAGCCTCCTTC	To generate VdAMP3 complementation mutant
Promoter_VdAMP3_Fw	CTCGGAATTAACCCTCACTAAAGGGAACAAAAGCTGGAGCTCACA CAACATCTATGCTTCAGAAGGTGGCAAAAGTG	To generate pVdAMP3::eGFP transformant
Promoter_VdAMP3_Rv	ATGATGGCCATGTTATCCTCCTCGCCCTTGCTCACCATATTAATTAA GATTGATGGTGTCAAGAGGGTCTGGGATATGATTG	To generate pVdAMP3::eGFP transformant

Chapter 3

Structural and functional characterization of a host microbiota-targeting antimicrobial protein from the plant pathogen *Verticillium dahliae*

Gabriella C. Petti[1]*, Nick C. Snelders[1,2]*, Ashok K. Rout[3], Biwen Wang[4], Kathrin König[8], Edgar A. Chavarro-Carrero[2], Tjalling Siersma[4], Jacob Biboy[5], Ayesha Safoor[6], Filipe Cabreiro[6], Waldemar Vollmer[5], Leendert Hamoen[4], Jeroen R. Mesters[7], Daniel Friedrich[8], Alvaro Mallagaray[3], Bart P.H.J. Thomma[1]

[1]University of Cologne, Institute for Plant Sciences, Cluster of Excellence on Plant Sciences (CEPLAS), 50674 Cologne, Germany

[2]Laboratory of Phytopathology, Wageningen University & Research, 6708 PB Wageningen, The Netherlands

[3]University of Lübeck, Institute of Chemistry and Metabolomics, 23562 Lübeck, Germany

[4]University of Amsterdam, Swammerdam Institute for Life Sciences, 1098 XH Amsterdam, The Netherlands

[5]Newcastle University, Centre for Bacterial Cell Biology, Institute for Cell and Molecular Biosciences, NE2 4AX Newcastle upon Tyne, United Kingdom

[6]University of Cologne, Cologne Excellence Cluster for Cellular Stress Responses in Aging-Associated Diseases (CECAD), 50931 Cologne, Germany

[7]University of Lübeck, Institute of Biochemistry, 23562 Lübeck, Germany

[8]University of Cologne, Department of Chemistry and Biochemistry, 50939 Cologne, Germany

*These authors contributed equally to this work.

Author contributions:

G.C.P. performed the VdAve1 structure determination (Figure 1), the VdAve1 antimicrobial activity spectrum analysis (Figure 3), the VdAve1-derived peptides antimicrobial tests (Figure 4, 5), and the VdAve1 binding assays (Figure 7, 8) and wrote the chapter.

Abstract

Antimicrobial proteins are ancient and widespread molecules, which play key roles in survival across all domains of life. Fungal plant pathogens secrete antimicrobial proteins to selectively suppress host-associated microbial antagonists, and thus promote host colonization. We previously demonstrated that the soil-borne plant pathogen *Verticillium dahliae* employs the bactericidal protein VdAve1 to suppress bacterial competitors during host colonization. Here, we uncover the mode of action of VdAve1. Using nuclear magnetic resonance (NMR), we solved the three-dimensional structure of VdAve1, revealing a β-barrel-like fold. We show that VdAve1 disrupts microbial plasma membranes and exhibits broad-spectrum antimicrobial activity against bacteria, fungi, and amoebae. Furthermore, we show that synthetic peptides corresponding to positively charged regions of VdAve1 exhibit antimicrobial activity. We found that *Bacillus subtilis* responds to VdAve1 by modifying teichoic acid, and genetic disruption of genes involved in these modifications increases sensitivity to VdAve1, suggesting that VdAve1 targets these molecules. Supporting this hypothesis, we observed that VdAve1 binds purified lipoteichoic acid (LTA), a major component of the Gram-positive cell wall. Our current findings support a model in which VdAve1 binds LTA, promoting its association with the bacterial surface, from where it perturbs the plasma membrane, ultimately leading to membrane dissipation and cell death.

Introduction

Plants associate with diverse and complex sets of microbes, which collectively form their microbiota. Microbiota profiling has revealed that plant-associated communities are highly dynamic, and their composition is determined by various factors, such as environmental conditions, plant genotype and organs (Trivedi et al. 2020). Plants actively shape their microbiota by recruiting mutualists and beneficial microbes through the secretion of exudates (Berendsen et al. 2012; Harbort et al. 2020; Hu et al. 2018). These beneficial microbes contribute to plant growth and health by influencing nutrient acquisition, stress tolerance and mitigating disease development (Trivedi et al., 2020). Besides beneficial microbes, the plant microbiota comprises neutral and pathogenic microbes. Under conducive circumstances, such as host immunity imbalances or abiotic stresses, pathogenic members of the plant microbiota and invading pathogenic microbes can cause disease (Chen et al. 2020; Pfeilmeier et al. 2021; Velásquez et al. 2018). Disease development can be mitigated by the plant microbiota through competitive intermicrobial interactions, such as resource competition and secretion of antimicrobial compounds (Carrión et al. 2019; Vogel et al. 2021). Additionally, microbes can stimulate plant immunity, enhancing plant responsiveness to biotic stresses and therefore increasing the capacity to withstand pathogen attack (Mauch-Mani et al. 2017; Pieterse et al. 2014). By these means, the plant microbiota expands the endogenous immune functions of the host and represents an additional barrier to be breached for the invading pathogen (Carrión et al. 2019; Hacquard et al. 2017).

Plant pathogens secrete effector proteins to facilitate host colonization. Initially thought to be solely involved in pathogen suppression of host immune responses, it is now recognized that effector proteins serve broader functions, such as protection against host-derived antimicrobial compounds and nutrient acquisition (Cook et al. 2015). Given that plant-associated microbial communities contribute significantly to plant health, acting as an extension of the plant immunity, it was hypothesized that pathogens have evolved effectors to target not only the host physiology but also its microbiota (Snelders et al. 2018). Growing evidence support this hypothesis, showing that fungal pathogens secrete effector proteins with antimicrobial properties to selectively suppress microbial competitors during host, and more broadly niche, colonization (Chavarro-Carrero et al. 2024; Gómez-Pérez et al. 2023;

Kettles et al. 2018; Ökmen et al. 2023; Snelders et al. 2020; Snelders et al. 2021; Snelders et al. 2023).

Verticillium dahliae is a soilborne fungus that causes vascular wilt disease in a wide range of plant species, including crops (Fradin and Thomma 2006). It persists in the soil as resilient resting structures called microsclerotia, which germinate in response to nutrient-rich root exudates (Mol and van Riessen 1995). The emerging hyphae grow through the soil and rhizosphere, eventually penetrating plant roots. Once inside, *V. dahliae* colonizes the xylem, producing conidiospores that spread through the vasculature via the sap stream. This systemic infection leads to chlorosis, necrosis, and ultimately plant senescence. The fungus then transitions to a saprophytic phase, exiting the vasculature to colonize decaying plant material, where it forms new microsclerotia that return to the soil upon tissue decomposition (Fradin and Thomma 2006). It was recently shown that *V. dahliae* secretes antimicrobial effector proteins during both pathogenic and saprotrophic stages of its life-cycle to antagonize microbial niche competitors (Snelders et al. 2020; Snelders et al. 2021; Snelders et al. 2023). For instance, the *V. dahliae* antimicrobial effector protein VdAve1 contributes to *V. dahliae* virulence by selectively suppressing bacterial antagonists in the host rhizosphere (Snelders et al. 2020). Interestingly, VdAve1 is not only expressed during host colonization, but also in soil, during soil-dwelling life stages (Snelders et al. 2020).

VdAve1 was previously identified as an avirulence factor that is recognized by the tomato immune receptor Ve1, whereas during *V. dahliae* infection on susceptible hosts lacking the Ve1 receptor VdAve1 acts as a virulence factor, promoting disease development (de Jonge et al. 2012). Interestingly, VdAve1 is homologous to a widespread class of plant peptides, called plant natriuretic peptides (PNPs). Phylogenetic analysis revealed that the evolutionary relationships of VdAve1 homologs is incongruent with species phylogeny, suggesting that VdAve1 was acquired by *V. dahliae* from plants via horizontal gene transfer (de Jonge et al. 2012). VdAve1 homologs were also found in other fungal plant pathogens, such as *Colletotrichum higginsianum*, *Cercospora beticola* and *Fusarium oxysporum* (de Jonge et al. 2012). Additionally, the bacterial plant pathogen *Xanthomonas citri* carries a VdAve1 homolog, which was shown to contribute to virulence function during host colonization (Gottig et al. 2008).

PNPs are signalling molecules that regulate water and ion homeostasis in plants, influencing physiological processes such as stomatal opening, photosynthesis, and stress responses (Wang et al. 2011). Additionally, AtPNP-A, a PNP from *Arabidopsis thaliana*, has been implicated in plant defense, as its overexpression enhances resistance to *Pseudomonas syringae* (Ficarra et al. 2018). However, contrasting findings have also been reported, where AtPNP-A overexpression resulted in increased *P. syringae* growth (Lee et al. 2020). AtPNP-A signalling is mediated by two receptors, AtPNP-R1 and AtPNP-R2 (Di Paolo et al. 2023; Lee et al. 2020). AtPNP-R1 is essential for AtPNP-A-induced stomatal opening (Di Paolo et al. 2023), while both receptors are required for the regulation of water homeostasis in response to AtPNP-A perception (Lee et al. 2020). Interestingly, it was previously shown that AtPNP-A inhibits the growth of *Bacillus subtilis*, indicating that the antimicrobial activity also occurs among plant homologs and suggesting that VdAve1 antimicrobial activity may not be the result of neofunctionalization upon horizontal gene transfer (Snelders et al. 2020).

VdAve1 is a small (~13 kDa) positively charged, cysteine-rich secreted protein that does not share structural or sequence homology with known antimicrobial proteins (Snelders et al. 2020). To gain insights into the antimicrobial properties of VdAve1, *in vitro* antimicrobial activity assays were performed using purified VdAve1 against a panel of plant-associated bacteria, revealing a selective antimicrobial activity. While Gram-negative bacteria showed differential sensitivity, all tested Gram-positive were inhibited, including the model Gram-positive bacterium *B. subtilis* (Snelders et al. 2020). Notably, scanning electron microscopy revealed that VdAve1 induces *B. subtilis* cells lysis, indicating that VdAve1 has bactericidal activity (Snelders et al. 2020). However, the mode of action of VdAve1 remained unknown.

Results

VdAve1 structure determination by NMR

To elucidate the mode of action of VdAve1, we determined the protein structure by liquid-state NMR spectroscopy. To this end, uniformly ^{15}N- and ^{15}N, ^{13}C-labelled mature VdAve1 was heterologously produced in *Escherichia coli* and purified. To acquire high-quality NMR spectra, protein samples should be highly concentrated. However, intermolecular interactions might increase as protein concentration increases, leading to fast T_2 relaxation rates and broadening

of the signals. This in turn may preclude the acquisition of long 3D NMR experiments required for the assignment of NMR spectra and structural calculations (Mallagaray et al. 2019). To investigate whether intermolecular interactions arise in highly concentrated VdAve1 samples, we estimated the rotational correlation time (τ_c) using $^{1}H,^{15}N$-TRACT NMR experiments (Lee et al. 2006) at different protein concentrations, ranging from 200 to 766 µM (Figure 1a). The τ_c, which is the average time a molecule takes to rotate one radian, remained constant at the different protein concentrations, evidencing no protein aggregation even at high protein concentrations. However, upon overnight incubation at room temperature, we observed protein precipitation in the VdAve1 sample with the highest concentration (766 µM), making this concentration unsuitable for long-running NMR measurements. Consequently, the VdAve1 concentration was set at 650 µM for subsequent NMR measurements.

Next, we acquired a set of multidimensional NMR spectra for structure determination (Table S 1). Upon obtaining the spectra, we first assigned the VdAve1 backbone manually, reaching a chemical shift assignment completeness of 94% for the backbone amide groups. Then we made use of the automated deep learning-based approach ARTINA (Klukowski et al. 2022) to assign the VdAve1 backbone and verified the deep learning-based assignment with the manual assignment. Next, we determined the VdAve1 structure with ARTINA (Klukowski et al. 2022), obtaining an ensemble of 20 structures with a root mean square deviation of 2.22 Å (Figure 1b; Table S2). Secondary structure analysis revealed model 1 (out of 20) comprises 7% alpha-helix, 23.2% beta-sheet, 13.4% turn and 56.4% coil (Kabsch and Sander 1983). Four anti-parallel β-strands form a curved sheet (L2-T4, N110-Q115, Y49-C53 and M65-R73) that is capped by a 7-residue long alpha-helix (Q91-I97) and a small anti-parallel β-sheet (V32-V34, M87-L89). This arrangement of six β-strands into two sheets is reminiscent of a jelly-roll fold/barrel where neighbouring strands in the protein sequence alternate between the two sheets. The VdAve1 fold results in an overall surface charge of +6.21 (Figure 1c).

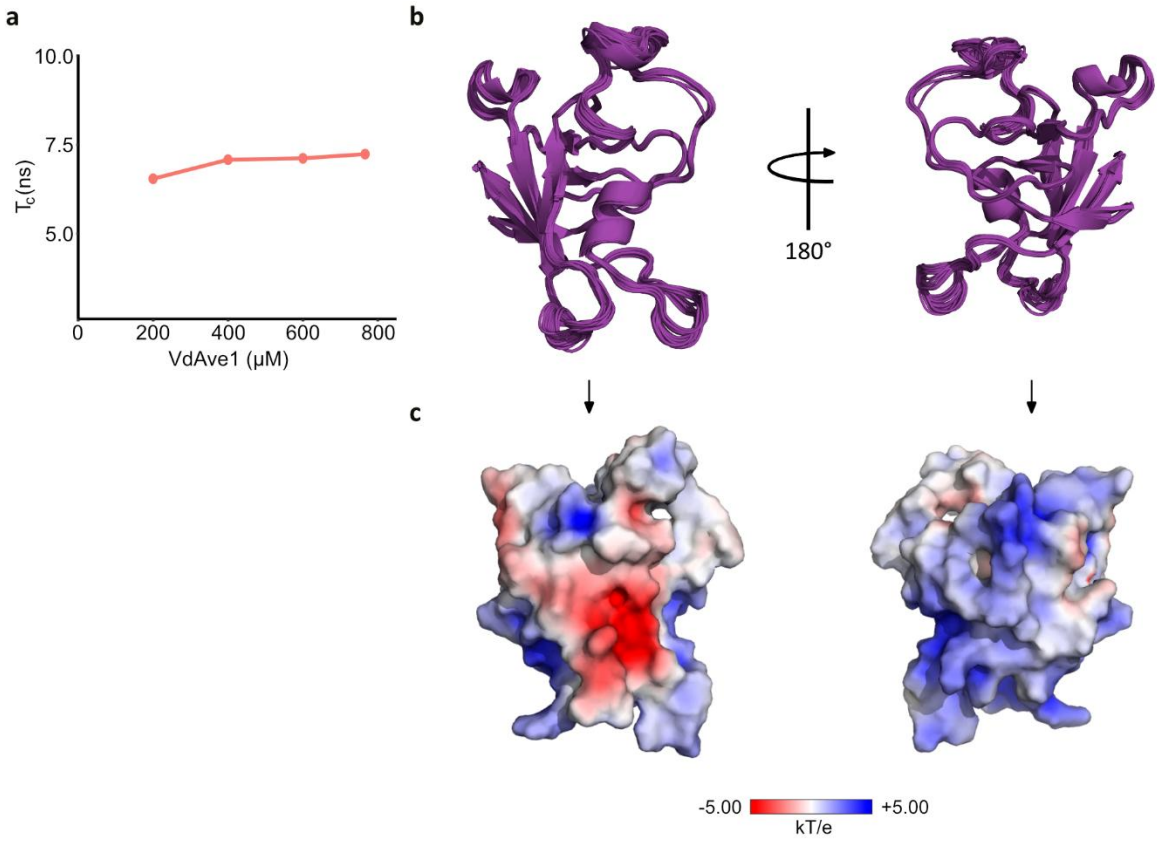

Figure 1. VdAve1 structure solved by liquid-state NMR spectroscopy. a. Rotational correlation times (τ_c) calculated from $^{1}H,^{15}N$ TRACT experiments at different VdAve1 concentrations. **b.** Overlay of the 20 most energetically favored VdAve1 conformers determined by NMR spectroscopy. Structure ensemble has a root mean square deviation of 2.22 Å. The protein global fold comprises two β-sheets forming a β-barrel-like fold flanked by an α-helix. **c.** VdAve1 surface charge distribution depicting positively charged (blue), negatively charged (red) and uncharged (white) regions of the protein.

In an attempt to find leads towards a possible mode of action of VdAve1, we performed a structural homology search with the solved VdAve1 structure, showing that VdAve1 displays homology to domain 1 (D1) of expansins. The top four hits comprised expansins from *Clavibacter michiganensis* (E values = $2.41e^{-4}$ and $2.26e^{-4}$), an alpha-like expansin from *Gossypium hirsutum* (E value = $2.29e^{-3}$) and a beta-expansin from *Zea mays* (E value = $1.28e^{-3}$) (Table 1). Expansins are non-enzymatic plant cell wall-loosening proteins involved in diverse plant developmental processes (Sampedro and Cosgrove 2005), and typically made up of two domains, D1 and D2, with the latter mediating cell wall polysaccharide binding (Georgelis et al. 2012). Cell wall loosening by expansins is thought to be achieved by disrupting non-covalent interactions, which requires the presence of both domains (Georgelis et al. 2011). While the exact molecular mechanism of expansin-mediated cell wall modification and the specific role

of D1 remain to be fully elucidated, the structural homology of VdAve1 to the expansin D1 suggests a potential role in cell wall interactions, such as carbohydrate binding.

Table 1. List of the top four VdAve1 structural homologs.

Description	Organism	Seq. Id.	E-Value
Crystal structure of apo-clavibacter Michiganensis expansin	*Clavibacter michiganensis*	19.4	0.000241
Crystal structure of d78n mutant clavibacter michiganensis expansin in complex with cellohexaose	*Clavibacter michiganensis subsp. michiganensis NCPPB 382*	16.6	0.000226
Crystal structure of cotton alpha-like expansin GhEXLA1	*Gossypium hirsutum*	20.1	0.00229
Crystal structure of EXPB1 (Zea m 1), a beta-expansin and group-1 pollen allergen from maize	*Zea mays*	16.9	0.00128

VdAve1 induces dissipation of *Bacillus subtilis* cell membranes

Many cationic AMPs exert their antimicrobial activity by targeting plasma membranes (Ciumac et al. 2019). Based on its overall net positive charge, we speculated that a similar mechanism is employed by VdAve1. Assessing membrane depolarization gives indication of whether a compound targets the cell membrane. To this end, we monitored the cellular localization of the cell division regulator protein MinD upon incubation of *B. subtilis* with VdAve1 (Marston et al. 1998). MinD accumulates at the cell poles and division sites by associating to the plasma membrane in a membrane potential-dependent manner (Marston et al. 1998). Consequently, MinD localization using fluorescence microscopy following a MinD-GFP reporter strain has been used as a proxy of membrane depolarization (Eun et al. 2012; Müller et al. 2016; Wenzel et al. 2013). Interestingly, after 10 minutes of incubation with VdAve1, clear delocalization of MinD-GFP from the cell poles and cell division sites was observed (Figure 2a). In contrast, exposure to water or the unrelated *V. dahliae* effector protein Vd-D that is not known to possess antimicrobial activity (Li 2019), did not lead to MinD-GFP delocalization (Figure 2a). These findings suggest that VdAve1 induces dissipation of *B. subtilis* plasma membranes.

Several positively charged membrane-active antimicrobial proteins exert their activity by establishing electrostatic interactions with negatively charged target molecules on, or in close proximity to, the plasma membrane. Antimicrobial proteins relying on these interactions are often characterized by salt sensitivity, as the presence of positively charged ions reduces the electrostatic interaction with the negatively charged target (Aerts et al. 2008; Yeaman and

Yount 2003). Given its positive charge, we hypothesized that VdAve1 activity similarly requires electrostatic interactions. To test this, we monitored *B. subtilis* growth inhibition by VdAve1 in the presence of different salts at various concentrations. Interestingly, increasing concentrations of Na^+ reduced VdAve1 activity and concentrations as low as 6.25 mM of Mg^{2+} and Ca^{2+} completely abolished its activity (Figure 2b), indicating that VdAve1 displays strong sensitivity to positively charged ions. Thus, VdAve1 salt-sensitivity suggests that the protein targets a negatively charged component of the bacterial cell envelope through electrostatic interactions.

To investigate whether the bactericidal activity of VdAve1 is a consequence of direct action on the plasma membrane, we tested its activity on fungal protoplasts. Even though plasma membrane compositions differ between fungi and bacteria, many membrane-targeting AMPs display both antibacterial and antifungal activity (Ciumac et al. 2019). Notably, VdAve1 caused lysis of the protoplast from the fungal species *Trichoderma viride* and *Monilinia fructicola* (Figure 2c). Collectively, these findings indicate that VdAve1 displays membrane-lytic activity.

Many cationic AMPs disrupt membranes through the formation of pores (Kim et al. 2022), leading to complete depolarization of the membrane (Spindler et al. 2011). To further study the effect of VdAve1 on plasma membranes, we analyzed its killing kinetics on *B. subtilis.* To this end, we incubated *B. subtilis* with the fluorescence potentiometric probe $DiSC_3(5)$ (Te Winkel et al. 2016) and monitored the release of fluorescence as a means of membrane depolarization. The pore-forming peptides gramicidin A, B and C were used as positive controls and caused immediate membrane depolarization (Figure 2d), in a fashion observed for pore-forming compounds (Barbour et al. 2016). Interestingly, VdAve1 induced a gradual membrane depolarization (Figure 2d), suggesting that membrane disruption is not achieved through pore formation.

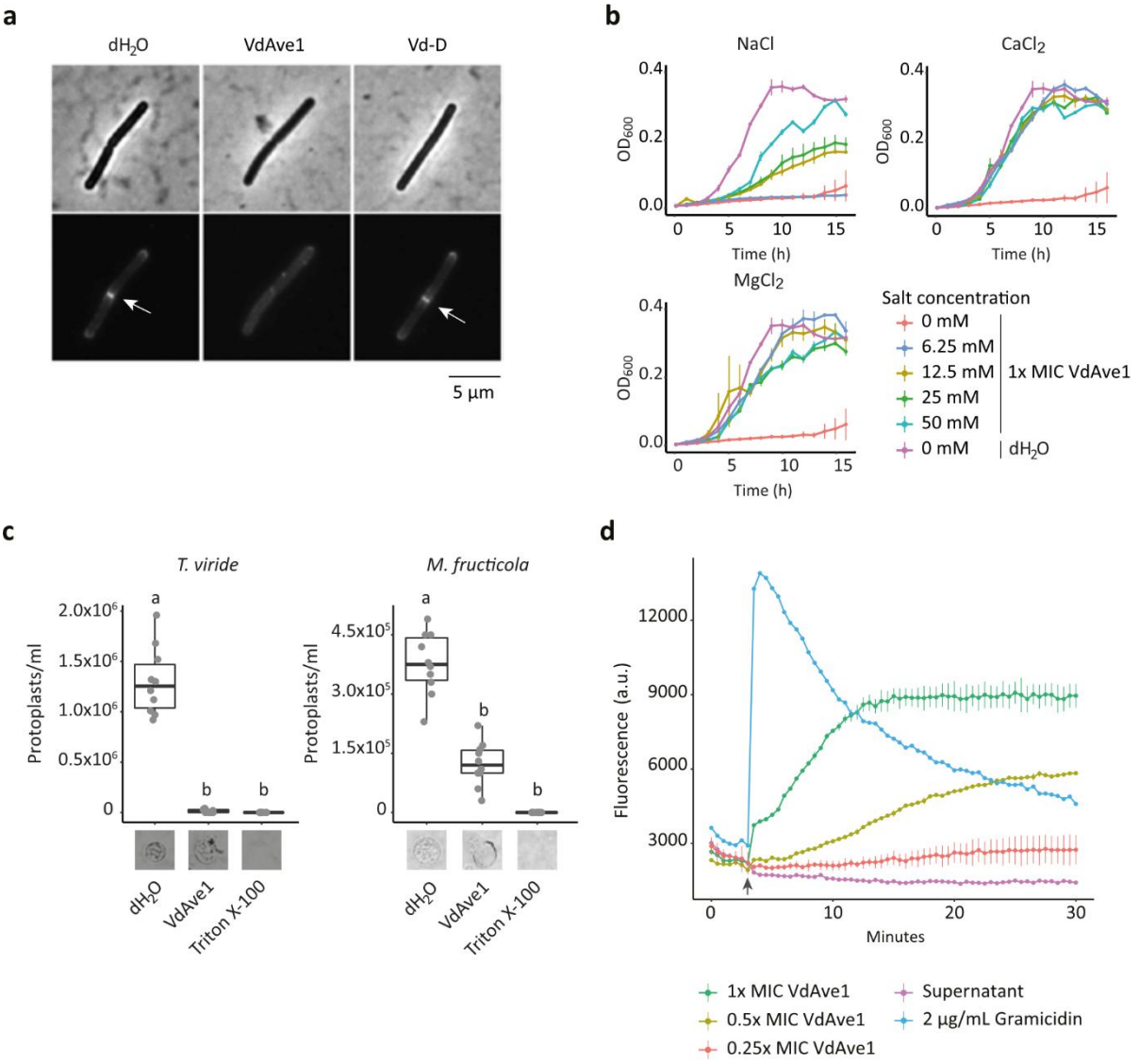

Figure 2. VdAve1 induces dissipation of *Bacillus subtilis* cell membranes. a. Cellular localization of the cell division regulator protein MinD-GFP in a *B. subtilis* reporter strain, upon 10 min of incubation with VdAve1, Vd-D or water. Treatment with 8 µM of VdAve1 induced delocalization of MinD-GFP from the cell poles and cell division sites. **b.** VdAve1 displays sensitivity to positively charged ions. VdAve1 activity on *B. subtilis* was tested in the presence of increasing NaCl, $CaCl_2$ and $MgCl_2$ concentrations. Growth curves represent mean OD_{600} values ± standard deviation (n=3). **c.** VdAve1 causes lysis of protoplasts from the fungal species *Trichoderma viride* and *Monilinia fructicola*. Triton X-100 was used as positive control. Representative pictures of the corresponding protoplasts are displayed under the boxplots. Different letter labels represent statistically significant differences according to one-way ANOVA and Tukey's post-hoc test; $p<0.0001$, N=10. **d.** VdAve1 induces gradual depolarization of *B. subtilis* cell membranes. Release of the fluorescence potentiometric probe $DiSC_3(5)$ was monitored over time as a means of membrane depolarization after incubation with different VdAve1 concentrations or the pore-forming peptides gramicidin. The arrow indicates the time point of protein administration. Graphs represent mean values ± standard deviation (n=3).

VdAve1 displays broad-spectrum activity

Membrane-targeting AMPs are usually characterized by broad-spectrum activity. The observed activity of VdAve1 on *B. subtilis* membranes, as well as the induced lysis of *T. viride* and *M. fructicola* protoplasts, led us to hypothesize that VdAve1 may have a broader activity spectrum. To explore this hypothesis, we tested the activity of VdAve1 against the yeast *Cyberlindnera jadinii* as well as the filamentous fungi *Alternaria brassicicola* and *Cladosporium cucumerinum*. Interestingly, growth of all fungi was inhibited by VdAve1 (Figure 3a,b), indicating that VdAve1 has antifungal activity. The broad-spectrum activity exhibited by VdAve1 suggests that its inhibitory effect extends beyond bacteria and fungi. To this end, we examined the effect of VdAve1 on the amoeba *Leptophrys vorax*. This amoeba has different life stages that are characterized by distinct cellular morphologies. Motile trophozoites are able to feed on algae by engulfing entire cells and finally forming immobile digestive cysts. Mature cysts hatch, releasing a motile trophozoite and leaving an empty cyst (Hess et al. 2012). To test VdAve1 activity on *L. vorax*, we treated a suspension of immobile digestive cysts with VdAve1. After 24 h of incubation, *L. vorax* cysts hatched in the negative control, releasing trophozoites and empty cysts, whereas VdAve1 treatment impeded hatching of the cysts (Figure 3c). Finally, we examined the effect of VdAve1 on mammalian cells. To this end, we incubated VdAve1 with human colon cancer (HCT116) cells. VdAve1 did not suppress cell growth, in contrast to the positive control, 5-FU, which effectively inhibited proliferation (Figure 3d).

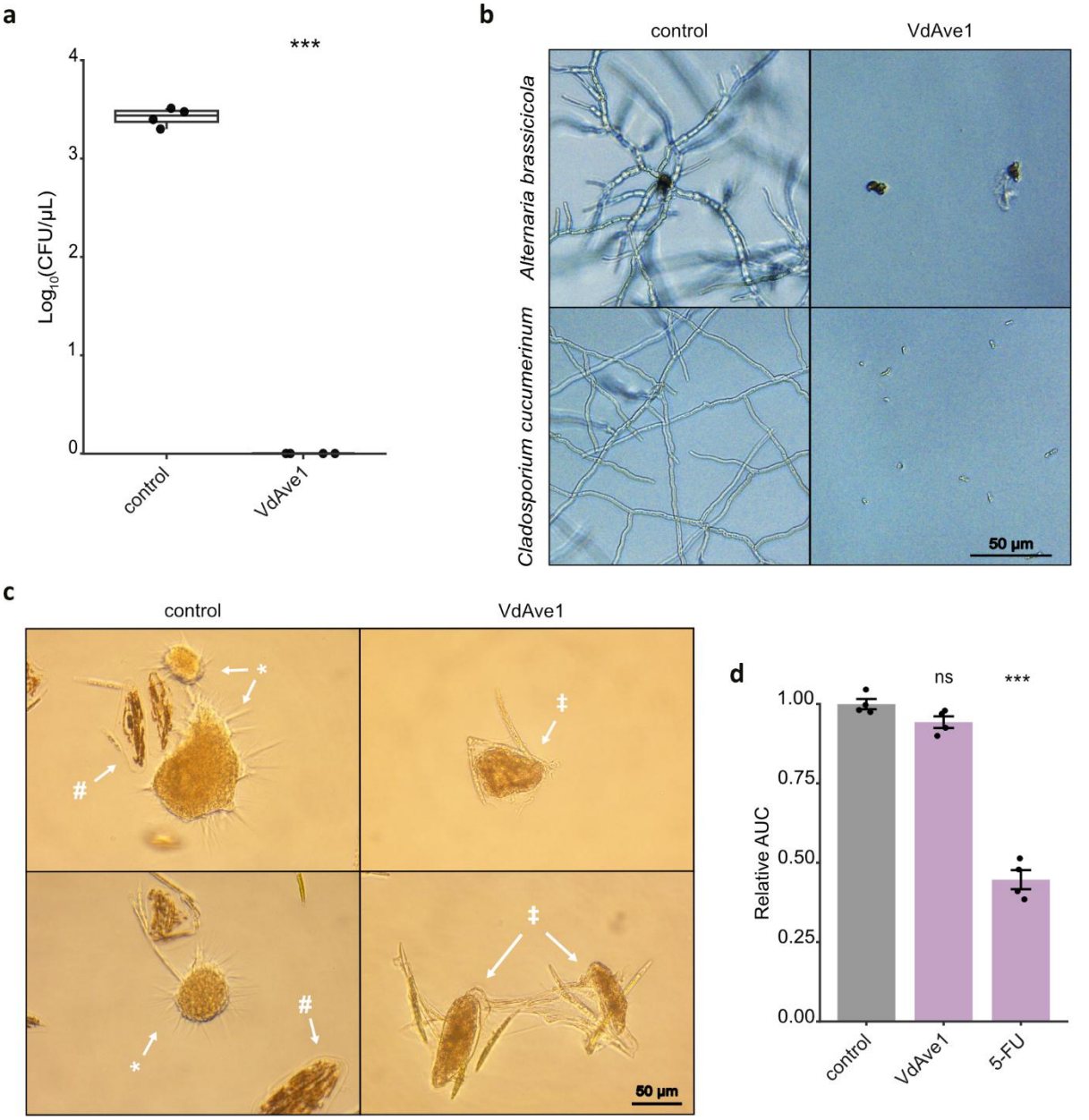

Figure 3. VdAve1 has broad-spectrum activity. a. Antifungal activity test of VdAve1 against the yeast *Cyberlindnera jadinii*. Upon 24 h incubation with VdAve1, yeast cultures were plated and colony-forming units (CFUs) were determined. Data is shown as $\log_{10}(x)$-transformed CFUs (n=4), individual data points are shown (n=4) Statistical significance was assessed by one-way ANOVA and post-hoc Tukey HSD test (***$P \leq 0.001$). **b.** Antifungal activity test of VdAve1 against the filamentous fungi *Alternaria brassicicola* and *Cladosporium cucumerinum*. Representative microscopic pictures of the fungal isolates after 24h incubation with VdAve1. **c.** Representative microscopic pictures of a *Leptophrys vorax* culture of immobile digestive cysts treated with VdAve1. *L. vorax* immobile digestive cysts hatched in the negative control, leaving free trophozoites (*) and empty cysts (#), whereas VdAve1 treatment impeded hatching of the immobile digestive cysts (‡). Pictures were taken after 24 h of incubation. **d.** VdAve1 activity test on human colon cancer cells, HCT 116. The plot shows area under the growth curve (AUC) of HCT 116 treated with VdAve1 or the positive control, 5-FU, relative to the negative control. Bars indicate means, error bars represent standard errors, individual data points are shown (n=4). Statistical significance was assessed by one-way ANOVA and post-hoc Tukey HSD test (***$P \leq 0.001$; ns, not significant).

VdAve1-derived cationic peptides display antimicrobial activity

To investigate whether specific regions of VdAve1 are responsible for the membrane disruption that is observed in *B. subtilis*, we designed partially overlapping 20 amino acid-long VdAve1-derived peptides that collectively span the mature protein sequence (Table 2) and screened them for antimicrobial activity. Strikingly, two peptides, aa41-60 and aa101-116 completely inhibited *B. subtilis* growth (Figure 4a). Interestingly, the VdAve1-derived peptides that display antimicrobial activity are predicted to have the highest positive charge; +4.91 for aa41-60 and +3.09 for aa101-116. In the 3D structure of VdAve1, these two peptides form two separate antiparallel, surface-exposed, beta strands that localize adjacent to each other (Figure 4b). Collectively, these findings suggest that these regions can directly interact with, and consequently perturb, bacterial plasma membranes.

Next, we focused on the characterization of the antimicrobial activity of peptide aa41-60, showing the highest charge. We first narrowed down the active region of the peptide by screening truncated versions for antimicrobial activity against *B. subtilis* (Table 2): aa41-60 (20 aa-long, +4.91 charge), aa43-58 (16 aa-long, +4.91 charge), aa46-58 (13 aa-long, +4.95), and aa45-54 (10 aa-long, +3.91). Interestingly, the antimicrobial activity of the peptides correlated with their charge and length, with a 13 aa-long peptide, aa46-58, showing the strongest bacterial growth inhibition (Figure 4c). To elucidate the antimicrobial activity of this peptide, we tested whether individual residues contribute to its activity. To this end, we mutated single amino acids (Table 2) and screened the mutants for loss of antimicrobial activity against *B. subtilis*. Interestingly, all mutated peptides equally inhibited bacterial growth (Figure 4d), indicating that the antimicrobial activity cannot be assigned to a particular amino acid.

Next, we investigated whether the activity of peptide aa46-58 depends on its charge. As this peptide has five positively charged residues, we gradually decreased its charge by gradually replacing an increasing number of positively charged residues with alanines, resulting in peptides with positively charged residues ranging from four to zero. Interestingly, the antimicrobial activity decreased with decreasing positive charge and was completely lost when four of the five positively charged residues were mutated (Figure 4e).

Next, we tested whether side chain properties of the positively charged residues are relevant for the antimicrobial activity of this peptide. To this end, we replaced positively charged residues of the peptide with another positively charged amino acid, replacing arginines (R)

with lysines (K) and *vice versa*, resulting in a peptide with the same overall charge but opposite R to K ratio (Table 2; Figure 4e). Interestingly, the peptide retained its antimicrobial activity, suggesting that the activity depends on the presence of positively charged residues, irrespective from their side chains.

To test whether peptide aa46-58 function is sequence-dependent, we randomized its sequence, resulting in a peptide with the same length and amino acid composition but with a different amino acid order (Table 2). Interestingly, the scrambled peptide completely inhibited bacterial growth (Figure 4e), suggesting that the activity of the peptide does not dependent on the exact amino acid sequence, but rather on other physicochemical properties provided by the amino acids, such as charge. Additionally, it suggests that the antimicrobial activity of the peptide does not rely on sequence-specific interactions, like receptor-binding. Overall, our findings suggest that the antimicrobial activity of aa46-58 depends on its net charge.

Table 2. List of peptides used in this study.

ID	Sequence
aa1-20	DLGTASYYNPPYLPTACGGS
aa11-30	PYLPTACGGSNPSQFPSGNL
aa21-40	NPSQFPSGNLFVAVSDGLWD
aa31-50	FVAVSDGLWDNGAACGRRYR
aa41-60	NGAACGRRYRIKCLSGARGS
aa51-70	IKCLSGARGSCKDGMIDVRV
aa61-80	CKDGMIDVRVVDRAKTTVTK
aa71-90	VDRAKTTVTKAAHKATMILS
aa81-100	AAHKATMILSQDSYDAIVNQ
aa91-110	QDSYDAIVNQWKGTRHKAVN
aa101-116	WKGTRHKAVNIEFRQI
aa43-58	AACGRRYRIKCLSGAR
aa46-58	GRRYRIKCLSGAR
aa45-54	CGRRYRIKCL
aa45-53	CGRRYRIKC
aa47-52	RRYRIK
G1A	ARRYRIKCLSGAR
R2A	GARYRIKCLSGAR

ID	Sequence
R3A	GRAYRIKCLSGAR
Y4A	GRRARIKCLSGAR
R5A	GRRYAIKCLSGAR
I6A	GRRYRAKCLSGAR
K7A	GRRYRIACLSGAR
C8A	GRRYRIKALSGAR
L9A	GRRYRIKCASGAR
S10A	GRRYRIKCLAGAR
G11A	GRRYRIKCLSAAR
R13A	GRRYRIKCLSGAA
5 (+) aa	GRRYRIKCLSGAR
4 (+) aa	GRRYRIACLSGAR
3 (+) aa	GRRYAIACLSGAR
2 (+) aa	GRAYAIACLSGAR
1 (+) aa	GAAYAIACLSGAR
0 (+) aa	GAAYAIACLSGAA
(+) aa swapped	GKKYKIRCLSGAK
scrambled	RSRCIGLGRKAYR

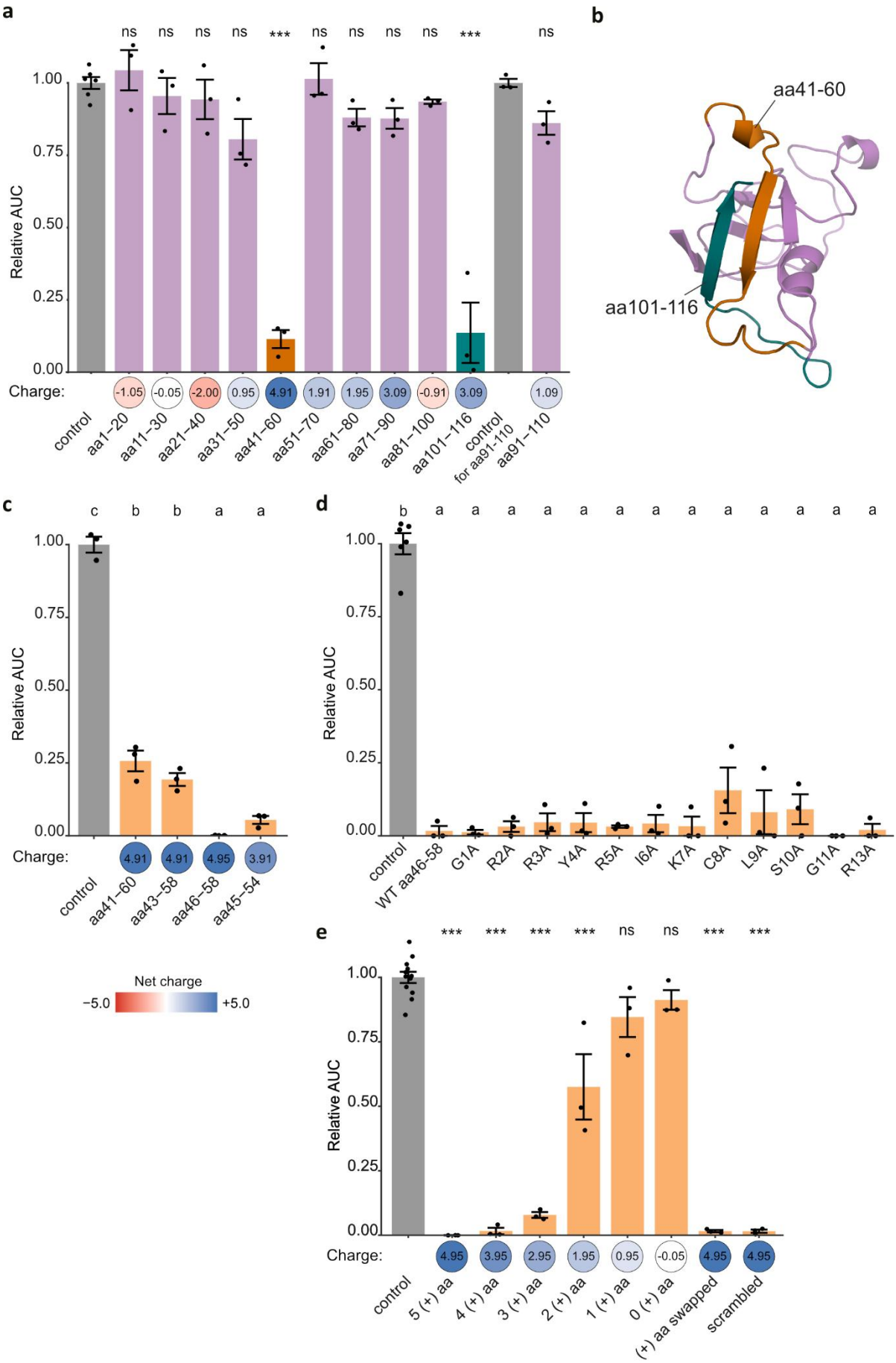
a
ns ns ns ns *** ns ns ns ns *** ns
1.00
0.75
0.50
0.25
0.00
Relative AUC
Charge:
-1.05 -0.05 -2.00 0.95 4.91 1.91 1.95 3.09 -0.91 3.09 1.09
control
aa1–20
aa11–30
aa21–40
aa31–50
aa41–60
aa51–70
aa61–80
aa71–90
aa81–100
aa101–116
control for aa91-110
aa91–110
b
aa41-60
aa101-116
c
c b b a a
Relative AUC
Charge:
4.91 4.91 4.95 3.91
control
aa41–60
aa43–58
aa46–58
aa45–54
Net charge
−5.0
+5.0
d
b a a a a a a a a a a a a a
Relative AUC
control
WT aa46-58
G1A
R2A
R3A
Y4A
R5A
I6A
K7A
C8A
L9A
S10A
G11A
R13A
e
*** *** *** *** ns ns *** ***
Relative AUC
Charge:
4.95 3.95 2.95 1.95 0.95 -0.05 4.95 4.95
control
5 (+) aa
4 (+) aa
3 (+) aa
2 (+) aa
1 (+) aa
0 (+) aa
(+) aa swapped
scrambled

Figure 4. VdAve1-derived cationic peptides display antimicrobial activity. a. Antimicrobial activity test of 20 aa long partially overlapping peptides that collectively span the mature VdAve1 sequence against *B. subtilis*. Peptides aa41-60 (orange bar) and aa101-116 (petrol bar) significantly reduced *B. subtilis* growth. The plot shows area under the growth curve (AUC) of *B. subtilis* treated with the respective peptide relative to the corresponding control. Bars indicate means, error bars represent standard errors, individual data points are shown (n=6 for the control, n=3 for all others). Statistical significance was assessed by one-way ANOVA and post-hoc Tukey HSD test (***$P \leq 0.001$; ns, not significant). Charges of corresponding peptides are displayed below the bar plot. **b.** VdAve1 structure indicating the regions corresponding to the antimicrobial peptides: aa41-60 (orange) and aa101-116 (petrol). **c.** Antimicrobial activity test of truncated variants of peptide aa41-60. Plot shows area under the growth curve (AUC) of *B. subtilis* treated with the respective peptide relative to the control. Bars indicate means, error bars represent standard errors, individual data points are shown (n=3). Letters indicate significant differences based on one-way ANOVA and post-hoc Tukey HSD test. Charges of corresponding peptides are displayed below the bar plot. **d.** Antimicrobial activity test of single amino acid mutants of peptide aa46-58. The plot shows area under the growth curve (AUC) of *B. subtilis* treated with the respective peptide relative to the control treatment. Bars indicate mean, error bars represent standard error, individual data points are shown (n=6 for the control, n=3 for all others). Different letter labels indicate significant differences based on one-way ANOVA and post-hoc Tukey HSD test. **e.** Antimicrobial activity test of aa46-58 mutated in increasing number of positively charged residues as well as a randomized version of the peptide. The plot shows area under the growth curve (AUC) of *B. subtilis* treated with the respective peptide relative to the control treatment. Bars indicate mean, error bars represent standard error, individual data points are shown (n=12 for the control, n=3 for all others). Statistical significance was assessed by one-way ANOVA and post-hoc Tukey HSD test (***$P \leq 0.001$; ** $P \leq 0.001$; * $P \leq 0.05$; ns, not significant). Charges of corresponding peptides are displayed below the bar plot.

Antimicrobial activity of the VdAve1-derived peptide against a Gram-negative bacterium

It was previously shown that VdAve1 has antimicrobial activity against Gram-negative bacteria (Snelders et al. 2020). To investigate whether our findings on the activity of aa46-58 also extends to Gram-negative bacteria, we tested the peptide aa46-58 and its single amino acids mutants (Table 2) against *Sphingopyxis macrogoltabida* (Figure 5). Surprisingly, substitution of the cysteine with alanine, C8A, completely impaired the peptide activity. Since cysteine and alanine differ in their chemical properties, this loss of activity may be a result of structural alterations in the peptide. To minimize structural disruption, we replaced cysteine with serine (C8S), a biochemically similar amino acid that retains polarity but lacks a thiol group, and tested it for inhibition of *S. macrogoltabida* growth. Interestingly, replacement of the cysteine with serine did not restore the peptide activity (Figure 5), suggesting that the presence of the thiol group, which can form disulfide bonds, is crucial for the activity of the peptide against *S. macrogoltabida.*

Next, we investigated whether the antimicrobial activity of aa46-58 against *S. macrogoltabida* depends on its charge. To this end, we tested the ability of the aa46-58 mutant which lacks positively charged amino acids to inhibit *S. macrogoltabida* growth. Interestingly, the antimicrobial activity was completely lost when the positively charged amino acids were mutated (Figure 5), indicating that the activity of the peptide depends on its charge also in the case of Gram-negative bacteria.

To assess whether the peptide antimicrobial activity against *S. macrogoltabida* relies on its precise amino acid sequence, we tested the activity of the scramble peptide against *S. macrogoltabida* (Table 2). Also against this bacterium, the scramble peptide retained its antimicrobial activity (Figure 5), confirming that the activity of the peptide does not dependent on its exact amino acid sequence. Furthermore, the retention of the antimicrobial activity of the scramble peptide indicates that the cysteine contribution to the peptide activity is independent of its position in the peptide sequence.

Overall, our findings indicate that the antimicrobial activity of peptide aa46-58 against *S. macrogoltabida* depends on both its charge and presence of a cysteine, possibly required for disulfide bridges between two peptides, leading to the formation of a dimer with a further increased overall molecular charge.

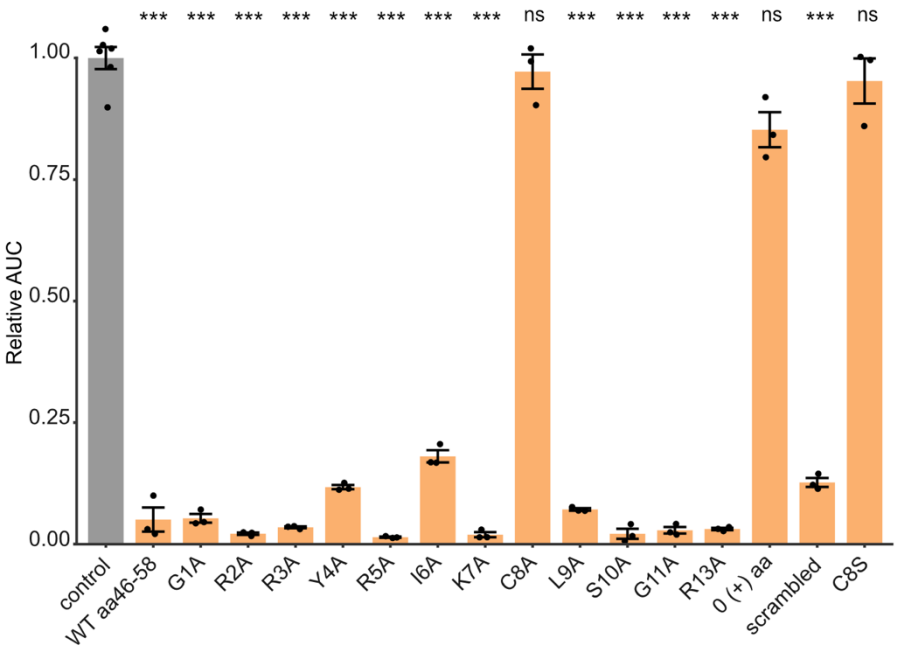

Figure 5. VdAve1 derived peptide activity against *Sphingopyxis macrogoltabida*. Antimicrobial activity test of peptide aa46-58 and its mutants. The plot shows area under the growth curve (AUC) of *S. macrogoltabida* treated with the respective peptide relative to the control treatment. Bars indicate

mean, error bars represent standard error, individual data points are shown (n=6 for the control, n=3 for all others). Statistical significance was assessed by one-way ANOVA and post-hoc Tukey HSD test (***$P \leq 0.001$; ** $P \leq 0.001$; * $P \leq 0.05$; ns, not significant).

Identification of genes involved in the response and resistance to VdAve1

To improve our understanding of the mode of action of VdAve1, we examined transcriptional changes of *B. subtilis* upon exposure to sub-minimal inhibitory concentrations of the protein, 0.5x MIC (Snelders et al. 2020). To capture immediate transcriptional changes that provide insight into the bacterial response to the protein, we collected bacterial cells after 5- and 20-minutes of incubation with 0.5x MIC of VdAve1. The *sigV* operon genes, *sigV*, *rsiV*, *oatA* and *yrhK*, were the most strongly induced genes in response to VdAve1 at both time points (Table 3). Interestingly, the *sigV* gene encodes the σ^V sigma factor which regulates genes involved in peptidoglycan modifications and it was previously implicated in resistance to lysozyme (Ho et al. 2011). One of the sigV operon genes, *oatA,* mediates O-acetylation of peptidoglycan which hinders lysozyme activity (Guariglia-Oropeza and Helmann 2011). Besides its own operon, σ^V mediates induction of the *dlt* operon, which encodes proteins that mediate D-alanylation of teichoic acids (Guariglia-Oropeza and Helmann 2011). Accordingly, we also observed the induction of the entire *dlt* operon in response to VdAve1 treatment. Moreover, exposure to VdAve1 led to the induction of genes involved in cation export, such as *ydbO*, *cadA*, *ykkD* and *nhaK* (Fujisawa et al. 2005; Jack et al. 2000; Kunst et al. 1997; Tsai et al. 1992) (Table 4). Cation export might hinder electrostatic interactions between VdAve1 and its potential negatively charged target, in a similar fashion as observed when testing VdAve1 activity in the presence of salts (Figure 2b). Finally, the phospholipid desaturase *des*, which increases membrane fluidity (Aguilar et al. 1998), was downregulated in response to VdAve1, suggesting that VdAve1 increases membrane fluidity.

Table 3. The ten most strongly induced *B. subtilis* genes in response to 0.5x MIC of VdAve1.

	5 minutes		20 minutes	
Gene	Log2FC VdAve1/ MQ	Adjusted p value	Log2FC VdAve1/ MQ	Adjusted p value
sigV	5.04	9.08E-150	6.19	5.97E-186
rsiV	4.72	2.20E-112	5.67	5.09E-211
oatA	4.26	8.48E-213	5.35	0.00E+00
yrhK	4.21	1.72E-52	4.72	8.74E-108
ymaE	3.84	7.59E-75	2.65	1.38E-23
ymzB	3.70	3.45E-60	2.36	1.78E-13
ydbO	2.11	2.21E-22	2.33	1.40E-72
maeA	1.65	6.71E-06	2.01	3.22E-22
mmgD	1.51	1.09E-14	1.99	7.47E-09
bcrC	1.50	1.08E-10	1.99	2.40E-49

Table 4. Selected differentially expressed *B. subtilis* genes upon incubation with 0.5x MIC of VdAve1.

		5 minutes		20 minutes	
	Gene	Log2FC VdAve1/ MQ	Adjusted p value	Log2FC VdAve1/ MQ	Adjusted p value
SigV operon	*sigV*	4.72	2.20E-112	6.19	5.97E-186
	rsiV	5.04	9.08E-150	5.67	5.09E-211
	oatA	4.26	8.48E-213	5.35	0.00E+00
	yrhK	3.70	3.45E-60	4.72	8.74E-108
Cell wall	*cwlO*	-1.96	9.98E-55	0.15	0.57
metabolism	*lytE*	-1.26	2.87E-22	0.32	6.53E-02
	iseA	4.21	1.72E-52	1.95	5.58E-11
Teichoic acid	*dltA*	0.34	2.79E-03	0.85	4.17E-20
synthesis or	*dltB*	0.23	0.29	0.80	1.34E-09
modification	*dltC*	0.16	0.47	0.77	9.05E-11
	dltD	0.33	5.52E-03	0.80	3.02E-17
	dltE	0.32	4.19E-02	0.85	4.33E-13
	tagT	0.68	1.86E-09	0.75	1.77E-11
	ugtP	0.33	4.54E-02	0.32	3.82E-02
	yfnI	0.53	2.42E-06	0.47	2.68E-05
Cation export/uptake	*cadA*	0.81	3.85E-06	0.18	0.57
	ydbO	0.90	2.51E-10	2.33	1.40E-72
	ykkD	0.81	9.26E-03	0.35	0.45
	nhaK	-0.07	0.91	1.01	9.53E-07
Membrane fluidity	*des*	-1.15	2.46E-06	0.02	0.98

To further substantiate the involvement of the differentially expressed genes in protection to VdAve1, and find a possible molecular binding target, we generated a transposon insertion library and screened for mutants with differential sensitivity to VdAve1. To this end, the *B. subtilis* transposon insertion library was incubated with either VdAve1 or ultrapure water and, after a total of nine generations, bacterial cells were harvested and sequenced. Consistent with the transcriptome analysis, mutagenesis of the σ^V-regulated genes *oatA* and *dltA-E* led to enhanced sensitivity to VdAve1 (Table 5). Similarly, disruption of *rsiV*, which regulates σ^V activity (Zellmeier et al. 2005), significantly improved survivability in the presence of VdAve1. Disruption of additional genes involved in teichoic acid synthesis or modification, such as *galE*, *gtaB*, and *ugtP* (Jorasch et al. 1998; Soldo et al. 2003; Yasbin et al. 1976), resulted in increased sensitivity to VdAve1. Moreover, the inactivation of genes implicated in cell wall integrity or metabolism, the peptidase genes *pbpX*, *cwlO* and *dacA* (Atrih et al. 1999; Wilson et al. 2023; Yamaguchi et al. 2004), increased sensitivity to VdAve1. Interestingly, inactivation of *rsiX*, which regulates the sigma factor of *SigX* (Brutsche and Braun 1997) (Table 5), enhanced *B. subtilis* tolerance to VdAve1, suggesting that genes within the *SigX* regulon also contribute to protection against VdAve1. It was previously shown that *SigX* contributes to resistance to cationic antimicrobial peptides by regulating cell surface modifications through the activation of other operons, including the *dlt* operon (Helmann 2016). Even though we could not identify a specific molecular target at the cell envelope, the transposon screen corroborated the relevance of genes involved in cell envelope modification for tolerance of *B. subtilis* to VdAve1 treatment.

Table 5. Genes affecting *B. subtilis* sensitivity to VdAve1 identified by transposon sequencing.

	Gene	Relative fitness VdAve1/ MQ	Adjusted p value
SigV operon	*rsiV*	2.61	2.53E-18
	oatA	0.68	1.75E-05
Cell wall metabolism	*pbpX*	1.90E-02	1.56E-235
	cwlO	2.66E-03	9.25E-94
	dacA	0.16	1.10E-26
Teichoic acid synthesis or modification	*dltA*	1.76E-03	1.74E-292
	dltB	9.86E-03	0.00E+00
	dltC	2.52E-03	2.47E-65
	dltD	2.59E-03	0.00E+00
	dltE	0.27	1.77E-24
	galE	8.72E-02	5.29E-150
	gtaB	0.24	1.60E-21
	ugtP	0.12	4.25E-45
Other genes	*greA*	0.16	3.41E-18
	miaA	0.31	4.70E-08
	rsiX	2.36	1.06E-16

VdAve1 does not hydrolyse peptidoglycan

The transcriptome analysis and transposon screen resulted in the identification of the *SigV* operon as a key player in the response of *B. subtilis* to VdAve1. Notably, *SigV* has previously been implicated in *B. subtilis* resistance to lysozyme treatment (Ho et al. 2011). Additionally, the bacterial response to VdAve1 involved genes associated with teichoic acid modification and biosynthesis, which are also known to contribute to lysozyme resistance (Ho et al. 2011). These parallels between the *B. subtilis* responses to VdAve1 and lysozyme suggest that VdAve1 may function as a lysozyme. To test this hypothesis, we performed high-performance liquid chromatography (HPLC) of *B. subtilis* peptidoglycan incubated with VdAve1. The elution profile did not show distinct peaks corresponding to muropeptides, indicating that VdAve1 alone does not degrade peptidoglycan in a lysozyme-like manner (Figure 6). As a reference, we analyzed muropeptides derived from peptidoglycan digestion with cellosyl, a lysozyme from *Streptomyces coelicolor* (Rau et al. 2001), which exhibited the expected elution profile. To further assess potential muropeptides modifications by VdAve1, we incubated peptidoglycan with both cellosyl and VdAve1. In all control conditions, distinct muropeptide peaks were observed (Figure 6), supporting that VdAve1 does not possess lysozyme-like activity.

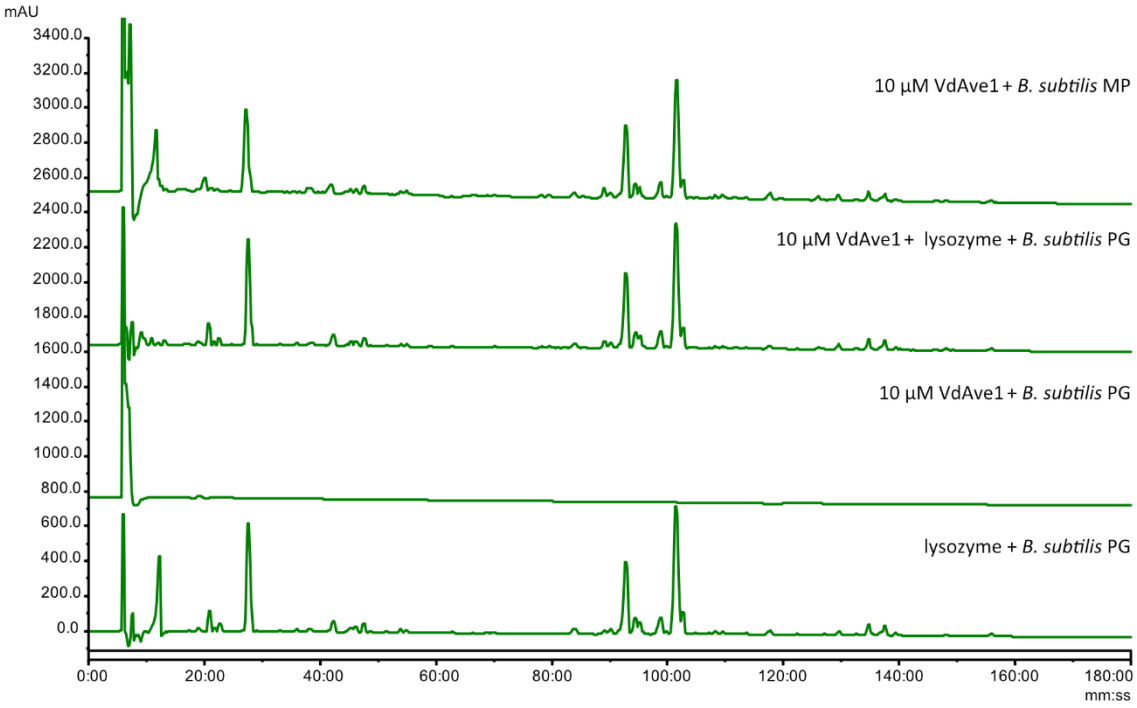

Figure 6. VdAve1 does not hydrolyse peptidoglycan. HPLC analyses of peptidoglycan (PG) from *Bacillus subtilis* incubated with VdAve1 for 16h. The lysozyme cellosyl and muropeptides (MP) generated from cellosyl-digested peptidoglycan were used as controls.

VdAve1 binds lipoteichoic acid

The transcriptomic and transposon screening analysis highlighted the importance of peptidoglycan and teichoic acid modifications for *B. subtilis* tolerance to VdAve1. In order to evaluate possible interactions of VdAve1 with these molecules we performed chemical shift perturbation (CSP) of VdAve1 upon binding in 1H, 15N HSQC spectra. Changes in the chemical shift of the protein amide signals reflect alterations of their chemical environments, typically caused by ligand binding or associated structural changes (Williamson 2013). Exposure to *B. subtilis* peptidoglycan up to concentrations of 1 mg/mL did not lead to CSPs, suggesting that the protein does not bind peptidoglycan (Figure 7a). In contrast, exposure to *B. subtilis* lipoteichoic acid (LTA; 1 mg/mL) induced CSPs in VdAve1 (Figure 7b), suggesting that the protein binds LTA. To shed more light on the interaction of VdAve1 with LTA, we performed chemical shift titrations by gradually increasing the concentration of LTA to 0.2, 0.4, and 0.6 mg/mL and monitored backbone CSP of VdAve1 (Figure 8a). We identified amino acids, such as K84 and A85 (Figure 8a, expanded view), that showed CSP as a function of LTA concentration, suggesting involvement in LTA binding. Next, we calculated the CSPs ($\Delta\delta_{NH}$) of VdAve1 in the absence of LTA when compared with the presence of 0.6 mg/mL LTA for each

backbone amide (Figure 8b) and mapped these changes onto the VdAve1 structure (Figure 8c). The residues experiencing CSPs are found on one side of the VdAve1 structure and we could distinguish two areas with both large CSPs ($\Delta\delta_{NH}>2\sigma$, pink-colored residues in Figure 8c) and small CSPs ($\Delta\delta_{NH}>\sigma$, orange-colored residues in Figure 8c). The residue experiencing the largest CSP is K84, suggesting a potential involvement of this residue in the binding of LTA. We also observed small CSPs ($\Delta\delta_{NH}>\sigma$) in the His-tag used for affinity purification after heterologous expression in *E. coli* (Figure S 1), which might be caused by unspecific interactions or allosteric effects due to LTA binding.

To investigate the relevance of LTA binding for the mode of action of VdAve1, we preincubated VdAve1 with LTA from *B. subtilis* and monitored its antimicrobial activity against *B. subtilis* (Figure 8d). Interestingly, VdAve1 activity was inhibited in the presence of LTA, suggesting that the protein binds LTA and it is therefore not able to reach the bacterial cell envelope and, consequently, unable to inhibit bacterial growth.

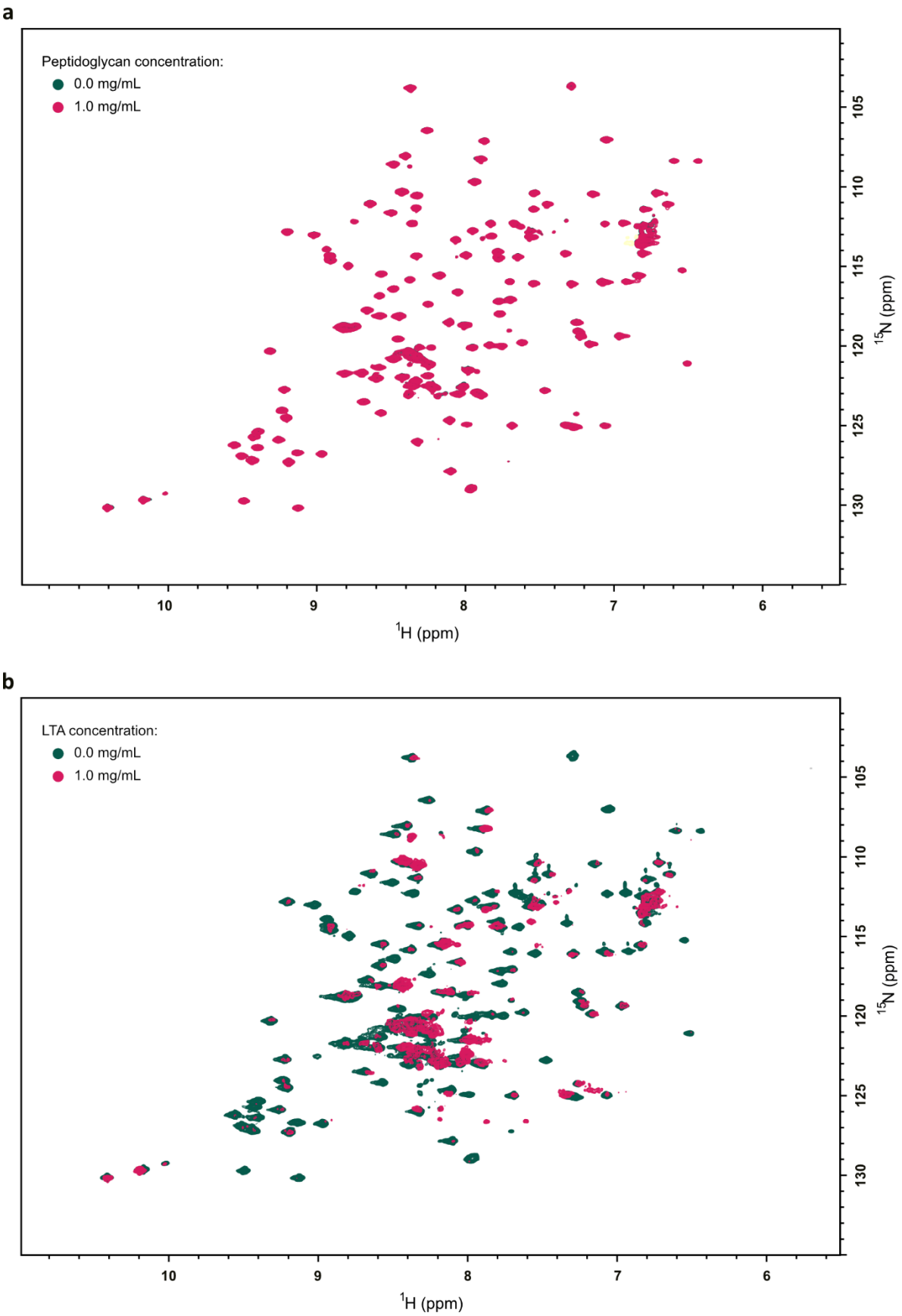

Figure 7. VdAve1 interactions with *Bacillus subtilis* cell wall components. a. ^{1}H,^{15}N HSQC spectra of VdAve1 (green) and VdAve1 with 1 mg/mL peptidoglycan (pink). **b.** ^{1}H,^{15}N HSQC spectra of VdAve1 (green) and VdAve1 with 1 mg/mL LTA (pink).

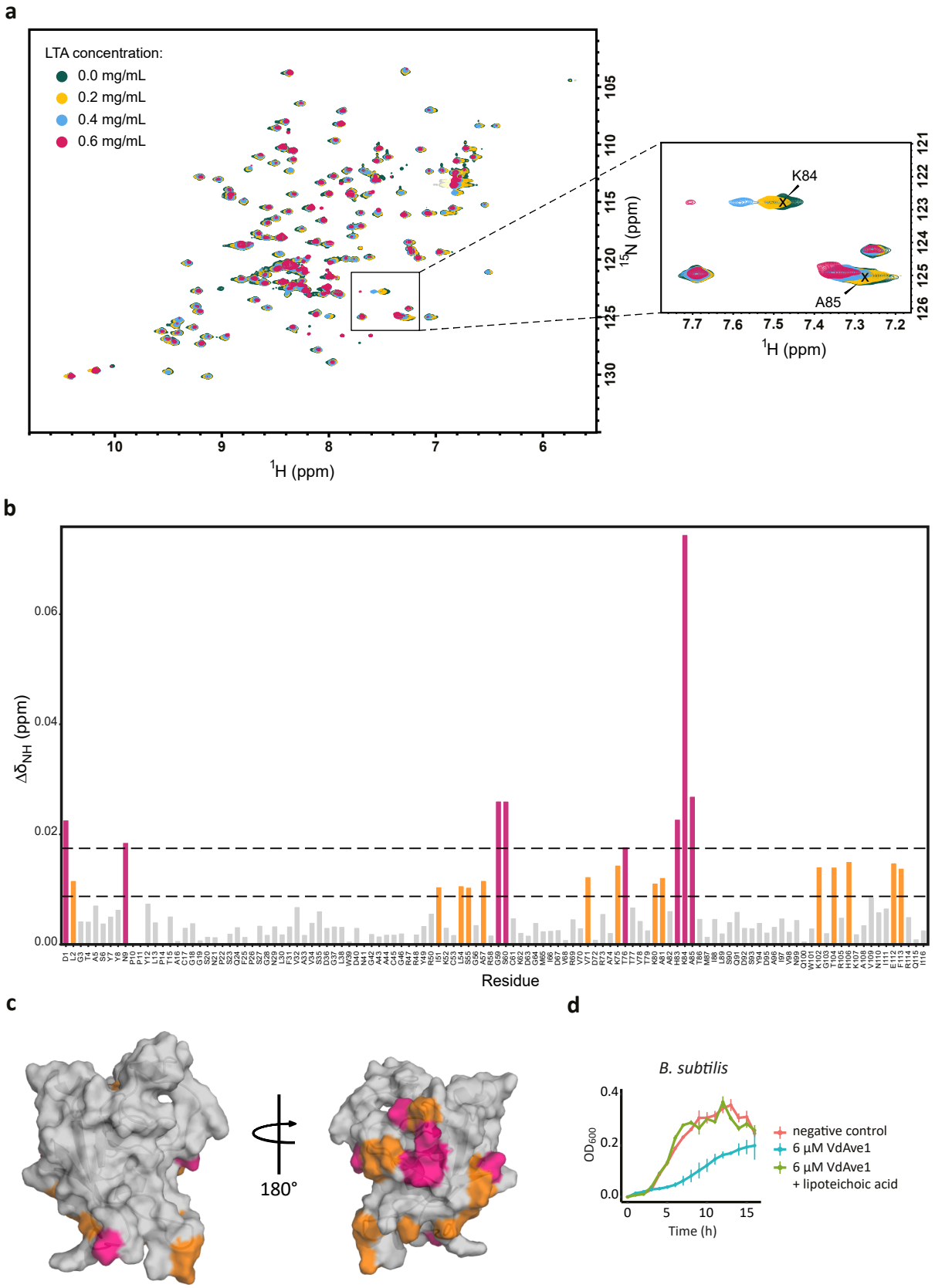

Figure 8. VdAve1 binds lipoteichoic acid. a. ^{1}H, ^{15}N HSQC spectra of VdAve1 upon binding with increasing concentrations of lipoteichoic acid (LTA): 0.0 mg/mL (green), 0.2 mg/mL (yellow), 0.4 mg/mL (cyan), 0.6 mg/mL (pink). Full spectra (left) and the expanded view (right) show peaks perturbations. **b.** Chemical shift perturbations (CSPs) for each VdAve1 residue induced by 0.6 mg/mL LTA. The $\Delta\delta_{NH}$ values were color-coded, $\Delta\delta_{NH}>2\sigma$ pink and $\Delta\delta_{NH}>\sigma$ orange. **c.** CSPs mapped onto VdAve1 structure. **d.**

Preincubation VdAve1 with an equal concentration of LTA from *B. subtilis* inhibits VdAve1 activity. Curves represent mean values ± standard deviation (n=3).

Discussion

Antimicrobial proteins (AMPs) are ancient and widely distributed molecules that play fundamental roles in defence and survival across all forms of life (Ageitos et al. 2017). Irrespective of their diversity in sequence, structure, and mechanism of action, AMPs are generally small, cationic molecules with broad-spectrum antimicrobial activity. They act either by killing microbes, through microbicidal activity, or inhibiting their growth, through microbistatic activity. One of the most common bactericidal strategies employed by AMPs is membrane disruption (Bortolotti et al. 2023). Through their positive charge, electrostatic interactions with negatively charged microbial plasma membranes take place, leading to structural destabilization and membrane leakage that ultimately results in cell death. Various models have been proposed to explain AMP-mediated membrane disruption, which can be broadly classified into pore-forming and non-pore-forming mechanisms. In pore-forming mechanisms, AMPs integrate into the lipid bilayer, and assemble into transmembrane pores that are typically composed of multiple AMP monomers and compromise membrane integrity. In non-pore-forming models, AMPs accumulate on the membrane surface, disrupting its structure (Chen et al. 2023).

We have previously shown that the soil-borne plant pathogen *V. dahliae* makes use of the bactericidal effector protein VdAve1 to suppress bacterial antagonists during host colonization (Snelders et al. 2020). In this study, we investigated the mode of action of VdAve1. Our findings reveal that VdAve1 induces dissipation of the *B. subtilis* plasma membrane, leading to cell leakage and bacterial death. This activity appears to be primarily driven by charge-mediated interactions, as evidenced by the requirement for positively charged residues in active VdAve1-derived peptides. The salt sensitivity of the antimicrobial activity provides further support for a model in which electrostatic interactions facilitate membrane binding. Finally, whereas bacterial, fungal, and amoebic membranes are negatively charged due to the presence of anionic lipids, mammalian membranes predominantly consist of neutral lipids (Josefsson 1966; Rautenbach et al. 2016; Zasloff 2002). The finding that VdAve1 also inhibits fungi and

amoebae, but does not lyse mammalian cells, further supports the hypothesis that VdAve1 selectively interacts with microbial membranes via electrostatic interactions.

To explain the antibacterial activity, we further investigated the activity of VdAve1 on *B. subtilis* and found that genes involved in cell wall modification contribute to *B. subtilis* tolerance to VdAve1 treatment. Particularly, D-alanylation of teichoic acid appeared to be an important contributor to this tolerance. Teichoic acids are negatively charged molecules in the bacterial cell wall, which can be either anchored to the plasma membrane as lipoteichoic acid (LTA) or connected to the cell wall as wall teichoic acid (Percy and Gründling 2014). D-alanylation of these molecules reduces their negative charge, decreasing the electrostatic attraction between cationic AMPs and the bacterial surface (Kristian et al. 2005). The observation that in response to VdAve1 *B. subtilis* induces genes involved in teichoic acid modification led us to hypothesize that these molecules might be a direct target of VdAve1. In support of this hypothesis, we showed that VdAve1 binds purified LTA.

It was previously proposed that membrane-disrupting AMPs interact with cell wall components and cell wall precursors prior to membrane disruption (Malanovic and Lohner 2016). For instance, the membrane disrupting AMP nisin binds lipid II, a precursor for peptidoglycan synthesis, prior to membrane disruption (Breukink et al. 1999). Interestingly, it was shown that lipid II binding, besides inhibiting cell wall biosynthesis, aids membrane permeabilization by nisin (Breukink et al. 1999). Lipid II is anchored in the plasma membrane, positioning AMPs in close proximity to their secondary target and promoting AMP insertion into bacterial membranes (Breukink et al. 1999; Wiedemann et al. 2001). Similarly, LTA has been proposed as a potential AMP interaction site (Malanovic and Lohner 2016). LTA, being anchored in the plasma membrane, may function as a docking platform, facilitating AMP accumulation at the bacterial surface before translocation to the cytoplasmic membrane, where disruption occurs. Several membrane-disrupting AMPs, including the lipopeptide brevibacillin produced by *B. laterosporus*, the peptide lactoferricin B derived from bovine lactoferrin, and the lipopeptide serrawettin produced by *Serratia marcescens*, have been suggested to interact with LTA, as indicated by experiments showing that exogenously added LTA reduces their antimicrobial activity (Decker et al. 2024; Vorland et al. 1999; Yang et al. 2017). However, direct experimental evidence demonstrating LTA binding by these membrane-disrupting AMPs is still lacking.

Building on our findings, we propose a model for VdAve1 mode of action against Gram-positive bacteria in which VdAve1 initially binds LTA, increasing its local concentration at the bacterial surface. From this anchored position, VdAve1 may either directly disrupt the plasma membrane or be released from LTA before interacting with the membrane, ultimately leading to dissipation and cell death. Determining the binding affinity of VdAve1 for LTA could provide insights into whether it remains anchored or is released before exerting its antimicrobial effect.

We previously showed that *V. dahliae* exploits VdAve1 to target bacterial antagonists during host colonization. Bacterial community profiling of host plants infected with *V. dahliae* revealed that VdAve1 inhibits the growth of Gram-negative Sphingomonads (Snelders et al. 2020). While Gram-negative bacteria lack LTA, they possess lipopolysaccharide (LPS). LTA and LPS play essential roles in bacterial envelope integrity and share functional and structural similarities. As amphiphilic molecules they are anchored in the membrane via a glycolipid moiety and carry a strong negative charge (Adams et al. 2014; Percy and Gründling 2014). Therefore, we can speculate that LPS could serve as an alternative binding target for VdAve1 at the outer membrane of Gram-negative bacteria. Interestingly, our data suggest that for the synthesized active VdAve1-derived peptide, in addition to charge-based interactions, cysteine residues are critical for its activity against Gram-negative bacteria. Cysteine is highly nucleophilic and susceptible to oxidation, allowing the formation of covalent disulfide bonds, which can impact protein folding, stability, and function (Giles et al. 2003). We speculate that disulfide bond formation between VdAve1-derived peptides may enhance their overall charge and structural stability, potentially optimizing their interaction with Gram-negative outer membranes. However, it remains unclear why this feature is required for targeting Gram-negative bacteria but not Gram-positive bacteria.

Interestingly, previous studies testing the antibacterial activity of VdAve1 against a panel of plant-associated bacteria *in vitro* revealed that while all tested Gram-positive bacteria were inhibited, Gram-negative bacteria exhibited varying degrees of sensitivity (Snelders et al. 2020). Bacteria have evolved diverse resistance mechanisms to counteract AMPs present in their natural environments. These strategies include reducing AMP binding affinity through modifications of cell envelope components and surface charge, thickening the cell wall to create a physical barrier, and inactivating AMPs via the secretion of proteases (Andersson et

al. 2016). Consequently, the observed differential sensitivity among the tested bacteria is not surprising.

We show that VdAve1 exhibits broad-spectrum antimicrobial activity, inhibiting yeast, filamentous fungi and amoeba besides bacteria, although these microbes lack LTA and LPS in their cell walls. Whether the antimicrobial activity of VdAve1 involves interaction with other cell wall components in these organisms presently remains unknown.

By solving the VdAve1 structure using nuclear magnetic resonance (NMR), we present the first experimentally determined structure of a PNP-like protein, providing a foundation for understanding the biological function of this underexplored protein family. Given the structural homology between PNPs and expansins (Gehring and Irving 2003), it is not surprising that our analysis revealed a strong similarity between VdAve1 and domain 1 (D1) of expansins, a class of plant proteins involved in cell wall loosening (Sampedro and Cosgrove 2005). These findings still raise the intriguing possibility that expansins may possess previously unrecognized antimicrobial properties. While expansins primarily function in plant cell wall modification, their ability to alter polysaccharide structures could have consequences for microbial cell walls, potentially influencing bacterial envelope integrity.

In conclusion, our findings demonstrate that VdAve1 has broad-spectrum activity, inhibiting microbial growth by disrupting plasma membranes through electrostatic interactions. Additionally, we show that VdAve1 binds LTA in the cell wall of Gram-positive bacteria, likely serving as a docking platform that facilitates its accumulation at the bacterial surface before membrane destabilization.

Materials and Methods

Expression and purification of recombinant VdAve1

VdAve1 protein production and purification were performed as previously described (Snelders et al. 2020). Briefly, a pre-inoculum of *Escherichia coli* BL21 transformed with pET15b harboring the sequence for expression of mature VdAve1 was grown in 2x Yeast Extract Tryptone (YT) medium supplemented with 100 µg/mL of ampicillin at 37°C and 180 rpm overnight. The bacteria were resuspended in 1 L of 2xYT medium supplemented with 100

µg/mL of ampicillin and grown at 37°C and 200 rpm until the culture reached an optical density (OD_{600}) of 2. Protein production was induced with isopropyl-β-d-thiogalactoside at a final concentration of 1 mM and cultures were grown at 42°C and 200 rpm for 2h. Next, the cells were harvested by pelleting at approximately 4500 x g for 1 h, washed in dH_2O, pelleted at 12,000 x g for 30 min and snap-frozen in liquid nitrogen. The cells were resuspended in 10 mM Tris, 6 M guanidinium chloride and 10 mM β-mercaptoethanol at pH 8.0 and stirred overnight at 4°C to lyse cells. The lysate was centrifuged at 12,000 x g for 40 min at 4°C and the supernatant was collected. Protein purification was performed under denaturing conditions using the liquid chromatography system ÄKTA go (Cytiva, Marlborough, USA) and a column packed with His60 Ni^{2+} Superflow Resin (Takara Bio, Kusatsu, Japan). The chromatography system was equilibrated with wash buffer: 10 mM Tris, 6 M guanidinium chloride and 20 mM imidazole at pH 8.0. The protein sample was loaded and the column was washed with wash buffer. After all weakly interacting proteins were washed off, the column was eluted with elution buffer: 10 mM Tris, 6 M guanidinium chloride and 200 mM imidazole at pH 8.0. The flow-through of each step was collected and analysed on mini-protean TGX stain-free precast gels (Bio-Rad, Hercules, USA). In order to confirm the presence of the proteins of interest, western blots were performed with Anti-Polyhistidine antibody (Sigma-Aldrich, St. Louis, USA) to detect His-tagged proteins. Purified proteins were refolded *in vitro* by step-wise dialysis using Spectra/Por 3 Dialysis Membrane (Repligen, Waltham, USA) with a molecular weight cut off of 3.5 kDa. Each dialysis step lasted at least 24h. The first dialysis buffer consisted of 4 M guanidinium chloride, 50 mM BisTris, 10 mM reduced glutathione and 2 mM oxidized glutathione at pH 7.0. The second dialysis buffer consisted of 3 M guanidinium chloride, 50 mM BisTris, 10 mM reduced glutathione and 2 mM oxidized glutathione at pH 6.5. The third dialysis buffer consisted of 2 M guanidinium chloride, 100 mM BisTris, 125 mM Ammonium sulfate, 10 mM reduced glutathione and 2 mM oxidized glutathione at pH 6.0. The fourth dialysis buffer consisted of 1 M guanidinium chloride, 100 mM BisTris, 250 mM Ammonium sulfate, 10 mM reduced glutathione and 2 mM oxidized glutathione at pH 5.8. The fifth dialysis buffer consisted of 100 mM BisTris, 250 mM Ammonium sulfate, 10 mM reduced glutathione and 2 mM oxidized glutathione at pH 5.8. Finally, the protein sample was dialyzed against 30 mM potassium phosphate buffer at pH 6.5. Protein samples were concentrated with a centrifugal filter unit (Sigma-Aldrich, St. Louis, USA), and concentrations were determined with NanoDrop (Thermo Fisher Scientific, Carlsbad, USA).

For production of isotopically labelled VdAve1, *E. coli* BL21 cells were grown in M9 minimal medium prepared according to a publicly available protocol from EMBL-EBI (Heidelberg, Germany). For [^{15}N] labelling, the medium was supplemented with 0.5 g/L ammonium-^{15}N chloride (Sigma-Aldrich, St. Louis, USA). For [^{13}C, ^{15}N] labelling, 4 g/L D-Glucose-$^{13}C_6$ (Deutero, Kastellaun, Germany) was added as the sole carbon source in addition to ammonium-^{15}N chloride. The M9 medium further contained 0.6 g Na_2HPO_4, 0.3 g KH_2PO_4, 0.5 g NaCl, 120 mg $MgSO_4$, 33 mg $CaCl_2$, 1 mg biotin, 1 mg thiamine, 0.05 g EDTA, 8.3 mg $FeCl_3$-$6H_2O$, 0.84 mg $ZnCl_2$, 0.13 mg $CuCl_2$-$2H_2O$, 0.1 mg $CoCl_2$-$6H_2O$, 0.1 mg H3BO3, 10.6 µg MnCl2-6H2O per L, supplemented with 100 µg/mL of ampicillin. Production, purification and refolding were performed as described above.

Sample preparation and NMR spectroscopy

3D NMR experiments required for spectral assignment and structural calculation (see Table S 1), as well as ^{1}H,^{15}N TRACT experiments were prepared in 1.7 mm NMR tubes at 40 µL final sample volume, and were acquired in a Bruker Avance III HD 600 MHz spectrometer equipped with TCI Microcryoprobe^{TM}. Titrations were performed in 5 mm NMR tubes at 600 µL final sample volume either in a Bruker Avance III HD 600 MHz or a Bruker Avance III HDX 500 MHz spectrometer equipped with a TCI cryogenic probe. All experiments were acquired at 298 K, unless otherwise stated. NMR spectra were processed with NMRPipe (Delaglio et al. 1995) or TopSpin 3.6 (Bruker, Billerica, USA) and analysed using CcpNmr 3.1 software suit (Vranken et al. 2005).

Samples containing 600 µM or 650 µM [^{13}C, ^{15}N] VdAve1 were prepared for 3D experiments. For ^{1}H, ^{15}N-TRACT experiments four samples at 200, 400, 600 and 766 µM VdAve1 concentration were prepared. LTA and peptidoglycan were titrated over samples containing 150 µM VdAve1 concentration. All samples were prepared in 30 mM phosphate buffer, 8% D_2O, 200 µM DSS-d_6, and 0.01% NaN_3 (pH 6.6).

Spectral assignment and structure calculation

Backbone and side chain resonances were assigned using 2D ^{1}H-^{15}N HSQC, ^{1}H-^{13}C HSQC, 3D HNCO, HN(CA)CO, HNCA, CBCA(CO)NH, HNCACB, HN(CO)CA, HCC(CO)NH, HBHA(CO)NH,

CC(CO)NH, HNHA, HCCH-TOCSY, ^{1}H-^{15}N TOCSY-HSQC, ^{1}H-^{15}N NOESY-HSQC with 90, 100 and 150 ms mixing times, ^{1}H-^{13}C NOESY-HSQC with 200 ms mixing time. For more details see Table S 1. Automated protein assignment and structure calculation were performed with ARTINA (Klukowski et al. 2022). All figures showing structures were generated with PyMOL (The PyMOL Molecular Graphics System, Version 3.0 Schrödinger, LLC). The APBS Electrostatics Plugin 3.4.1 was used to visualize surface charge distribution. The structure homology search was performed with Foldseek (van Kempen et al. 2024).

Chemical shift perturbation (CSP) NMR experiments

^{1}H-^{15}N HSQC spectra for CSP NMR experiments were collected in the presence of 1 mg/mL of *Bacillus subtilis* peptidoglycan, and 0.2, 0.4, 0.6, 1.0 mg/mL of *B. subtilis* lipoteichoic acid (LTA) (Sigma-Aldrich, St. Louis, USA). CSPs were calculated based on $CSP = \frac{1}{3}\sqrt{(\Delta\delta_{15N} \times 0.2)^2 - (\Delta\delta_{1H})^2)}$ and are listed in Table S 3. CSPs greater than 2σ were considered significant and further interpreted as signals that reflect interacting residues.

^{1}H,^{15}N TRACT experiments

Thirty delays were acquired (in s): 0, 0.0015, 0.003, 0.0045, 0.006, 0.0075, 0.009, 0.0105, 0.012, 0.0135, 0.015, 0.01875, 0.0225, 0.02625, 0.03, 0.0375, 0.045, 0.0525, 0.060, 0.0675, 0.075, 0.09, 0.1125, 0.135, 0.15, 0.3, 0.6, 0.75, 1.125 and 1.5. For experimental set-up see Table S 1.

MinD Delocalization Assay

The MinD delocalization assay was conducted as previously described (Müller et al. 2016; Saeloh et al. 2018) with minor modifications. *B. subtilis* strain TB35, expressing MinD-GFP, was cultivated in 0.5× YT medium (4 g/L tryptone, 2.5 g/L yeast extract, 1.25 g/L NaCl) supplemented with 0.1% xylose at 30°C until reaching an OD_{600} of 0.1. The culture was then treated with 8 µM (1× MIC) VdAve1 for 10 minutes, followed by immobilization on a 1% agarose thin film. MinD-GFP localization was analyzed using an Olympus BX 50 microscope equipped with a Photometrics CoolSNAP fx digital camera.

VdAve1 activity assay on bacteria

In order to test VdAve1 activity against *B. subtilis* strain 168, bacteria were grown on lysogeny broth agar (LBA) at 28 °C. A single colony was selected and grown overnight in low salt LB (10 g/L Tryptone, 5 g/L Yeast Extract, 0.5g/L NaCl) at 28°C and 200 rpm. Bacterial cultures were resuspended to an OD_{600} of 0.05 and mixed in a 1:1 ratio with 16 µM of VdAve1 and/or NaCl, $CaCl_2$ and $MgCl_2$ in a 96-well clear plate with flat bottom to reach a final OD_{600} of 0.025 and final protein concentration of 8 µM and 0, 6.25, 12.5, 25, 50 mM salts. Bacterial growth was followed by measuring the OD_{600} overtime with a CLARIOstar® plate reader (BMG LABTECH, Ortenberg, Germany). The microplate Reader was set at 22 °C and the plate was shaken before each measurement for 10 seconds at 300 rpm.

To investigate the importance of LTA binding for VdAve1 antimicrobial activity, 240 µg/mL VdAve1 was preincubated with 240 µg/mL of purified *B. subtilis* LTA (Sigma-Aldrich, St. Louis, MO, USA) for 30 min at room temperature. Then, the VdAve1-LTA suspension was mixed in a 1:1 ratio with a *B. subtilis* culture with an OD_{600} of 0.05. The growth assay was performed as described above.

VdAve1 activity assay on fungal protoplasts

Protoplasts from the fungal species *Trichoderma viride* and *Monilinia fructicola* were obtained as previously described (Leisen et al. 2020). Protoplasts were pelleted at 100 x g for 1 min and resuspended in 1 M sorbitol and 10 mM MOPS at pH 6.3 to a final concentration of 10^5-10^6 protoplasts/mL. Protoplasts were incubated with 8 µM of VdAve1, Triton X-100 or sterile ultrapure water. Following 30 minutes of incubation, intact protoplasts were quantified for the different treatments using a haemocytometer.

Membrane potential measurements

B. subtilis membrane potential measurements were performed as described previously (Saeloh et al. 2018; Te Winkel et al. 2016). *B. subtilis* cultures were grown at 30°C in 0.5x YT, until OD_{600} of 0.1. Cultures were supplemented with 8, 4 or 2 µM VdAve1 (1, 0.5 and 0.25x MIC) or 2 µg/mL Gramicidin.

VdAve1 activity assay on fungi

To test VdAve1 activity against yeast, *Cyberlindnera jadinii* was grown on potato dextrose agar (PDA) at 28°C. A single colony was selected and grown overnight in 5% potato dextrose broth (PDB) at 28°C at 180 rpm. Overnight cultures were resuspended to an OD_{600} of 0.01 in fresh 5% PDB supplemented with 8 µM VdAve1 or filter-sterilized potassium phosphate buffer in a 96-well clear plate with flat bottom and incubated overnight at 28°C. To determine yeast abundance, a dilution series of the yeast cultures was plated on PDA plates and incubated at 28°C. After overnight incubation, colony-forming units (CFUs) were enumerated and the Log_{10}(CFU/µL) was calculated.

To test VdAve1 activity against filamentous fungi, *Alternaria brassicicola* and *Cladosporium cucumerinum* were grown on PDA at 28°C. Conidiospores were harvested and suspended in 5% PDB to a final concentration of 10^4 spores/mL with filter sterilized potassium phosphate buffer or VdAve1, at a final concentration of 8 µM. 100 µL were aliquoted in 96-well clear plate with flat bottom and incubated overnight at 28°C. Fungal growth was imaged using Olympus CK 40 microscope (Shinjuku City, Tokyo, Japan).

VdAve1 activity assay on amoeba

Leptophrys vorax was cultured in half-strength Waris-H without soil extract, supplemented with the algal prey *Closterium cornu*, as described previously (Hess 2017). A culture of *L. vorax* digestive cysts were incubated with 8 µM VdAve1 in 24-well clear plate with flat bottom at room temperature. Microscopy pictures were taken with an Olympus CK 40 microscope (Shinjuku City, Tokyo, Japan) after 20 h of incubation.

VdAve1 activity assay on cancer cells

Human colon cancer cells, HCT116 cell line, were seeded (500 cells/well) in a 96-well clear plate with flat bottom and supplemented with 100 µL RPMI 1640 and 8 µM VdAve1, 2.5 µM 5-fluorouracil (5-FU) or sterile phosphate buffer. Cell proliferation was monitored with a

Multiskan SkyHigh microtiter plate spectrophotometer (Thermo Fisher Scientific, Carlsbad, USA) at an absorbance wavelength of 450 nm for 190 h.

VdAve1-derived peptide activity test

VdAve1-derived peptides were chemically synthesized by GenScript (Piscataway, NJ, USA) and Proteogenix (City, France). *B. subtilis* and *Sphingopyxis macrogoltabida* were grown in ¼ lysogeny broth (LB) low salt (2.5 g/L tryptone, 1.25 g /L yeast extract and 0.125 g/L NaCl) or tryptic soy broth (TSB) low salt (17 g/L tryptone, 3 g/L soy peptone, 2.5 g/L dipotassium phosphate, 2.5 g/L glucose and 0.5 g/L NaCl), respectively, at 28°C and 180 rpm. Overnight cultures were resuspended to an OD_{600} of 0.05 supplemented with 50 µM peptides in a 96-well clear plate with flat bottom. Bacterial growth was followed by measuring the OD_{600} overtime with a CLARIOstar Plus Microplate Reader (BMG LABTECH, Ortenberg, Germany). The Microplate Reader was set at 25°C and plate was shaken before each measurement for 10 seconds at 300 rpm. The net charge of the peptides was calculated as the sum of the charges of every ionizable group in the peptide with an online tool (https://www.bachem.com/knowledge-center/peptide-calculator/).

Transcriptome Analysis

100 µL of an overnight *B. subtilis* strain 168 culture was inoculated with 10 mL of fresh low-salt LB medium (10 g/L tryptone, 5 g/L yeast extract, 0.5 g/L NaCl) and incubated at 30°C while shaking at 200 rpm. The culture was then used to inoculate multiple 100 mL flasks containing 10 mL of low-salt LB, adjusting the final OD_{600} to 0.05. Bacterial suspensions were grown at 30°C while shaking at 200 rpm until reaching OD_{600} of 0.3. Four µM of VdAve1 or sterile ultrapure water were added to the cultures. Following 5 and 20 minutes of incubation under the same conditions, 0.5 mL of bacterial culture was transferred to 2 mL screw-cap tubes containing 1.5 g of 0.1 mm glass beads, 500 µL phenol-chloroform-isoamyl alcohol (25:24:1), and 50 µL of 10% SDS. The samples were mixed and immediately snap-frozen in liquid nitrogen. To ensure cell lysis, samples were subjected to bead beating (10× for 30 seconds at 6,000 rpm).

After lysis, tubes were centrifuged at 13,000 × g for 5 minutes, and the aqueous phase was transferred to a new tube containing 400 µL chloroform. Following mixing and a second

centrifugation (13,000 × g for 5 minutes), the aqueous phase was collected, and RNA was precipitated using ethanol and sodium acetate. The RNA pellets were recovered by centrifugation (30 minutes at 13,000 × g), resuspended in ultrapure water, and treated with DNase.

To remove ribosomal RNA, the MICROBExpress™ Bacterial mRNA Enrichment Kit (Thermo Fisher Scientific, Carlsbad, USA) was used. Sequencing libraries were prepared with the NEBNext® Ultra™ II Directional RNA Library Prep Kit for Illumina®, following the manufacturer's protocol (New England Biolabs, Ipswich, MA, USA). The libraries were sequenced on an Illumina NextSeq 550 platform, using the NextSeq 500/550 High Output v2.5 kit (75-bp read length).

For data analysis, sequencing reads were processed using the web-based Galaxy platform, and differential expression analysis was performed using DESeq2 (Galaxy Version 2.11.40.6+galaxy1).

Transposon Sequencing (Tn-seq) Analysis

The construction of the *B. subtilis* transposon insertion library and sequencing library was performed following previously established protocols (Johnson and Grossman 2014; van Opijnen et al. 2014), with minor modifications. To generate the transposon insertion library, 6 µg of genomic DNA isolated from *B. subtilis* strain BSB1 was mixed with 2 µg of the transposon-harboring plasmid pCJ4 and 0.4 µg of the mariner transposase Himar1-C9. The reaction mixture contained 9.5% glycerol, 93.5 mM NaCl, 9.5 mM $MgCl_2$, 3.6 µM BSA, 1.9 mM dithiothreitol, and 20.5 mM HEPES (pH 7.9), and was incubated overnight at 30°C to facilitate transposition. The DNA was then precipitated, purified, and resuspended in 15 µL of 10 mM $MgCl_2$, 1 mM dithiothreitol, and 50 mM Tris-HCl (pH 7.8). To repair transposon insertion junctions, 4 µL of 2.5 mM dNTPs and 0.5 µL of T4 DNA Polymerase (New England Biolabs, Ipswich, MA, USA) were added, and the reaction was incubated at 12°C for 20 minutes. Following heat inactivation, 0.2 µL of 2.6 mM NAD and 0.5 µL of *E. coli* DNA ligase were added, and the mixture was incubated overnight at 16°C to repair nicked DNA strands. The resulting transposon-inserted genomic DNA (Tn-gDNA) was then transformed into competent *B. subtilis*

BSB1 cells. Approximately 250,000 transformants were selected on agar plates, pooled in liquid medium, and stored at -80°C for further analysis.

The transposon insertion library was grown for 1h in low-salt LB medium (10 g/L tryptone, 5 g/L yeast extract, 0.5 g/L NaCl) at 28°C and aliquoted to three flasks containing 6 mL of low-salt LB medium supplemented with sterile ultrapure water or 4 µM VdAve1, to have a final OD_{600} of 0.1. When bacterial cultures reached OD_{600} of 0.8, 0.75 mL was transferred to new flasks containing fresh 6 mL of low-salt LB medium supplemented with sterile ultrapure water or 4 µM VdAve1, to have a final OD_{600} of 0.1. After a total of three transfers in media supplemented with ultrapure water or VdAve1, corresponding to a total of nine generations, bacterial cells were harvested and genomic DNA was isolated.

Genomic DNA isolated from treated bacterial samples was digested with MmeI (New England Biolabs, Ipswich, MA, USA) and treated with calf intestinal phosphatase before purification. Meanwhile, a customized Illumina sequencing R1 adapter was annealed using oligonucleotides BW-TnR1-S and BW-TnR1-AntiS (Table S 4), followed by ligation using T4 DNA ligase. Adapter-ligated DNA fragments were purified with AMPure XP beads (Beckman Coulter, Indianapolis, IN, USA). PCR amplification was performed using the universal BW-TnPCR-Uni primer and a specific barcoded primer (Table S 4) to generate Illumina sequencing libraries. The resulting PCR-enriched Tn-seq libraries were separated via native 8% acrylamide gel electrophoresis, and DNA fragments (~165 bp) were extracted and resuspended in 0.1X TE buffer. The libraries were sequenced using an Illumina NextSeq 550 platform with a NextSeq 500/550 High Output v2.5 kit (75-bp read length). Data processing was conducted using Python and the web-based Galaxy platform. Reads were filtered and trimmed with Trimmomatic (Galaxy Version 0.36.5), and transposon inverted repeats were removed from the 3’ ends using Cutadapt (Galaxy Version 1.16.5). Reads between 13-18 bp were selected and mapped to the B. subtilis reference genome (NC_000913) using Bowtie2 (Galaxy Version 2.3.4.3+galaxy0). To determine transposon insertion sites, a customized *map_functions* identified 183,963 TA dinucleotide sequences across gene coding regions. The number of reads per TA dinucleotide was calculated for each treatment condition. On average, 9.53 million reads per library were obtained, covering 112,457 TA sites across 4,280 coding sequences, with an average of 85 reads per insertion. To assess the impact of transposon insertions on B. subtilis proliferation under different experimental conditions we first estimated the expected

read count per gene based on the total number of TA dinucleotide sites in each coding sequence. Then we calculated the ratio of observed-to-expected reads for each gene. Finally, we identified statistically significant differences between conditions using an unpaired two-sided Student's t-test.

HPLC analysis of *Bacillus subtilis* peptidoglycan incubated with VdAve1

Peptidoglycan was isolated from *B. subtilis* strain bFB66, muropeptides were prepared by overnight cellosyl-digestion of peptidoglycan. Fifty µL of reaction mix were prepared as following: 10 µM VdAve1 in 20 mM of sodium phosphate at pH 7.5, 50 mM NaCl, 1 mM MgCl2, peptidoglycan or muropeptides. The reaction mix was incubated for 16h at 37°C and 900 rpm in a thermal shaker. The reaction was stopped by boiling and samples were reduced and acidified to pH 3.5-4.0. High-performance liquid chromatography (HPLC) was performed as previously described (Atrih et al. 1999).

Supplementary information

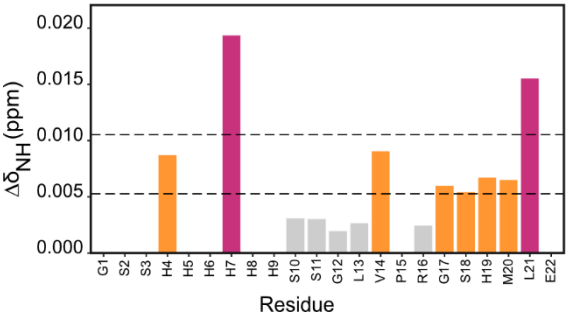

Figure S1. Chemical shift perturbances of the protein His-tag. The $\Delta\delta_{NH}$ values were color-coded, $\Delta\delta_{NH}>2\sigma$ pink and $\Delta\delta_{NH}>\sigma$ orange.

Table S 1. Details on experimental set-up of NMR experiments

Exp.	Name from Bruker library	NS	SW* (ppm)	TD*	O1* (ppm)	D1 (s)	Comments
$^{1}H,^{15}N$ HSQC	trosyetf3gpsi.2	4-16	32/16	128/2048	117/4.68	1.5	J=90 Hz
$^{1}H,^{13}C$ HSQC	hsqcetgpsp.2	8	70/16	128/2048	40/4.68	1	J=145 Hz
HNCO	hncogpwg3d	16	14/29/16	128/80/2048	173.5/116.5/4.68	1	NUS 40%
HN(CA)CO	hncacogpwg3d	16	14/29/16	128/80/2048	173.5/116.5/4.68	1	NUS 40%
HNCA	hncagpwg3d	16	30/29/16	128/80/2048	53.2/116.5/4.68	1	NUS 40%

HNCACB	hncacbgpwg3d	104	69/29/14	128/64/2048	42/116.5/4.68	1	NUS 40%
CBCA(CO)NH	cbcaconhgpwg3d	32	69/29/14	128/64/2048	42/116.5/4.68	1	NUS 40%
HN(CO)CA	hncocagpwg3d	16	30/29/16	128/80/2048	53.2/116.5/4.68	1	NUS 40%
HCC(CO)NH	hccconhgpwg3d3	64	16/29/16	128/64/2048	4.68/116.5/4.68	1.5	NUS 40%
HBHA(CO)NH	hbhaconhgpwg3d	56	16/29/14	128/64/2048	4.68/116.5/4.68	1	NUS 40%
CC(CO)NH	ccconhgp3d	48	80.8/29/14	128/64/2048	43/116.5/4.68	1	NUS 40%
HNHA	hnhagp3d	16	30/14/14	64/128/2048	115/4.68/4.68	1	NUS 405
HCCH-TOCSY	hcchdigp3d2	32	80.8/80.8/14	96/96/2048	40/40/4.7	1	-
^{1}H-^{15}N TOCSY-HSQC	mlevhsqcetf3gp3d	32	16/29/16	128/80/2048	4.68/116.5/4.68	2	NUS 43%
^{1}H-^{15}N NOESY-HSQC	noesyhsqcetf3gp3d	16	16/29/14	128/80/2048	4.68/116.5/4.68	1.5	NUS 53%, 100 ms and 150 ms
^{1}H-^{15}N NOESY-HSQC	noesyhsqcetf3gp3d	16	16/29/14	128/80/2048	4.68/116.5/4.68	1.5	90 ms
^{1}H-^{13}C NOESY-HSQC	noesyhsqcetgp3d	32	14/80/14	128/80/2048	4.7/43/4.7	1.2	200 ms
^{1}H,^{15}N-TRACT	15n1h-tract-alpha, 15n1h-tract-beta	40	33.3/16	30/2048	98.65/4.68	2	-

* F1/F2/F3

Table S 2. Structure calculation statistics

NMR distances and constraints	
Total number of distance restraints	1643
Number of intraresidual restraints (|*i-j*| = 0)	355
Number of sequential restraints (|*i-j*| = 1)	516
Number of medium-range restraints (1 < |*i-j*| < 5)	202
Number of long-range restraints (|*i-j*| ≥ 5)	570
Number of torsion angle restraints	182
Structure statistics	
Distance restraint violations > 0.1 Å	8 ± 3
Max. distance restraint violation (Å)	0.26 ± 0.04
Angle restraint violations > 5.0°	7 ± 1
Maximal angle restraint violation (°)	19.10 ± 0.52
Residues in most favored Ramachandran plot regions	81.50%

Residues in additionally allowed regions	18.50%

Table S 3. ^{15}N and ^{1}H chemical shit perturbances of VdAve1 in presence of 0.6 mg/mL of *Bacillus subtilis* lipoteichoic acid (LTA).

Residue	^{15}N APO	^{1}H APO	^{15}N LTA	^{1}H LTA	CSP
TAG-4_H	120.4523	8.387343	120.6381	8.368723	0.008762
TAG-7_H	122.4554	8.237324	122.1859	8.264064	0.019404
TAG-10_S	118.1251	8.447731	118.1044	8.439253	0.003144
TAG-11_S	115.9366	7.704725	115.8929	7.70177	0.003077
TAG-12_G	110.5392	8.329976	110.5202	8.33463	0.002005
TAG-13_L	121.5195	7.983124	121.4834	7.986825	0.002707
TAG-14_V	122.5274	8.012086	122.3928	8.007606	0.009102
TAG-16_R	121.9394	8.423916	121.9451	8.431334	0.002502
TAG-17_G	110.2877	8.419199	110.2102	8.428501	0.006024
TAG-18_S	115.5516	8.173207	115.4899	8.162376	0.005475
TAG-19_H	121.1535	8.239946	121.0956	8.22328	0.006763
TAG-20_M	120.0795	8.226194	120.1612	8.237116	0.006551
TAG-21_L	122.9937	8.381109	122.767	8.392446	0.015584
1_D	120.8645	8.299526	120.8884	8.284171	0.022694
2_L	118.6624	8.014717	118.534	7.990885	0.01168
3_G	108.0174	8.401788	107.9609	8.395443	0.004324
4_T	113.0153	9.023672	113.0175	9.036509	0.004282
5_A	120.3038	9.316472	120.2195	9.302913	0.007215
6_S	113.0814	7.826013	113.0603	7.814948	0.003947
7_Y	118.0852	8.577985	118.0816	8.593559	0.005197
8_Y	117.3648	8.2519	117.276	8.244358	0.006433
9_N	120.0713	7.952252	120.2727	7.990849	0.018599
12_Y	118.7541	8.739156	118.5777	8.713501	0.007548
13_L	115.5534	6.846573	115.4912	6.845851	0.004152
15_T	108.5629	8.4845	108.5197	8.471447	0.005217
16_A	122.7156	9.220758	122.7039	9.220712	0.00078
17_C	110.4272	7.149753	110.3909	7.143641	0.003163
18_G	106.4415	8.25882	106.3823	8.260775	0.003998
19_G	112.7424	7.951866	112.7338	7.953881	0.000883
20_S	114.4382	7.778157	119.34	6.969261	0.001527
21_N	119.3546	6.972481	114.2526	7.992354	0.00145
23_S	114.2772	7.996249	115.1756	6.544095	0.002088
24_Q	115.2241	6.545453	119.8442	7.166179	0.003267
25_F	119.8553	7.170107	116.7786	8.569063	0.001504
27_S	116.8188	8.575994	113.9022	8.927551	0.003537
28_G	113.8952	8.933022	111.2753	8.325585	0.001884
29_N	111.3223	8.329757	121.0514	6.508832	0.003425
30_L	121.0806	6.509531	119.0732	7.236117	0.001961

31_F	119.0714	7.246307	112.1815	8.351965	0.003399
32_V	112.2815	8.357677	127.1468	9.436887	0.006932
33_A	127.1745	9.4377	109.5939	7.938774	0.001869
34_V	109.6549	7.938729	118.0027	7.784731	0.004067
35_S	117.9555	7.768877	118.1044	8.439253	0.00615
36_D	118.1251	8.447731	119.0732	7.236117	0.003144
37_G	119.0714	7.246307	118.4466	7.254958	0.003399
38_L	118.4947	7.257652	119.7799	7.617937	0.003326
39_W	119.7805	7.620018	118.1044	8.439253	0.000695
40_D	118.1251	8.447731	114.3029	8.912121	0.003144
42_G	114.3175	8.906756	124.9549	7.691248	0.002035
43_A	124.9734	7.688246	113.4892	6.841147	0.001587
44_A	113.5069	6.836661	113.4892	6.841147	0.001907
45_C	113.5069	6.836661	111.6019	8.494053	0.001907
46_G	111.6105	8.500213	122.1702	8.333526	0.002133
47_R	122.1652	8.334223	121.633	8.69047	0.000405
48_R	121.6429	8.69596	117.7355	8.651603	0.001946
49_Y	117.7284	8.66195	124.0688	9.223151	0.003482
50_R	124.04	9.239356	125.5327	9.416497	0.005732
51_I	125.6775	9.429115	122.459	8.358298	0.01053
52_K	122.5032	8.361853	126.221	9.559077	0.003174
53_C	126.1933	9.558955	129.8572	9.514199	0.001847
54_L	129.7234	9.49634	112.1613	7.812596	0.010728
55_S	112.2896	7.830638	107.0714	7.868123	0.010458
56_G	107.1118	7.875492	125.8302	8.338632	0.003645
57_A	125.987	8.322918	123.064	8.183094	0.01169
58_R	123.054	8.178193	111.8211	8.722055	0.001763
59_G	112.1858	8.750826	114.1194	7.593763	0.026135
60_S	114.3868	7.651039	118.4353	8.119616	0.026121
61_C	118.4889	8.109593	121.8497	8.247925	0.004893
62_K	121.8427	8.254483	120.321	8.388286	0.002235
63_D	120.308	8.383797	108.2048	7.882684	0.001729
64_G	108.2319	7.893534	116.5681	8.047356	0.004043
65_M	116.6005	8.051265	114.3008	8.320794	0.002525
66_I	114.3147	8.328113	122.9478	8.048956	0.002609
67_D	122.9888	8.048386	112.7892	9.202627	0.002737
68_V	112.8023	9.201639	119.9223	7.745113	0.000934
69_R	120.0036	7.758462	125.8555	9.252807	0.004707
70_V	125.8841	9.260005	118.6966	8.758663	0.003065
71_V	118.8663	8.773732	117.0379	7.700476	0.012376
72_D	117.0521	7.69964	123.5131	8.666819	0.000982
73_R	123.4934	8.683381	127.8156	8.093438	0.005675
74_A	127.8336	8.099024	114.7291	8.797848	0.002215
75_K	114.9398	8.787368	103.411	7.268914	0.014476
76_T	103.657	7.289496	115.9908	7.065962	0.017776

77_T	115.9463	7.084486	121.3133	8.592283	0.006849
78_V	121.3312	8.579588	115.4386	8.557062	0.004398
79_T	115.4468	8.564992	122.6998	8.205716	0.002699
80_K	122.5587	8.224018	124.7813	8.1249	0.01121
81_A	124.6289	8.104524	122.99	7.902139	0.012221
82_A	123.0746	7.894492	115.7006	7.534487	0.006191
83_H	116.0393	7.544528	122.7613	7.703196	0.022823
84_K	122.772	7.479459	124.9077	7.355078	0.074582
85_A	125.0864	7.282408	117.1248	7.788707	0.026994
86_T	117.1796	7.779485	114.4153	7.777955	0.004775
87_M	114.4382	7.778157	121.6388	8.80485	0.001527
88_I	121.7028	8.811229	130.1564	9.133678	0.004764
89_L	130.1603	9.127317	112.2572	7.06364	0.002136
90_S	112.3162	7.067901	119.8406	7.837827	0.004183
91_Q	119.9311	7.839288	113.279	8.07293	0.006051
92_D	113.3059	8.065172	115.8929	7.70177	0.003146
93_S	115.9366	7.704725	124.1381	8.57255	0.003077
94_Y	124.1906	8.566472	115.7973	8.376162	0.004048
95_D	115.8282	8.373174	119.3376	7.228434	0.002288
96_A	119.3839	7.232252	106.9723	7.069189	0.003336
97_I	107.0213	7.058408	122.8604	7.917277	0.00486
98_V	122.877	7.923767	126.3099	9.406648	0.002431
99_N	126.3631	9.397991	120.8094	8.483699	0.004574
100_Q	120.8024	8.485173	122.0434	8.595461	0.00068
101_W	121.9979	8.59456	126.5565	8.951941	0.003044
102_K	126.7552	8.967003	103.7694	8.36235	0.014166
103_G	103.7735	8.368874	114.2554	7.802649	0.002192
104_T	114.0756	7.78022	120.5487	8.324944	0.014124
105_R	120.6223	8.327704	125.0672	9.393698	0.004995
106_H	125.3299	9.396101	124.4658	9.206029	0.015133
107_K	124.4944	9.207678	116.1149	7.301206	0.001986
108_A	116.0768	7.293411	110.9109	8.633157	0.003634
109_V	111.0384	8.638703	118.7092	8.806259	0.008696
110_N	118.7819	8.816786	114.6743	8.921473	0.005984
111_I	114.5937	8.909597	119.3167	8.466539	0.006673
112_E	119.5308	8.453869	118.7092	8.806259	0.014885
113_F	118.8984	8.823867	116.3356	8.492281	0.01391
114_R	116.4101	8.488763	127.2965	9.189065	0.005106
115_Q	127.3124	9.188696	128.8872	7.970267	0.00107
116_I	128.883	7.962245	108.3528	6.434694	0.002688

Table S 4. Primers used in the Tn-seq analysis.

Name	Name Sequence (5’ --> 3’) Application	Application

BW-TnR1-S	TCTTTCCCTACACGACGCTCTTCCGATCTNN	Tn-seq library preparation
BW-TnR1-AntiS	AGATCGGAAGAGCGTCGTGTAGGGAAAGA	Tn-seq library preparation
BW-TnPCR-Uni	AATGATACGGCGACCACCGAGATCTACACTCTTTCCCTACACGACGCTCTTCCGATCT	Tn-seq library preparation
BW-TnPCR-BC43	CAAGCAGAAGACGGCATACGAGATGCTGTAGTGACTGGAGTTCAGACGTGTGCTCTTCCGATCAGACCGGGGACTTATCATCCAACCTGT	Tn-seq library preparation
BW-TnPCR-BC44	CAAGCAGAAGACGGCATACGAGATATTATAGTGACTGGAGTTCAGACGTGTGCTCTTCCGATCAGACCGGGGACTTATCATCCAACCTGT	Tn-seq library preparation
BW-TnPCR-BC45	CAAGCAGAAGACGGCATACGAGATGAATGAGTGACTGGAGTTCAGACGTGTGCTCTTCCGATCAGACCGGGGACTTATCATCCAACCTGT	Tn-seq library preparation
BW-TnPCR-BC46	CAAGCAGAAGACGGCATACGAGATTCGGGAGTGACTGGAGTTCAGACGTGTGCTCTTCCGATCAGACCGGGGACTTATCATCCAACCTGT	Tn-seq library preparation
BW-TnPCR-BC47	CAAGCAGAAGACGGCATACGAGATCTTCGAGTGACTGGAGTTCAGACGTGTGCTCTTCCGATCAGACCGGGGACTTATCATCCAACCTGT	Tn-seq library preparation
BW-TnPCR-BC48	CAAGCAGAAGACGGCATACGAGATTGCCGAGTGACTGGAGTTCAGACGTGTGCTCTTCCGATCAGACCGGGGACTTATCATCCAACCTGT	Tn-seq library preparation

References

Adams, Peter G.; Lamoureux, Loreen; Swingle, Kirstie L.; Mukundan, Harshini; Montaño, Gabriel A. (2014): Lipopolysaccharide-induced dynamic lipid membrane reorganization: tubules, perforations, and stacks. In *Biophysical journal* 106 (11), pp. 2395–2407. DOI: 10.1016/j.bpj.2014.04.016.

Aerts, A. M.; François, I. E. J. A.; Cammue, B. P. A.; Thevissen, K. (2008): The mode of antifungal action of plant, insect and human defensins. In *Cellular and molecular life sciences: CMLS* 65 (13), pp. 2069–2079. DOI: 10.1007/s00018-008-8035-0.

Ageitos, J. M.; Sánchez-Pérez, A.; Calo-Mata, P.; Villa, T. G. (2017): Antimicrobial peptides (AMPs): Ancient compounds that represent novel weapons in the fight against bacteria. In *Biochemical pharmacology* 133, pp. 117–138. DOI: 10.1016/j.bcp.2016.09.018.

Aguilar, P. S.; Cronan, J. E.; Mendoza, D. de (1998): A Bacillus subtilis gene induced by cold shock encodes a membrane phospholipid desaturase. In *Journal of bacteriology* 180 (8), pp. 2194–2200. DOI: 10.1128/JB.180.8.2194-2200.1998.

Andersson, D. I.; Hughes, D.; Kubicek-Sutherland, J. Z. (2016): Mechanisms and consequences of bacterial resistance to antimicrobial peptides. In *Drug resistance updates: reviews and commentaries in antimicrobial and anticancer chemotherapy* 26, pp. 43–57. DOI: 10.1016/j.drup.2016.04.002.

Atrih, A.; Bacher, G.; Allmaier, G.; Williamson, M. P.; Foster, S. J. (1999): Analysis of peptidoglycan structure from vegetative cells of Bacillus subtilis 168 and role of PBP 5 in peptidoglycan maturation. In *Journal of bacteriology* 181 (13), pp. 3956–3966. DOI: 10.1128/JB.181.13.3956-3966.1999.

Barbour, Abdelahhad; Tagg, John; Abou-Zied, Osama K.; Philip, Koshy (2016): New insights into the mode of action of the lantibiotic salivaricin B. In *Scientific reports* 6, p. 31749. DOI: 10.1038/srep31749.

Berendsen, Roeland L.; Pieterse, Corné M. J.; Bakker, Peter A. H. M. (2012): The rhizosphere microbiome and plant health. In *Trends in plant science* 17 (8), pp. 478–486. DOI: 10.1016/j.tplants.2012.04.001.

Bortolotti, A.; Troiano, C.; Bobone, S.; Konai, M. M.; Ghosh, C.; Bocchinfuso, G. et al. (2023): Mechanism of lipid bilayer perturbation by bactericidal membrane-active small molecules. In *Biochimica et biophysica acta. Biomembranes* 1865 (1), p. 184079. DOI: 10.1016/j.bbamem.2022.184079.

Breukink, E.; Wiedemann, I.; van Kraaij, C.; Kuipers, O. P.; Sahl, H. G.; Kruijff, B. de (1999): Use of the cell wall precursor lipid II by a pore-forming peptide antibiotic. In *Science (New York, N.Y.)* 286 (5448), pp. 2361–2364. DOI: 10.1126/science.286.5448.2361.

Brutsche, S.; Braun, V. (1997): SigX of Bacillus subtilis replaces the ECF sigma factor fecI of Escherichia coli and is inhibited by RsiX. In *Molecular & general genetics : MGG* 256 (4), pp. 416–425. DOI: 10.1007/s004380050585.

Carrión, Víctor J.; Perez-Jaramillo, Juan; Cordovez, Viviane; Tracanna, Vittorio; Hollander, Mattias de; Ruiz-Buck, Daniel et al. (2019): Pathogen-induced activation of disease-suppressive functions in the endophytic root microbiome. In *Science (New York, N.Y.)* 366 (6465), pp. 606–612. DOI: 10.1126/science.aaw9285.

Chavarro-Carrero, Edgar A.; Snelders, Nick C.; Torres, David E.; Kraege, Anton; López-Moral, Ana; Petti, Gabriella C. et al. (2024): The soil-borne white root rot pathogen Rosellinia necatrix expresses antimicrobial proteins during host colonization. In *PLoS pathogens* 20 (1), e1011866. DOI: 10.1371/journal.ppat.1011866.

Chen, Eric H-L; Wang, Chun-Hsiung; Liao, Yi-Ting; Chan, Feng-Yueh; Kanaoka, Yui; Uchihashi, Takayuki et al. (2023): Visualizing the membrane disruption action of antimicrobial peptides by cryo-electron tomography. In *Nature communications* 14 (1), p. 5464. DOI: 10.1038/s41467-023-41156-2.

Chen, Tao; Nomura, Kinya; Wang, Xiaolin; Sohrabi, Reza; Xu, Jin; Yao, Lingya et al. (2020): A plant genetic network for preventing dysbiosis in the phyllosphere. In *Nature* 580 (7805), pp. 653–657. DOI: 10.1038/s41586-020-2185-0.

Ciumac, Daniela; Gong, Haoning; Hu, Xuzhi; Lu, Jian Ren (2019): Membrane targeting cationic antimicrobial peptides. In *Journal of colloid and interface science* 537, pp. 163–185. DOI: 10.1016/j.jcis.2018.10.103.

Cook, David E.; Mesarich, Carl H.; Thomma, Bart P. H. J. (2015): Understanding plant immunity as a surveillance system to detect invasion. In *Annual review of phytopathology* 53, pp. 541–563. DOI: 10.1146/annurev-phyto-080614-120114.

de Jonge, Ronnie de; van Esse, H. Peter; Maruthachalam, Karunakaran; Bolton, Melvin D.; Santhanam, Parthasarathy; Saber, Mojtaba Keykha et al. (2012): Tomato immune receptor Ve1 recognizes effector of multiple fungal pathogens uncovered by genome and RNA sequencing. In *Proceedings of the National Academy of Sciences of the United States of America* 109 (13), pp. 5110–5115. DOI: 10.1073/pnas.1119623109.

Decker, Tanya; Rautenbach, Marina; Khan, Sehaam; Khan, Wesaal (2024): Antibacterial efficacy and membrane mechanism of action of the Serratia-derived non-ionic lipopeptide, serrawettin W2-FL10. In *Microbiology spectrum* 12 (7), e0295223. DOI: 10.1128/spectrum.02952-23.

Di Paolo, Valeria; Masotti, Fiorella; Vranych, Cecilia V.; Grandellis, Carolina; Garavaglia, Betiana S.; Gottig, Natalia; Ottado, Jorgelina (2023): Xanthomonas natriuretic peptide is recognized by the Arabidopsis natriuretic peptide receptor 1 and through this interaction triggers similar plant responses to its plant counterpart. In *Plant science: an international journal of experimental plant biology* 326, p. 111494. DOI: 10.1016/j.plantsci.2022.111494.

Eun, Ye-Jin; Foss, Marie H.; Kiekebusch, Daniela; Pauw, Daniel A.; Westler, William M.; Thanbichler, Martin; Weibel, Douglas B. (2012): DCAP: a broad-spectrum antibiotic that targets the cytoplasmic membrane of bacteria. In *Journal of the American Chemical Society* 134 (28), pp. 11322–11325. DOI: 10.1021/ja302542j.

Ficarra, Florencia A.; Grandellis, Carolina; Garavaglia, Betiana S.; Gottig, Natalia; Ottado, Jorgelina (2018): Bacterial and plant natriuretic peptides improve plant defence responses against pathogens. In *Molecular plant pathology* 19 (4), pp. 801–811. DOI: 10.1111/mpp.12560.

Fradin, Emilie F.; Thomma, Bart P. H. J. (2006): Physiology and molecular aspects of Verticillium wilt diseases caused by V. dahliae and V. albo-atrum. In *Molecular plant pathology* 7 (2), pp. 71–86. DOI: 10.1111/j.1364-3703.2006.00323.x.

Fujisawa, Makoto; Kusumoto, Ayumi; Wada, Yuko; Tsuchiya, Takahiro; Ito, Masahiro (2005): NhaK, a novel monovalent cation/H+ antiporter of Bacillus subtilis. In *Archives of microbiology* 183 (6), pp. 411–420. DOI: 10.1007/s00203-005-0011-6.

Gehring, C. A.; Irving, H. R. (2003): Natriuretic peptides—a class of heterologous molecules in plants. In *The international journal of biochemistry & cell biology* 35 (9), pp. 1318–1322. DOI: 10.1016/s1357-2725(03)00032-3.

Georgelis, Nikolaos; Tabuchi, Akira; Nikolaidis, Nikolas; Cosgrove, Daniel J. (2011): Structure-function analysis of the bacterial expansin EXLX1. In *The Journal of biological chemistry* 286 (19), pp. 16814–16823. DOI: 10.1074/jbc.M111.225037.

Georgelis, Nikolaos; Yennawar, Neela H.; Cosgrove, Daniel J. (2012): Structural basis for entropy-driven cellulose binding by a type-A cellulose-binding module (CBM) and bacterial expansin. In *Proceedings of the National Academy of Sciences of the United States of America* 109 (37), pp. 14830–14835. DOI: 10.1073/pnas.1213200109.

Giles, Niroshini M.; Watts, Aaron B.; Giles, Gregory I.; Fry, Fiona H.; Littlechild, Jennifer A.; Jacob, Claus (2003): Metal and redox modulation of cysteine protein function. In *Chemistry & biology* 10 (8), pp. 677–693. DOI: 10.1016/s1074-5521(03)00174-1.

Gómez-Pérez, Daniel; Schmid, Monja; Chaudhry, Vasvi; Hu, Yiheng; Velic, Ana; Maček, Boris et al. (2023): Proteins released into the plant apoplast by the obligate parasitic protist Albugo selectively repress phyllosphere-associated bacteria. In *The New phytologist* 239 (6), pp. 2320–2334. DOI: 10.1111/nph.18995.

Gottig, Natalia; Garavaglia, Betiana S.; Daurelio, Lucas D.; Valentine, Alex; Gehring, Chris; Orellano, Elena G.; Ottado, Jorgelina (2008): Xanthomonas axonopodis pv. citri uses a plant natriuretic peptide-like protein to modify host homeostasis. In *Proceedings of the National Academy of Sciences of the United States of America* 105 (47), pp. 18631–18636. DOI: 10.1073/pnas.0810107105.

Guariglia-Oropeza, Veronica; Helmann, John D. (2011): Bacillus subtilis σ(V) confers lysozyme resistance by activation of two cell wall modification pathways, peptidoglycan O-acetylation and D-alanylation of teichoic acids. In *Journal of bacteriology* 193 (22), pp. 6223–6232. DOI: 10.1128/JB.06023-11.

Hacquard, Stéphane; Spaepen, Stijn; Garrido-Oter, Ruben; Schulze-Lefert, Paul (2017): Interplay Between Innate Immunity and the Plant Microbiota. In *Annual review of phytopathology* 55, pp. 565–589. DOI: 10.1146/annurev-phyto-080516-035623.

Harbort, Christopher J.; Hashimoto, Masayoshi; Inoue, Haruhiko; Niu, Yulong; Guan, Rui; Rombolà, Adamo D. et al. (2020): Root-Secreted Coumarins and the Microbiota Interact to Improve Iron Nutrition in Arabidopsis. In *Cell host & microbe* 28 (6), 825-837.e6. DOI: 10.1016/j.chom.2020.09.006.

Helmann, John D. (2016): Bacillus subtilis extracytoplasmic function (ECF) sigma factors and defense of the cell envelope. In *Current opinion in microbiology* 30, pp. 122–132. DOI: 10.1016/j.mib.2016.02.002.

Hess, Sebastian (2017): Hunting for agile prey: trophic specialisation in leptophryid amoebae (Vampyrellida, Rhizaria) revealed by two novel predators of planktonic algae. In *FEMS microbiology ecology* 93 (9). DOI: 10.1093/femsec/fix104.

Hess, Sebastian; Sausen, Nicole; Melkonian, Michael (2012): Shedding light on vampires: the phylogeny of vampyrellid amoebae revisited. In *PloS one* 7 (2), e31165. DOI: 10.1371/journal.pone.0031165.

Ho, Theresa D.; Hastie, Jessica L.; Intile, Peter J.; Ellermeier, Craig D. (2011): The Bacillus subtilis extracytoplasmic function σ factor σ(V) is induced by lysozyme and provides resistance to lysozyme. In *Journal of bacteriology* 193 (22), pp. 6215–6222. DOI: 10.1128/JB.05467-11.

Hu, Lingfei; Robert, Christelle A. M.; Cadot, Selma; Zhang, Xi; Ye, Meng; Li, Beibei et al. (2018): Root exudate metabolites drive plant-soil feedbacks on growth and defense by shaping the rhizosphere microbiota. In *Nature communications* 9 (1), p. 2738. DOI: 10.1038/s41467-018-05122-7.

Jack, D. L.; Storms, M. L.; Tchieu, J. H.; Paulsen, I. T.; Saier, M. H. (2000): A broad-specificity multidrug efflux pump requiring a pair of homologous SMR-type proteins. In *Journal of bacteriology* 182 (8), pp. 2311–2313. DOI: 10.1128/JB.182.8.2311-2313.2000.

Johnson, Christopher M.; Grossman, Alan D. (2014): Identification of host genes that affect acquisition of an integrative and conjugative element in Bacillus subtilis. In *Molecular microbiology* 93 (6), pp. 1284–1301. DOI: 10.1111/mmi.12736.

Jorasch, P.; Wolter, F. P.; Zähringer, U.; Heinz, E. (1998): A UDP glucosyltransferase from Bacillus subtilis successively transfers up to four glucose residues to 1,2-diacylglycerol: expression of ypfP in Escherichia coli and structural analysis of its reaction products. In *Molecular microbiology* 29 (2), pp. 419–430. DOI: 10.1046/j.1365-2958.1998.00930.x.

Josefsson, J. O. (1966): Some bioelectrical properties of Amoeba proteus. In *Acta physiologica Scandinavica* 66 (4), pp. 395–405. DOI: 10.1111/j.1748-1716.1966.tb03216.x.

Kabsch, Wolfgang; Sander, Christian (1983): Dictionary of protein secondary structure: Pattern recognition of hydrogen-bonded and geometrical features. In *Biopolymers* 22 (12), pp. 2577–2637. DOI: 10.1002/bip.360221211.

Kettles, Graeme J.; Bayon, Carlos; Sparks, Caroline A.; Canning, Gail; Kanyuka, Kostya; Rudd, Jason J. (2018): Characterization of an antimicrobial and phytotoxic ribonuclease secreted by the fungal wheat pathogen Zymoseptoria tritici. In *The New phytologist* 217 (1), pp. 320–331. DOI: 10.1111/nph.14786.

Kim, Shanghyeon; Lee, Jaehoo; Lee, Sol; Kim, Hyein; Sim, Ji-Yeong; Pak, Boryeong et al. (2022): Matching amino acids membrane preference profile to improve activity of antimicrobial peptides. In *Communications biology* 5 (1), p. 1199. DOI: 10.1038/s42003-022-04164-4.

Klukowski, Piotr; Riek, Roland; Güntert, Peter (2022): Rapid protein assignments and structures from raw NMR spectra with the deep learning technique ARTINA. In *Nature communications* 13 (1), p. 6151. DOI: 10.1038/s41467-022-33879-5.

Kristian, Sascha A.; Datta, Vivekanand; Weidenmaier, Christopher; Kansal, Rita; Fedtke, Iris; Peschel, Andreas et al. (2005): D-alanylation of teichoic acids promotes group a streptococcus antimicrobial peptide resistance, neutrophil survival, and epithelial cell invasion. In *Journal of bacteriology* 187 (19), pp. 6719–6725. DOI: 10.1128/JB.187.19.6719-6725.2005.

Kunst, F.; Ogasawara, N.; Moszer, I.; Albertini, A. M.; Alloni, G.; Azevedo, V. et al. (1997): The complete genome sequence of the gram-positive bacterium Bacillus subtilis. In *Nature* 390 (6657), pp. 249–256. DOI: 10.1038/36786.

Lee, Donghan; Hilty, Christian; Wider, Gerhard; Wüthrich, Kurt (2006): Effective rotational correlation times of proteins from NMR relaxation interference. In *Journal of magnetic resonance (San Diego, Calif.: 1997)* 178 (1), pp. 72–76. DOI: 10.1016/j.jmr.2005.08.014.

Lee, Keun Pyo; Liu, Kaiwei; Kim, Eun Yu; Medina-Puche, Laura; Dong, Haihong; Duan, Jianli et al. (2020): PLANT NATRIURETIC PEPTIDE A and Its Putative Receptor PNP-R2 Antagonize Salicylic Acid-Mediated Signaling and Cell Death. In *The Plant cell* 32 (7), pp. 2237–2250. DOI: 10.1105/tpc.20.00018.

Leisen, Thomas; Bietz, Fabian; Werner, Janina; Wegner, Alex; Schaffrath, Ulrich; Scheuring, David et al. (2020): CRISPR/Cas with ribonucleoprotein complexes and transiently selected telomere vectors allows highly efficient marker-free and multiple genome editing in Botrytis cinerea. In *PLoS pathogens* 16 (8), e1008326. DOI: 10.1371/journal.ppat.1008326.

Li, J. (2019): Identification of host-specific effectors mediating pathogenicity of the vascular wilt pathogen Verticillium dahliae. Wageningen university & Research.

Malanovic, Nermina; Lohner, Karl (2016): Gram-positive bacterial cell envelopes: The impact on the activity of antimicrobial peptides. In *Biochimica et biophysica acta* 1858 (5), pp. 936–946. DOI: 10.1016/j.bbamem.2015.11.004.

Mallagaray, Alvaro; Creutznacher, Robert; Dülfer, Jasmin; Mayer, Philipp H. O.; Grimm, Lena Lisbeth; Orduña, Jose Maria et al. (2019): A post-translational modification of human Norovirus capsid protein attenuates glycan binding. In *Nature communications* 10 (1), p. 1320. DOI: 10.1038/s41467-019-09251-5.

Marston, A. L.; Thomaides, H. B.; Edwards, D. H.; Sharpe, M. E.; Errington, J. (1998): Polar localization of the MinD protein of Bacillus subtilis and its role in selection of the mid-cell division site. In *Genes & development* 12 (21), pp. 3419–3430. DOI: 10.1101/gad.12.21.3419.

Mauch-Mani, Brigitte; Baccelli, Ivan; Luna, Estrella; Flors, Victor (2017): Defense Priming: An Adaptive Part of Induced Resistance. In *Annual review of plant biology* 68, pp. 485–512. DOI: 10.1146/annurev-arplant-042916-041132.

Mol, L.; van Riessen, H. W. (1995): Effect of plant roots on the germination of microsclerotia ofVerticillum dahliae. In *Eur J Plant Pathol* 101 (6), pp. 673–678. DOI: 10.1007/BF01874871.

Müller, Anna; Wenzel, Michaela; Strahl, Henrik; Grein, Fabian; Saaki, Terrens N. V.; Kohl, Bastian et al. (2016): Daptomycin inhibits cell envelope synthesis by interfering with fluid membrane microdomains. In *Proceedings of the National Academy of Sciences of the United States of America* 113 (45), E7077-E7086. DOI: 10.1073/pnas.1611173113.

Ökmen, Bilal; Katzy, Philipp; Huang, Luyao; Wemhöner, Raphael; Doehlemann, Gunther (2023): A conserved extracellular Ribo1 with broad-spectrum cytotoxic activity enables smut fungi to compete with host-associated bacteria. In *The New phytologist* 240 (5), pp. 1976–1989. DOI: 10.1111/nph.19244.

Percy, Matthew G.; Gründling, Angelika (2014): Lipoteichoic acid synthesis and function in gram-positive bacteria. In *Annual review of microbiology* 68, pp. 81–100. DOI: 10.1146/annurev-micro-091213-112949.

Pfeilmeier, Sebastian; Petti, Gabriella C.; Bortfeld-Miller, Miriam; Daniel, Benjamin; Field, Christopher M.; Sunagawa, Shinichi; Vorholt, Julia A. (2021): The plant NADPH oxidase RBOHD is required for microbiota homeostasis in leaves. In *Nature microbiology* 6 (7), pp. 852–864. DOI: 10.1038/s41564-021-00929-5.

Pieterse, Corné M. J.; Zamioudis, Christos; Berendsen, Roeland L.; Weller, David M.; van Wees, Saskia C. M.; Bakker, Peter A. H. M. (2014): Induced systemic resistance by beneficial microbes. In *Annual review of phytopathology* 52, pp. 347–375. DOI: 10.1146/annurev-phyto-082712-102340.

Rau, A.; Hogg, T.; Marquardt, R.; Hilgenfeld, R. (2001): A new lysozyme fold. Crystal structure of the muramidase from Streptomyces coelicolor at 1.65 A resolution. In *The Journal of biological chemistry* 276 (34), pp. 31994–31999. DOI: 10.1074/jbc.M102591200.

Rautenbach, Marina; Troskie, Anscha M.; Vosloo, J. Arnold (2016): Antifungal peptides: To be or not to be membrane active. In *Biochimie* 130, pp. 132–145. DOI: 10.1016/j.biochi.2016.05.013.

Saeloh, Dennapa; Tipmanee, Varomyalin; Jim, Kin Ki; Dekker, Marien P.; Bitter, Wilbert; Voravuthikunchai, Supayang P. et al. (2018): The novel antibiotic rhodomyrtone traps membrane proteins in vesicles with increased fluidity. In *PLoS pathogens* 14 (2), e1006876. DOI: 10.1371/journal.ppat.1006876.

Sampedro, Javier; Cosgrove, Daniel J. (2005): The expansin superfamily. In *Genome biology* 6 (12), p. 242. DOI: 10.1186/gb-2005-6-12-242.

Snelders, Nick C.; Boshoven, Jordi C.; Song, Yin; Schmitz, Natalie; Fiorin, Gabriel L.; Rovenich, Hanna et al. (2023): A highly polymorphic effector protein promotes fungal virulence through suppression of plant-associated Actinobacteria. In *The New phytologist* 237 (3), pp. 944–958. DOI: 10.1111/nph.18576.

Snelders, Nick C.; Kettles, Graeme J.; Rudd, Jason J.; Thomma, Bart P. H. J. (2018): Plant pathogen effector proteins as manipulators of host microbiomes? In *Molecular plant pathology* 19 (2), pp. 257–259. DOI: 10.1111/mpp.12628.

Snelders, Nick C.; Petti, Gabriella C.; van den Berg, Grardy C. M.; Seidl, Michael F.; Thomma, Bart P. H. J. (2021): An ancient antimicrobial protein co-opted by a fungal plant pathogen for in planta mycobiome manipulation. In *Proceedings of the National Academy of Sciences of the United States of America* 118 (49). DOI: 10.1073/pnas.2110968118.

Snelders, Nick C.; Rovenich, Hanna; Petti, Gabriella C.; Rocafort, Mercedes; van den Berg, Grardy C. M.; Vorholt, Julia A. et al. (2020): Microbiome manipulation by a soil-borne fungal plant pathogen using effector proteins. In *Nature plants* 6 (11), pp. 1365–1374. DOI: 10.1038/s41477-020-00799-5.

Soldo, Blazenka; Scotti, Claudio; Karamata, Dimitri; Lazarevic, Vladimir (2003): The Bacillus subtilis Gne (GneA, GalE) protein can catalyse UDP-glucose as well as UDP-N-acetylglucosamine 4-epimerisation. In *Gene* 319, pp. 65–69. DOI: 10.1016/s0378-1119(03)00793-5.

Spindler, E. C.; Hale, J. D. F.; Giddings, T. H.; Hancock, R. E. W.; Gill, R. T. (2011): Deciphering the mode of action of the synthetic antimicrobial peptide Bac8c. In *Antimicrobial agents and chemotherapy* 55 (4), pp. 1706–1716. DOI: 10.1128/AAC.01053-10.

Te Winkel, J. Derk; Gray, Declan A.; Seistrup, Kenneth H.; Hamoen, Leendert W.; Strahl, Henrik (2016): Analysis of Antimicrobial-Triggered Membrane Depolarization Using Voltage Sensitive Dyes. In *Frontiers in cell and developmental biology* 4, p. 29. DOI: 10.3389/fcell.2016.00029.

Trivedi, Pankaj; Leach, Jan E.; Tringe, Susannah G.; Sa, Tongmin; Singh, Brajesh K. (2020): Plant-microbiome interactions: from community assembly to plant health. In *Nature reviews. Microbiology* 18 (11), pp. 607–621. DOI: 10.1038/s41579-020-0412-1.

Tsai, K. J.; Yoon, K. P.; Lynn, A. R. (1992): ATP-dependent cadmium transport by the cadA cadmium resistance determinant in everted membrane vesicles of Bacillus subtilis. In *Journal of bacteriology* 174 (1), pp. 116–121. DOI: 10.1128/jb.174.1.116-121.1992.

van Kempen, Michel; Kim, Stephanie S.; Tumescheit, Charlotte; Mirdita, Milot; Lee, Jeongjae; Gilchrist, Cameron L. M. et al. (2024): Fast and accurate protein structure search with Foldseek. In *Nature biotechnology* 42 (2), pp. 243–246. DOI: 10.1038/s41587-023-01773-0.

van Opijnen, Tim; Lazinski, David W.; Camilli, Andrew (2014): Genome-Wide Fitness and Genetic Interactions Determined by Tn-seq, a High-Throughput Massively Parallel Sequencing Method for Microorganisms. In *Current protocols in molecular biology* 106, 7.16.1-7.16.24. DOI: 10.1002/0471142727.mb0716s106.

Velásquez, André C.; Castroverde, Christian Danve M.; He, Sheng Yang (2018): Plant-Pathogen Warfare under Changing Climate Conditions. In *Current biology: CB* 28 (10), R619-R634. DOI: 10.1016/j.cub.2018.03.054.

Vogel, Christine M.; Potthoff, Daniel B.; Schäfer, Martin; Barandun, Niculò; Vorholt, Julia A. (2021): Protective role of the Arabidopsis leaf microbiota against a bacterial pathogen. In *Nature microbiology* 6 (12), pp. 1537–1548. DOI: 10.1038/s41564-021-00997-7.

Vorland, L. H.; Ulvatne, H.; Rekdal, O.; Svendsen, J. S. (1999): Initial binding sites of antimicrobial peptides in Staphylococcus aureus and Escherichia coli. In *Scandinavian journal of infectious diseases* 31 (5), pp. 467–473. DOI: 10.1080/00365549950163987.

Wang, Yu Hua; Gehring, Chris; Irving, Helen R. (2011): Plant natriuretic peptides are apoplastic and paracrine stress response molecules. In *Plant & cell physiology* 52 (5), pp. 837–850. DOI: 10.1093/pcp/pcr036.

Wenzel, Michaela; Patra, Malay; Senges, Christoph Helmut Rudi; Ott, Ingo; Stepanek, Jennifer Janina; Pinto, Antonio et al. (2013): Analysis of the mechanism of action of potent antibacterial hetero-tri-organometallic compounds: a structurally new class of antibiotics. In *ACS chemical biology* 8 (7), pp. 1442–1450. DOI: 10.1021/cb4000844.

Wiedemann, I.; Breukink, E.; van Kraaij, C.; Kuipers, O. P.; Bierbaum, G.; Kruijff, B. de; Sahl, H. G. (2001): Specific binding of nisin to the peptidoglycan precursor lipid II combines pore formation and inhibition of cell wall biosynthesis for potent antibiotic activity. In *The Journal of biological chemistry* 276 (3), pp. 1772–1779. DOI: 10.1074/jbc.M006770200.

Williamson, Mike P. (2013): Using chemical shift perturbation to characterise ligand binding. In *Progress in nuclear magnetic resonance spectroscopy* 73, pp. 1–16. DOI: 10.1016/j.pnmrs.2013.02.001.

Wilson, Sean A.; Tank, Raveen K. J.; Hobbs, Jamie K.; Foster, Simon J.; Garner, Ethan C. (2023): An exhaustive multiple knockout approach to understanding cell wall hydrolase function in Bacillus subtilis. In *mBio* 14 (5), e0176023. DOI: 10.1128/mbio.01760-23.

Yamaguchi, Hiroyuki; Furuhata, Kazumi; Fukushima, Tatsuya; Yamamoto, Hiroki; Sekiguchi, Junichi (2004): Characterization of a new Bacillus subtilis peptidoglycan hydrolase gene, yvcE (named cwlO), and the enzymatic properties of its encoded protein. In *Journal of bioscience and bioengineering* 98 (3), pp. 174–181. DOI: 10.1016/S1389-1723(04)00262-2.

Yang, Xu; Huang, En; Yousef, Ahmed E. (2017): Brevibacillin, a cationic lipopeptide that binds to lipoteichoic acid and subsequently disrupts cytoplasmic membrane of Staphylococcus aureus. In *Microbiological research* 195, pp. 18–23. DOI: 10.1016/j.micres.2016.11.002.

Yasbin, R. E.; Maino, V. C.; Young, F. E. (1976): Bacteriophage resistance in Bacillus subtilis 168, W23, and interstrain transformants. In *Journal of bacteriology* 125 (3), pp. 1120–1126. DOI: 10.1128/jb.125.3.1120-1126.1976.

Yeaman, Michael R.; Yount, Nannette Y. (2003): Mechanisms of antimicrobial peptide action and resistance. In *Pharmacological reviews* 55 (1), pp. 27–55. DOI: 10.1124/pr.55.1.2.

Zasloff, Michael (2002): Antimicrobial peptides of multicellular organisms. In *Nature* 415 (6870), pp. 389–395. DOI: 10.1038/415389a.

Zellmeier, Stephan; Hofmann, Claudia; Thomas, Sylvia; Wiegert, Thomas; Schumann, Wolfgang (2005): Identification of sigma(V)-dependent genes of Bacillus subtilis. In *FEMS microbiology letters* 253 (2), pp. 221–229. DOI: 10.1016/j.femsle.2005.09.056.

Chapter 4

Antimicrobial activity of plant natriuretic peptides and their potential role in microbiota interactions

Gabriella C. Petti[1], Zoe Prockl[1], Lila Cadiou[1], Anton Kraege[1], Nick C. Snelders[2], Bart P.H.J. Thomma[1]

[1]University of Cologne, Institute for Plant Sciences, Cluster of Excellence on Plant Sciences (CEPLAS), 50674 Cologne, Germany

[2]Laboratory of Phytopathology, Wageningen University & Research, 6708 PB Wageningen, The Netherlands

Abstract

Plants assemble diverse microbial communities across above- and belowground tissues, comprising mutualistic, commensal, and pathogenic members. To maintain microbiota balance and prevent disease, they employ a range of strategies to regulate microbial colonization, including the production of antimicrobial proteins. Plant natriuretic peptides (PNPs) are small, secreted proteins conserved throughout the plant kingdom, mainly known for their roles in regulation of water household and stress responses. Notably, *PNP* gene homologs have been horizontally acquired by particular plant-associated organisms, including the fungal pathogen *Verticillium dahliae*, where a PNP homolog was shown to display selective antimicrobial activity and promote host colonization by modulating the host-associated microbiota. Here, we show that diverse PNPs from *Arabidopsis thaliana*, *Solanum lycopersicum*, *Physcomitrium patens*, but also the plant pest insect *Bemisia tabaci* exhibit antibacterial and antifungal activity *in vitro*. The antimicrobial activity of the diverse PNPs correlates with a net positive surface charge, suggesting a charge-dependent mechanism for the antimicrobial activity. Additionally, we show that deletion of *PNP* genes in *A. thaliana* alters phyllosphere bacterial community compositions, as determined by amplicon sequencing-based microbiota profiling, whereas fungal communities remained unaffected. These findings suggest that plant PNPs function as charge-dependent antimicrobial proteins and shape phyllosphere bacterial communities.

Introduction

Plant natriuretic peptides (PNPs) are a class of small (approximately 14 kDa) signalling proteins that are secreted into the apoplast, where they contribute to diverse physiological processes (Boudart et al. 2005; Wang et al. 2011). The best-characterized is AtPNP-A, one of two PNPs encoded by *Arabidopsis thaliana*, which has been shown to play a role in stomatal aperture regulation, osmotic-dependent cell volume changes, ion flux modulation, cellular redox homeostasis and biotic stress responses (Maryani et al. 2001; Ludidi et al. 2002; Wang et al. 2007; Ficarra et al. 2018). Several of these processes are mediated via elevation of intracellular cyclic guanosine monophosphate (cGMP) levels (Ludidi et al. 2002; Pharmawati et al. 2001; Wang et al. 2007). Two plasma membrane-localized receptors, AtPNP-R1 and AtPNP-R2, act as interactors of AtPNP-A (Turek and Gehring 2016; Lee et al. 2020). AtPNP-R1 contains a guanylyl cyclase (GC) catalytic center that converts GTP to cGMP and is involved in the regulation of stomatal aperture (Turek and Gehring 2016; Di Paolo et al. 2023). In contrast, AtPNP-R2 lacks a GC catalytic domain and, although its mode of action is less well characterized, it influences defence signalling by negatively regulating salicylic acid levels (Lee et al. 2020). Although both receptors act in the AtPNP-A-mediated regulation of water homeostasis, they are thought to have distinct, nonoverlapping functions (Lee et al. 2020).

The involvement of AtPNP-A in biotic stress responses is supported by gene expression analysis and pathogen infection assays. Transcriptomic analyses have shown that AtPNP-A is co-expressed with genes involved in systemic acquired resistance, such as the pathogenesis related (PR) genes *PR-1*, *PR-2* and *PR-3* (Meier et al. 2008). Additionally, overexpression of AtPNP-A in *Arabidopsis* results in enhanced resistance to *Pseudomonas syringae*, characterized by milder disease symptoms and reduced bacterial proliferation, while *AtPNP-A* knockout mutants display increased *P. syringae* susceptibility, including enhanced bacterial titres (Ficarra et al. 2018). Furthermore, AtPNP-A expression is induced upon *P. syringae* infection, supporting its role in defence responses (Ficarra et al. 2018).

PNP genes are widely conserved across the plant kingdom, occurring in bryophytes, gymnosperms, and angiosperms, with some species encode multiple paralogs (Patané et al. 2022). Interestingly, PNP-like genes were also found in organisms that interact with plants, including plant pathogens and pests that have acquired these PNP homologs through horizontal gene transfer (HGT) from plants (de Jonge et al. 2012; Gottig et al. 2008, 2008;

Patané et al. 2022). For instance, the bacterial plant pathogen *Xanthomonas citri* carries a PNP-like gene, *XacPNP*, acquired via HGT and contributes to virulence during host colonization (Gottig et al. 2008; Moreira et al. 2010). Deletion of *XacPNP* results in more necrotic lesions and earlier bacterial death, along with reduced photosynthetic efficiency and impaired net water flux in infected leaves (Gottig et al. 2008). Therefore, it was suggested that XacPNP enhances virulence by minimizing host damage and supporting water homeostasis (Gottig et al. 2008). Similarly, the fungal plant pathogen *Verticillium dahliae* carries the PNP-like gene *VdAve1* which was acquired from plants through HGT and contributes to virulence during host colonization (de Jonge et al. 2012). Interestingly, it was shown that VdAve1 contributes to *V. dahliae* host colonization by suppressing microbial antagonists present in the host microbiota (Snelders et al. 2020). Functional characterization revealed that VdAve1 is a bactericidal protein that exerts its antimicrobial activity by establishing electrostatic interactions with negatively charged bacterial plasma membranes, leading to membrane disruption and cell death (Snelders et al. 2020; Chapter 3). These findings suggested that PNPs may act as antimicrobials.

To determine whether antimicrobial activity may occur among plant PNPs, or is more likely a function that emerged in VdAve1 following horizontal gene transfer, an Arabidopsis PNP, AtPNP-A, was tested for antimicrobial activity. Notably, AtPNP-A inhibited the growth of the bacterium *Bacillus subtilis*, suggesting that antimicrobial activity occurs among plant homologs too (Snelders et al. 2020). Besides in plants and in plant-associated microbes, also a plant-associated pest was reported to harbour a PNP homolog, as the tobacco whitefly *Bemisia tabaci* harbors a PNP homolog that was gained via HGT (Patané et al. 2022).

Plants live in close association with a dynamic microbiota composed of bacteria, fungi, and other microorganisms that support nutrient uptake, enhance stress tolerance, and modulate immunity (Berendsen et al. 2012; Bulgarelli et al. 2013; Hacquard et al. 2017; Trivedi et al. 2020). The composition of these communities varies across different plant compartments, such as the rhizosphere, phyllosphere, and endosphere, and is shaped by both environmental factors and host genotype (Trivedi et al. 2020). The plant microbiota comprises microbes with mutualistic, beneficial and pathogenic potential (Trivedi et al. 2020). Accordingly, plants must regulate microbial colonization to maintain microbiota balance and prevent disease. To this

end, plants deploy a range of defence strategies, including the production of antimicrobial proteins (van Loon et al. 2006).

Plants produce a broad arsenal of antimicrobial proteins to defend against microbial pathogens and maintain a balanced microbiota. These proteins can be constitutively expressed or induced upon pathogen recognition and act through diverse mechanisms to inhibit microbial growth and colonization (van Loon et al. 2006). Among the most extensively studied are the pathogenesis-related (PR) proteins, which are typically upregulated in response to pathogen infection. PR proteins encompass several functionally distinct families, including glucanases, chitinases, and defensins, many of which exhibit direct antimicrobial activity by targeting microbial cell walls or membranes (van Loon et al. 2006). These proteins participate in the plant immune system and contribute to both local and systemic resistance responses (Dorey et al. 1997; Durrant and Dong 2004).

Given the antimicrobial activity of AtPNP-A, its role in responses against *P. syringae*, and considering that the fungal homolog VdAve1 modulates host-associated microbiota, we hypothesize that PNPs may represent a previously unrecognized class of antimicrobial plant proteins that contribute to microbiota regulation *in planta*. To explore this hypothesis, we tested PNPs from diverse plant species for antimicrobial activity and analysed microbiota shifts in Arabidopsis *PNP* deletion mutants.

Results

PNPs display antimicrobial activity

To assess whether the antimicrobial activity of the PNP family extends to other members beyond AtPNP-A (Snelders et al. 2020), we selected PNP homologs from diverse plant lineages; the dicotyledons *A. thaliana* and *Solanum lycopersicum*, and the bryophyte *Physcomitrium patens*. More specifically, the two previously identified *A. thaliana* PNPs, AtPNP-A (gene locus AT2G18660) and AtPNP-B (gene locus AT4G30380), were selected (Ludidi et al. 2002). In *S. lycopersicum*, one PNP homolog had been previously reported, here referred to as SlPNP-A (gene locus Solyc08g061060) (de Jonge et al. 2012). To identify additional PNP homologs, a phmmer search (Finn et al. 2011) was performed using the amino acid sequence of the PNP-like protein VdAve1 as a query against the UniProt Reference Proteomes database (The UniProt

Consortium 2023), with an E-value cutoff of 1e−5. This search identified three more homologs in tomato, corresponding to the following gene loci: Solyc08g067390 (E = 5.2e−26, referred to as SlPNP-B), Solyc08g061063 (E = 1.5e−22), and Solyc07g006390 (E = 1.6e−5, referred to as SlPNP-C). However, the protein encoded by Solyc08g061063 was predicted by UniProt to contain an N-terminal intrinsically disordered region and lacked a signal peptide, which is an atypical feature for a PNP (Boudart et al. 2005; Ludidi et al. 2002) and was therefore excluded from further analysis. For *P. patens*, the best phmmer hit was selected, corresponding to the gene locus LOC112290798 (PpPNP-A). Finally, we also included the previously reported PNP-like gene horizontally acquired from plants by the whitefly *B. tabaci*, gene locus LOC109042916 (BtPNP).

To evaluate their potential antimicrobial activity, PNPs were heterologously produced in *Escherichia coli* and their effects on microbial growth were tested. Given that *V. dahliae* Ave1 and *A. thaliana* AtPNP-A were previously shown to inhibit *Bacillus subtilis* growth, we focused on *Bacillus* as target genus and tested the impact on the plant-associated species *B. drentensis* (Chavarro-Carrero et al. 2024). Interestingly, all tested PNPs, except SlPNP-B and SlPNP-C, strongly inhibited growth of *B. drentensis* at low micromolar concentrations (Figure 1a), confirming that several PNPs have antibacterial activity. We then tested the activity of the *A. thaliana PNPs* on two plant-associated bacteria, *Pseudomonas syringae* and *Xanthomonas campestris*. Both bacteria were inhibited by the AtPNPs (Figure 1b). Furthermore, we screened the PNPs for antifungal activity against the yeast *Cyberlindnera jadinii*, showing that, similar to the antibacterial activity, all PNPs except SlPNP-B and SlPNP-C inhibited fungal growth (Figure 1c). Finally, we tested the activity of the *A. thaliana PNPs* on two plant-associated fungi, *Alternaria brassicicola* and *Verticillium dahliae*. Growth of both fungi was inhibited by the AtPNPs (Figure 1d).

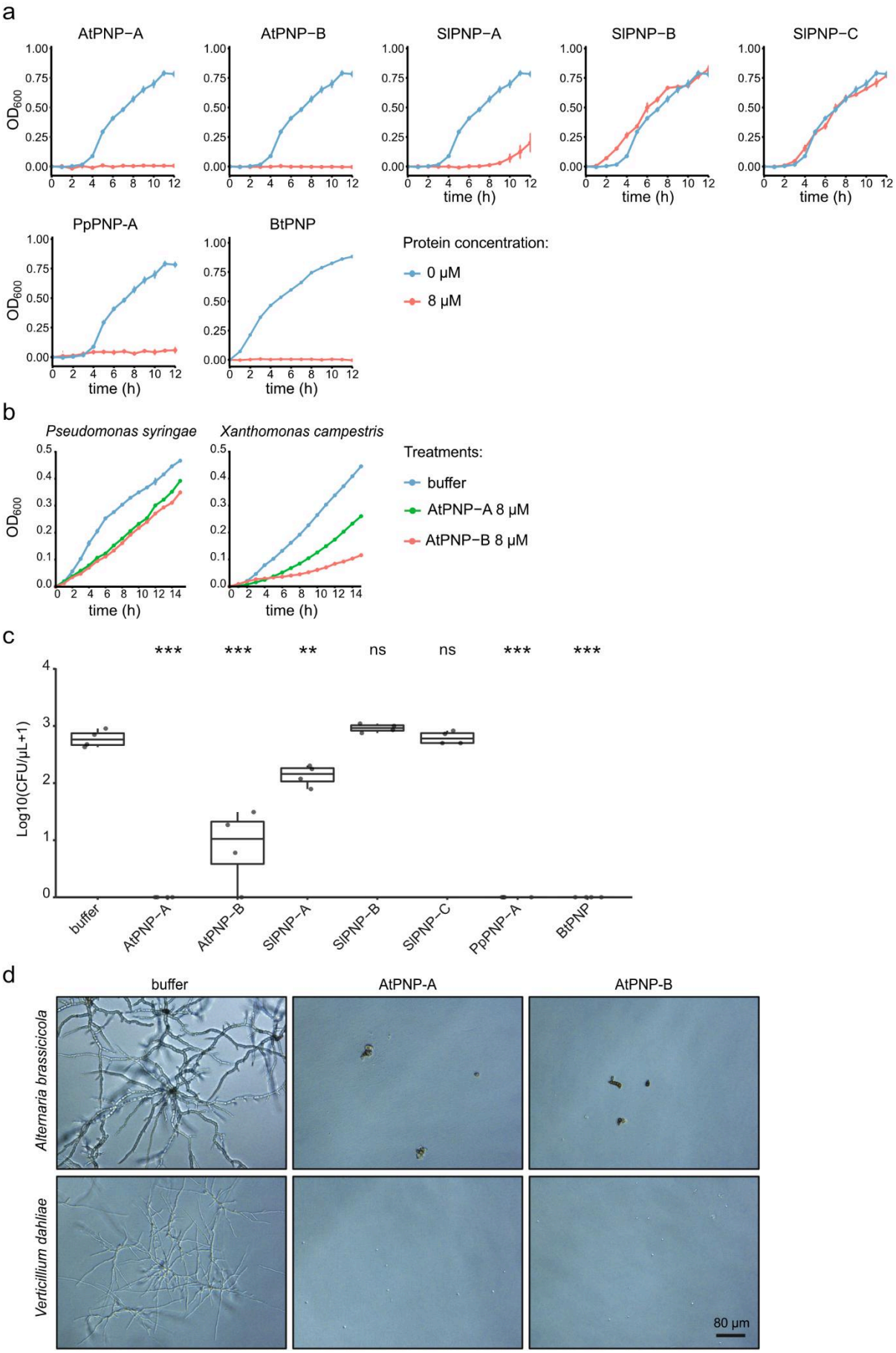
a
AtPNP−A
AtPNP−B
SlPNP−A
SlPNP−B
SlPNP−C
PpPNP−A
BtPNP
OD600
time (h)
Protein concentration:
0 μM
8 μM
b
Pseudomonas syringae
Xanthomonas campestris
Treatments:
buffer
AtPNP−A 8 μM
AtPNP−B 8 μM
c
*** *** ** ns ns *** ***
Log10(CFU/μL+1)
buffer
AtPNP−A
AtPNP−B
SlPNP−A
SlPNP−B
SlPNP−C
PpPNP−A
BtPNP
d
buffer
AtPNP-A
AtPNP-B
Alternaria brassicicola
Verticillium dahliae
80 μm

Figure 1. PNPs display antimicrobial activity. a. Growth curves of *Bacillus drentensis* incubated in the presence (red) or absence (blue) of 8 μM of *Arabidopsis thaliana* AtPNP-A and AtPNP-B, *Solanum lycopersicum* SlPNP-A, SlPNP-B and SlPNP-C, *Physcomitrella patens* PpPNP-A and *Bemisia tabaci* BtPNP. Graphs represent mean OD_{600} values ± standard error (n=3). **b.** Growth curves of *Pseudomonas syringae* and *Xanthomonas campestris* incubated with buffer (red), AtPNP-A (green) or AtPNP-B (blue). Graphs represent mean values ± standard error (n=3). **c.** *Cyberlindnera jadinii* colony-forming units (CFUs) after overnight incubation with corresponding PNPs at a final concentration of 8 μM. Data are shown as $\log_{10}(x+1)$-transformed CFUs (n=4). All treatments were compared to the buffer control, with statistical analysis performed using one-way ANOVA followed by Tukey's post hoc test (*P*-values: **p*-value < 0.05, ***p*-value < 0.01, ****p*-value < 0.001). **d.** Representative microscopic pictures of the fungal plant pathogens *Alternaria brassicicola* and *Verticillium dahliae* grown in 5% potato dextrose broth (PDB) supplemented with buffer, AtPNP-A or AtPNP-B at a final concentration of 8 μM. Pictures were taken after 18h of incubation.

PNPs displaying antimicrobial activity are positively charged

To better understand PNP antimicrobial activity, we examined the sequences and predicted structures of the PNPs included in this study. Multiple sequence alignment revealed pairwise identities ranging from 31% to 66% (Figure 2a,b). Notably, PpPNP-A contains an extended N-terminal region that lacks in the other homologs. To address the possibility that this unique N-terminal extension might result from a genome annotation artifact, we queried publicly available RNA-sequencing data for RNA-seq reads spanning the canonical PNP domain and the upstream N-terminal region. The identification of such reads confirmed that this extension is transcribed as part of a single transcript (Figure S 1), suggesting that the N-terminal domain is a genuine feature of *PpPNP-A*. Using AlphaFold (Jumper et al. 2021), we predicted three-dimensional structures of the PNPs. Despite the relative low degree of sequence conservation all PNPs displayed a conserved overall fold, with the exception of PpPNP-A in which the additional N-terminal domain protrudes from the core structure (Figure 2c).

The activity of many antimicrobial proteins depends on their positive charge, which promotes interactions with negatively charged microbial surfaces and causes microbial membrane disruption (Shai 2002). We previously showed that the antimicrobial activity of the PNP-like protein VdAve1 is primarily driven by charge-mediated interactions (Chapter 3). Accordingly, we hypothesized that a similar mechanism may underlie the activity of other PNPs. To test this, we quantified the surface charge of the predicted protein structures by calculating their mean electrostatic surface potential. Strikingly, all PNPs that showed antimicrobial activity (AtPNP-A, AtPNP-B, SlPNP-A, PpPNP-A, BtPNP) have an overall positive surface charge, whereas the two PNPs that did no show antimicrobial activity (SlPNP-B and SlPNP-C) are negatively charged

(Figure 3). These findings suggest that the positive charge of the active PNPs contributes to their antimicrobial activity by facilitating electrostatic interactions with microbial surfaces.

a

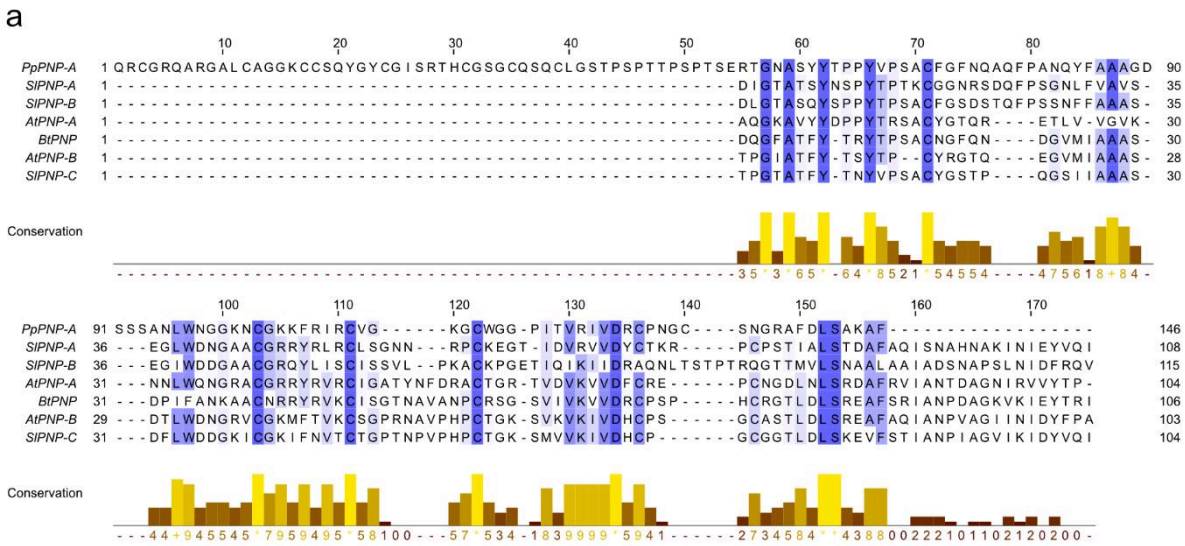

b

	AtPNP-A	AtPNP-B	SlPNP-A	SlPNP-B	SlPNP-C	PpPNP-A	BtPNP
AtPNP-A	100.00	44.34	40.91	31.03	38.10	36.73	44.34
AtPNP-B		100.00	39.64	31.62	65.71	36.73	52.83
SlPNP-A			100.00	43.48	36.94	35.79	42.34
SlPNP-B				100.00	35.04	39.60	35.90
SlPNP-C					100.00	41.84	50.94
PpPNP-A						100.00	36.73
BtPNP							100.00

c

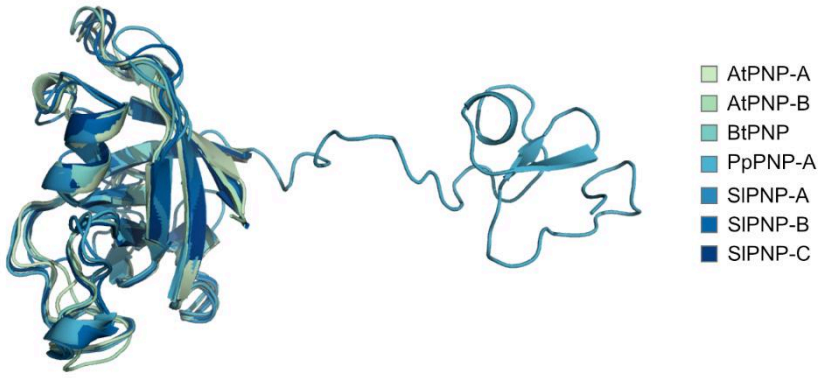

Figure 2. Multiple sequence and structural alignment of PNPs. a. Multiple amino acid sequence alignment of *Arabidopsis thaliana* AtPNP-A and AtPNP-B, *Solanum lycopersicum* SlPNP-A, SlPNP-B and SlPNP-C, *Physcomitrella patens* PpPNP-A and *Bemisia tabaci* BtPNP. Amino acids are colored based on conservation. **b.** PNPs pairwise identity values (%) among the PNP sequences shown in panel a. **c.** AlphaFold-predicted structure alignment of PNPs displayed in panel a.

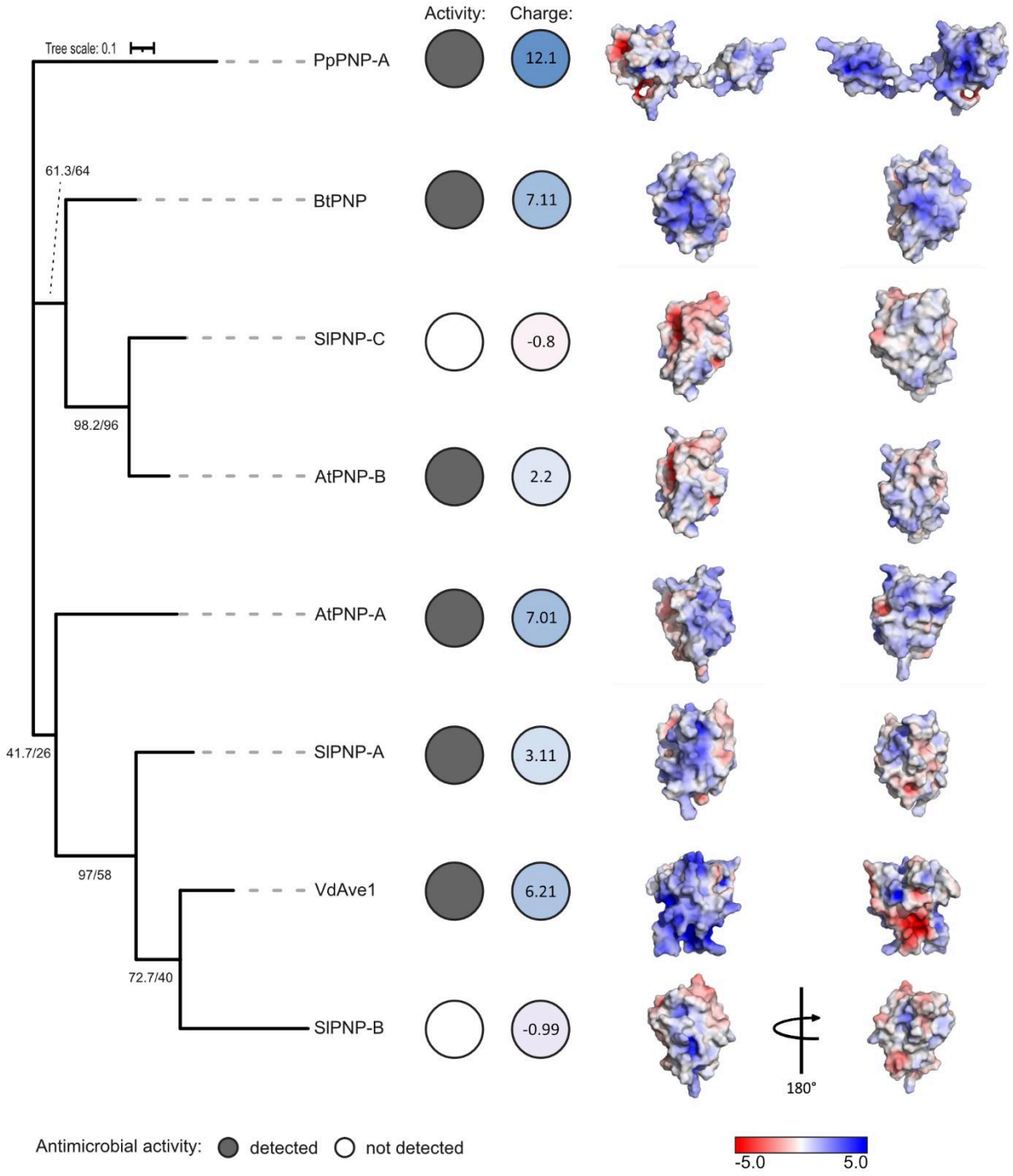

Figure 3. PNPs displaying antimicrobial activity are predicted to have a positive surface charge. The unrooted maximum likelihood phylogenetic tree of PNP homologs was constructed from protein sequences. Branch support values are given as SH-aLRT (%) / ultrafast bootstrap (%) and shown at the corresponding node. Dots next to each protein indicate observed activity in the assays shown in Figure 1 (white: no activity detected; black: activity detected in the tested microbial species) and mean electrostatic surface potential (quantified in kT/e). Predicted 3D structures of the PNPs are shown and colored by electrostatic surface potential, ranging from –5.0 kT/e (red, negative) to +5.0 kT/e (blue, positive).

Arabidopsis thaliana PNPs influence phyllosphere bacterial community composition

Antimicrobials have been shown to contribute to plant-microbiota interactions (Hacquard et al. 2017). In line with this, we previously demonstrated that the plant pathogen *V. dahliae* employs the PNP-like protein VdAve1 during host colonization to modulate host microbiota (Snelders et al. 2020). Given our observation that PNPs exhibit antimicrobial activity (Figure 1), we hypothesized that these proteins may contribute to microbial community regulation in the hosts that produces them.

As a first step toward testing this hypothesis, we examined the expression of *AtPNP-A* and *AtPNP-B* in different *A. thaliana* tissues using a publicly available *A. thaliana* RNA-seq database (Zhang et al. 2020), which comprises over 20,000 datasets from plants subjected to diverse experimental conditions, including (a)biotic stresses. We selected the following tissues: endosperm, flower, seed, root, leaf, silique, seedling, and stem. *AtPNP-A* showed predominant expression in the leaf, seedling, stem, and flower (Figure 4a), whereas *AtPNP-B* expression was mainly detected in the endosperm and silique (Figure 4b).

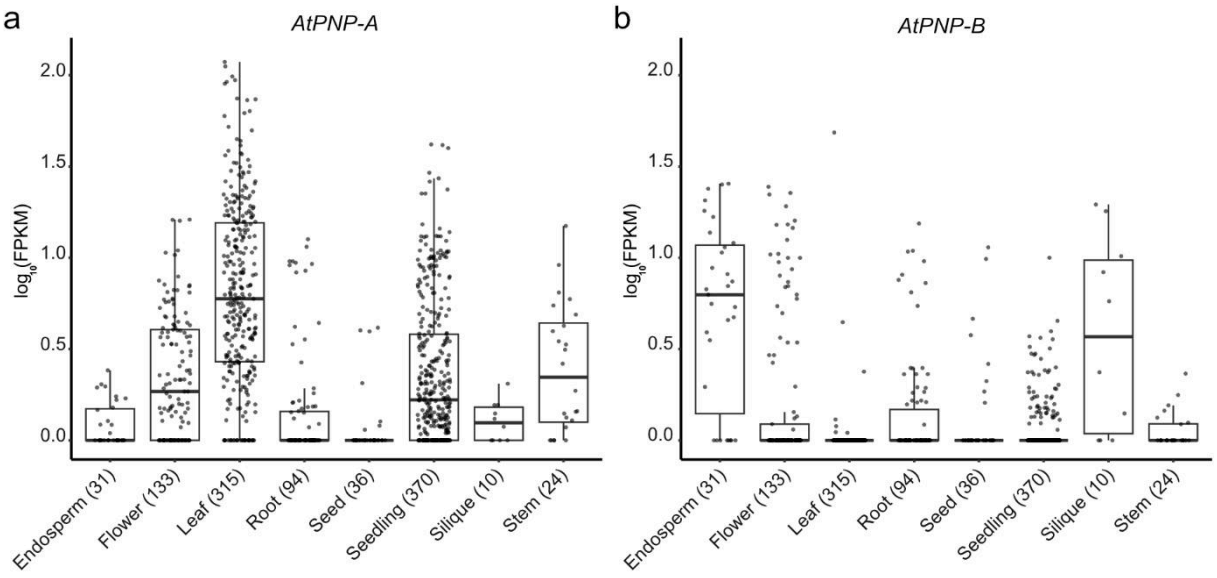

Figure 4. Tissue-specific expression of *Arabidopsis thaliana* PNPs. Expression levels of *AtPNP-A* (**a**) and *AtPNP-B* (**b**) across various *A. thaliana* tissues are shown as $\log_{10}$-transformed fragments per kilobase of transcript per million mapped reads (FPKM) values, based on publicly available RNA-seq data. Each dot represents the $\log_{10}$(FPKM) of the corresponding PNP in an individual RNA-seq dataset. Numbers in brackets indicate the total number of libraries for each tissue.

Given the strong expression of *AtPNP-A* in leaves, we next analysed the bacterial and fungal microbiota in the phyllosphere of *A. thaliana* wild-type (Col-0) plants as well as knock-out

mutants of *PNP-A*, *PNP-B* and double mutants. Although *AtPNP-B* is mainly expressed in reproductive tissues, we included *pnp-b* and *pnp-a/pnp-b* mutants to test for potential indirect effects of *AtPNP-B* on the phyllosphere microbiota. The *A. thaliana* bacterial composition was determined by 16S rDNA amplicon sequencing and visualized via principal coordinate analysis (PCoA) based on Bray-Curtis dissimilarities (Figure 5a). To statistically assess the impact of genotype on microbial variation, we performed PERMANOVA (adonis), which quantifies the proportion of variance explained by a given factor as effect size (R^2). This analysis revealed a clear genotype-dependent shift in the microbiota (Figure 5b), with the *pnp-a* mutant explaining the largest proportion of variation (29%). Surprisingly, the *pnp-b* and *pnp-a/pnp-b* mutants also accounted for 20% of community variation each, despite *AtPNP-B* not being expressed in the phyllosphere. A significant PERMANOVA result can arise from either differences in community composition or differences in the variation between groups. To determine whether variation between genotypes contributed to the significant PERMANOVA result, we performed a beta-dispersion analysis. The analysis revealed no significant differences between genotypes ($F = 1.27$, $p = 0.31$; Table S 1), showing that the PERMANOVA result arises solely from differences in community composition.

Although phylum-level analysis showed no major compositional changes in the overall community (Figure 5c), pairwise comparisons revealed differences when comparing the wild-type to *pnp-a*, showing an increase of Verrucomicrobia and Acidobacteria in the *pnp-a* mutant (Figure 5d). No significant differences were detected between the wild-type and the *pnp-b* or *pnp-a/pnp-b* double mutant at this taxonomic level. At higher taxonomic resolution, more pronounced differences emerged. Pairwise comparisons at the order level identified taxa with differential abundance between wild-type and the PNPs mutants (Figure 5e-g). The Acidobacteria Gp16 and the Proteobacteria Sphingomonadales were increased in *pnp-a* compared to the wild-type, while the Proteobacteria Legionellales were decreased. Notably, although changes in Verrucomicrobia were detected at the phylum level, these differences were not observed at the order level, suggesting that the variation may be dispersed across multiple orders and thus lost at higher taxonomic resolution. The *pnp-b* mutant compared to the wild-type showed an increase in Burkholderiales, and a decrease in unclassified Gammaproteobacteria (Gammaproteobacteria/i.s.). In the *pnp-a/pnp-b* double mutant, the absence of both homologs led to shifts in higher number of orders, including increased

abundance of Cellvibrionales, Burkholderiales, and Acidobacteria Gp16, along with decreased levels of Mycobacteriales, Pseudonocardiales, and Gammaproteobacteria/i.s.

Interestingly, while the *pnp-a* and *pnp-b* mutants showed distinct changes, the double mutant did not simply reflect an additive combination of these alterations. Besides changes in the Acidobacteria Gp16, Burkholderiales and Gammaproteobacteria/i.s which were observed also in the single mutants, several additional taxa were uniquely altered in the double mutant. This includes the increase of Cellvibrionales and decrease in Mycobacteriales and Pseudonocardiales in the double mutant compared to the wild-type, which were not affected in either single mutant. These results suggest that PNPs alter bacterial communities. However, we cannot exclude the possibility that some of the observed differences arise indirectly, for example due to altered physiological traits in the mutants that affect microbiota assemblies.

Despite displaying antifungal activity *in vitro* (Figure 1), ITS-based analysis of fungal communities revealed no significant differences in the mycobiota composition across wild-type, single, or double mutants (Figure 6a, b), indicating that PNPs do not impact the growth of the fungi present in these communities.

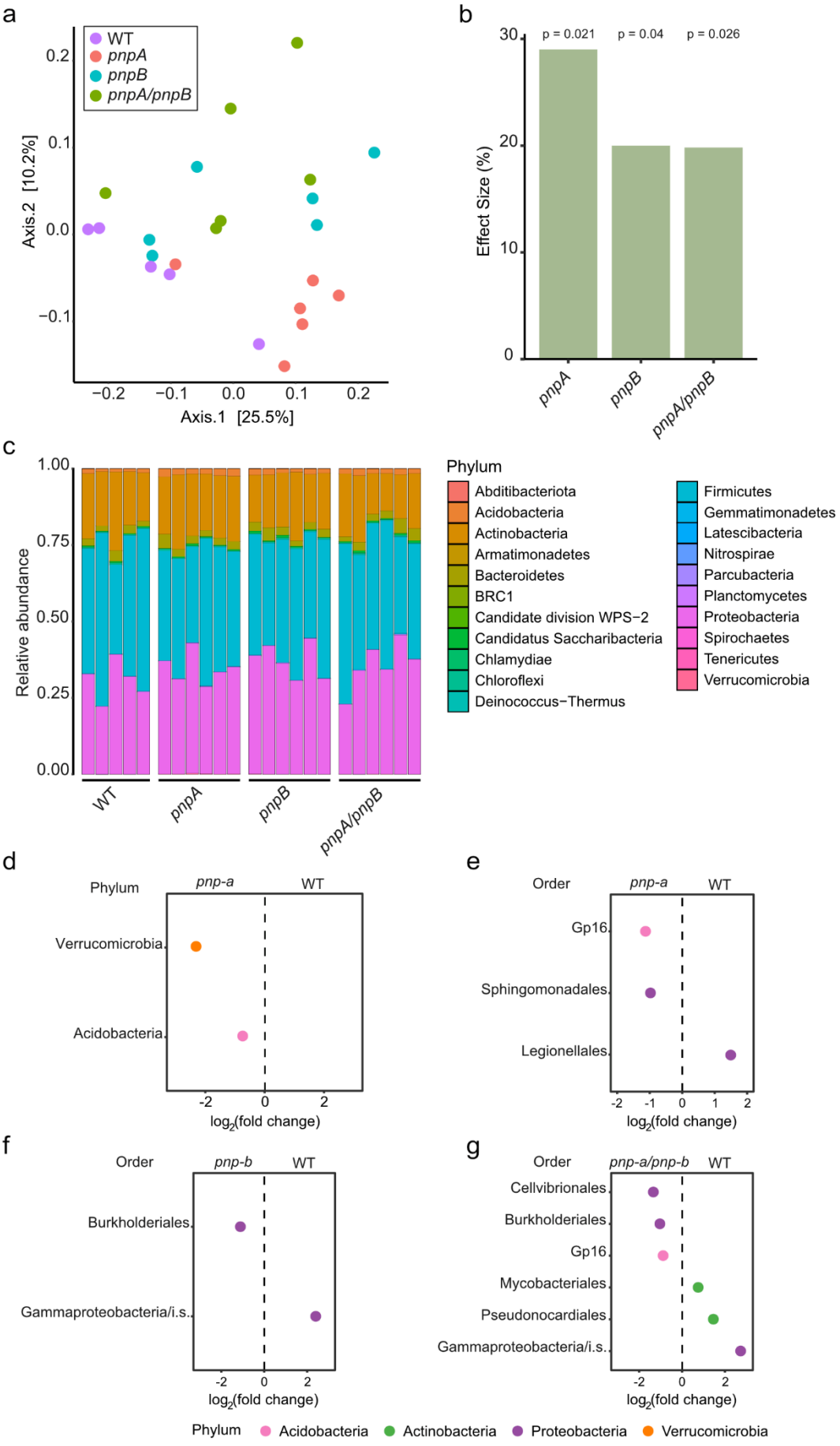
a
WT
pnpA
pnpB
pnpA/pnpB
Axis.2 [10.2%]
Axis.1 [25.5%]
b
p = 0.021
p = 0.04
p = 0.026
Effect Size (%)
pnpA
pnpB
pnpA/pnpB
c
Relative abundance
WT
pnpA
pnpB
pnpA/pnpB
Phylum
Abditibacteriota
Acidobacteria
Actinobacteria
Armatimonadetes
Bacteroidetes
BRC1
Candidate division WPS−2
Candidatus Saccharibacteria
Chlamydiae
Chloroflexi
Deinococcus−Thermus
Firmicutes
Gemmatimonadetes
Latescibacteria
Nitrospirae
Parcubacteria
Planctomycetes
Proteobacteria
Spirochaetes
Tenericutes
Verrucomicrobia
d
Phylum
pnp-a
WT
Verrucomicrobia
Acidobacteria
log2(fold change)
e
Order
pnp-a
WT
Gp16
Sphingomonadales
Legionellales
log2(fold change)
f
Order
pnp-b
WT
Burkholderiales
Gammaproteobacteria/i.s.
log2(fold change)
g
Order
pnp-a/pnp-b
WT
Cellvibrionales
Burkholderiales
Gp16
Mycobacteriales
Pseudonocardiales
Gammaproteobacteria/i.s.
log2(fold change)
Phylum
Acidobacteria
Actinobacteria
Proteobacteria
Verrucomicrobia

Figure 5. PNPs shape the *A. thaliana* phyllosphere bacterial microbiota composition. a. Principal Coordinate Analysis (PCoA) based on Bray-Curtis dissimilarities showing genotype-dependent shifts in bacterial community composition of *A. thaliana* wild-type (Col-0) and PNP mutants (*pnp-a*, *pnp-b*, *pnp-a/pnp-b*). **b.** Effect size (R^2) of genotypic impact on the bacterial community structure, determined with PERMANOVA (permutations, 999) on Bray-Curtis distances. P-values were adjusted using the Benjamini-Hochberg method (n=5 for the wild-type, n=6 for the mutants). **c.** Phylum-level analysis of bacterial community composition showing no major compositional changes across genotypes. **d.** Differential abundance of bacterial phyla in pairwise comparisons between *A. thaliana* wild-type (Col-0) and *pnp-a* (Wald test and Benjamini–Hochberg correction, padj < 0.05). **e-g.** Differential abundance of bacterial orders in pairwise comparisons between *A. thaliana* wild-type (Col-0) and *pnp-a* (**e**), *pnp-b* (**f**) and *pnp-a/pnp-b* (**g**) (Wald test and Benjamini–Hochberg correction, padj < 0.05). Taxa are colored according to phylum identity.

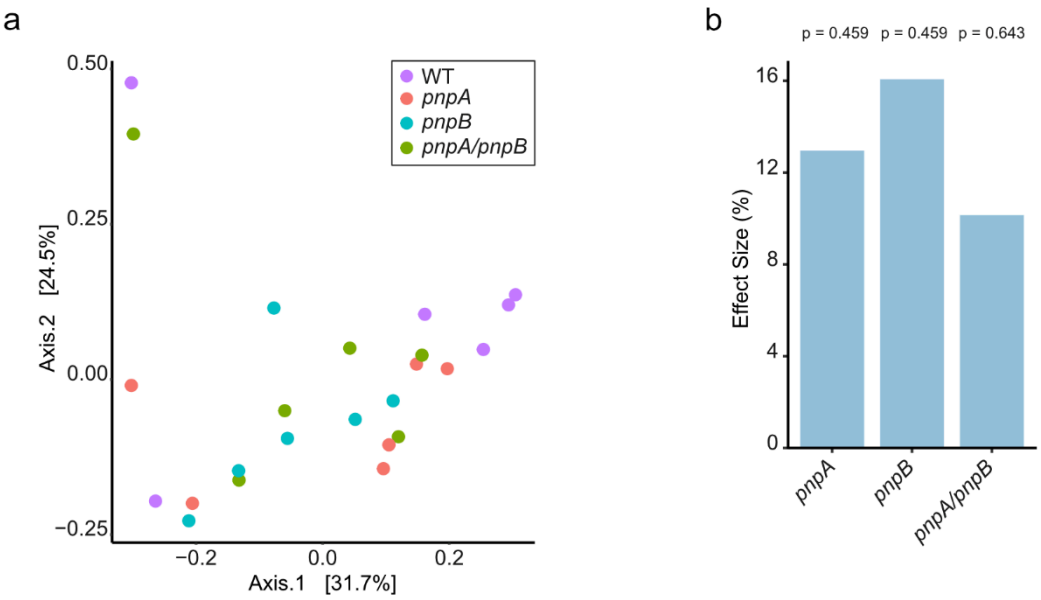

Figure 6. PNPs do not significantly affect the phyllosphere fungal microbiota composition in *A. thaliana*. a. Principal Coordinate Analysis (PCoA) based on Bray-Curtis dissimilarities showing no significant genotype-dependent shifts in fungal community composition among *A. thaliana* wild-type (Col-0) and PNP mutants (*pnp-a*, *pnp-b*, *pnp-a/pnp-b*). **b.** Effect size (R^2) of genotypic impact on fungal community structure, determined with PERMANOVA (permutations, 999) on Bray-Curtis distances (n=6). P-values were adjusted using the Benjamini-Hochberg method. No statistically significant differences were observed between genotypes.

Discussion

Our findings establish PNPs as a previously unrecognized class of antimicrobial proteins. While PNPs have been traditionally associated with the regulation of water homeostasis and stress responses (Maryani et al. 2001; Ludidi et al. 2002; Wang et al. 2007; Ficarra et al. 2018), we demonstrate that their functional repertoire extends to direct antimicrobial activity and potential modulation of bacterial community composition in the phyllosphere.

Our *in vitro* assays demonstrate that PNPs from a phylogenetically diverse set of organisms, including the angiosperms *A. thaliana* and *S. lycopersicum*, the bryophyte *P. patens*, and the insect *B. tabaci*, exert antibacterial and antifungal effects. These findings indicate that antimicrobial activity is a common feature of PNPs across multiple lineages. Among the tested PNPs, only those with a net positive charge displayed antimicrobial activity, supporting the hypothesis that electrostatic interactions underlie their activity. This is consistent with findings on the *V. dahliae* PNP-like protein VdAve1, which binds the cell wall component lipoteichoic acid, potentially increasing the protein concentration at the bacterial surface, and subsequently disrupts the plasma membrane via electrostatic interactions between its positively charged regions and the negatively charged microbial membranes (Chapter 3). Since protein charge is pH-dependent, it remains possible that SlPNP-B and SlPNP-C acquire activity under different physiological conditions.

Beyond *in vitro* activity, we examined the influence of plant PNPs on the composition of the phyllosphere microbiota in *A. thaliana*, revealing significant shifts in bacterial community composition in the *PNP* mutants. Distinct alterations in phyllosphere bacterial communities were observed in *pnp-a* and *pnp-b*, with *pnp-a* having the strongest impact. In the *pnp-a/pnp-b* double mutant, a broader range of bacterial orders was affected. Notably, while all taxa altered in the *pnp-b* mutant were also differentially abundant in the double mutant, only a partial overlap was observed with those affected in *pnp-a*. This indicates that the community shift in the double mutant is not simply the sum of the effects of the single mutants. Instead, the combined loss of *AtPNP-A* and *AtPNP-B* may lead to a reorganization of the microbial community. The distinct microbiota profiles associated with *pnp-a* and *pnp-b* mutants may arise from variations in their primary sequences that could influence target binding or biological activity. Although *in vitro* assays revealed no differences in the activity of the Arabidopsis PNPs against the tested microbes, differences in their activity might still occur on

microbes different from the ones we tested. Alternatively, the differential microbiota effects could result from the distinct expression patterns of the two PNPs.

The transcriptomic data indicate that *AtPNP-A* is predominantly expressed in leaves, whereas *AtPNP-B* expression was detected primarily in siliques and the endosperm, suggesting tissue-specific functions. The observed alteration of the phyllosphere microbiota in the *pnp-b* mutant was therefore unexpected. The expression of *AtPNP-B* in the endosperm indicates a potential role in early seedling defense, as this tissue contains antimicrobial compounds that protect emerging seedlings after seed coat rupture (Terras et al. 1995). The influence of *AtPNP-B* on phyllosphere bacterial composition may thus originate from its early activity during seed germination, when initial microbial colonization from soil occurs (Mayer et al. 2025). Because early colonizers strongly influence subsequent community assembly on mature plants (Carlström et al. 2019), *AtPNP-B* activity during germination could have lasting effects on phyllosphere microbiota structure. In contrast, *AtPNP-A* may act predominantly in the leaves, modulating microbial dynamics once the phyllosphere is established. This temporal distinction could explain why *AtPNP-A* loss exhibits different effects in the single and double mutants. To test this hypothesis, future studies should investigate microbiota compositions at early developmental stages, such as in seedlings. Moreover, repeating the microbiota profiling using complementation lines and performing expression analyses under identical growth conditions will be crucial to validate our findings.

An important consideration is the potential for indirect effects on microbial communities via host physiology. AtPNP-A, for instance, has been implicated in stomatal regulation, where its overexpression increases stomatal aperture and knockout lines show reduced opening (Ficarra et al. 2018). Given that stomata are entry points for microbial colonizers (Wippel 2023), it is conceivable that altered stomatal physiology in PNP mutants could influence microbial colonization indirectly. To disentangle direct antimicrobial activity from such physiological effects, one approach would be to mutate regions of PNPs specifically involved in stomatal regulation. The segment spanning amino acids 11–44 in AtPNP-A is known to induce protoplast swelling and overlaps with a positively charged region, raising the possibility that this domain contributes to both antimicrobial and stomatal functions. Whether these two activities can be functionally separated remains an open question. Alternatively, *P. patens*, which forms stomata only in the diploid sporophyte, could serve as a model to study PNP–modulation of

microbiota interactions in the absence of stomatal influences, particularly using available stomata-deficient mutants (Chater et al. 2016).

While our bacterial microbiome analyses revealed significant genotype-dependent shifts, our ITS-based fungal community profiling did not detect major changes across PNP mutant lines. In general, the fungal population size in the phyllosphere is smaller than that of bacteria (Rastogi et al. 2013; Sohrabi et al. 2023). Therefore, it is possible that fungi sensitive to PNPs are absent or present at low abundance, making community-level differences difficult to detect.

Our findings also raise important questions about the broader ecological and evolutionary relevance of PNP-mediated antimicrobial activity. The presence of PNP-like proteins in diverse plant-associated organisms, such as *V. dahliae*, *X. citri*, and *B. tabaci*, suggests that these proteins may be exploited to influence microbial communities in ways that benefit the producing organism. In *V. dahliae*, the PNP-like effector VdAve1 has been shown to enhance host colonization by selectively suppressing microbial competitors (Snelders et al. 2020). Similarly, *B. tabaci* PNPs might function to shape the insect's gut microbiota or modulate the microbiota of the plant during feeding. Functional studies, such as expression profiling, microbiome analysis, and knockout-based fitness assays, will be essential to test this hypothesis. It would also be worthwhile to examine whether XacPNP, which influences host physiology during infection infection (Gottig et al. 2008), also affects microbial community composition, as observed for VdAve1.

Finally, our results support the view that PNPs may function as PR proteins. AtPNP-A is pathogen-inducible and co-expressed with canonical PR genes (Meier et al. 2008). While antimicrobial activity is not a required criterion for PR classification, many PR proteins were later found to possess antimicrobial properties (van Loon et al. 2006). In this context, our finding that PNPs display antimicrobial activity reinforces their potential role in plant defense. However, further studies are needed to assess local and systemic induction, as well as induction in response to the defense hormones salicylic acid, ethylene and jasmonic acid, which are known to regulate PR protein expression (van Loon et al. 2006).

In conclusion, we identify PNPs as charge-dependent antimicrobial proteins that shape phyllosphere bacterial communities, extending their functional roles in plant biology and highlighting their importance in host–microbe interactions. Our findings not only broaden our

understanding of plant antimicrobial strategies but also raise new questions about the role of PNP-like proteins in microbiota modulation across different kingdoms of life.

Materials and methods

PNP production and purification

Signal peptides were predicted by using the SignalP 5.0 server (Almagro Armenteros et al. 2019). The DNA sequences encoding mature PNPs were codon-optimized for expression in *Escherichia coli*, synthesized, and cloned into pET15b with an N-terminal His_6-tag sequence by BioCat GmbH (Heidelberg, Germany). These expression vectors were transformed into *E. coli* strain BL21. Protein production and purification was performed as described previously (Snelders et al. 2020). Single colonies were used to inoculate 100 mL of 2× yeast extract tryptone (YT) medium (16 g/L tryptone, 10 g/L yeast extract, 5 g/L NaCl) containing 100 µg/mL ampicillin, and cultures were grown overnight at 37 °C with shaking at 180 rpm. Next, the overnight cultures were used to inoculate 1 L of fresh 2×YT medium supplemented with 100 µg/mL ampicillin, and incubated at 37 °C and 200 rpm until the optical density at 600 nm (OD_{600}) reached 2. Protein production was induced by adding isopropyl-β-d-thiogalactoside at a final concentration of 1 mM and the cultures were incubated at 42°C, 200 rpm. After 2h, the cells were harvested by pelleting at 4,500 x g for 1 h, washed in dH_2O, pelleted at 12,000 x g for 30 min and snap-frozen in liquid nitrogen. Next, the cells were lysed by resuspending in 10 mM Tris, 6 M guanidinium chloride and 10 mM β-mercaptoethanol at pH 8.0 and overnight stirring at 4°C. The lysate was clarified by centrifugation at 12,000 x g for 40 min at 4°C and the supernatant was collected. Protein purification was performed under denaturing conditions using a column packed with His60 Ni^{2+} Superflow Resin (Takara Bio, Kusatsu, Japan) on a liquid chromatography ÄKTA go system (Cytiva, Marlborough, USA). For equilibration of the chromatography system wash buffer (10 mM Tris, 6 M guanidinium chloride and 20 mM imidazole at pH 8.0) was used. Upon loading of the protein sample, the column was washed with wash buffer until the UV absorbance at 280 nm returned to basal levels and subsequently eluted with elution buffer (10 mM Tris, 6 M guanidinium chloride and 200 mM imidazole at pH 8.0). For each step, the flow-through was collected and analysed on mini-protean TGX stain-free precast gels (Bio-Rad, Hercules, USA). To confirm presence of the proteins of interest,

western blots were performed with Anti-Polyhistidine antibody (Sigma-Aldrich, St. Louis, USA). Purified proteins were refolded *in vitro* by step-wise dialysis using Spectra/Por 3 Dialysis Membrane (Repligen, Waltham, USA) with a molecular weight cut off of 3.5 kDa. Each dialysis step was performed for a minimum of 24 hours. The first dialysis buffer consisted of 4 M guanidinium chloride, 50 mM BisTris, 10 mM reduced glutathione, and 2 mM oxidized glutathione and 15% glycerol at pH 7.0. The second dialysis buffer consisted of 3 M guanidinium chloride, 50 mM BisTris, 10 mM reduced glutathione, 2 mM oxidized glutathione and 15% glycerol at pH 6.5. The third dialysis buffer consisted of 2 M guanidinium chloride, 100 mM BisTris, 125 mM ammonium sulfate, 10 mM reduced glutathione, 2 mM oxidized glutathione and 20% glycerol at pH 6.0. The fourth dialysis buffer consisted of 1 M guanidinium chloride, 100 mM BisTris, 200 mM glycine, 250 mM ammonium sulfate, 10 mM reduced glutathione, 2 mM oxidized glutathione and 20% glycerol at pH 5.8. The fifth dialysis buffer consisted of 100 mM BisTris, 150 mM glycine, 250 mM ammonium sulfate, 10 mM reduced glutathione, 2 mM oxidized glutathione and 25% glycerol at pH 5.8. The sixth dialysis buffer consisted of 50 mM glycine and 15% glycerol at pH 6.0. Finally, samples were dialyzed into 30 mM potassium phosphate buffer at pH 6.5. Refolded proteins were concentrated using centrifugal filter units (Sigma-Aldrich, St. Louis, USA), and protein concentrations were measured using a NanoDrop spectrophotometer (Thermo Fisher Scientific, Waltham, USA).

Antimicrobial activity assays

To test the antibacterial activity of the PNPs, the bacteria *B. drentensis, P. syringae* and *X. campestris* were grown on tryptic soy agar (TSA; Sigma-Aldrich, St. Louis, USA) at 28°C. Single colonies were selected and grown overnight in tryptic soy broth (TSB) low-salt (17 g/L tryptone, 3 g/L soy peptone, 2.5 g/L dipotassium phosphate, 2.5 g/L glucose and 0.5 g/L NaCl) at 28 °C, 180 rpm. The overnight bacterial cultures were diluted in fresh low-salt TSB to an OD_{600} of 0.05 and mixed in a 1:1 ratio with 16 µM of purified PNPs in 96-well clear plate with flat bottom. Filter-sterilized 30 mM potassium phosphate buffer at pH 6.5 was used as a negative control. Bacterial growth was followed by measuring OD_{600} overtime with a CLARIOstar Plus Microplate Reader (BMG LABTECH, Ortenberg, Germany). The Microplate Reader was set at 25 °C and the plate was shaken before each measurement for 10 seconds at 300 rpm.

To test the antifungal activity of the PNPs, fungi were grown on potato dextrose agar (PDA; Carl Roth, Karlsruhe, Germany) at 28 °C. For the yeast *C. jadinii,* a single colony was selected and grown overnight in 5% potato dextrose broth (PDB; VWR, Radnor, United States) at 28 °C, 180 rpm. The overnight cultures were diluted to an OD_{600} of 0.01 in fresh 5% PDB supplemented with 8 µM PNPs or filter-sterilized 30 mM potassium phosphate buffer at pH 6.5 in a 96-well clear plate with flat bottom and incubated overnight at 28°C. To determine yeast abundance, a dilution series of the yeast cultures was plated on PDA plates and incubated at 28°C. After overnight incubation, colony-forming units (CFUs) were enumerated. For the filamentous fungi *A. brassicicola* and *V. dahliae*, conidiospores were first harvested in sterile distilled water, washed, and subsequently diluted to a final concentration of 10^4 spores/mL in 5% PDB supplemented with 8 µM of the respective PNP in 30 mM potassium phosphate buffer (pH 6.5) or 30 mM potassium phosphate buffer (pH 6.5). 100 µL were aliquoted in 96-well clear plate with flat bottom and incubated overnight at 28°C. Fungal growth was imaged using Olympus CK 40 microscope (Shinjuku City, Tokyo, Japan).

Multiple sequence alignment and structure predictions

The multiple sequence alignment was performed with Clustal Omega (Sievers et al. 2011) and visualized with Jalview (Waterhouse et al. 2009). The percentage identity of the pairwise alignment was determined with Jalview (Waterhouse et al. 2009). The unrooted maximum likelihood phylogenetic tree of the PNP homologs was constructed from the multiple sequence alignment using IQ-TREE (Nguyen et al. 2015) and visualized with iTOL (Letunic and Bork 2021).

Protein structure predictions were performed with AlphaFold v2.1.0 (Jumper et al. 2021), using the mature PNPs sequences. The multiple structure alignment was performed with PyMOL (The PyMOL Molecular Graphics System, Version 3.0 Schrödinger, LLC). The surface charge prediction was performed using the Adaptive Poisson–Boltzmann Solver (APBS) electrostatic plugin in PyMOL (Baker et al. 2001).

PpPNP transcript validation using RNA-Seq data

To verify the presence of the N-terminal extension of PpPNP-A, a BLAST search was performed with the mRNA sequence of PpPNP-A and the NCBI RNA-Seq archives (Leinonen et al. 2010); reads from the ERX3966793 Illumina HiSeq 4000 library (Lebeis et al. 2015) were used.

Plant material and growth conditions

The following T-DNA insertion lines, all in the *A. thaliana* Col-0 ecotype, were obtained from the Nottingham Arabidopsis Stock Centre (NASC) (University of Nottingham, UK): *pnp-a* (SALK_000951C); *pnp-b* (SALK_005318C, SALK_110534C) (Alonso et al. 2003). The *pnp-a/pnp-b* mutant was generated by crossing the *pnp-a* and *pnp-b* (At4g30380) mutants. The resulting F1 progeny was self-fertilized, and individuals from the F2 population were subjected to PCR-based genotyping using gene-specific and T-DNA border primers to identify plants homozygous for both insertions. The primers used were the SALK LBb1-3 ATTTTGCCGATTTCGGAAC; *AtPNP-A* forward TTTCCGGATATCCGAAATTTC; *AtPNP-A* reverse ATGTGATTTAGGGTCTGCGTG; *AtPNP-B* forward CTTCCTCGGTAACTCCATTCC; *AtPNP-B* reverse CGACAGGATTAGCGATCTGAG. Plants were grown in potting soil (Balster Einheitserde, Frödenberg, Germany) in a greenhouse with a relative humidity of 55% at 22°C, and 17-hour light/7-hour dark photoperiod. For microbiota analysis, three-week-old plants were harvested and immediately snap-frozen in liquid nitrogen. Two plants were randomly selected and pooled as one biological replicate prior to tissue homogenization and DNA extraction.

***PNPs* expression analysis**

AtPNP-A and *AtPNP-B* tissue-specific RNAseq data were retrieved from the *Arabidopsis* RNA-seq database (Zhang et al. 2020).

Microbiota sequencing

A. thaliana samples were manually ground to fine powder using a mortar and pestle with liquid nitrogen. Around 400 mg of powder was used for DNA extraction with the the DNeasy PowerSoil Pro Kit (Qiagen, Venlo, The Netherlands). The DNA was further purified using the Monarch PCR&DNA Clean Up kit (New England Biolabs, Ipswich, USA). Next, the DNA purity

and concentration were determined using a NanoDrop spectrophotometer (Thermo Fisher Scientific, Waltham, USA). The DNA was used to amplify the variable regions V3–V4 of the 16S rRNA gene using the primers 341f (ACTCCTACGGGAGGCAGCAG) and 806r (GGACTACHVGGGTWTCTAAT), along with mPNA (GGCAAGTGTTCTTCGGA) and pPNA (GGCTCAACCCTGGACAG) blocking clamps (PNABio, Newbury Park, USA). For fungal community profiling, the ITS2 region was amplified using the primers ITS3 (GCATCGATGAAGAACGCAGC) and ITS4 (TCCTCCGCTTATTGATATGC), in the presence of the ITS2-specific PNA clamp (CGAGGGCACGTCTGCCTGG) from the same supplier. Amplifications and amplicon sequencing (Illumina MiSeq) were performed by BGI-Genomics (Shenzhen, China). Only samples with a minimum of 10,000 reads were included in the analysis. Data processing and analysis were performed as previously described (Callahan et al. 2016; Snelders et al. 2020).

Microbiota analysis

The sequencing data were processed in R v4.2.0 as previously described (Callahan et al. 2016; Snelders et al. 2020). The reads were demultiplexed using *cutadapt* (v4.1; (Martin 2011)), then trimmed and filtered to a mean paired-read length of 412 bp with a minimum Phred score of 30. Amplicon sequence variants (ASVs) were inferred using the DADA2 pipeline (v1.24; (Callahan et al. 2016)), and taxonomy was assigned with the Ribosomal Database Project (RDP, v18; (Cole et al. 2014)). Community compositions were visualised using Principal Coordinates Analysis (PCoA) based on Bray-Curtis dissimilarity matrices computed with phyloseq (v1.50.0; (McMurdie and Holmes 2013)). Differences in microbial community structure across genotypes were statistically assessed using permutational multivariate analysis of variance (PERMANOVA) using the vegan package (v2.6-4; (Oksanen et al. 2024)). Effect sizes (R^2) and adjusted p-values (Benjamini-Hochberg method) were calculated, and results were visualised as bar plots. Differential abundance analysis was performed using DESeq2 (v1.46.0; (Love et al. 2014)); a Wald test was applied under a negative binomial model to identify significantly different taxa between genotypes, adjusted p-value < 0.05. Beta dispersion (homogeneity of multivariate dispersions) among genotypes was tested using Bray–Curtis dissimilarities calculated in phyloseq (v1.50.0; (McMurdie and Holmes 2013)). Differences in dispersion were assessed by ANOVA followed by Tukey's HSD.

Data visualization

Data was visualized using the ggplot2 (Wickham 2009) with R (v4.4.2).

Supplementary information

Table S 1. Pairwise Tukey's HSD post hoc test for beta dispersion based on Bray–Curtis dissimilarities.

Comparison	Adjusted p-value
pnp-a/pnp-b - pnp-a	0.528
pnp-b - pnp-a	0.484
WT - *pnp-a*	1.000
pnp-b - pnp-a/pnp-b	1.000
WT - *pnp-a/pnp-b*	0.570
WT - *pnp-b*	0.527

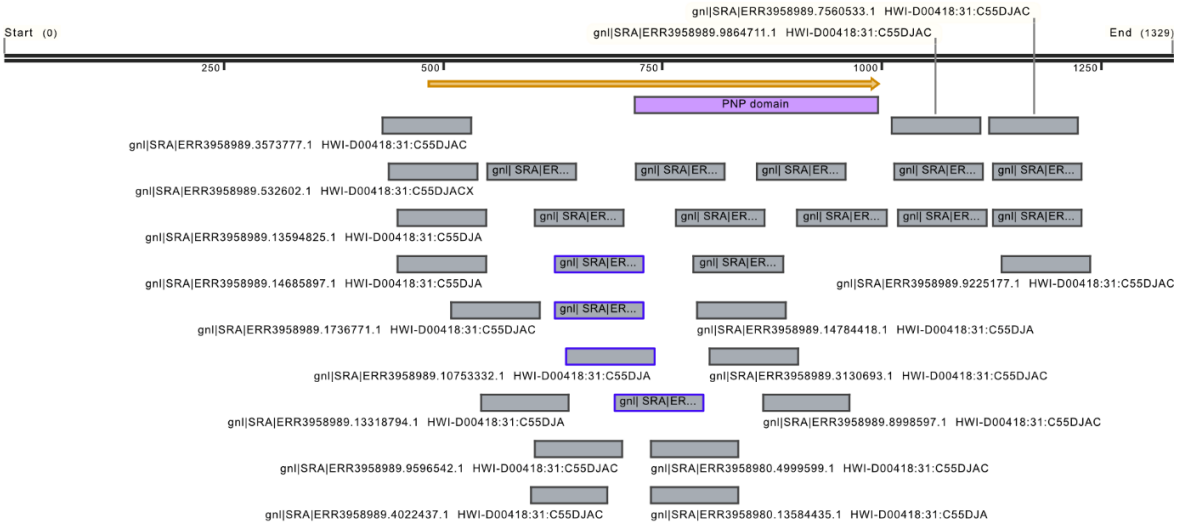

Figure S 1. RNA-seq read support for N-terminal extension of PpPNP-A. Visualization of RNA-seq read alignments over the PpPNP-A mRNA of *Physcomitrella patens*. The annotated coding region is indicated by an orange arrow, and the PNP domain is indicated by a purple box. Aligned RNA-seq reads are shown as grey bars. Reads spanning the PNP domain and part of the N terminal region are highlighted with blue outlining.

References

Almagro Armenteros, José Juan; Tsirigos, Konstantinos D.; Sønderby, Casper Kaae; Petersen, Thomas Nordahl; Winther, Ole; Brunak, Søren et al. (2019): SignalP 5.0 improves signal peptide predictions using deep neural networks. In *Nature biotechnology* 37 (4), pp. 420–423. DOI: 10.1038/s41587-019-0036-z.

Alonso, José M.; Stepanova, Anna N.; Leisse, Thomas J.; Kim, Christopher J.; Chen, Huaming; Shinn, Paul et al. (2003): Genome-wide insertional mutagenesis of Arabidopsis thaliana. In *Science (New York, N.Y.)* 301 (5633), pp. 653–657. DOI: 10.1126/science.1086391.

Baker, N. A.; Sept, D.; Joseph, S.; Holst, M. J.; McCammon, J. A. (2001): Electrostatics of nanosystems: application to microtubules and the ribosome. In *Proceedings of the National Academy of Sciences of the United States of America* 98 (18), pp. 10037–10041. DOI: 10.1073/pnas.181342398.

Berendsen, Roeland L.; Pieterse, Corné M. J.; Bakker, Peter A. H. M. (2012): The rhizosphere microbiome and plant health. In *Trends in plant science* 17 (8), pp. 478–486. DOI: 10.1016/j.tplants.2012.04.001.

Boudart, Georges; Jamet, Elisabeth; Rossignol, Michel; Lafitte, Claude; Borderies, Gisèle; Jauneau, Alain et al. (2005): Cell wall proteins in apoplastic fluids of Arabidopsis thaliana rosettes: identification by mass spectrometry and bioinformatics. In *Proteomics* 5 (1), pp. 212–221. DOI: 10.1002/pmic.200400882.

Bulgarelli, Davide; Schlaeppi, Klaus; Spaepen, Stijn; Ver Loren Themaat, Emiel; Schulze-Lefert, Paul (2013): Structure and functions of the bacterial microbiota of plants. In *Annual review of plant biology* 64, pp. 807–838. DOI: 10.1146/annurev-arplant-050312-120106.

Callahan, Benjamin J.; McMurdie, Paul J.; Rosen, Michael J.; Han, Andrew W.; Johnson, Amy Jo A.; Holmes, Susan P. (2016): DADA2: High-resolution sample inference from Illumina amplicon data. In *Nature methods* 13 (7), pp. 581–583. DOI: 10.1038/nmeth.3869.

Carlström, Charlotte I.; Field, Christopher M.; Bortfeld-Miller, Miriam; Müller, Barbara; Sunagawa, Shinichi; Vorholt, Julia A. (2019): Synthetic microbiota reveal priority effects and keystone strains in the Arabidopsis phyllosphere. In *Nature ecology & evolution* 3 (10), pp. 1445–1454. DOI: 10.1038/s41559-019-0994-z.

Chater, Caspar C.; Caine, Robert S.; Tomek, Marta; Wallace, Simon; Kamisugi, Yasuko; Cuming, Andrew C. et al. (2016): Origin and function of stomata in the moss Physcomitrella patens. In *Nature plants* 2, p. 16179. DOI: 10.1038/nplants.2016.179.

Chavarro-Carrero, Edgar A.; Snelders, Nick C.; Torres, David E.; Kraege, Anton; López-Moral, Ana; Petti, Gabriella C. et al. (2024): The soil-borne white root rot pathogen Rosellinia necatrix expresses antimicrobial proteins during host colonization. In *PLoS pathogens* 20 (1), e1011866. DOI: 10.1371/journal.ppat.1011866.

Cole, James R.; Wang, Qiong; Fish, Jordan A.; Chai, Benli; McGarrell, Donna M.; Sun, Yanni et al. (2014): Ribosomal Database Project: data and tools for high throughput rRNA analysis. In *Nucleic acids research* 42 (Database issue), D633-42. DOI: 10.1093/nar/gkt1244.

de Jonge, Ronnie de; van Esse, H. Peter; Maruthachalam, Karunakaran; Bolton, Melvin D.; Santhanam, Parthasarathy; Saber, Mojtaba Keykha et al. (2012): Tomato immune receptor Ve1 recognizes effector of multiple fungal pathogens uncovered by genome and RNA sequencing. In *Proceedings of the National Academy of Sciences of the United States of America* 109 (13), pp. 5110–5115. DOI: 10.1073/pnas.1119623109.

Di Paolo, Valeria; Masotti, Fiorella; Vranych, Cecilia V.; Grandellis, Carolina; Garavaglia, Betiana S.; Gottig, Natalia; Ottado, Jorgelina (2023): Xanthomonas natriuretic peptide is recognized by the Arabidopsis natriuretic peptide receptor 1 and through this interaction triggers similar plant responses to its plant counterpart. In *Plant science: an international journal of experimental plant biology* 326, p. 111494. DOI: 10.1016/j.plantsci.2022.111494.

Dorey, Stephan; Baillieul, Fabienne; Pierrel, Marie-Agnès; Saindrenan, Patrick; Fritig, Bernard; Kauffmann, Serge (1997): Spatial and Temporal Induction of Cell Death, Defense Genes, and Accumulation of Salicylic Acid in Tobacco Leaves Reacting Hypersensitively to a Fungal Glycoprotein Elicitor. In *Molecular plant-microbe interactions: MPMI* 10 (5), pp. 646–655. DOI: 10.1094/MPMI.1997.10.5.646.

Durrant, W. E.; Dong, X. (2004): Systemic acquired resistance. In *Annual review of phytopathology* 42, pp. 185–209. DOI: 10.1146/annurev.phyto.42.040803.140421.

Ficarra, Florencia A.; Grandellis, Carolina; Garavaglia, Betiana S.; Gottig, Natalia; Ottado, Jorgelina (2018): Bacterial and plant natriuretic peptides improve plant defence responses against pathogens. In *Molecular plant pathology* 19 (4), pp. 801–811. DOI: 10.1111/mpp.12560.

Finn, Robert D.; Clements, Jody; Eddy, Sean R. (2011): HMMER web server: interactive sequence similarity searching. In *Nucleic acids research* 39 (Web Server issue), W29-37. DOI: 10.1093/nar/gkr367.

Gottig, Natalia; Garavaglia, Betiana S.; Daurelio, Lucas D.; Valentine, Alex; Gehring, Chris; Orellano, Elena G.; Ottado, Jorgelina (2008): Xanthomonas axonopodis pv. citri uses a plant natriuretic peptide-like protein to modify host homeostasis. In *Proceedings of the National Academy of Sciences of the United States of America* 105 (47), pp. 18631–18636. DOI: 10.1073/pnas.0810107105.

Hacquard, Stéphane; Spaepen, Stijn; Garrido-Oter, Ruben; Schulze-Lefert, Paul (2017): Interplay Between Innate Immunity and the Plant Microbiota. In *Annual review of phytopathology* 55, pp. 565–589. DOI: 10.1146/annurev-phyto-080516-035623.

Jumper, John; Evans, Richard; Pritzel, Alexander; Green, Tim; Figurnov, Michael; Ronneberger, Olaf et al. (2021): Highly accurate protein structure prediction with AlphaFold. In *Nature* 596 (7873), pp. 583–589. DOI: 10.1038/s41586-021-03819-2.

Lebeis, Sarah L.; Paredes, Sur Herrera; Lundberg, Derek S.; Breakfield, Natalie; Gehring, Jase; McDonald, Meredith et al. (2015): PLANT MICROBIOME. Salicylic acid modulates colonization of the root microbiome by specific bacterial taxa. In *Science (New York, N.Y.)* 349 (6250), pp. 860–864. DOI: 10.1126/science.aaa8764.

Lee, Keun Pyo; Liu, Kaiwei; Kim, Eun Yu; Medina-Puche, Laura; Dong, Haihong; Duan, Jianli et al. (2020): PLANT NATRIURETIC PEPTIDE A and Its Putative Receptor PNP-R2 Antagonize Salicylic Acid-Mediated Signaling and Cell Death. In *The Plant cell* 32 (7), pp. 2237–2250. DOI: 10.1105/tpc.20.00018.

Leinonen, Rasko; Sugawara, Hideaki; Shumway, Martin (2010): The sequence read archive. In *Nucleic acids research* 39 (Database issue), D19-21. DOI: 10.1093/nar/gkq1019.

Letunic, Ivica; Bork, Peer (2021): Interactive Tree Of Life (iTOL) v5: an online tool for phylogenetic tree display and annotation. In *Nucleic acids research* 49 (W1), W293-W296. DOI: 10.1093/nar/gkab301.

Love, Michael I.; Huber, Wolfgang; Anders, Simon (2014): Moderated estimation of fold change and dispersion for RNA-seq data with DESeq2. In *Genome biology* 15 (12), p. 550. DOI: 10.1186/s13059-014-0550-8.

Ludidi, N. N.; Heazlewood, J. L.; Seoighe, C.; Irving, H. R.; Gehring, C. A. (2002): Expansin-like molecules: novel functions derived from common domains. In *Journal of molecular evolution* 54 (5), pp. 587–594. DOI: 10.1007/s00239-001-0055-4.

Martin, Marcel (2011): Cutadapt removes adapter sequences from high-throughput sequencing reads. In *EMBnet j.* 17 (1), p. 10. DOI: 10.14806/ej.17.1.200.

Maryani, M. M.; Bradley, G.; Cahill, D. M.; Gehring, C. A. (2001): Natriuretic peptides and immunoreactants modify osmoticum-dependent volume changes in Solanum tuberosum L. mesophyll cell protoplasts. In *Plant Science* 161 (3), pp. 443–452. DOI: 10.1016/S0168-9452(01)00423-X.

Mayer, Teresa; Teutloff, Erik; Unger, Kerstin; Lehenberger, Pamela; Agler, Matthew T. (2025): Deterministic colonization arises early during the transition of soil bacteria to the phyllosphere and is shaped by plant-microbe interactions. In *Microbiome* 13 (1), p. 102. DOI: 10.1186/s40168-025-02090-1.

McMurdie, Paul J.; Holmes, Susan (2013): phyloseq: an R package for reproducible interactive analysis and graphics of microbiome census data. In *PloS one* 8 (4), e61217. DOI: 10.1371/journal.pone.0061217.

Meier, Stuart; Bastian, René; Donaldson, Lara; Murray, Shane; Bajic, Vladimir; Gehring, Chris (2008): Co-expression and promoter content analyses assign a role in biotic and abiotic stress responses to plant natriuretic peptides. In *BMC plant biology* 8, p. 24. DOI: 10.1186/1471-2229-8-24.

Moreira, Leandro M.; Almeida, Nalvo F.; Potnis, Neha; Digiampietri, Luciano A.; Adi, Said S.; Bortolossi, Julio C. et al. (2010): Novel insights into the genomic basis of citrus canker based on the genome sequences of two strains of Xanthomonas fuscans subsp. aurantifolii. In *BMC genomics* 11, p. 238. DOI: 10.1186/1471-2164-11-238.

Nguyen, Lam-Tung; Schmidt, Heiko A.; Haeseler, Arndt von; Minh, Bui Quang (2015): IQ-TREE: a fast and effective stochastic algorithm for estimating maximum-likelihood phylogenies. In *Molecular biology and evolution* 32 (1), pp. 268–274. DOI: 10.1093/molbev/msu300.

Oksanen, Jari; Simpson, Gavin L.; Blanchet, F. Guillaume; Kindt, Roeland; Legendre, Pierre; Minchin, Peter R. et al. (2024): vegan: Community Ecology Package. Available online at URL http://CRAN. R-project. org/package= vegan (2024).

Patané, José S. L.; Moreira, Leandro M.; Melo Teixeira, Marcus de; Martins, Joaquim; Setubal, João C.; Varani, Alessandro M. (2022): New insights into plant natriuretic peptide evolution: From the lysogenic conversion in

Xanthomonas to the lateral transfer to the whitefly Bemisia tabaci. In *Gene* 821, p. 146326. DOI: 10.1016/j.gene.2022.146326.

Pharmawati, Made; Maryani, Maria M.; Nikolakopoulos, Theo; Gehring, Christoph A.; Irving, Helen R. (2001): Cyclic GMP modulates stomatal opening induced by natriuretic peptides and immunoreactive analogues. In *Plant Physiology and Biochemistry* 39 (5), pp. 385–394. DOI: 10.1016/S0981-9428(01)01252-9.

Rastogi, Gurdeep; Coaker, Gitta L.; Leveau, Johan H. J. (2013): New insights into the structure and function of phyllosphere microbiota through high-throughput molecular approaches. In *FEMS microbiology letters* 348 (1), pp. 1–10. DOI: 10.1111/1574-6968.12225.

Sievers, Fabian; Wilm, Andreas; Dineen, David; Gibson, Toby J.; Karplus, Kevin; Li, Weizhong et al. (2011): Fast, scalable generation of high-quality protein multiple sequence alignments using Clustal Omega. In *Molecular systems biology* 7, p. 539. DOI: 10.1038/msb.2011.75.

Snelders, Nick C.; Rovenich, Hanna; Petti, Gabriella C.; Rocafort, Mercedes; van den Berg, Grardy C. M.; Vorholt, Julia A. et al. (2020): Microbiome manipulation by a soil-borne fungal plant pathogen using effector proteins. In *Nature plants* 6 (11), pp. 1365–1374. DOI: 10.1038/s41477-020-00799-5.

Sohrabi, Reza; Paasch, Bradley C.; Liber, Julian A.; He, Sheng Yang (2023): Phyllosphere Microbiome. In *Annual review of plant biology* 74, pp. 539–568. DOI: 10.1146/annurev-arplant-102820-032704.

Terras, F. R.; Eggermont, K.; Kovaleva, V.; Raikhel, N. V.; Osborn, R. W.; Kester, A. et al. (1995): Small cysteine-rich antifungal proteins from radish: their role in host defense. In *The Plant cell* 7 (5), pp. 573–588. DOI: 10.1105/tpc.7.5.573.

The UniProt Consortium (2023): UniProt: the Universal Protein Knowledgebase in 2023. In *Nucleic acids research* 51 (D1), D523-D531. DOI: 10.1093/nar/gkac1052.

Trivedi, Pankaj; Leach, Jan E.; Tringe, Susannah G.; Sa, Tongmin; Singh, Brajesh K. (2020): Plant-microbiome interactions: from community assembly to plant health. In *Nature reviews. Microbiology* 18 (11), pp. 607–621. DOI: 10.1038/s41579-020-0412-1.

Turek, Ilona; Gehring, Chris (2016): The plant natriuretic peptide receptor is a guanylyl cyclase and enables cGMP-dependent signaling. In *Plant molecular biology* 91 (3), pp. 275–286. DOI: 10.1007/s11103-016-0465-8.

van Loon, L. C.; Rep, M.; Pieterse, C. M. J. (2006): Significance of inducible defense-related proteins in infected plants. In *Annual review of phytopathology* 44, pp. 135–162. DOI: 10.1146/annurev.phyto.44.070505.143425.

Wang, Yu Hua; Gehring, Chris; Cahill, David M.; Irving, Helen R. (2007): Plant natriuretic peptide active site determination and effects on cGMP and cell volume regulation. In *Functional plant biology: FPB* 34 (7), pp. 645–653. DOI: 10.1071/FP06316.

Wang, Yu Hua; Gehring, Chris; Irving, Helen R. (2011): Plant natriuretic peptides are apoplastic and paracrine stress response molecules. In *Plant & cell physiology* 52 (5), pp. 837–850. DOI: 10.1093/pcp/pcr036.

Waterhouse, Andrew M.; Procter, James B.; Martin, David M. A.; Clamp, Michèle; Barton, Geoffrey J. (2009): Jalview Version 2--a multiple sequence alignment editor and analysis workbench. In *Bioinformatics (Oxford, England)* 25 (9), pp. 1189–1191. DOI: 10.1093/bioinformatics/btp033).

Wickham, Hadley (2009): ggplot2. DOI: 10.1007/978-0-387-98141-3.

Wippel, Kathrin (2023): Plant and microbial features governing an endophytic lifestyle. In *Current opinion in plant biology* 76, p. 102483. DOI: 10.1016/j.pbi.2023.102483.

Zhang, Hong; Zhang, Fei; Yu, Yiming; Feng, Li; Jia, Jinbu; Liu, Bo et al. (2020): A Comprehensive Online Database for Exploring ~20,000 Public Arabidopsis RNA-Seq Libraries. In *Molecular plant* 13 (9), pp. 1231–1233. DOI: 10.1016/j.molp.2020.08.001.

Chapter 5: General discussion

Introduction

The microbiota constitutes a fundamental component of host biology across different organisms, including animals and plants, contributing to a wide range of essential functions such as nutrient acquisition and resistance against (a)biotic stresses (Hacquard et al. 2015). Within these microbial communities, individual members can have beneficial, neutral or pathogenic potential (Round and Mazmanian 2009; Trivedi et al. 2020). In plants, the immune system is crucial to maintain a balanced and healthy microbiota, to support the establishment and persistence of beneficial microbes while simultaneously restricting the proliferation of pathogenic ones (Chen et al. 2020; Pfeilmeier et al. 2021; Song et al. 2021). Beyond the host immune system itself, the plant microbiota also influences the outcome of plant–pathogen interactions, acting both directly and indirectly to suppress disease (Vannier et al. 2019). Owing to these roles, the microbiota has been described as an additional layer of the plant immune system, extending host defence capabilities (Hacquard et al. 2017).

In order to promote host colonization, plant pathogens secrete effector proteins (Lo Presti et al. 2015). Initially described as secreted molecules that suppress host immunity and alter host metabolism to facilitate infection, effectors are now recognized to have broader functions, including microbial self-protection and the reprogramming of host physiology (Cox et al. 2017; de Jonge et al. 2010; Hu et al. 2022). Recent discoveries further expanded the functional repertoire of effectors, revealing that some effectors act directly against microbiota members (Kettles et al. 2018; Snelders et al. 2020; Chang et al. 2021; Gómez-Pérez et al. 2023; Ökmen et al. 2023; Snelders et al. 2023; Chavarro-Carrero et al. 2024; Kraege et al. 2025; Mesny et al. 2024). By exerting antimicrobial activity, they suppress microbial antagonists both within the host and in soil microbiota, thereby enhancing pathogen niche colonization. In this PhD research, I seeked to advance our understanding of antimicrobial effector proteins by elucidating the mechanisms of action and ecological functions of selected effectors in fungal pathogens and their homologs in other organisms.

In this PhD thesis, I describe the first *V. dahliae* effector protein with antifungal activity, VdAMP3. This effector protein is an ancient antimicrobial protein which has been co-opted by *V. dahliae* to manipulate the host mycobiota (Chapter 2). VdAMP3 is specifically expressed during the formation of resting structures in senescing plant tissues, where it acts to suppress

fungal competitors. *V. dahliae* secretes the bactericidal effector VdAve1 to facilitate niche colonization by inhibiting bacterial antagonists (Snelders et al. 2020). In this thesis, I present the structural and functional characterization of the VdAve1 effector (Chapter 3). I show that VdAve1 binds lipoteichoic acid, a cell wall component of Gram-positive bacteria, and disrupts microbial membranes in a charge-dependent manner. I also show that its activity extends beyond bacteria, targeting also eukaryotic microbes. Finally, I show that plant homologs of VdAve1, known as plant natriuretic peptides (PNPs), from diverse plant species display antibacterial and antifungal activity (Chapter 4). Loss of PNP genes in *Arabidopsis thaliana* leads to alteration of bacterial but not fungal phyllosphere communities, suggesting that PNPs modulate microbiota compositions. In this chapter, I place the key findings of this PhD research into a broader scientific context and discuss their implications.

Antimicrobial effectors enable *V. dahliae* survival across ecological niches

V. dahliae is a soil-borne fungal pathogen with a complex life cycle that spans multiple ecological niches, including bulk soil, host rhizosphere, vascular tissues, and senescing plant material. Each of these environments harbors distinct microbial communities, and the broad host range of *V. dahliae* further requires adaptation to plant species with different microbiota (Tkacz et al. 2020). Additionally, pathogen infection itself perturbs the host microbiota (Durán et al. 2021; Pfeilmeier et al. 2024; Seybold et al. 2020). In these niches, *V. dahliae* must contend with competitors and predators, ranging from bacterial and fungal antagonists to fungivorous nematodes and mycophagous amoebae (Chakraborty et al. 1983; Friberg et al. 2005). To establish itself across such diverse environments, *V. dahliae* relies on a suite of effector proteins with antimicrobial activities that act in a niche- and stage-specific manner (Kettles et al. 2018; Snelders et al. 2020; Chang et al. 2021; Gómez-Pérez et al. 2023; Ökmen et al. 2023; Snelders et al. 2023; Chavarro-Carrero et al. 2024; Kraege et al. 2025; Mesny et al. 2024). The VdAve1 effector alters the composition of the rhizosphere microbiota by depleting members of the order Sphingomonadales, which are antagonistic to *V. dahliae* (Snelders et al. 2020). A related protein, VdAve1L2, also displays antibacterial activity and was shown to suppress Actinobacteria, another group of bacterial antagonists, in the host rhizosphere (Snelders et al. 2023). The recently described effector Av2 inhibits beneficial *Pseudomonas* spp. recruited by the plant in response to the infection as part of a “cry for help” strategy, thereby suppressing

their antagonistic activity and promoting fungal colonization (Kraege et al. 2025). Effector-mediated microbiome manipulation extends into the latest stages of the disease cycle, when the host begins to senesce and *V. dahliae* shifts toward a saprophytic lifestyle. During this phase, the host microbiota undergoes changes, with an increase in fungi and a decrease in bacteria, conditions under which *V. dahliae* deploys the antifungal effector VdAMP3 to compete with fungal antagonists and ensure the successful formation of its resting structures, the microsclerotia (Chapter 2). Beyond their roles within the host, effectors also function during the saprophytic phase in soil. VdAve1, for example, promotes *V. dahliae* soil colonization. Similarly, VdAMP2 is expressed in soil, but displays a distinct antibacterial spectrum compared to VdAve1, enhancing fungal competitiveness in the microbe-rich soil environment (Snelders et al. 2020). These examples illustrate that *V. dahliae* secretes a diverse arsenal of antimicrobial effectors to shape microbiota composition across its life cycle. Given that more than half of the *V. dahliae* secretome encodes putative antimicrobial proteins (Mesny et al. 2025), the effectors characterized to date likely represent only a subset of the antimicrobial repertoire employed by the fungus to colonize diverse niches.

From plants to pathogens: VdAve1 and PNPs as charge-dependent antimicrobials

The *V. dahliae* VdAve1 effector is a small (~13 kDa), positively charged, bactericidal protein (Snelders et al. 2020). VdAve1 is homologous to a widespread class of plant proteins, the plant natriuretic peptides (PNPs) (de Jonge et al. 2012). The abundance of plant homologs, together with the distribution of the few microbial homologs within the plant PNPs, suggests that VdAve1 was acquired from plants (de Jonge et al. 2012).

In Chapter 3, we elucidated the mode of action of VdAve1 through a combination of structural and functional analyses. We show that VdAve1 induces dissipation of bacterial cell membranes, consistent with the mechanism of many positively charged antimicrobial proteins that disrupt negatively charged microbial membranes (Yeaman and Yount 2003). This activity is charge-mediated, as positively charged residues are essential for the antimicrobial function of VdAve1-derived peptides. Similarly, during functional characterization of PNPs from phylogenetically diverse plants in Chapter 4, antimicrobial activity was observed only in proteins carrying a net positive charge, supporting the idea that electrostatic interactions are central to the mode of action of PNP-like proteins.

We show that exposure of *Bacillus subtilis* to VdAve1 triggers D-alanylation of teichoic acids, a negatively charged cell wall component present in Gram-positive bacteria, which reduces surface charge. Mutants lacking these modifications are more sensitive to the effector, suggesting that VdAve1 targets these molecules. Direct binding assays confirmed VdAve1–LTA interactions, supporting a model in which VdAve1 binds LTA to concentrate at the bacterial surface, facilitating plasma membrane disruption through its positive charge and ultimately leading to cell death (Figure 1). While LTA has been proposed as a docking site for membrane-disrupting AMPs (Malanovic and Lohner 2016), our study provides the first direct experimental evidence of such binding. Whether PNPs similarly bind LTA, and whether this is necessary for their activity, remains unknown.

Structural characterization using nuclear magnetic resonance revealed that VdAve1 adopts a β-barrel-like fold (Chapter 3), representing the first experimentally determined structure of a PNP-like protein. Intriguingly, VdAve1 exhibits structural similarity to domain 1 (D1) of expansins, a class of plant proteins involved in cell wall loosening. Expansins proteins primarily involved in loosening of plant cell walls for cell growth. Expansins typically consist of two domains, D1 and D2, with D2 responsible for binding cell wall polysaccharides (Georgelis et al. 2012). Plant cell walls are physical barriers against invading pathogens, and reduced cell wall integrity is often associated with increased pathogen susceptibility (Cantu et al. 2008). Localized loosening of the cell wall mediated by expansins, while essential for plant growth, may create a more favourable environment for pathogen ingress. Given the structural homology of D1 to VdAve1, it is tempting to speculate that this domain may have evolved to act as a protective barrier, counterbalancing the heightened susceptibility that arises when the cell wall is transiently loosened.

PNP genes have been horizontally acquired from plants by a variety of plant-associated organisms including multiple bacterial species within the *Xanthomonas* genus, multiple ascomycete fungi (*Colletotrichum, Fusarium, Verticillium, Cercospora, Venturia, Teratosphaeria, Pseudocercospora, Trichoderma*), a basidiomycete (*Thanatephorus cucumeris*), and the insect *Bemisia tabaci* (de Jonge et al. 2012; Gottig et al. 2008; Patané et al. 2022), suggesting that PNPs provide adaptive benefits when deployed by these organisms. Functional studies demonstrate that some of these horizontally acquired PNP-like proteins possess antimicrobial properties, as exemplified by the *V. dahliae* effector VdAve1 (Snelders et

al. 2020; Chapter3) and the *B. tabaci* protein BtPNP (Chapter 4). In the bacterial plant pathogen *Xanthomonas citri*, the PNP-like protein XacPNP has been implicated in virulence, and while its contribution has been attributed to the alteration of host physiology (Gottig et al. 2008), its effects on other microbes have yet to be experimentally investigated. Intriguingly, VdAve1 has been shown to promote *V. dahliae* virulence even in the absence of host microbiota, indicating that its function cannot be solely explained by antimicrobial activity (Punt et al. 2025). Instead, this observation points toward an additional role in host physiology manipulation. Taken together, these findings raise the possibility that PNP-like proteins have been repeatedly acquired across kingdoms to serve dual roles, the modulation of host physiology and microbial competition.

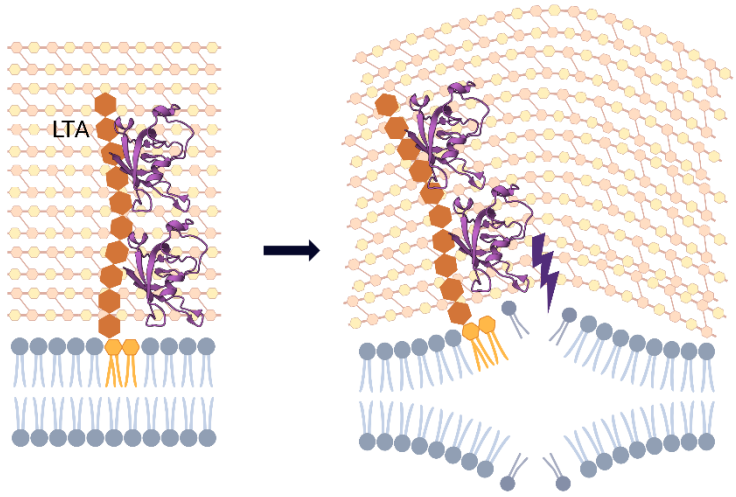

Figure 1. Model of the mode of action of the antimicrobial *Verticillium dahliae* VdAve1 effector against Gram-positive bacteria. VdAve1 binds lipoteichoic acid (LTA) in the cell wall of Gram-positive bacteria. LTA serves as a docking platform that concentrates the effector close to the bacterial plasma membrane, facilitating charge-dependent membrane disruption and cell death.

Many fungal antimicrobial effectors have ancient origins

Antimicrobial effectors are widespread across the fungal kingdom, with large and diverse repertoires predicted in both plant pathogenic and non-plant pathogenic species (Mesny et al. 2025). Their broad occurrence, and overrepresentation among the most conserved secreted protein families, indicate that antimicrobial effectors have an ancient origin (Snelders et al. 2022; Mesny et al. 2025). In fungal ancestors, antimicrobial proteins likely functioned in

microbial competition with complex microbial communities, long before fungi evolved interactions with plant hosts. Such proteins may have evolved as effectors for microbiota manipulation observed in plant-associated fungi today (Figure 2a). For instance, the *V. dahliae* effector VdAMP3 belongs to the cysteine-stabilized αβ defensin family (Chapter 2), a group of antimicrobial proteins conserved across animals, fungi, and plants. This conservation suggests a common ancestral origin and highlights that the antimicrobial function of VdAMP3 is an ancient trait. This protein functions as an antimicrobial effector secreted by *V. dahliae* to manipulate the host mycobiome. Although some antimicrobial effectors have an ancient origin, others have a more recent origin, emerging during host adaptation (Figure 2b). A notable example is the horizontally acquired *V. dahliae* effector VdAve1 (de Jonge et al. 2012). Its plant homologs, the PNPs, regulate water and ion homeostasis (Wang et al. 2011) and display antimicrobial activity (Chapter 4). Interestingly, our preliminary data suggests that PNPs have an additional role in microbiota manipulation. Both of these functions, microbiota modulation and host physiology regulation, appear to have been hijacked by *V. dahliae* for the manipulation of soil and host-associated microbial communities as well as host physiological processes.

The ancient origin of many antimicrobial effectors, combined with the fact that fungi interacted with other microbes before establishing associations with plants, has led to the hypothesis that immunomodulatory effectors evolved from ancestral antimicrobial proteins (Mesny et al. 2025). Supporting this hypothesis, more than half of functionally characterized immune-modulating effectors registered in the PHI-base database are predicted to possess antimicrobial properties (Mesny et al. 2025). Interestingly, a small set of these effectors has been shown to directly inhibit microbial growth *in vitro*. Homologs of these proteins are found in fungi that do not associate with plants, suggesting that the antimicrobial activity is ancestral and that the immunomodulatory ability has been acquired during the co-evolution with plant hosts (Mesny et al. 2025). This led to the hypothesis that immunomodulatory fungal effectors with predicted antimicrobial properties manipulate host physiology and inhibit microbial antagonists. To test this, the *V. dahliae* effector Vd424Y was analysed. Vd424Y has xylanolytic and cytotoxic activity in planta. Notably, within this effector family the nuclear localization signal, which is required for the immunomodulatory and cytotixic activity, is present only in the fungal clade composed of fungal pathogens, suggesting that this function evolved during the co-evolution with plant hosts. Interestingly, Vd424Y plays a role in microbiota manipulation

during host colonization, indicating that the antimicrobial property was retained during the co-evolution with the plant hosts.

Leveraging antimicrobial effectors in disease management

The need to reduce the use of agrochemicals, due to their negative environmental impacts, has driven the search for more environmentally friendly alternatives to reduce disease impacts in crop cultivation (Ayilara et al.). One alternative is the use of microbes as biocontrol agents for plant protection against pathogens. Biocontrol products can consist of single microbial strains or consortia, and they can suppress pathogen growth through direct antagonism or by stimulating host defences (Sheoran et al. 2025). For example, *Trichoderma* spp. are widely applied for their antagonistic activity against soil-borne pathogens such as *Fusarium* spp. and *Rhizoctonia* spp. (Mukesh et al. 2015). However, despite many years of use, the efficacy of biocontrol agents in the field remains inconsistent (Besset-Manzoni et al. 2019). It is increasingly clear that the persistence and functionality of microbial inoculants depend on a complex interplay of environmental variables, including both abiotic and biotic factors that shape microbial communities in soils and plants (Saad et al. 2020). One of these factors that has only recently gained attention is the ability of pathogens to suppress the growth of microbial antagonists through the secretion of antimicrobial effectors (Kettles et al. 2018; Snelders et al. 2020; Chang et al. 2021; Gómez-Pérez et al. 2023; Ökmen et al. 2023; Snelders et al. 2023; Chavarro-Carrero et al. 2024; Kraege et al. 2025; Mesny et al. 2024). Antimicrobial effectors secreted by pathogens can directly inhibit the growth of biocontrol agents, preventing their establishment in a given niche and thereby undermining their effectiveness. Antimicrobial effector deployment by pathogens is highly dynamic. Different effectors can be expressed at distinct infection stages (Snelders et al. 2022), and their contribution to pathogen fitness likely depends on the microbial community composition in each environment. While candidate biocontrol strains are often tested in the presence of the pathogen, this approach may not detect effectors expressed only under different environmental conditions. For instance, the antimicrobial effector VdAMP2 of *V. dahliae* is expressed in soil but not on growth media or *in planta* (Snelders et al. 2020). Similarly, the effector VdAve1L2 is not expressed in growth media, whereas it is expressed *in planta* (Snelders et al. 2023). Consequently, a biocontrol agent may appear effective in laboratory or greenhouse assays but prove ineffective

in the field, where pathogen-secreted antimicrobial effectors are expressed and suppress the biocontrol strain.

Plants under pathogen attack can actively shape their microbiota through a strategy known as the “cry for help,” in which they alter root exudates to recruit beneficial microorganisms that suppress disease (Spooren et al. 2024). These recruited microbes inhibit pathogens through multiple mechanisms, such as antibiosis, nutrient competition, and siderophore-mediated iron sequestration (Mendes et al. 2011; Kwak and Weller 2013; Carrión et al. 2018). This recruitment can occur both locally at infection sites and systemically in distal tissues, likely mediated by plant defense signalling. However, recent work has shown that pathogens can counteract this defence. *V. dahliae* employs the effector Av2 to inhibit the growth of beneficial *Pseudomonas* species that are recruited by the plant through the “cry for help” response (Kraege et al. 2025). Interestingly, the plant-driven recruitment of beneficial microbes in response to pathogen attack can have long-lasting effects, creating disease-suppressive soil legacies that protect future plant generations. A classic example is the take-all decline, where the severity and incidence of take-all disease, caused by *Gaeumannomyces graminis*, decline upon a severe disease outbreak during monoculture of a host crop, due to the accumulation of antibiotic-producing Pseudomonads (Weller et al. 2002). Interestingly, the build-up of disease-suppressive soils typically takes years of pathogen pressure to develop (Weller et al. 2002; Kwak and Weller 2013). This slow progression may result from the suppression of plant-recruited beneficial microbes by antimicrobial effectors secreted by the pathogen, which is only gradually overcome by the host recruitment (Mesny et al. 2024; Kraege et al. 2025).

The importance of the host microbiota in suppressing pathogen growth is not limited to plants. In animals, including humans, the host microbiota similarly plays a critical role in defense against invading pathogens. For example, the human gut microbiota provides a protective barrier by suppressing pathogens through nutrient and space competition as well as by stimulating host immune responses (Kamada et al. 2013). Perturbations of this barrier can favor the growth of opportunistic fungal pathogens. For instance, antibiotic-induced alterations of the gut microbiota increase susceptibility to the opportunistic yeast *Candida albicans* (Gutierrez et al. 2020). Thus, successful colonization and disease progression by fungal pathogens likely require not only evasion of host immunity but also the ability to modulate the host microbiota. Genome analysis of soil- and plant-associated fungi has revealed that

antimicrobial effectors are widely conserved across the fungal kingdom, indicating that fungi have relied on these tools for microbial competition before the establishment of symbioses with multicellular eukaryotes (Mesny et al. 2025). Most human fungal pathogens are opportunistic and primarily cause disease in immunocompromised individuals (Rokas 2022). Many of these pathogens persist in soils as saprotrophs, and occasionally cause disease, implying that their effector repertoires have not specifically co-evolved with their hosts (Snelders et al. 2022). Given that the host microbiota represents a barrier to pathogen colonization and disease, it is plausible that opportunistic pathogens co-opt antimicrobial proteins originally used in soil microbial competition as effectors for host microbiota modulation to promote infection.

Antimicrobial resistance poses a growing global health crisis, with drug-resistant pathogen infections projected to cause up to 10 million deaths annually by 2050 (O'Neill 2016). The urgent need for novel therapeutic strategies has intensified the search for alternatives to traditional antibiotics. Antimicrobial proteins have emerged as promising candidates for drug development. Among these, fungal antimicrobial effectors represent an underexplored reservoir of bioactive molecules. Many antimicrobial proteins have demonstrated efficacy against drug-resistant bacteria (Wang et al. 2024), and can act synergistically with conventional antibiotics, thereby enhancing therapeutic effectiveness (Lazzaro et al. 2020). For instance, some antimicrobial peptides (AMPs) increase bacterial membrane permeability, which facilitates antibiotic entry into the cell and boosts drug potency (Wang et al. 2024). Others are capable of inhibiting or disrupting biofilms, thereby exposing previously protected bacterial populations to antibiotic action (Mataraci and Dosler 2012). These mechanisms highlight the potential of antimicrobial proteins both as stand-alone agents and as adjuvants to conventional therapies. Nevertheless, important risks remain. A key concern is that the evolution of pathogen resistance to therapeutic antimicrobial proteins could result in cross-resistance to endogenous host proteins, which form an essential component of innate immunity (Lazzaro et al. 2020). One strategy to mitigate this risk is to prioritize the vast diversity of antimicrobial proteins derived from non-animal organisms, whose sequences and structures differ from animal antimicrobial proteins, reducing the likelihood of cross-resistance. Fungal antimicrobial effectors represent a largely unexplored catalogue of diverse antimicrobial proteins that could be leveraged for the development of novel therapeutics.

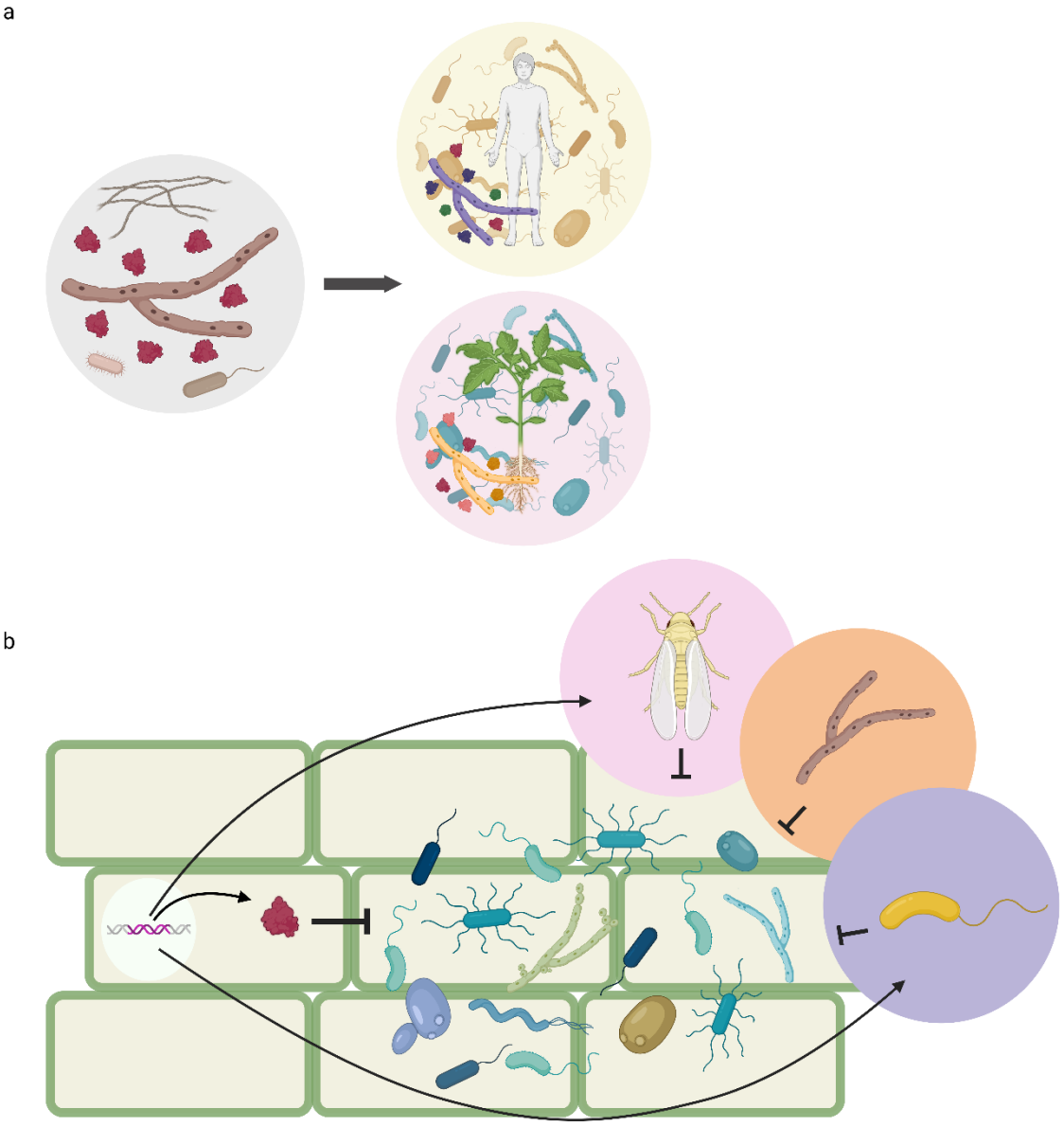

Figure 2. The evolution of effector-mediated microbiota manipulation. To establish symbioses with multicellular organisms, fungi secrete effectors, some of which display antimicrobial activity. Antimicrobial effectors are broadly conserved across the fungal kingdom, and even occur in early-diverging lineages, suggesting an ancient origin in microbial competition that predates the emergence of land plants. These ancestral proteins evolved in pathogenic fungi as effectors for the manipulation of host microbiota (a). While many fungal antimicrobial effectors have an ancient origin, others arose during host adaptation. The fungal pathogen *Verticillium dahliae* horizontally acquired the effector VdAve1 from plants, whose homologs are annotated as plant natriuretic peptides (PNPs). PNPs have also been independently acquired by other plant-associated organisms, where they contribute to niche colonization. Both plant-derived and non-plant PNPs exhibit antimicrobial activity, suggesting a role in microbiota manipulation (b).

References

Abdelfattah, Ahmed; Tack, Ayco J. M.; Lobato, Carolina; Wassermann, Birgit; Berg, Gabriele (2023): From seed to seed: the role of microbial inheritance in the assembly of the plant microbiome. In *Trends in microbiology* 31 (4), pp. 346–355. DOI: 10.1016/j.tim.2022.10.009.

Ayilara, Modupe S.; Akinola, Saheed A.; Adebajo, Mosimininuoluwa T.: Benefits and Drawbacks of Microbial Inoculant in Terms of Human Health and the Environment, pp. 411–435. DOI: 10.1007/978-981-97-0633-4_17.

Bakker, Peter A. H. M.; Pieterse, Corné M. J.; van Loon, L. C. (2007): Induced Systemic Resistance by Fluorescent Pseudomonas spp. In *Phytopathology* 97 (2), pp. 239–243. DOI: 10.1094/PHYTO-97-2-0239.

Besset-Manzoni, Yoann; Joly, Pierre; Brutel, Aline; Gerin, Florence; Soudière, Olivier; Langin, Thierry; Prigent-Combaret, Claire (2019): Does in vitro selection of biocontrol agents guarantee success in planta? A study case of wheat protection against Fusarium seedling blight by soil bacteria. In *PloS one* 14 (12), e0225655. DOI: 10.1371/journal.pone.0225655.

Boutrot, Freddy; Zipfel, Cyril (2017): Function, Discovery, and Exploitation of Plant Pattern Recognition Receptors for Broad-Spectrum Disease Resistance. In *Annual review of phytopathology* 55, pp. 257–286. DOI: 10.1146/annurev-phyto-080614-120106.

Bulgarelli, Davide; Schlaeppi, Klaus; Spaepen, Stijn; Ver Loren Themaat, Emiel; Schulze-Lefert, Paul (2013): Structure and functions of the bacterial microbiota of plants. In *Annual review of plant biology* 64, pp. 807–838. DOI: 10.1146/annurev-arplant-050312-120106.

Cantu, Dario; Vicente, Ariel R.; Labavitch, John M.; Bennett, Alan B.; Powell, Ann L. T. (2008): Strangers in the matrix: plant cell walls and pathogen susceptibility. In *Trends in plant science* 13 (11), pp. 610–617. DOI: 10.1016/j.tplants.2008.09.002.

Carrión, Víctor J.; Cordovez, Viviane; Tyc, Olaf; Etalo, Desalegn W.; Bruijn, Irene de; Jager, Victor C. L. de et al. (2018): Involvement of Burkholderiaceae and sulfurous volatiles in disease-suppressive soils. In *The ISME journal* 12 (9), pp. 2307–2321. DOI: 10.1038/s41396-018-0186-x.

Chakraborty, S.; Old, K. M.; Warcup, J. H. (1983): Amoebae from a take-all suppressive soil which feed on Gaeumannomyces graminis tritici and other soil fungi. In *Soil Biology and Biochemistry* 15 (1), pp. 17–24. DOI: 10.1016/0038-0717(83)90113-X.

Chang, Hao-Xun; Noel, Zachary A.; Chilvers, Martin I. (2021): A β-lactamase gene of Fusarium oxysporum alters the rhizosphere microbiota of soybean. In *The Plant journal : for cell and molecular biology* 106 (6), pp. 1588–1604. DOI: 10.1111/tpj.15257.

Chavarro-Carrero, Edgar A.; Snelders, Nick C.; Torres, David E.; Kraege, Anton; López-Moral, Ana; Petti, Gabriella C. et al. (2024): The soil-borne white root rot pathogen Rosellinia necatrix expresses antimicrobial proteins during host colonization. In *PLoS pathogens* 20 (1), e1011866. DOI: 10.1371/journal.ppat.1011866.

Chen, Tao; Nomura, Kinya; Wang, Xiaolin; Sohrabi, Reza; Xu, Jin; Yao, Lingya et al. (2020): A plant genetic network for preventing dysbiosis in the phyllosphere. In *Nature* 580 (7805), pp. 653–657. DOI: 10.1038/s41586-020-2185-0.

Cheng, Saisai; Gong, Xin; Xue, Wenfeng; Kardol, Paul; Delgado-Baquerizo, Manuel; Ling, Ning et al. (2024): Evolutionarily conserved core microbiota as an extended trait in nitrogen acquisition strategy of herbaceous species. In *The New phytologist* 244 (4), pp. 1570–1584. DOI: 10.1111/nph.20118.

Cook, David E.; Mesarich, Carl H.; Thomma, Bart P. H. J. (2015): Understanding plant immunity as a surveillance system to detect invasion. In *Annual review of phytopathology* 53, pp. 541–563. DOI: 10.1146/annurev-phyto-080614-120114.

Cox, Kevin L.; Meng, Fanhong; Wilkins, Katherine E.; Li, Fangjun; Wang, Ping; Booher, Nicholas J. et al. (2017): TAL effector driven induction of a SWEET gene confers susceptibility to bacterial blight of cotton. In *Nature communications* 8, p. 15588. DOI: 10.1038/ncomms15588.

de Jonge, Ronnie; van Esse, H. Peter; Kombrink, Anja; Shinya, Tomonori; Desaki, Yoshitake; Bours, Ralph et al. (2010): Conserved fungal LysM effector Ecp6 prevents chitin-triggered immunity in plants. In *Science (New York, N.Y.)* 329 (5994), pp. 953–955. DOI: 10.1126/science.1190859.

de Jonge, Ronnie; van Esse, H. Peter; Maruthachalam, Karunakaran; Bolton, Melvin D.; Santhanam, Parthasarathy; Saber, Mojtaba Keykha et al. (2012): Tomato immune receptor Ve1 recognizes effector of multiple fungal pathogens uncovered by genome and RNA sequencing. In *Proceedings of the National Academy of Sciences of the United States of America* 109 (13), pp. 5110–5115. DOI: 10.1073/pnas.1119623109.

Durán, Paloma (2024): The core microbiota across the green lineage. In *Current opinion in plant biology* 77, p. 102487. DOI: 10.1016/j.pbi.2023.102487.

Durán, Paloma; Reinstädler, Anja; Rajakrut, Anna Lisa; Hashimoto, Masayoshi; Garrido-Oter, Ruben; Schulze-Lefert, Paul; Panstruga, Ralph (2021): A fungal powdery mildew pathogen induces extensive local and marginal systemic changes in the Arabidopsis thaliana microbiota. In *Environmental microbiology* 23 (10), pp. 6292–6308. DOI: 10.1111/1462-2920.15768.

Durrant, W. E.; Dong, X. (2004): Systemic acquired resistance. In *Annual review of phytopathology* 42, pp. 185–209. DOI: 10.1146/annurev.phyto.42.040803.140421.

Edwards, Joseph; Johnson, Cameron; Santos-Medellín, Christian; Lurie, Eugene; Podishetty, Natraj Kumar; Bhatnagar, Srijak et al. (2015): Structure, variation, and assembly of the root-associated microbiomes of rice. In *Proceedings of the National Academy of Sciences of the United States of America* 112 (8), E911-20. DOI: 10.1073/pnas.1414592112.

Epple, P.; Apel, K.; Bohlmann, H. (1997): Overexpression of an endogenous thionin enhances resistance of Arabidopsis against Fusarium oxysporum. In *The Plant cell* 9 (4), pp. 509–520. DOI: 10.1105/tpc.9.4.509.

Ficarra, Florencia A.; Grandellis, Carolina; Garavaglia, Betiana S.; Gottig, Natalia; Ottado, Jorgelina (2018): Bacterial and plant natriuretic peptides improve plant defence responses against pathogens. In *Molecular plant pathology* 19 (4), pp. 801–811. DOI: 10.1111/mpp.12560.

Fradin, Emilie F.; Thomma, Bart P. H. J. (2006): Physiology and molecular aspects of Verticillium wilt diseases caused by V. dahliae and V. albo-atrum. In *Molecular plant pathology* 7 (2), pp. 71–86. DOI: 10.1111/j.1364-3703.2006.00323.x.

Friberg, Hanna; Lagerlöf, Jan; Rämert, Birgitta (2005): Influence of soil fauna on fungal plant pathogens in agricultural and horticultural systems. In *Biocontrol Science and Technology* 15 (7), pp. 641–658. DOI: 10.1080/09583150500086979.

Gao, A. G.; Hakimi, S. M.; Mittanck, C. A.; Wu, Y.; Woerner, B. M.; Stark, D. M. et al. (2000): Fungal pathogen protection in potato by expression of a plant defensin peptide. In *Nature biotechnology* 18 (12), pp. 1307–1310. DOI: 10.1038/82436.

Georgelis, Nikolaos; Yennawar, Neela H.; Cosgrove, Daniel J. (2012): Structural basis for entropy-driven cellulose binding by a type-A cellulose-binding module (CBM) and bacterial expansin. In *Proceedings of the National Academy of Sciences of the United States of America* 109 (37), pp. 14830–14835. DOI: 10.1073/pnas.1213200109.

Gómez-Pérez, Daniel; Schmid, Monja; Chaudhry, Vasvi; Hu, Yiheng; Velic, Ana; Maček, Boris et al. (2023): Proteins released into the plant apoplast by the obligate parasitic protist Albugo selectively repress phyllosphere-associated bacteria. In *The New phytologist* 239 (6), pp. 2320–2334. DOI: 10.1111/nph.18995.

Gottig, Natalia; Garavaglia, Betiana S.; Daurelio, Lucas D.; Valentine, Alex; Gehring, Chris; Orellano, Elena G.; Ottado, Jorgelina (2008): Xanthomonas axonopodis pv. citri uses a plant natriuretic peptide-like protein to modify host homeostasis. In *Proceedings of the National Academy of Sciences of the United States of America* 105 (47), pp. 18631–18636. DOI: 10.1073/pnas.0810107105.

Gu, Shaohua; Wei, Zhong; Shao, Zhengying; Friman, Ville-Petri; Cao, Kehao; Yang, Tianjie et al. (2020): Competition for iron drives phytopathogen control by natural rhizosphere microbiomes. In *Nature microbiology* 5 (8), pp. 1002–1010. DOI: 10.1038/s41564-020-0719-8.

Gutierrez, Daniel; Weinstock, Anthony; Antharam, Vijay C.; Gu, Haiwei; Jasbi, Paniz; Shi, Xiaojian et al. (2020): Antibiotic-induced gut metabolome and microbiome alterations increase the susceptibility to Candida albicans colonization in the gastrointestinal tract. In *FEMS microbiology ecology* 96 (1). DOI: 10.1093/femsec/fiz187.

Hacquard, Stéphane; Garrido-Oter, Ruben; González, Antonio; Spaepen, Stijn; Ackermann, Gail; Lebeis, Sarah et al. (2015): Microbiota and Host Nutrition across Plant and Animal Kingdoms. In *Cell host & microbe* 17 (5), pp. 603–616. DOI: 10.1016/j.chom.2015.04.009.

Hacquard, Stéphane; Spaepen, Stijn; Garrido-Oter, Ruben; Schulze-Lefert, Paul (2017): Interplay Between Innate Immunity and the Plant Microbiota. In *Annual review of phytopathology* 55, pp. 565–589. DOI: 10.1146/annurev-phyto-080516-035623.

Hu, Yezhou; Ding, Yanxia; Cai, Boying; Qin, Xiaohui; Wu, Jingni; Yuan, Minhang et al. (2022): Bacterial effectors manipulate plant abscisic acid signaling for creation of an aqueous apoplast. In *Cell host & microbe* 30 (4), 518-529.e6. DOI: 10.1016/j.chom.2022.02.002.

Jones, Jonathan D. G.; Dangl, Jeffery L. (2006): The plant immune system. In *Nature* 444 (7117), pp. 323–329. DOI: 10.1038/nature05286.

Kamada, Nobuhiko; Chen, Grace Y.; Inohara, Naohiro; Núñez, Gabriel (2013): Control of pathogens and pathobionts by the gut microbiota. In *Nature immunology* 14 (7), pp. 685–690. DOI: 10.1038/ni.2608.

Kesel, Jonas de; Conrath, Uwe; Flors, Víctor; Luna, Estrella; Mageroy, Melissa H.; Mauch-Mani, Brigitte et al. (2021): The Induced Resistance Lexicon: Do's and Don'ts. In *Trends in plant science* 26 (7), pp. 685–691. DOI: 10.1016/j.tplants.2021.01.001.

Kettles, Graeme J.; Bayon, Carlos; Sparks, Caroline A.; Canning, Gail; Kanyuka, Kostya; Rudd, Jason J. (2018): Characterization of an antimicrobial and phytotoxic ribonuclease secreted by the fungal wheat pathogen Zymoseptoria tritici. In *The New phytologist* 217 (1), pp. 320–331. DOI: 10.1111/nph.14786.

Klosterman, Steven J.; Subbarao, Krishna V.; Kang, Seogchan; Veronese, Paola; Gold, Scott E.; Thomma, Bart P. H. J. et al. (2011): Comparative genomics yields insights into niche adaptation of plant vascular wilt pathogens. In *PLoS pathogens* 7 (7), e1002137. DOI: 10.1371/journal.ppat.1002137.

Kraege, Anton; Punt, Wilko; Doddi, Andrea; Zhu, Jinyi; Schmitz, Natalie; Snelders, Nick C.; Thomma, Bart P.H.J. (2025): Undermining the cry for help: The phytopathogenic fungus Verticillium dahliae secretes an antimicrobial effector protein to undermine host recruitment of antagonistic Pseudomonas bacteria. DOI: 10.1101/2025.06.09.658588.

Kwak, Youn-Sig; Weller, David M. (2013): Take-all of Wheat and Natural Disease Suppression: A Review. In *The plant pathology journal* 29 (2), pp. 125–135. DOI: 10.5423/PPJ.SI.07.2012.0112.

Lazzaro, Brian P.; Zasloff, Michael; Rolff, Jens (2020): Antimicrobial peptides: Application informed by evolution. In *Science (New York, N.Y.)* 368 (6490). DOI: 10.1126/science.aau5480.

Lemanceau, Philippe; Blouin, Manuel; Muller, Daniel; Moënne-Loccoz, Yvan (2017): Let the Core Microbiota Be Functional. In *Trends in plant science* 22 (7), pp. 583–595. DOI: 10.1016/j.tplants.2017.04.008.

Lo Presti, Libera; Lanver, Daniel; Schweizer, Gabriel; Tanaka, Shigeyuki; Liang, Liang; Tollot, Marie et al. (2015): Fungal effectors and plant susceptibility. In *Annual review of plant biology* 66, pp. 513–545. DOI: 10.1146/annurev-arplant-043014-114623.

Malanovic, Nermina; Lohner, Karl (2016): Gram-positive bacterial cell envelopes: The impact on the activity of antimicrobial peptides. In *Biochimica et biophysica acta* 1858 (5), pp. 936–946. DOI: 10.1016/j.bbamem.2015.11.004.

Mataraci, Emel; Dosler, Sibel (2012): In vitro activities of antibiotics and antimicrobial cationic peptides alone and in combination against methicillin-resistant Staphylococcus aureus biofilms. In *Antimicrobial agents and chemotherapy* 56 (12), pp. 6366–6371. DOI: 10.1128/aac.01180-12.

Mauch-Mani, Brigitte; Baccelli, Ivan; Luna, Estrella; Flors, Victor (2017): Defense Priming: An Adaptive Part of Induced Resistance. In *Annual review of plant biology* 68, pp. 485–512. DOI: 10.1146/annurev-arplant-042916-041132.

Meier, Stuart; Bastian, René; Donaldson, Lara; Murray, Shane; Bajic, Vladimir; Gehring, Chris (2008): Co-expression and promoter content analyses assign a role in biotic and abiotic stress responses to plant natriuretic peptides. In *BMC plant biology* 8, p. 24. DOI: 10.1186/1471-2229-8-24.

Mendes, Rodrigo; Kruijt, Marco; Bruijn, Irene de; Dekkers, Ester; van der Voort, Menno; Schneider, Johannes H. M. et al. (2011): Deciphering the rhizosphere microbiome for disease-suppressive bacteria. In *Science (New York, N.Y.)* 332 (6033), pp. 1097–1100. DOI: 10.1126/science.1203980.

Mesny, Fantin; Bauer, Martha; Zhu, Jinyi; Thomma, Bart P. H. J. (2024): Meddling with the microbiota: Fungal tricks to infect plant hosts. In *Current opinion in plant biology* 82, p. 102622. DOI: 10.1016/j.pbi.2024.102622.

Mesny, Fantin; Wolf, Valentina; López-Moral, Ana; Kraege, Anton; Punt, Wilko; Park, Jiyeun et al. (2025): Plant-associated fungi co-opt ancient antimicrobials for host manipulation. DOI: 10.1101/2024.01.04.574150.

Mukesh, Srivastava; Mohammad, Shahid; Sonika, Pandey; Vipul, Kuma; Anuradha, Singh; Shubha, Trived et al. (2015): Trichoderma: A scientific approach against soil borne pathogens. In *Afr. J. Microbiol. Res.* 9 (50), pp. 2377–2384. DOI: 10.5897/AJMR2015.7788.

Ngou, Bruno Pok Man; Ahn, Hee-Kyung; Ding, Pingtao; Jones, Jonathan D. G. (2021): Mutual potentiation of plant immunity by cell-surface and intracellular receptors. In *Nature* 592 (7852), pp. 110–115. DOI: 10.1038/s41586-021-03315-7.

Ökmen, Bilal; Katzy, Philipp; Huang, Luyao; Wemhöner, Raphael; Doehlemann, Gunther (2023): A conserved extracellular Ribo1 with broad-spectrum cytotoxic activity enables smut fungi to compete with host-associated bacteria. In *The New phytologist* 240 (5), pp. 1976–1989. DOI: 10.1111/nph.19244.

O'Neill, Jim (2016): Tackling drug-resistant infections globally: final report and recommendations.

Paasch, Bradley C.; Sohrabi, Reza; Kremer, James M.; Nomura, Kinya; Cheng, Yu Ti; Martz, Jennifer et al. (2023): A critical role of a eubiotic microbiota in gating proper immunocompetence in Arabidopsis. In *Nature plants* 9 (9), pp. 1468–1480. DOI: 10.1038/s41477-023-01501-1.

Patané, José S. L.; Moreira, Leandro M.; Melo Teixeira, Marcus de; Martins, Joaquim; Setubal, João C.; Varani, Alessandro M. (2022): New insights into plant natriuretic peptide evolution: From the lysogenic conversion in Xanthomonas to the lateral transfer to the whitefly Bemisia tabaci. In *Gene* 821, p. 146326. DOI: 10.1016/j.gene.2022.146326.

Pfeilmeier, Sebastian; Petti, Gabriella C.; Bortfeld-Miller, Miriam; Daniel, Benjamin; Field, Christopher M.; Sunagawa, Shinichi; Vorholt, Julia A. (2021): The plant NADPH oxidase RBOHD is required for microbiota homeostasis in leaves. In *Nature microbiology* 6 (7), pp. 852–864. DOI: 10.1038/s41564-021-00929-5.

Pfeilmeier, Sebastian; Werz, Anja; Ote, Marine; Bortfeld-Miller, Miriam; Kirner, Pascal; Keppler, Andreas et al. (2024): Leaf microbiome dysbiosis triggered by T2SS-dependent enzyme secretion from opportunistic Xanthomonas pathogens. In *Nature microbiology* 9 (1), pp. 136–149. DOI: 10.1038/s41564-023-01555-z.

Pieterse, Corné M. J.; Zamioudis, Christos; Berendsen, Roeland L.; Weller, David M.; van Wees, Saskia C. M.; Bakker, Peter A. H. M. (2014): Induced systemic resistance by beneficial microbes. In *Annual review of phytopathology* 52, pp. 347–375. DOI: 10.1146/annurev-phyto-082712-102340.

Pritchard, Leighton; Birch, Paul R. J. (2014): The zigzag model of plant-microbe interactions: is it time to move on? In *Molecular plant pathology* 15 (9), pp. 865–870. DOI: 10.1111/mpp.12210.

Pruitt, Rory N.; Locci, Federica; Wanke, Friederike; Zhang, Lisha; Saile, Svenja C.; Joe, Anna et al. (2021): The EDS1-PAD4-ADR1 node mediates Arabidopsis pattern-triggered immunity. In *Nature* 598 (7881), pp. 495–499. DOI: 10.1038/s41586-021-03829-0.

Punt, Wilko; Park, Jiyeun; Roevenich, Hanna; Kraege, Anton; Schmitz, Natalie; Wieneke, Jan et al. (2025): A gnotobiotic system reveals multifunctional effector roles in plant-fungal pathogen dynamics. DOI: 10.1101/2025.03.27.645772.

Rokas, Antonis (2022): Evolution of the human pathogenic lifestyle in fungi. In *Nature microbiology* 7 (5), pp. 607–619. DOI: 10.1038/s41564-022-01112-0.

Round, June L.; Mazmanian, Sarkis K. (2009): The gut microbiota shapes intestinal immune responses during health and disease. In *Nature reviews. Immunology* 9 (5), pp. 313–323. DOI: 10.1038/nri2515.

Saad, Maged M.; Eida, Abdul Aziz; Hirt, Heribert (2020): Tailoring plant-associated microbial inoculants in agriculture: a roadmap for successful application. In *Journal of experimental botany* 71 (13), pp. 3878–3901. DOI: 10.1093/jxb/eraa111.

Sasse, Joelle; Martinoia, Enrico; Northen, Trent (2018): Feed Your Friends: Do Plant Exudates Shape the Root Microbiome? In *Trends in plant science* 23 (1), pp. 25–41. DOI: 10.1016/j.tplants.2017.09.003.

Sels, Jan; Mathys, Janick; Coninck, Barbara M. A. de; Cammue, Bruno P. A.; Bolle, Miguel F. C. de (2008): Plant pathogenesis-related (PR) proteins: a focus on PR peptides. In *Plant Physiology and Biochemistry* 46 (11), pp. 941–950. DOI: 10.1016/j.plaphy.2008.06.011.

Seybold, Heike; Demetrowitsch, Tobias J.; Hassani, M. Amine; Szymczak, Silke; Reim, Ekaterina; Haueisen, Janine et al. (2020): A fungal pathogen induces systemic susceptibility and systemic shifts in wheat metabolome and microbiome composition. In *Nature communications* 11 (1), p. 1910. DOI: 10.1038/s41467-020-15633-x.

Shalev, Or; Ashkenazy, Haim; Neumann, Manuela; Weigel, Detlef (2022): Commensal Pseudomonas protect Arabidopsis thaliana from a coexisting pathogen via multiple lineage-dependent mechanisms. In *The ISME journal* 16 (5), pp. 1235–1244. DOI: 10.1038/s41396-021-01168-6.

Sheoran, Asha Rani; Lakra, Nita; Saharan, Baljeet Singh; Luhach, Annu; Kumar, Ravinder; Seth, Chandra Shekhar; Duhan, Joginder Singh (2025): Enhancing Plant Disease Resistance: Insights from Biocontrol Agent Strategies. In *J Plant Growth Regul* 44 (2), pp. 436–459. DOI: 10.1007/s00344-024-11480-y.

Snelders, Nick C.; Boshoven, Jordi C.; Song, Yin; Schmitz, Natalie; Fiorin, Gabriel L.; Rovenich, Hanna et al. (2023): A highly polymorphic effector protein promotes fungal virulence through suppression of plant-associated Actinobacteria. In *The New phytologist* 237 (3), pp. 944–958. DOI: 10.1111/nph.18576.

Snelders, Nick C.; Rovenich, Hanna; Petti, Gabriella C.; Rocafort, Mercedes; van den Berg, Grardy C. M.; Vorholt, Julia A. et al. (2020): Microbiome manipulation by a soil-borne fungal plant pathogen using effector proteins. In *Nature plants* 6 (11), pp. 1365–1374. DOI: 10.1038/s41477-020-00799-5.

Snelders, Nick C.; Rovenich, Hanna; Thomma, Bart P. H. J. (2022): Microbiota manipulation through the secretion of effector proteins is fundamental to the wealth of lifestyles in the fungal kingdom. In *FEMS microbiology reviews* 46 (5). DOI: 10.1093/femsre/fuac022.

Song, Yi; Wilson, Andrew J.; Zhang, Xue-Cheng; Thoms, David; Sohrabi, Reza; Song, Siyu et al. (2021): FERONIA restricts Pseudomonas in the rhizosphere microbiome via regulation of reactive oxygen species. In *Nature plants* 7 (5), pp. 644–654. DOI: 10.1038/s41477-021-00914-0.

Spooren, Jelle; van Bentum, Sietske; Thomashow, Linda S.; Pieterse, Corné M. J.; Weller, David M.; Berendsen, Roeland L. (2024): Plant-Driven Assembly of Disease-Suppressive Soil Microbiomes. In *Annual review of phytopathology* 62 (1), pp. 1–30. DOI: 10.1146/annurev-phyto-021622-100127.

Terras, F. R.; Eggermont, K.; Kovaleva, V.; Raikhel, N. V.; Osborn, R. W.; Kester, A. et al. (1995): Small cysteine-rich antifungal proteins from radish: their role in host defense. In *The Plant cell* 7 (5), pp. 573–588. DOI: 10.1105/tpc.7.5.573.

Thomma, Bart P. H. J.; Nürnberger, Thorsten; Joosten, Matthieu H. A. J. (2011): Of PAMPs and effectors: the blurred PTI-ETI dichotomy. In *The Plant cell* 23 (1), pp. 4–15. DOI: 10.1105/tpc.110.082602.

Tkacz, Andrzej; Bestion, Eloïne; Bo, Zhiyan; Hortala, Marion; Poole, Philip S. (2020): Influence of Plant Fraction, Soil, and Plant Species on Microbiota: a Multikingdom Comparison. In *mBio* 11 (1). DOI: 10.1128/mbio.02785-19.

Trivedi, Pankaj; Leach, Jan E.; Tringe, Susannah G.; Sa, Tongmin; Singh, Brajesh K. (2020): Plant-microbiome interactions: from community assembly to plant health. In *Nature reviews. Microbiology* 18 (11), pp. 607–621. DOI: 10.1038/s41579-020-0412-1.

van de Mortel, Judith E.; Vos, Ric C. H. de; Dekkers, Ester; Pineda, Ana; Guillod, Leandre; Bouwmeester, Klaas et al. (2012): Metabolic and transcriptomic changes induced in Arabidopsis by the rhizobacterium Pseudomonas fluorescens SS101. In *Plant physiology* 160 (4), pp. 2173–2188. DOI: 10.1104/pp.112.207324.

van de Velde, Willem; Zehirov, Grigor; Szatmari, Agnes; Debreczeny, Monika; Ishihara, Hironobu; Kevei, Zoltan et al. (2010): Plant peptides govern terminal differentiation of bacteria in symbiosis. In *Science (New York, N.Y.)* 327 (5969), pp. 1122–1126. DOI: 10.1126/science.1184057.

van Loon, L. C.; Rep, M.; Pieterse, C. M. J. (2006): Significance of inducible defense-related proteins in infected plants. In *Annual review of phytopathology* 44, pp. 135–162. DOI: 10.1146/annurev.phyto.44.070505.143425.

Vandenkoornhuyse, Philippe; Quaiser, Achim; Duhamel, Marie; Le Van, Amandine; Dufresne, Alexis (2015): The importance of the microbiome of the plant holobiont. In *The New phytologist* 206 (4), pp. 1196–1206. DOI: 10.1111/nph.13312.

Vannier, Nathan; Agler, Matthew; Hacquard, Stéphane (2019): Microbiota-mediated disease resistance in plants. In *PLoS pathogens* 15 (6), e1007740. DOI: 10.1371/journal.ppat.1007740.

Wang, Yeji; Song, Minghui; Chang, Wenqiang (2024): Antimicrobial peptides and proteins against drug-resistant pathogens. In *Cell surface (Amsterdam, Netherlands)* 12, p. 100135. DOI: 10.1016/j.tcsw.2024.100135.

Wang, Yu Hua; Gehring, Chris; Irving, Helen R. (2011): Plant natriuretic peptides are apoplastic and paracrine stress response molecules. In *Plant & cell physiology* 52 (5), pp. 837–850. DOI: 10.1093/pcp/pcr036.

Weller, David M.; Raaijmakers, Jos M.; Gardener, Brian B. McSpadden; Thomashow, Linda S. (2002): Microbial populations responsible for specific soil suppressiveness to plant pathogens. In *Annual review of phytopathology* 40, pp. 309–348. DOI: 10.1146/annurev.phyto.40.030402.110010.

Yeaman, Michael R.; Yount, Nannette Y. (2003): Mechanisms of antimicrobial peptide action and resistance. In *Pharmacological reviews* 55 (1), pp. 27–55. DOI: 10.1124/pr.55.1.2.

Yeoh, Yun Kit; Dennis, Paul G.; Paungfoo-Lonhienne, Chanyarat; Weber, Lui; Brackin, Richard; Ragan, Mark A. et al. (2017): Evolutionary conservation of a core root microbiome across plant phyla along a tropical soil chronosequence. In *Nature communications* 8 (1), p. 215. DOI: 10.1038/s41467-017-00262-8.

Yuan, Minhang; Jiang, Zeyu; Bi, Guozhi; Nomura, Kinya; Liu, Menghui; Wang, Yiping et al. (2021): Pattern-recognition receptors are required for NLR-mediated plant immunity. In *Nature* 592 (7852), pp. 105–109. DOI: 10.1038/s41586-021-03316-6.